Delft University of Technology

Analysis and Remediation of the Salinized, Damour Coastal (Dolomitic) Limestone Aquifer in Lebanon

Khadra, Wisam

DOI
10.4233/uuid:6d4208be-65c1-43e8-afa0-5019f22c6167

Publication date
2017

Document Version
Final published version

Citation (APA)
Khadra, W. (2017). *Analysis and Remediation of the Salinized, Damour Coastal (Dolomitic) Limestone Aquifer in Lebanon*. [Dissertation (TU Delft), Delft University of Technology].
https://doi.org/10.4233/uuid:6d4208be-65c1-43e8-afa0-5019f22c6167

Important note
To cite this publication, please use the final published version (if applicable).
Please check the document version above.

Copyright
Other than for strictly personal use, it is not permitted to download, forward or distribute the text or part of it, without the consent of the author(s) and/or copyright holder(s), unless the work is under an open content license such as Creative Commons.

Takedown policy
Please contact us and provide details if you believe this document breaches copyrights.
We will remove access to the work immediately and investigate your claim.

This work is downloaded from Delft University of Technology.
For technical reasons the number of authors shown on this cover page is limited to a maximum of 10.

Analysis and Remediation of the Salinized, Damour Coastal (Dolomitic) Limestone Aquifer in Lebanon

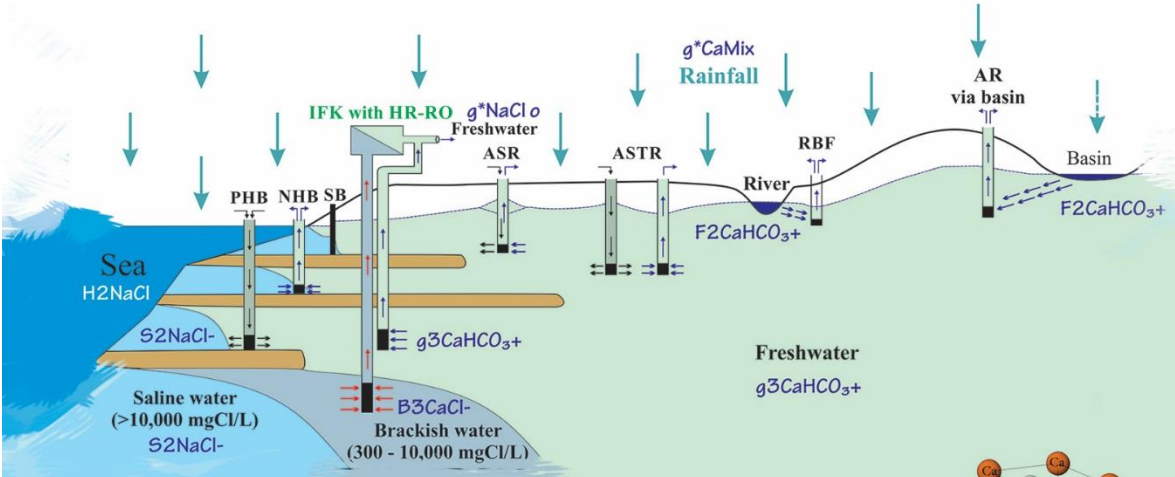

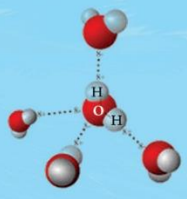

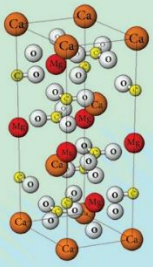

Wisam M. Khadra

Analysis and Remediation of the Salinized, Damour Coastal (Dolomitic) Limestone Aquifer in Lebanon

PROEFSCHRIFT

ter verkrijging van de graad Doctor aan
de Technische Universiteit Delft,
op gezag van de Rector Magnificus prof. ir. K.Ch.A.M.Luyben;
voorzitter van het College voor Promoties,
in het openbaar te verdedigen op
op woensdag 22 november 2017 om 15:00 uur

door

Wisam Mahmoud KHADRA
Master of Science in Geology, American University of Beirut
geboren te Saida, Libanon

This dissertation has been approved by the

Promotor: Prof. dr. P.J. Stuijfzand

Composition of the doctoral committee:

Rector magnificus chairperson

Prof. dr. P.J. Stuijfzand promotor

Independent members:

Prof. dr. ir. T.J. Heimovaara (CiTG, Technische Universiteit Delft)

Prof. dr. M. El-Fadel (FEA, American University of Beirut)

Prof. dr. ir. J.P. van der Hoek (CiTG, Technische Universiteit Delft)

Prof. dr. ir. T.N. Olsthoorn (CiTG, Technische Universiteit Delft)

Dr. B.M. van Breukelen (CiTG, Technische Universiteit Delft)

Reserve: Prof. dr. ir. M. Bakker (CiTG, Technische Universiteit Delft)

The work was carried out initially at the Critical Zone Hydrology Group (Department of Earth Sciences, Faculty of Earth and Life Sciences) at VU University Amsterdam, then completed at the section of Geo-environmental Engineering (Department of Geoscience and Engineering, Faculty of Civil Engineering and Geosciences) at Delft University of Technology. It was partially funded by the International Navigation Trading and Contracting Co. (INTC) - Lebanon.

ISBN: 978-94-6186-861-9

Table of Contents

Summary **9**
Samenvatting **15**

Chapter 1. General introduction **21**
1.1 Background 22
1.2 Management of salinized coastal aquifers 23
1.2.1 Reorganization of wells 24
1.2.2 Managed aquifer recharge 26
1.2.3 Seawater barriers 26
1.2.4 Desalination 27
1.2.5 Integrated Fresh-Keeper (IFK) wells 28
1.3 Conditions of the Eastern Mediterranean 28
1.4 The Lebanese context 29
1.5 Research objectives and questions 33
1.6 Outline of the thesis 33

Chapter 2. Separating baseline conditions from anthropogenic impacts: example of the Damour coastal aquifer (Lebanon) **37**
2.1 Introduction 38
2.2 Setting and methods 39
2.2.1 Geological and hydrogeological setting 39
2.2.2 Data collection 42
2.2.3 HydroChemical System Analysis 45
2.2.3.1 Identification of hydrosomes via environmental tracers 45
2.2.3.2 Determination of hydrochemical facies 45
2.2.3.4 Determination of chemical water type 46
2.2.3.5 Determination of mixing ratios 47
2.2.4 Determination of groundwater baseline composition 49
2.3 Results 50
2.3.1 Identified hydrosomes and their facies 50
2.3.1.1 Mountainous limestone water (M) 55
2.3.1.2 Damour river bank-filtrate (F) 56
2.3.1.3 Coastal plain water (C) 56
2.3.1.4 Landfill leachate (L) 56
2.3.1.5 Mixed M/S 57
2.3.1.6 Mixed M+S 57
2.3.1.7 Mixed (F/M)+S 57
2.3.2 Establishing baseline hydrochemistry for discerned units 58

2.3.3 Salinization sources 58
2.3.3.1 Sea spray and evapo(transpi)ration 58
2.3.3.2 Saltwater intrusion 60
2.3.4 Anthropogenic inputs 61
2.4 Discussion 62
2.4.1 Spatial patterns 62
2.4.1.1 Salinization pattern 62
2.4.1.2 Evolutionary trends 62
2.4.1.3 Recharge zones 63
2.4.2 Comparison with natural backgrounds elsewhere 64
2.4.3 Future outlook on salinization 65
2.5 Conclusions 65
Acknowledgements 66

Chapter 3. Hydrochemical effects of saltwater intrusion in a limestone and dolomitic limestone aquifer in Lebanon 67
3.1 Introduction 68
3.2 Setting and methods 70
3.2.1 Site description 70
3.2.2 Data collection 71
3.2.2.1 Hydrochemical data 71
3.2.2.2 Geochemical analyses 71
3.2.3 Statistical methods 71
3.2.4 Sea water input and correction procedure 72
3.2.5 Mixing Enrichment Factor 73
3.2.6 Forward reactive transport modeling 74
3.3 Results 76
3.3.1 Geochemistry of hosting rocks 76
3.3.2 Statistical results 78
3.3.3 Chemical equilibria 79
3.3.4 Seawater mixing effect 81
3.3.5 Flow path reactive transport modeling results 85
3.4 Discussion 89
3.4.1 Hydrogeochemical disparities 89
3.4.1.1 Main geochemical processes 89
3.4.1.2 Behavior of trace elements 90
3.4.1.3 TEs permissible levels 92
3.5 Conclusions 93
Acknowledgements 94
Appendix S3. Supplementary material 95

Chapter 4. Simulation of saltwater intrusion in a poorly karstified coastal aquifer in Lebanon (Eastern Mediterranean) 107
4.1 Introduction 108
4.2 Setting and methods 110
4.2.1 Site description 110
4.2.2 Description of aquifer hydrodynamics 111
4.2.3 Defining major geological (geo-)lineaments 113
4.2.4 Accounting for geo-lineaments in the model mesh 113
4.3 Model development 114
4.3.1 Numerical code and discretization 114
4.3.2 Boundary conditions 115
4.3.3 Hydraulic properties 117
4.4 Results 118
4.4.1 Time series analysis 118
4.4.2 Discrete features 119
4.4.3 Simulation results 120
4.4.4 Sensitivity analysis 124
4.5 Discussion 125
4.5.1 EPM vs. CDC resemblance 125
4.5.2 Options for mature karst 127
4.6 Conclusions 127
Acknowledgements 128
Appendix S4. Supplementary material 129

Chapter 5. Mitigation of saltwater intrusion by 'integrated fresh-keeper' wells combined with high recovery reverse osmosis 131
5.1 Introduction 132
5.2 Methods 133
5.2.1 Selection of proper vertical barrier 133
5.2.2 Design of high recovery RO system 134
5.3 Application to the Damour aquifer - Lebanon 137
5.4 Results and discussion 137
5.4.1 IFK pumping layout 137
5.4.2 Design of the HR-RO system 142
5.4.3 Assessment of permeate/concentrate quality and volume 144
5.4.4 Options of concentrate disposal 145
5.4.5 Economic assessment 147
5.5 Conclusions 148
Acknowledgements 150

Appendix S5. Supplementary material 151

Chapter 6. Synthesis and spin-off for water management 155
6.1 Summary of the findings 156
6.2 MAR in Lebanon 159
6.3 Assessment of MAR potential in the Damour area 162
6.3.1 Introduction 162
6.3.2 Hydrological analysis 163
6.3.2.1 RBF north of the Damour River 163
6.3.2.2 ASR in the Damour coastal plain 163
6.3.3 Hydrochemical analyses 164
6.3.4 Hydrogeochemical sustainability 165
6.3.5 Conclusions 165
6.4 Towards a structured multi-faceted approach to analyze and manage saltwater intrusion in coastal aquifers 166
6.5 Future challenges 168

Chapter 7. Acknowledgements 171

Chapter 8. Bibliography 175

Curriculum Vitae

Summary

Coastal aquifer management has recently emerged as a main scope in groundwater hydrology, especially in arid and semi-arid zones. About two thirds of the human population are currently gathered close to shorelines relying on coastal groundwater resources. Worldwide, these systems are subject to quality deterioration due to a multitude of anthropogenic impacts and subsequent saltwater intrusion (SWI).

Many hydrological and hydrochemical features of SWI have been disclosed during the past century through numerous case studies, column studies, scale models, flow and reactive transport modeling. Yet, many scientific and engineering challenges remain, some of which need to be addressed for a better prospecting of future coastal freshwater reserves. The scope of this thesis is to contribute to the analysis and remediation of SWI by studying the following aspects: (1) response of carbonate aquifers with varying Ca/Mg content to SWI, (2) behavior of trace elements (TEs) where fresh and intruded seawater mix, (3) derivation of groundwater baseline levels in polluted settings, notably salinized aquifers, (4) identification and quantification of major hydrogeochemical processes stimulated by SWI, (5) reliability of complex models (especially in karst) with variable-density and solute transport formulations, and (6) feasibility of SWI mitigation strategies. A structured multi-faceted approach to analyze and manage SWI in coastal aquifers from detection to remediation is then provided. It was expanded based on the overall outcome of this research. The proposed tools and methods were successfully applied to a stressed dolomitic limestone aquifer system in Lebanon (Eastern Mediterranean), suffering from salinization and other minor anthropogenic impacts, such as inputs from sewage effluents and agricultural processes. The potential of managed aquifer recharge (MAR) and in particular river bank filtration (RBF) is explored as well, for Lebanon in broad lines, and for the study area, as a karst example.

Methods

In order to reach the scope, some existing tools have been adapted and new tools developed. They include: (a) a method to establish natural background concentrations of salinized and/or contaminated groundwater, (b) a method to assess the mobilization of solutes notably TEs under various settings including mixing conditions, (c) guidelines for SWI modeling in poorly karstified aquifers, and (d) mitigation strategies especially recommended for karstic or fractured aquifers where a precise understanding of system dynamics is not possible.

A new structured approach is presented to derive groundwater baseline conditions. It builds on the HydroChemical System Analysis (HCSA) to map different groundwater bodies (hydrosomes) and hydrochemical zones within them, each of which showing significant differences in baseline chemistry. Complexities in assessing groundwater baseline conditions generally arise, where: (a) historical data of pristine water is lacking, (b) the hydrological system under investigation is facing a multitude of anthropogenic influences, or (c) groundwater bodies of different origins interfere. The introduced procedure includes an elimination scheme for biased data and data showing signs of

pollution, the definition of significant hydrochemical trends, and statistical analysis to discern new subfacies, identify any outliers, and choose representative values. All water bodies requiring natural concentrations are assigned through HCSA, precluding salinized samples, mixed redox and intermixed hydrosomes. This step of subdividing the population warrants a detailed determination of natural background concentrations by revealing the appropriate diversity for each hydrosome and its facies.

Eight major chemical constituents (Na, K, Ca, Mg, SO_4, TIC, Fe and Si) and 50 trace elements (TEs) were analyzed in 80 water and 65 rock samples in the Damour system, and interpreted with a quad-fold approach utilizing: (1) nonparametric statistical tests, (2) concentration deviations from ideal conservative freshwater-seawater mixing lines, (3) a new parameter called Mixing Enrichment Factor to assess the mobilization of chemical constituents under various settings, and (4) 1-D dual porosity flow path modeling with PHREEQC. This allowed the demonstration of groundwater quality differences between coastal limestone and dolomitic limestone aquifers, with and without ongoing moderate salinization.

SWI in the poorly karstified Damour aquifer was also simulated in various ways and compared to measurements. Two important steps were incorporated: (1) an initial time series analysis to discover the hydrodynamic response of the system and decide whether ignoring quickflow is justifiable, and (2) a coupled discrete-continuum (CDC) approach to check whether it warrants better results at the desired scale than an equivalent porous medium (EPM) model. Information on geo-lineaments (main fractures, faults, and discerned conduits) was used to embed discrete features into the 3-D continuum to obtain a more karst-representative CDC saltwater intrusion model. The simulation efforts utilized the SEAWAT code since it is density dependent and public-domain, and it enjoys widespread application. Including DF's necessitated manual handling because the selected code has no built-in option for such features.

Finally, a new coupled strategy to mitigate SWI in karstic or fractured aquifers is introduced as a localized remedy to protect shallow freshwater reserves while utilizing the deeper intercepted brackish water. It is a double sourcing application where fresh-keeper wells are installed at the bottom of a deepened borehole of selected salinized wells, and then supported by high recovery (HR) reverse osmosis (RO) desalination. This method sustainably produces 2 water types via its 2 separated well screens within the same borehole: freshwater from the shallow screen and brackish or slightly brackish water from the deeper one. The brackish water is treated to demineralized bottled water by utilizing a HR-RO tandem desalination unit. An axisymmetric (radial) profile model is used to define the proper layout of wells and warrant a stable saltwater interface with suitable feed volume and quality. The RO design has < 1 kWh/m^3 energy consumption, and up to 96% recovery in addition to low scaling propensity without use of any anti-scalant.

Results of separating baseline conditions from anthropogenic impacts

Baseline conditions for 16 main constituents, 59 trace elements and two isotopes were filtered out. Concentrations of Cl, Cl/Br, ^{2}H, ^{18}O and Ca/Sr in combination with major ions and less immobile trace elements (e.g. B and Li) were used to discern different hydrosomes. These are: (1) Mountainous limestone water, (2) coastal plain water, (3) Damour River bank-filtrate, and (4) mixed hydrosomes composed of freshwater from the limestone mountains, fresh river bank-filtrate and intruded saltwater of the Mediterranean Sea.

The characteristics of all hydrosomes were discussed and their areal extent was presented on a hydrochemical map with 2 cross-sections. The dominant hydrochemical facies was (sub)oxic, calcareous and salinized, indicating a very low reduction capacity of the aquifer system, strong dissolution of dolomitic limestone and clear traces of seawater encroachment. The aforementioned discrimination of groundwater bodies facilitated an easier hydrochemical analysis of the system, including salinization sources, anthropogenic inputs, recharge zones, and evolutionary trends.

Results of hydrochemical effects of SWI in limestone vs. dolomitic limestone

Dissolution/precipitation of $Ca_xMg_ySr_zCO_3$ and cation exchange were the main disclosed hydrogeochemical processes besides weak signs of little organic matter oxidation. In the dolomitic limestone aquifer, less carbonate dissolved as compared to the limestone aquifer, partly because of lower pCO_2 in addition to seawater inflow triggering Mg-calcite precipitation by cation exchange (Na expelling Ca and Mg). The presence of high Mg-calcite raised the Mg levels in groundwater, and enhanced the Mg participation (besides Ca) in the exchange for Na and K. Fe revealed no difference between the two aquifers. Silica (quartz or opal) showed higher concentrations in the limestone unit, which is, however, probably dictated by more dissolution in the overlying quaternary sand-rich unit.

SWI led to mobilization of As, Ba, Cu, Ni, Rb, Sr and U in both aquifers, partly by cation exchange (e.g. Ba and Sr). The geochemical contrast between limestone and dolomitic limestone proved to be an important factor explaining part of the observed variation in the concentration of TEs regardless of SWI. For example, As, Cu and Ni recorded stronger mobilization in the freshwater dolomitic limestone, whereas Ba, Rb, Sr and U were more mobilized in the limestone unit. Other elements such as Al, Be, Co, Cr, Pb and V showed no (im)mobilization in either rock type. The observed TE discrepancy between the limestone and dolomitic limestone units is mainly linked to the higher Sr content of limestone and its higher content of clay minerals and iron (hydro)oxides.

Results of simulating SWI in poorly coastal karstified aquifers

Time series analysis in the Damour aquifer revealed a relatively long response time of groundwater levels to rainfall inputs. This indicates that conduit quickflow is scarce, justifying an initial use of the EPM simplification. Comparison of the EPM and the CDC approaches showed that the latter had less difference between measured and computed salinity values than the EPM. This comparison relied on: (a) 5 statistical measures of

salinity or hydraulic head goodness-of-fit (root mean square (RMS) and normalized RMS error of salinity, correlation coefficient, Akaike Information Criterion, and Bayesian Information Criterion), and (b) the match of the simulated saltwater-freshwater interface with available data from 1965 and 2011. The CDC model improved the local-scale salinity values for the majority of wells including the position of the fresh-brackish water interface, and reduced the overall model error (RMS of chloride) by ca. 28%. For the EPM method, 26 simulated wells out of 59 were more than 200 mg/L off, whereas the count being 16 for the CDC model; only at a few wells CDC scored worse than EPM. Therefore, it is assumed that the CDC is better suited for modeling SWI in the poorly karstified Damour aquifer, which is worth its more complicated application, as is the case with any model seeking higher accuracy at local scale.

Results of mitigation of saltwater intrusion by 'integrated fresh-keeper' wells combined with HR-RO

A feasibility study of the introduced concept of 'integrated fresh-keeper' (IFK) wells coupled with HR-RO is presented as an example for a salinizing, brackish pilot well (TDS ~1600mg/L) in the Damour coastal aquifer. It is expected to produce 250 m^3/d of fresh groundwater by vertical hydraulic interception from the top well screen and 800 m^3/d of brackish groundwater (to be later desalinized with high recovery) from the fresh-keeper well screen below. Consequently, the IFK installation coupled with the HR-RO system may supply in a sustainable way a total of about 985 m^3/d of freshwater. About 735 m^3/d of this water is suitable for drinking purposes after a slight post-treatment to meet drinking standards, e.g. liming or blending with a small portion of brackish or fresh groundwater to stabilize the water and increase its alkalinity and TDS. The other 250 m^3/d of fresh water is good enough to supply as domestic water or to polish up the RO-permeate. The total expense of the desalting process was estimated at 0.99 US$/$m^3$ for a 10-year period life span, which could return back the plant capital cost in the first 1 to 4 years depending on the choice of selling bottled or tap water (the selling prices in Lebanon are 100 and 10 US$/$m^3$, respectively).

The usage of brackish groundwater from IFK wells thus serves 3 purposes: production of high quality drinking water, financial gain and mitigation of water stress by overpumping. The formulated strategy can be extrapolated to other sites, and the proposed treatment system could be used for similar feedwater conditions or be adapted after minor modification for more brackish waters. The disposal of concentrate in any RO system is a major environmental issue. Several options (though not ideal) exist: (a) disposal to surface water (ocean or river), sewer, deep saline aquifers (via injection), evaporation/salt ponds, or waste water treatment facilities, which either digest the low concentrate volume amidst the main stream or which are supplemented with e.g. electrodialysis reversal (EDR) treatment or eutectic freezing crystallization; (b) irrigation of plants tolerant to high salinity (e.g. halophytes); or (c) manufacturing of different by- products (e.g. fertilizers).

Conclusions

Various tools or methods to analyze SWI in coastal aquifers have been successfully applied in this thesis, such as: the HydroChemical System Analysis for mapping water quality, PHREEQC-2 for 1-D reactive transport modeling, and SEAWAT for density dependent groundwater flow modeling. Other existing tools have been adapted and new tools developed to: derive baseline groundwater conditions, assess the mobilization of chemical constituents under mixing conditions, simulate SWI in poorly karstified aquifers, and mitigate SWI in settings where a precise understanding of system dynamics is not possible, as in karstic or fractured aquifers. All together, they offer an interesting toolbox for investigating SWI anywhere.

In Lebanon as a particular case, more options of water buffering are urgently required. River bank filtration forms a forgotten but strong candidate of managed aquifer recharge (MAR) application to be added to the Lebanese national water strategy. Aquifer storage and recovery (ASR) in alluvial aquifers having nearby recharge sources (e.g. from rivers) also seem to be an attractive option. In addition, further research is needed to investigate the feasibility of utilizing other sources for recharge, for instance by harvesting rainwater, urban stormwater, or even treated effluent water, where rivers are far away or have a too bad water quality.

Samenvatting

Kustaquiferbeheer is recentelijk uitgegroeid tot een belangrijke taak van de grondwaterhydrologie, vooral in aride en semi-aride gebieden. Ongeveer twee derde van de mensheid woont momenteel dicht bij de kust en moet qua watervoorziening stellen met grondwaterreserves aldaar. Wereldwijd zijn deze voorraden echter onderhevig aan kwaliteitsverslechtering door een groot aantal antropogene invloeden waaronder zoutwaterintrusie (SWI).

Veel hydrologische en hydrochemische kennis van SWI is de afgelopen eeuw vergaard dankzij talrijke case studies, kolomstudies, schaalmodellen, en de modellering van grondwaterstroming en reactief stoftransport. Toch zijn er nog veel wetenschappelijke en technische uitdagingen, waarvan sommigen moeten worden aangepakt om tot een betere prospectie van toekomstige reserves aan grondwater in de kust te komen. Doel van dit proefschrift is bij te dragen aan de analyse, preventie en omkering van SWI door bestudering van de volgende aspecten: (1) reactie van carbonaataquifers met wisselend Ca/Mg gehalte op SWI, (2) gedrag van spore-elementen (SEn) waar zoet en geïntrudeerd zeewater mengen, (3) bepaling van de natuurlijke achtergrondsamenstelling van grondwater in vervuilde omgeving, met name in verzilte aquifers, (4) identificatie en kwantificering van belangrijke hydrogeochemische processen die door SWI gestimuleerd worden, (5) betrouwbaarheid van complexe modellen (vooral in karst), toegerust met variabele dichtheid en reactief stoftransport, en (6) haalbaarheid van strategieën om SWI te mitigeren. Met deze toegevoegde onderdelen is een gestructureerde, veelzijdige aanpak vormgegeven om SWI in kustwateraquifers te analyseren en te managen, van detectie tot en met remediëring. De voorgestelde gereedschappen en methoden zijn in dit proefschrift met succes toegepast op een gestreste, dolomitische kalksteenaquifer in Libanon (Oostelijke Middellandse Zee). Deze aquifer lijdt aan verzilting en andere (maar ondergeschikte) antropogene invloeden, zoals rioolwaterinputs en inputs vanuit de landbouw. De potentie van Managed Aquifer Recharge (MAR) en met name die van oeverfiltratie (RBF) wordt ook verkend, zowel voor Libanon als geheel (in grote lijnen) als voor het studiegebied (een voorbeeld van een karstaquifer).

Methoden

Om de gestelde doelen te realiseren, zijn enkele bestaande tools aangepast en nieuwe tools ontwikkeld. Zij omvatten: (a) een methode voor het vaststellen van natuurlijke achtergrondconcentraties van verzilt en/of anderszins verontreinigd grondwater, (b) een methode om de mobilisatie van opgeloste stoffen, met name SEn, vast te stellen en te kwantificeren onder verschillende omstandigheden waaronder die tijdens menging, (c) richtlijnen voor SWI modellering in weinig verkarste aquifers, en (d) mitigatiestrategieën, vooral aanbevolen voor verkarste of gebroken aquifers, waar het verkrijgen van nauwkeurig inzicht in de systeemdynamiek onmogelijk is.

Een nieuwe gestructureerde aanpak is gepresenteerd om de natuurlijke achtergrondsamenstelling van grondwater te bepalen. Zij is gebaseerd op de HydroChemical System Analysis (hydrochemische systeemanalyse; HCSA) ter kartering van verschillende grondwaterlichamen (hydrosomen) en hydrochemische zones daarbinnen,

die ieder voor zich significante verschillen in natuurlijke achtergrondkwaliteit vertonen. Complicaties bij het vaststellen van natuurlijke achtergrondconcentraties ontstaan over het algemeen, waar: (a) historische gegevens van ongerept water ontbreken, (b) het onderzochte hydrologische systeem geconfronteerd wordt met een groot aantal antropogene invloeden, of (c) grondwaterlichamen met verschillende oorsprong voorkomen. De voorgestelde aanpak omvat een schema ter eliminatie van foutieve gegevens en data die tekenen van verontreiniging vertonen, de bepaling van significante hydrochemische trends, en statistische analyse ter onderscheiding van nieuwe subfacies, ter identificatie van eventuele uitbijters en ter selectie van representatieve waarden. De natuurlijke achtergrondsamenstelling is vastgesteld voor alle door middel van HCSA onderscheiden waterlichamen en hun facies, onder uitsluiting van zones met verziltingsverschijnselen, gemengde redox en menging van verschillende hydrosomen. Deze discriminatiestap garandeert een gedetailleerde bepaling van natuurlijke achtergrondconcentraties door de diversiteit aan hydrochemische milieus binnen elk hydrosoom te onthullen.

Acht belangrijke chemische bestanddelen (Na, K, Ca, Mg, SO4, TIC, Fe en Si) en 50 spore-elementen (SEn) zijn geanalyseerd in 80 water- en 65 gesteentemonsters van het Damour-aquifersysteem, en geïnterpreteerd met een viervoudige benadering waarbij gebruik werd gemaakt van: (1) nonparametrische statistische tests, (2) concentratieafwijkingen van ideale conservatieve mengwaterlijnen voor zoetwater-zeewater, (3) een nieuwe parameter genaamd Mixing Enrichment Factor om de mobilisatie van chemische bestanddelen te beoordelen onder verschillende condities, en (4) 1-D dual porosity flow path modellering met PHREEQC. Dit maakte het mogelijk om grondwaterkwaliteitsverschillen aan te tonen tussen een kustaquifer van kalksteen en één van dolomitische kalksteen, met en zonder voortgaande (maar voorlopig nog milde) verzilting.

SWI in de weinig verkarste Damour aquifer is op verschillende manieren gesimuleerd en vergeleken met metingen. Twee belangrijke stappen zijn opgenomen: (1) als eerste een tijdreeksanalyse om de hydrodynamische respons van het systeem te ontdekken en te beslissen of het negeren van kortsluitstroming gerechtvaardigd is, en (2) een gekoppelde discreet-continuum (CDC) aanpak om te controleren of het betere resultaten op de gewenste schaal garandeert dan een equivalent poreus medium (EPM) model. Informatie over geo-lineamenten (hoofdbreuken, spleten en zich onderscheidende transportkanalen) is gebruikt om discrete eigenschappen in het 3-D continuum te integreren om een meer karst-representatief CDC zoutwaterintrusiemodel te verkrijgen. De simulaties zijn uitgevoerd met de SEAWAT-code, omdat deze code dichtheidsverschillen verdisconteert, publiek domein software is, en brede toepassing kent. Wel moesten ‘discrete features’ (DFs) noodzakelijkerwijs handmatig verwerkt worden, omdat de geselecteerde code geen ingebouwde optie heeft voor dergelijke functies.

Tenslotte, is een nieuwe, gekoppelde strategie geïntroduceerd om SWI te verminderen in verkarste of gebroken aquifers, door op lokale schaal de ondiepe zoetwaterreserve te beschermen, terwijl het dieper opgepompte brakwater tevens wordt gebruikt. Het is daardoor een dubbele bron-applicatie, waarbij een zoethouder put (fresh-keeper) aan de

onderzijde van een verdiept boorgat van een verzilte pompput wordt geïnstalleerd en vervolgens voorzien van een bovengrondse reverse osmosis (RO) ontzilting met hoog rendement (HR). Deze methode produceert duurzaam 2 watertypes via zijn 2 gescheiden putfilters in hetzelfde boorgat: zoetwater via het ondiepe filter en brak of licht brak water via het diepe. Het brakwater wordt behandeld tot gedemineraliseerd water door gebruik te maken van de HR-RO tandem ontziltingseenheid, en vervolgens gebotteld. Een axisymmetrisch (radiaal) 2D model is gebruikt om de geschikte lay-out van de putten te definiëren en een stabiel zoet/zout-grensvlak te waarborgen bij een gewenste wincapaciteit en kwaliteit. Het RO-ontwerp heeft een energieverbruik van < 1 kWh / m^3, een rendement (recovery) tot 96%, en geringe verstoppingspotentie zonder gebruik van een anti-scalant.

Resultaten van het scheiden van natuurlijke achtergrondcondities van antropogene effecten

De natuurlijke achtergrondconcentraties voor 16 hoofdbestanddelen, 59 spore-elementen en twee isotopen zijn vastgesteld. Concentraties van Cl, ^{2}H, ^{18}O en de verhouding Cl/Br en Ca/Sr in combinatie met (andere) hoofdbestanddelen en enkele relatief mobiele spoorelementen (bijv. B en Li) zijn gebruikt om verschillende hydrosomen te onderscheiden. Dit zijn: (1) kalksteenwater uit de bergen, (2) kustvlaktewater, (3) oeverfiltraat van de Damour Rivier, en (4) gemengde hydrosomen samengesteld uit zoet water uit het kalksteengebergte, zoet oeverfiltraat van de Damour Rivier en geïntrudeerd zoutwater van de Middellandse Zee.

De kenmerken van alle hydrosomen zijn besproken en hun ruimtelijke verspreiding is gepresenteerd op een hydrochemische kaart met 2 dwarsdoorsneden. De dominante hydrochemische facies was (sub)oxisch, kalkhoudend en verzilt, wat een zeer lage reductiecapaciteit van het aquifersysteem aangeeft, en tevens sterke oplossing van dolomitische kalksteen en duidelijke sporen van zeewaterintrusie. De in voorgaande genoemde discriminatie van grondwaterlichamen vergemakkelijkt de hydrochemische analyse van het systeem, door onderscheiding van verziltingsbronnen, antropogene inputs, voedingsgebieden en lijnen van kwaliteitsontwikkeling langs stroombanen.

Resultaten van hydrochemische effecten van SWI in kalksteen versus dolomitische kalksteen

Oplossing/neerslag van $Ca_xMg_ySr_zCO_3$ en kationuitwisseling vormden de belangrijkste hydrogeochemische processen naast een geringe mate van oxidatie van organische stof. In de dolomitische kalksteenaquifer werd minder carbonaat opgelost dan in de kalksteenaquifer, vooral door een lagere pCO_2 en in mindere mate door de neerslag van Mg-calciet veroorzaakt door kationuitwisseling (desorptie van Ca en Mg, adsorptie van Na) naar aanleiding van zeewaterintrusie. De aanwezigheid van Mg-calciet verhoogde de Mg-niveaus in grondwater en verhoogde de Mg-participatie (naast Ca) in de uitwisseling voor Na en K. Fe liet geen verschil tussen de twee aquifers zien. Silica (kwarts of opaal) vertoonde hogere concentraties in de kalksteeneenheid, die echter waarschijnlijk wordt gedicteerd door meer oplossing in de afdekkende zandrijke eenheid uit het Kwartair.

SWI leidde tot mobilisatie van As, Ba, Cu, Ni, Rb, Sr en U in beide aquifers, gedeeltelijk door kationuitwisseling (bijv. Ba en Sr). Het geochemische contrast tussen kalksteen en dolomitische kalksteen bleek een belangrijke factor te zijn die de waargenomen variatie in de concentratie van SEn gedeeltelijk verklaart, ongeacht SWI. Zo ondervonden As, Cu en Ni een sterkere mobilisatie in de zoete, dolomitische kalksteenaquifer, terwijl Ba, Rb, Sr en U meer in de zoete kalksteenaquifer werden gemobiliseerd. Andere elementen zoals Al, Be, Co, Cr, Pb en V vertoonden geen enkele (im)mobilisatie in één van beide gesteentes. De waargenomen SE-afwijking tussen de kalksteen- en dolomitische kalksteenaquifer is hoofdzakelijk gekoppeld aan het hogere gehalte aan Sr, kleimineralen en ijzer(hydro)oxiden van kalksteen.

Resultaten van het simuleren van SWI in weinig verkarste kustaquifers

Tijdreeksanalyse van waterstanden in de Damour aquifer leidde tot een relatief lange responstijd van het grondwaterpeil op regenval. Dit geeft aan dat er nauwelijks sprake is van korstsluitstroming via tunnelachtige afvoerkanalen, wat in eerste instantie het gebruik van de EPM-vereenvoudiging rechtvaardigt. Vergelijking van de EPM en de CDC benadering liet echter zien dat laatstgenoemde minder verschil vertoonde tussen gemeten en berekende zoutconcentraties dan EPM. Deze vergelijking was gebaseerd op: (a) 5 statistische parameters van de mate van overeenkomst tussen meetwaarden en berekende waarden van het zoutgehalte of stijghoogte (root mean square (RMS) en genormaliseerde RMS fout van zoutgehalte, correlatiecoëfficiënt, Akaike Information Criterion, en Bayesian Information Criterion), en (b) de overeenkomst tussen het gesimuleerde en het met beschikbare data van 1965 en 2011 gemeten zoet/zout-grensvlak. Het CDC-model verbeterde de simulatie van de lokale saliniteitswaarden voor de meerderheid van de bronnen, inclusief de positie van het zoet/zout-grensvlak, en verminderde de algemene modelfout (RMS van chloride) met ca. 28%. Met de EPM-methode bedroeg de fout > 200 mg/L voor 26 van de 59 gesimuleerde putten, terwijl dit aantal 16 was voor het CDC-model; bij slechts enkele putten scoorde CDC slechter dan EPM. Er is dan ook geconcludeerd dat CDC beter geschikt is voor het modelleren van SWI in de weinig verkarste Damour aquifer, en dat de ingewikkelder CDC applicatie de moeite loont, hetgeen voor elk model geldt dat op lokale schaal meer nauwkeurigheid wenst.

Resultaten van het mitigeren van zeewaterintrusie door 'geïntegreerde fresh-keeper'-putten in combinatie met HR-RO

Een haalbaarheidsstudie van het geïntroduceerde concept van 'geïntegreerde fresh-keeper' (IFK) putten in combinatie met HR-RO is gepresenteerd met als voorbeeld een verziltende pompput (TDS ~ 1600 mg/L) in de Damour kustaquifer. Naar verwachting wordt 250 m^3/d zoet grondwater geproduceerd via het bovenste filter en 800 m^3/d brak grondwater (te ontzilten met hoog rendement) via het zoethouderfilter eronder. Zodoende kan de IFK-installatie in combinatie met het HR-RO-systeem op duurzame wijze in totaal ongeveer 985 m^3/d zoet water leveren. Ongeveer 735 m^3/d van dit water is geschikt voor drinkwaterdoeleinden na een lichte nabehandeling om te voldoen aan de

drinkwaterstandaarden, bijv. door kalkdosering of vermenging met een klein deel brak of zoet grondwater om het water te stabiliseren en de alkaliniteit en TDS te verhogen. De overige 250 m^3/d zoet water is van voldoende kwaliteit om te leveren als huishoudwater of om het RO-permeaat bij te polijsten. De totale kosten van het ontzoutingsproces zijn geschat op 0.99 US$/$m^3$ bij een levensduur van 10 jaar. Dit betekent dat de kapitaalkosten van installatie al na 1 tot 4 jaar terug te verdienen zijn, afhankelijk van de keuze van verkoop als hetzij gebotteld water hetzij kraanwater (de verkoopprijzen in Libanon zijn respectievelijk 100 en 10 US$/$m^3$).

Het gebruik van brak grondwater uit IFK-putten kent dus drie doelen: productie van hoogwaardig drinkwater, financiële winst en vermindering van waterstress alsgevolg van overmatige winning. De geformuleerde strategie is toepasbaar op andere locaties, en het voorgestelde behandelingssysteem kan worden gebruikt voor soortgelijke voedingswateren of, na aanpassing, voor zouter water. De verwijdering van concentraat in een RO-systeem vormt een belangrijk milieuprobleem. Er zijn verschillende opties (hoewel niet ideaal): (a) afvoer naar oppervlaktewater (oceaan of rivier), riool, diepe zoute aquifers (via injectie), indampingspannen of afvalwater zuiveringsinstallaties, die het lage concentraat volume meenemen in de hoofdstroom of die worden toegerust met een extra behandelingsstap zoals electrodialysis reversal (EDR) of eutectische bevriezing kristallisatie; (b) irrigatie van planten die een hoog zoutgehalte tolereren (bijv. halofyten); of (c) vervaardiging van verschillende bijproducten (bijv. meststoffen).

Conclusies

Verschillende instrumenten of methoden om SWI te analyseren in kustaquifers zijn met succes toegepast in dit proefschrift, zoals: de HydroChemical System Analysis voor het in kaart brengen van waterkwaliteit, PHREEQC-2 voor 1-D reactieve transport modellering, en SEAWAT voor dichtheidsafhankelijke modellering van de grondwaterstroming. Andere bestaande gereedschappen zijn aangepast en nieuwe gereedschappen ontwikkeld met als doel: de natuurlijke grondwatersamenstelling af te leiden, de mobilisatie van chemische bestanddelen onder mengomstandigheden te beoordelen, SWI in weinig verkarste aquifers te simuleren, en SWI te mitigeren waar geen nauwkeurig inzicht in systeemdynamiek kan worden verkregen, zoals in verkarste of gebroken aquifers. Alles bij elkaar, bieden zij een interessante gereedschapskist voor het onderzoeken van SWI overal op aarde.

Libanon heeft dringend meer opties van waterbuffering nodig. Oeverfiltratie vormt een vergeten maar sterke Managed Aquifer Recharge (MAR) kandidaat die toegevoegd dient te worden aan de Libanese nationale waterstrategie. Aquifer Storage and Recovery (ASR) in alluviale aquifers met nabijgelegen bronnen van in te nemen infiltratiewater (dikwijls rivieren) lijkt ook een aantrekkelijke optie te zijn. Er is daarenboven verder onderzoek nodig om de haalbaarheid van het gebruik van andere bronnen van infiltratiewater te onderzoeken, bijvoorbeeld door het opvangen van regenwater, stedelijk water (urban runoff) of zelfs behandeld afvalwater, indien rivieren te ver weg zijn of een te slechte waterkwaliteit hebben.

Chapter 1

General introduction

1.1 Background

With a general demographic shift toward coastal urbanized lowlands, coastal areas are becoming densely populated exceeding about three times the global average. The high consumption rates put coastal water reserves under high stress, and lead to disruption of the hydrodynamic balance between on-shore freshwater and off-shore seawater. Eventually saltwater intrusion (SWI), the subsurface landward movement of saline water, is induced (Figure 1.1), which forms a major cause of groundwater quality deterioration in coastal areas.

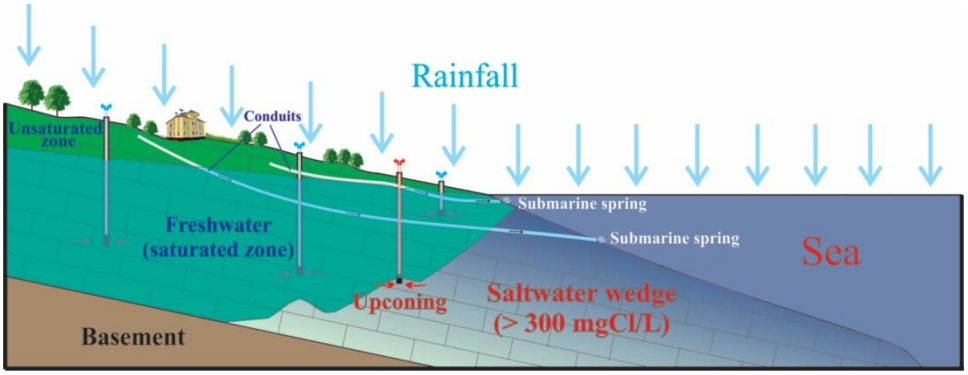

Figure 1.1 Simplified diagram of a dipping coastal aquifer, with pronounced conduits, threatened by SWI. Saltwater upconing is due to overpumping, but it is limited to deep wells. The saltwater wedge is expected to become wider if excessive pumping continues. Previously active submarine groundwater discharge (SGD) may menace today the aquifer system by short-circuiting seawater intrusion.

The basics of SWI and its main controlling factors have been thoroughly tackled since Badon-Ghyben (1888) and Herzberg (1901) discovered the physical principle of fresh groundwater floating on more saline groundwater. A multitude of studies followed in the 1950s and 1960s providing fundamental understanding of fresh salt groundwater interaction in aquifers (e.g. Todd 1953; Henry 1959; Carlston 1963; Bear and Dagan 1964; Charmonman 1965). Various methods have been applied since then to study the spread and extent of SWI. These include hydro(geo)logical studies with focus on hydraulic head distributions (e.g. Volker and Rushton 1982; Kim et al. 2007), airborne, surface and borehole geophysical investigations (e.g. Stewart 1999; Obikoya and Bennell 2012; Prinos et al. 2014; Himi et al. 2017), hydrochemical analyses (e.g. Stuyfzand 1993a; Drever 1997; Appelo and Postma 2005), and numerical models (e.g. De Filippis et al. 2016; Steiakakis et al. 2016; Zhao et al. 2016).

With the advent of fast computers, interpretations and visualizations have partly superated analytical solutions, by replacing simple homogeneous porous media by more realistic heterogeneous porous media in which variable-density flow can be easily coupled with advection and dispersion (Bear and Cheng 1999). Nevertheless, the complex conditions of carbonate aquifers including water-rock interactions, karstification or dolomitization, and field scale heterogeneities, are causes of many challenges arising in coastal areas. Some of these have direct implications on the prospecting of future freshwater reserves.

The scope of this thesis is to contribute to the analysis and remediation of SWI by studying the following aspects: (1) response of carbonate aquifers with varying Ca/Mg content to SWI, (2) behavior of trace elements (TEs) where fresh and intruded seawater mix, (3) derivation of groundwater baseline levels in polluted settings, notably salinized aquifers, (4) identification and quantification of major hydrogeochemical processes stimulated by SWI, (5) reliability of complex models (especially in karst) with variable-density and solute transport formulations, and (6) feasibility of SWI mitigation strategies.

1.2 Management of salinized coastal aquifers

Coastal aquifers are prone to saltwater intrusion to varying extents. In some cases (e.g. Beirut-Lebanon, Recife-Brazil, or Thrace-Greece), salinization is very intense, and it is exacerbated by population increases and urbanization. This makes the deterioration of water quality hardly reversible, and renders part of the groundwater reserves non-renewable at least for decades. Coastal aquifer management has therefore emerged as a main field in groundwater hydrology, especially in arid and semi-arid zones, for solving the following problem: *how to preserve or restore coastal fresh groundwater reserves?* The answer to this question is nowadays a main concern to hydrologists, stakeholders, water authorities, and policy makers. Replenishing deteriorated water is expensive and sometimes ineffective (Bear and Zhou 2007), whereas preventing salinization is hampered by the need to provide enough alternative water resources (Bear and Cheng 1999). So a key issue in coastal aquifer management is to develop proper planning strategies and to select the best alternative solutions capable of meeting water demands of suitable quality (Maimone et al. 2004; Bhattacharjya and Borah 2016).

Several countermeasures (elaborated below) to control SWI have been proposed over the last decades (Figure 1.2): (1) reducing pumping (Sherif et al. 2012), (2) changing extraction arrays (Polemio and Romanazzi 2014), (3) enhanced natural and/or artificial recharge (Papadopoulou et al. 2005; Sherif et al. 2013; Sophiya and Syed 2013), (4) direct reuse of treated wastewater or after its artificial recharge (Dausman 2008; Ouelhazi et al. 2014; Sana et al. 2013; Vandenbohede et al. 2013), (5) water transfer from other regions, (6) building subsurface physical barriers (Sugio et al. 1987; Ru et al. 2001; Abdoulhalik et al. 2017), (7) installing hydraulic barriers with/without injection wells (Sherif and Hamza

2001; Rastogi et al. 2004; Reichard and Johnson 2005; Sherif and Kacimov 2008) which are sometimes supported by desalination plants (Abd Elhamid and Javadi 2011; Payal 2014; Javadi et al. 2015), (8) integrated fresh-keeper (IFK) wells (Grakist et al. 2002; Kooiman et al. 2004; Stuyfzand and Raat 2010; Khadra et al. 2017a), or (9) stand-alone brackish water reverse osmosis (BWRO) or seawater reverse osmosis (SWRO) plants; the latter could utilize direct seawater intake or be fed via beach sand filtration (Bartak et al. 2012; Missimer et al. 2013). However, most of these measures have their specific limitations reducing their wide applicability. Each has demonstrated some pros and cons (Table 1.1), so that one could be advantageous compared to others for a particular setting such as in karstic aquifers.

Methodologies from outside the field of hydrology (e.g. empowerment, education, innovative treatment technologies, and public policy) could aid as well in protecting groundwater reserves. These elements, besides SWI countermeasures, are considered as part of a more broad sustainability plan to avoid unwanted environmental, economic and social consequences (Klein et al. 2014).

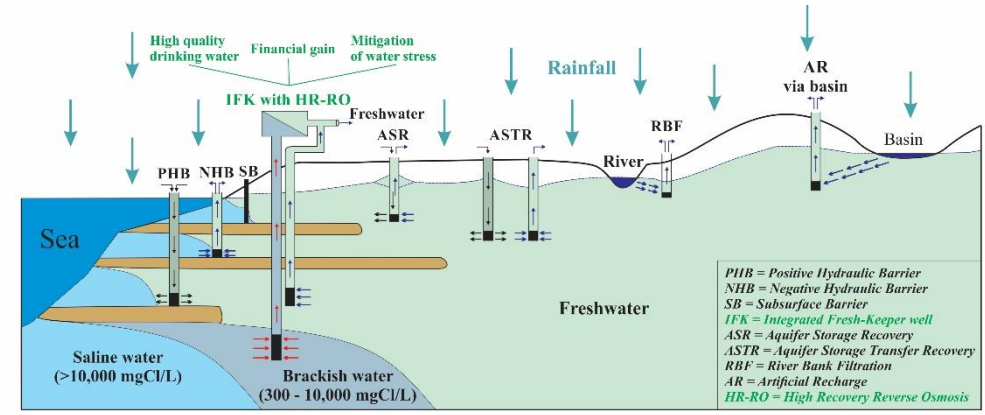

Figure 1.2 The most common countermeasures of saltwater intrusion. PHB = Positive Hydraulic Barrier; NHB = Negative Hydraulic Barrier; SB = Subsurface Barrier; IFK = Integrated Fresh-Keeper wells; ASR = Aquifer Storage Recovery; ASTR = Aquifer Storage Transfer Recovery; RBF = River Bank Filtration; AR = Artificial Recharge; RO = Reverse Osmosis (Khadra et al. 2017a).

1.2.1 Reorganization of wells

One goal of managing coastal aquifers is to minimize saltwater encroachment through pumping optimization (Post 2005). It is achieved by reducing pumping rates and relocating wells inland. It requires sustainable yield determination by considering the distribution of sources/sinks and their rates, and balancing the demand (outputs) with renewable water supply (inputs) (Bear and Cheng 2010). Modeling efforts including variable-density flow

and solute transport are needed to define the best pumping scheme (Scholze et al. 2002; Datta et al. 2009; Bear and Cheng 2010; Sherif et al. 2012; Adnan et al. 2013; Cai et al. 2015). However, this measure does not cope with the ever increasing water demands where modifying extraction rates does not suffice. Other complementary water resources are needed then.

Table 1.1 Main saltwater intrusion countermeasures with their pros and cons (Khadra et al. 2017a).

Mitigation	Description	Pros	Cons
Well field reorganization	Redesign well field by optimizing their withdrawal rates and/or distributing them landward	- Reduction of withdrawal is easy and direct without expenses - Decreases the chance of upconing at local scale	- Temporary solution - Not reliable when demand exceeds supply - Relocation of wells is costly
Aquifer recharge (AR)	Water artificially infiltrated into the underground, stored and then extracted	- Increases available storage and reduces seawater intrusion - Polluted water may suit as a recharge source	- Problematic in karst aquifers - If using basins, large areas may be needed, i.e. not always economically feasible - Clogging
Subsurface barriers (SB)	Artificial dams built underground	- Prevent seawater intrusion physically	- Feasibility limited to few meters in unconsolidated thin layers
Positive hydraulic barriers (PHB)	Artificial recharge wells	- Raise water level and push saltwater backwards	- Lack of chemically suitable recharge water
Negative hydraulic barriers (NHB)	Single or multi-pumping wells to intercept saltwater	- Protect freshwater wells from salinization - Good choice when raising water level is not possible - May be coupled with desalination plants	- Sensitive to pumping rates - Needs accurate understanding of aquifer dynamics - Requires a network of wells to form a complete barrier - May salinize freshwater reserves if not implemented properly
Desalination	Desalting of brackish or salt groundwater	- Provides alternative water resource - Reduces the stress on groundwater	- Problem of reject disposal - Operation and maintenance costs - Extraction of brackish groundwater may accelerate saltwater intrusion
Integrated fresh-keeper wells (IFK)	Create a stable fresh-brackish interface by vertical interception of upconing brackish water within individual wells	- More feasible than negative hydraulic barriers - Suitable in complex dynamic settings - Local remedy and can be individually implemented - May be coupled with desalination plants	- Not applicable if aquifer is fully salinized to the water table - Heterogeneous macroporosity (typical in karstified rock and faulted rock)

1.2.2 Managed aquifer recharge

Managed aquifer recharge (MAR) is becoming a widespread solution to make groundwater abstraction sustainable. It serves double purposes in many coastal aquifers by increasing available storage and reducing saltwater intrusion (Kresic 2007). It can turn a lot of surface water (otherwise often lost) into safe and reliable groundwater storage. Even polluted water can be used as recharge source, thanks to the role of geologic units in transforming it to better quality (Stuyfzand 1989a,b; Bouwer 2002; Stuyfzand 2002). MAR systems include (Figure 1.2): (a) aquifer storage recovery (ASR; water injected, stored and then extracted from same well), (b) aquifer storage transfer recovery (ASTR; water injected and then extracted by another well downgradient), (c) river bank filtration (RBF; induced water recharge from a hydraulically connected river), (d) basin recharge (recharge via basin(s)), (e) rainwater harvesting (rainfall collected at roof tops then directed to trenches or shafts to recharge underlying shallow aquifers), and (f) in-channel structures (subsurface dams, sand dams and gabions, which are usually built across ephemeral streams with the aim of building a new groundwater reservoir behind these barriers).

Most MAR options are problematic in karstic and highly fractured aquifers due to the combination of high permeability (with limited purification and chemical attenuation), low overall porosity, high dispersivity, low recovery efficiency, and complex surface terrains often inappropriate for recharge basins (dolines may offer opportunities however, e.g. the arid karst systems in Saudi Arabia; Schulz et al. 2016). Such aquifers have a non-uniform response to recharge and random preferential groundwater flow paths. To date, MAR sites in karst are relatively scarce worldwide. Few sites are found in the European Union (e.g. UK and Italy; Sprenger et al. 2017) although Europe was at the forefront of artificial recharge utilization, and very few examples exist elsewhere, e.g. the Wala reservoir in Jordan (Xanke et al. 2015; 2016), the karstic Gambier Limestone aquifer, South Australia (Vanderzalm et al. 2014), the Caldas Novas aquifer, Brazil (Troeger 2010), the Floridan karst aquifer system, USA (Bacchus et al. 2015a,b), or two incomplete trials in Lebanon (Daoud 1973; MoEW and UNDP 2014). Data from 18 sites with ASR in the Floridan aquifer show that their recovery is < 25% due to random preferential flow paths (Bacchus et al. 2015a,b). This is in line with the general perception that MAR is less effective in karstic media.

1.2.3 Seawater barriers

Seawater barriers aim at preventing the inland flow of saltwater. They are generally implemented by several means (Figure 1.2) (Pool and Carrera 2010):

1. Low permeability subsurface barriers (SB): These are artificial dams built underground to physically prevent water incursion. They are complex to build, expensive and often limited to thin layers close to land surface allowing a subsurface barrier of only few meters high (Ru et al. 2001). Several barriers, 11 to 25 m deep,

were built in southern Japan. They were constructed in both limestone (e.g. in Okinawa) and alluvial aquifers (e.g. in Ehime) (Sugio et al. 1987; Basri 2001). Construction material may consist of cement grout, silica gel, or in situ mixing technology where the soil is loosened then mixed with a self-hardening suspension (e.g. cement-bentonite or hydraulic lime). The latter is limited to unconsolidated sediments, and was successfully tested in the alluvial aquifer of the Nakajima site (Ehime). Alternatively, SBs can be created by induced gypsum precipitation in fractures and conduits of carbonate aquifers (Barcelona et al. 2006) although not advisable at large scales.

2. Positive hydraulic barriers (PHB): They are actually artificial recharge (AR) wells that inject freshwater or treated wastewater into the ground, e.g. the barrier wells installed at the West Coast Basin of Los Angeles (Reichard and Johnson 2005). They aim at raising the groundwater level and pushing the saltwater backwards. A main drawback is lack of suitable recharge water (regarding quantity, clogging potential and quality), which when available could be used as a direct feed source. Injecting compressed air or gas mixtures could be a substitute though it proved not adequate at some settings such as unconfined aquifers (Sun and Semprich 2013). Another drawback is that injection should never stop if the drawdown inland is far below sea level.
3. Negative hydraulic barriers (NHB): These are single or multi-pumping wells. They aim at catching saltwater close to the shoreline in order to protect inland groundwater. It is a good choice when raising water levels is not possible (Sherif and Hamza 2001; Sherif and Kacimov 2008; Kacimov et al. 2009). NHB may also be coupled with desalination plants, and utilized as feed sources for further production of water. However, unlike dams and positive barriers this solution is very sensitive to extraction rates and anisotropy, notably in complex dynamics (e.g. karstic aquifers), and hence definition of a salinity threshold becomes crucial to avoid deterioration of other freshwater wells. One option here, which is also applicable to PHB, is to substitute a number of vertical wells by one horizontal well. It may improve the well productivity due to more exposure to hosting formations (Labregère et al. 2006). A recent study by Hendizadeh et al. (2016) showed that freshwater horizontal wells perform dynamically better than vertical wells.

1.2.4 Desalination

With recent technological advances desalinated water has become the main source for drinking and domestic use in many countries, especially in the Middle East (Mohsen and Al-Jayyousi 1999; Ahmed et al. 2001; Al-Zubari 2003; Afonso et al. 2004; Jaber and Ahmed 2004; Stuyfzand et al. 2004, 2017). Desalinated seawater forms the main fresh water resource in the Middle East; Kuwait, Qatar, Saudi Arabia and United Arab Emirates are among the 10 top world producers (ESCWA 2009).

In the last decades, thermal desalination, e.g. multi-effect distillation (MED) and multi-stage flash (MSF), was the primary choice due to high salinity and poor feedwater quality. However, recently membrane technology has been introduced as a more viable alternative, mainly due to lower energy consumption (Karagiannis and Soldatos 2008; Triki et al. 2014). The wide application of desalination plants has been hindered not only by energy requirements but also by problems with suspended solids in feedwater, scaling/clogging of membranes and disposal of concentrate (Stuyfzand and Kappelhof 2005). Feed sources to reverse osmosis (RO) systems are either brackish water (TDS = 1,000-10,000 mg/L) or coastal seawater (TDS = 10,000-60,000 mg/L). Seawater reverse osmosis (SWRO) plants are sometimes fed by beach sand filtration to provide higher quality feed (Bartak et al. 2012; Missimer et al. 2013). The concept of DESIRES, an artificial floating DESalting Island on Renewable multi-Energy Supply, is another option integrating SWRO (Stuyfzand and Kappelhof 2005).

However, brackish water reverse osmosis (BWRO) is currently ca. 50% less expensive, and it can produce potable water with acceptable costs of < 1 US$/m^3 (Greenlee et al. 2009). BWRO with better feedwater quality has several advantages over SWRO leading to lower operational costs and less environmental problems. These include: (a) lower osmotic pressure (reducing energy costs), (b) lower water temperature (lowering osmotic pressure), (c) a lower clogging and biofouling potential thanks to less suspended solids, a lower turbidity and lower concentration of assimilable organic carbon, (d) fewer bacteria (Stein et al. 2016), and (e) either a higher recovery (of permeate) or lower salinity of the concentrate (brine).

1.2.5 Integrated Fresh-Keeper (IFK) wells

This concept is an innovative solution to salinizing wells introduced by KWR Watercycle Research Institute (The Netherlands) (Grakist et al. 2002; Kooiman et al. 2004; Stuyfzand and Raat 2010; Khadra et al. 2017a). IFK wells may be supported by desalination plants to treat the abstracted brackish water and thereby supply additional volumes of freshwater that could range from potable to domestic. This approach is presumably more convenient than creating a larger scale hydraulic gradient typical in negative barriers, especially in settings where a precise understanding of system dynamics is not possible, as in karstic or fractured aquifers.

1.3 Conditions of the Eastern Mediterranean

The Eastern Mediterranean, with a variety of geological/hydrological conditions, is among the many coastal areas in the world facing saltwater intrusion. Limestone aquifers dominate, and they are usually fractured or karstified. Rainfall is mostly low with relatively high potential evapo(transpi)ration (FAO 1997), and water scarcity is becoming a major concern (MED-EUWI 2007). The 2010-2011 joint program launched by the World Bank

and the League of Arab States for the MENA (Middle East and North Africa) region showed discouraging figures about their future climate. The Arab world with its vast tracts of deserts is expected to be one of the regions hardest hit by climate change, so it may consequently face about the worst water scarcity in the world. It is anticipated that the Eastern Mediterranean will become drier; less but more intense rainfall may cause increased frequency of droughts and floods; and the projected sea level rise along coastal zones will have significant impact. These factors will jointly pose more threat to groundwater supplies in coastal areas, which are first felt through SWI (World Bank 2011).

1.4 The Lebanese context

Lebanon is part of the MENA countries (Figure 1.3). It has a mesothermal Mediterranean climate characterized by dry summers, mild and moist winters, and abundant sunshine. Most of the precipitation falls between November and April; May, September and October have sparse precipitation; and the remaining period is generally dry. The cumulative annual rainfall in the coastal areas is about 600-1000 mm, increases to 1400 mm on the western flanks of Mount Lebanon thanks to relatively high orographic precipitation, and drops to less than 600 mm in the central regions due to the rain shadow on the leeward side of the orographic barrier. Figure 1.4 shows the longest available rainfall record in Lebanon collected in Beirut (coastal area) by the American University of Beirut weather station between 1876 and 2014.

The two major groundwater reservoirs in Lebanon are the Kesrouane Formation (Jurassic), and the Sannine-Maameltain (Cretaceous) (Figure 1.3). They cover ca. 54% of the country (43% for the Cretaceous alone), and are both made up of (dolomitic) limestone with varying degrees of karstification. Known karst features are karren, sinkholes, dolines, natural bridges, pinnacles, and flutes. The remaining groundwater reserves are hosted by other units. The most notable (from higher productivity) are: the Eocene limestones, the Miocene limestones, the early Cretaceous sandstones, the Aptian and Albian terrigenous clastics and limestones, and the recent Quaternary deposits.

Forty major streams and rivers and more than 2,000 springs spread over the Lebanese territory. Seventeen streams are perennial having their maximum and minimum discharge rates during March/April and September/October, respectively. The total annual flow of rivers is about 2,900 Mm^3, with nearly 18% flowing into neighbouring countries (MoE/UNDP/ECODIT 2011).

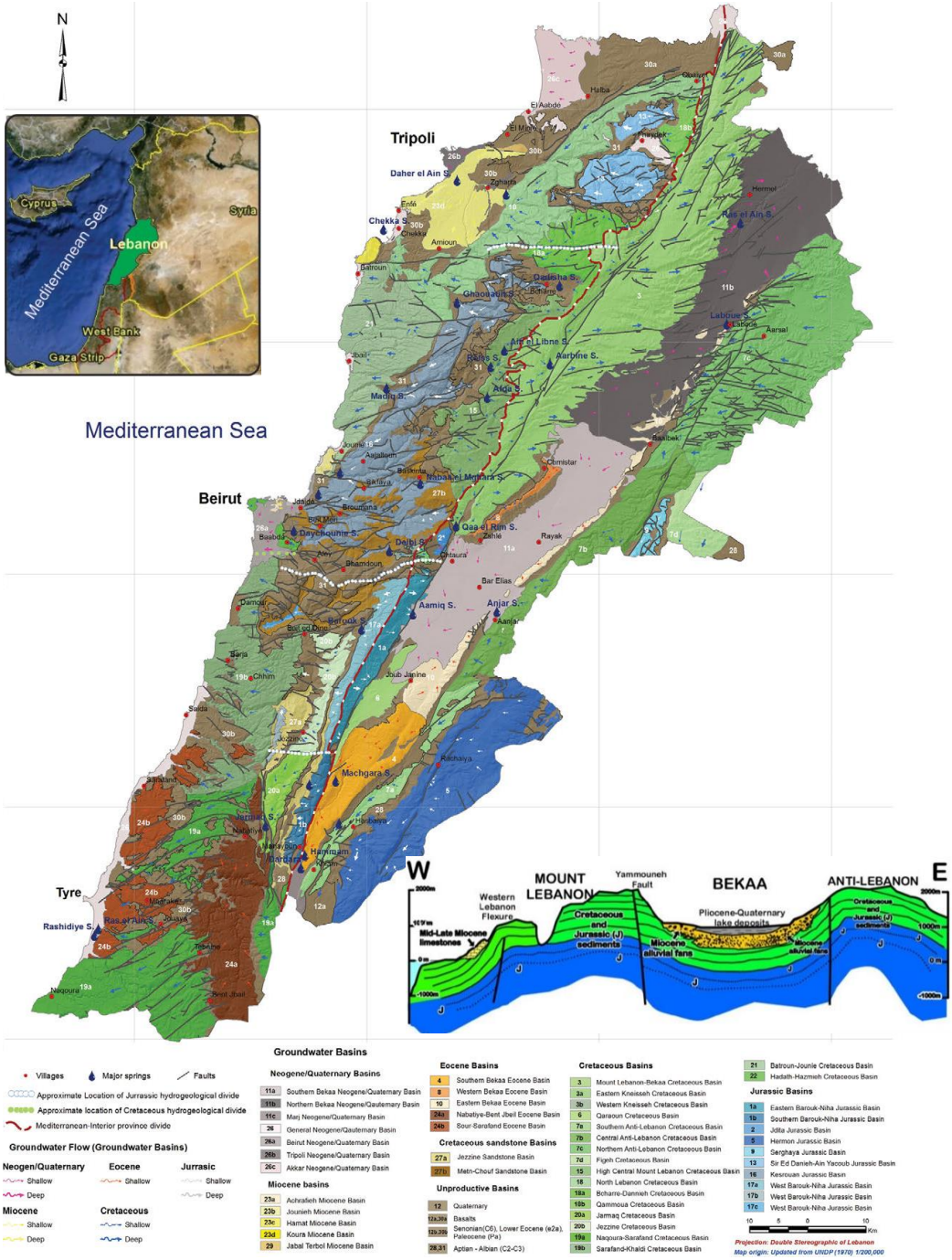

Figure 1.3 Geological map of Lebanon with major groundwater basins (MoEW and UNDP 2014). The schematic east-west cross section across Lebanon is adapted from C.D. Walley, The geology of Lebanon, Digital Documentation Center – AUB.

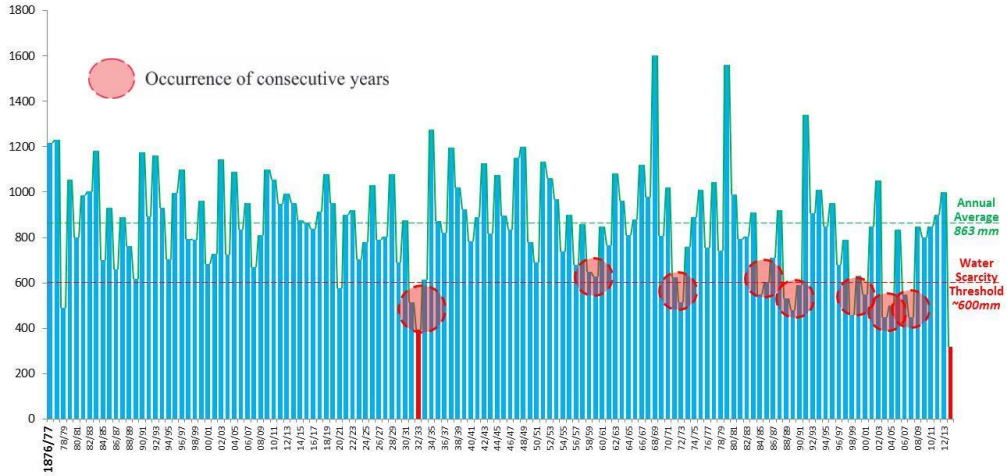

Figure 1.4 Total annual rainfall at the American University of Beirut weather station (Beirut) between 1876 and 2014 (ECODIT 2015).

The total available amount of surface and ground water in Lebanon averages 2,700 Mm^3/year. It exceeds the projected water demand estimated at ca. 1,800 Mm^3 in 2035 (MoE/UNDP/ECODIT 2011). So Lebanon has a surplus water budget (Figure 1.5); however, the groundwater reserves are significantly stressed while surface water is mostly lost to the sea if not detained in reservoirs (Figure 1.6). In fact, the Lebanese society relies more on groundwater reserves extracted via private and governmental wells. These are randomly distributed with no proper planning and monitoring in most instances, and consequently several coastal aquifers are partially or completely salinized, e.g. in Beirut (Acra et al. 1983; Lababidi et al. 1987), Koura-Zgharta (Khayat 2001) and Damour (Khadra 2003; Khadra and Stuyfzand 2014; Khadra et al. 2017b). The two main basins in Beirut and vicinity, the Hadath-Hazmieh Cretaceous Basin (basin 22 in Figure 1.3) and the Beirut Neogene-Quaternary Basin (basin 26a, Figure 1.3), show an annual deficiency of 7.2 Mm^3, and 38.4 Mm^3, respectively (MoEW and UNDP 2014). Water rationing there subsequently drops to ca. 3 hours/day during the dry season (MoE/UNDP/ECODIT 2011). A similar state of shortage characterizes other basins in Lebanon, e.g. the Bekaa Neogene-Quaternary Basins (basin 11a and 11b, Figure 1.3), which are stressed by heavy exploitation for irrigation purposes. Other water substitutes in Lebanon may not be eligible to date. For instance, many springs are contaminated due to increased urbanization and the widespread use of cesspits within their watersheds, and water treatment systems are mostly without advanced technologies.

Therefore, the weak water management and governance are among the main causes of water scarcity facing different Lebanese territories, notably the highly populated coastal zones. It is anticipated that these conditions will worsen soon due to population growth

(including more refugees due to the Syrian crisis), increasing urbanization and climate change. A hotter and drier climate is foreseen in which the dry seasons become longer and the wet seasons record less precipitation (MoE/UNDP/GEF 2016). Meanwhile, efficient management acts are still lacking or lagging behind, because the Lebanese Water Sector Strategy still needs a true collective will to implement serious nationwide measures.

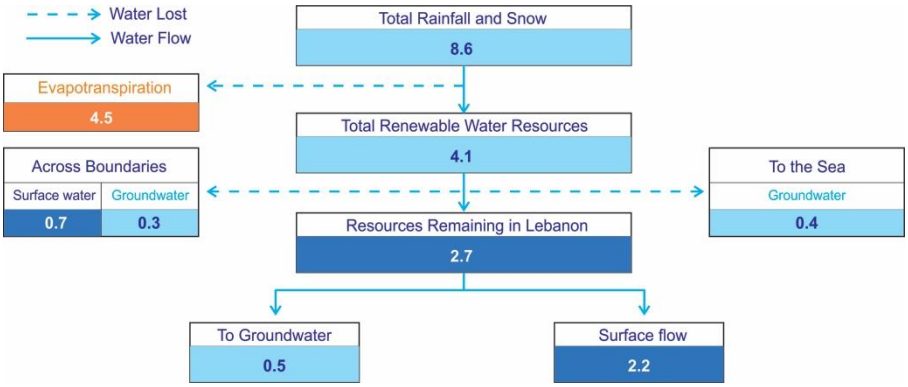

Figure 1.5 Water balance of Lebanon for an average year. Values in 1,000 Mm³/year (MoEW 2010).

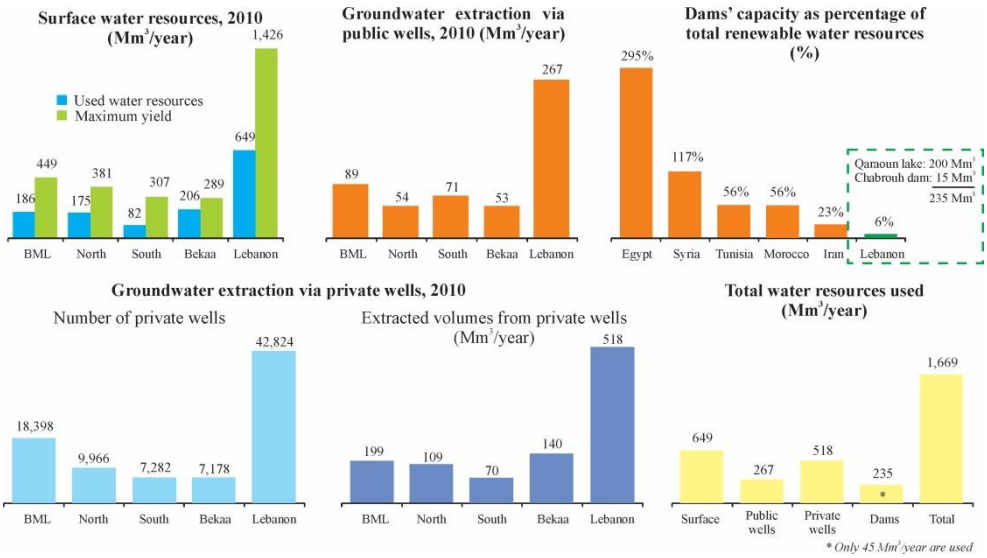

Figure 1.6 Distribution of surface and groundwater resources and their consumption in Lebanon in 2010 (MoEW 2010). BML = Beirut and Mount Lebanon.

1.5 Research objectives and questions

This PhD thesis aims at analyzing and mitigating the salinization of the Damour, coastal (dolomitic) limestone aquifer system in Lebanon (Eastern Mediterranean), and introducing some new tools or methods to diagnose, predict and manage SWI in general.

The Damour coastal aquifer, to which these new tools and methods are applied is a major part of the Khaldi Cretaceous Basin in Lebanon (basin 19b, Figure 1.3). It has crucial importance because it covers nearly one third (ca. 13 Mm^3/year) of the domestic water volume currently provided for more than one million people in part of the capital Beirut and its suburbs. This aquifer is special and scientifically interesting by its varying Ca/Mg ratio, poor karstification and moderate salinization. It therefore sheds light on some complexities in analyzing salinization processes in such aquifers, and forms a challenge in proposing relevant solutions to counteract SWI.

Different aspects are covered in this thesis; the most prominent objectives are to:

1. Develop a new comprehensive approach to establish groundwater baseline chemistry with a wide inorganic scan covering 74 elements.
2. Disclose major hydrochemical differences between the behavior of limestone and dolomitic limestone hosting units, with and without salinization. This includes the response of 8 major and 50 trace elements.
3. Develop a new parameter, called Mixing Enrichment Factor (MEF), to assess the (im)mobilization of major chemical constituents and trace elements in mixed groundwater (mainly fresh groundwater and intruded Mediterranean seawater).
4. Assess the adequacy of the equivalent porous medium (EPM) and the coupled discrete-continuum (CDC) approaches to simulate SWI in poorly karstified aquifers. It is supported by the use of time series analysis of rainfall and water table response as a prior step to decide where conduit quickflow in karst systems can be safely ignored.
5. Formulate a new efficient, feasible and profitable mitigation strategy of SWI, suitable for complex dynamics such as in karstic and fractured aquifers.
6. Apply and test objectives 1 to 5 as an example to manage and control groundwater reserves in an important dolomitic limestone coastal aquifer in Lebanon.
7. Offer a variety of tools and methods, for investigating SWI anywhere.

1.6 Outline of the thesis

This thesis is made up of eight chapters. Chapter 1 embodies a general introduction on coastal aquifers management, a review of the major countermeasures of SWI, the main research objectives, and thesis outline. Chapters 2 to 5 are based on peer-reviewed manuscripts that have been published (chapters 2, 3 and 5) or under review (chapter 4) in

highly acclaimed (Q1) international journals. Coupling objectives to chapters is illustrated in Figure 1.7.

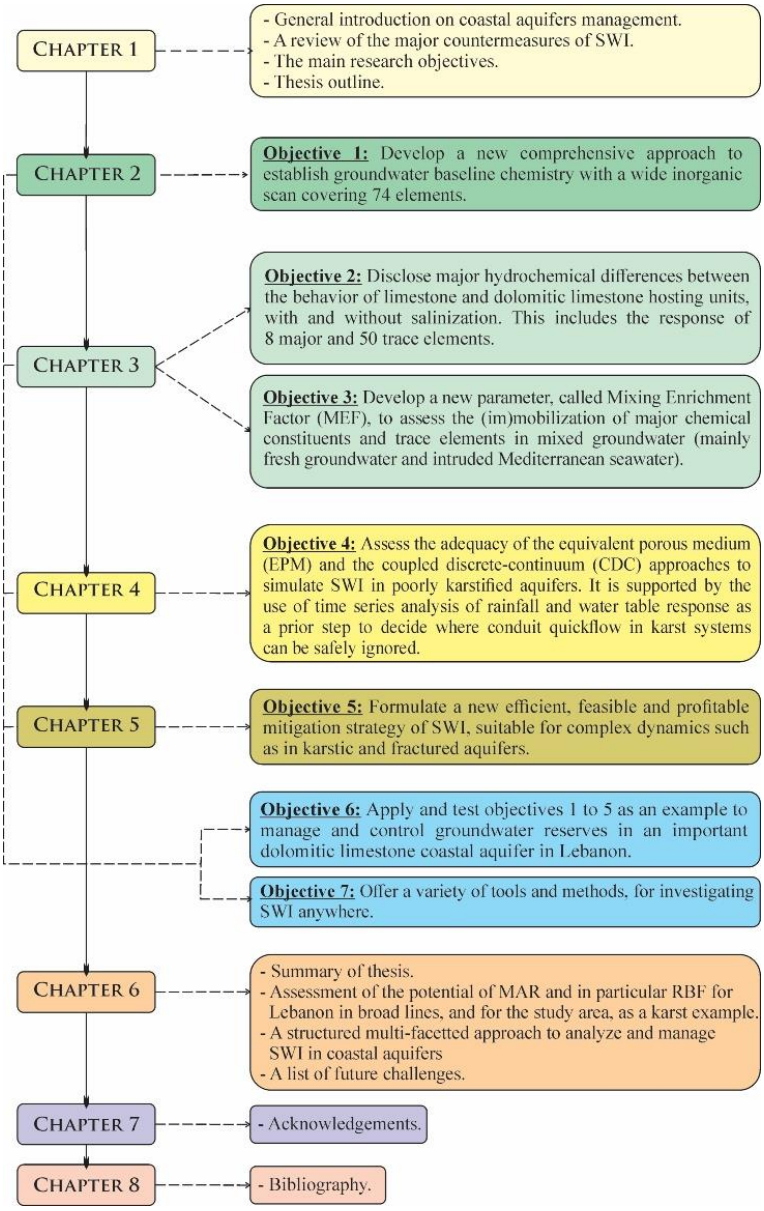

Figure 1.7 Structure of the thesis, and coupling of the objectives to the chapters.

In chapter 2, a new structured approach is presented to derive groundwater baseline conditions, in this case for the Damour coastal aquifer suffering from salinization and other anthropogenic impacts. The baseline conditions for 16 main constituents, 59 trace elements and two isotopes are filtered out. Multi-tracing is used to discern different hydrosomes (groundwater bodies of different origin) and their hydrochemical facies. Their characteristics are discussed and their areal extent is presented on a hydrochemical map with 2 cross-sections. Sources of salinization are defined, and recharge zones are delineated via environmental tracers and a special maturity index.

In chapter 3, the hydrochemical effects of saltwater intrusion in the Damour aquifer, on 8 major constituents and 50 trace elements in conjunction with potential geochemical differences between limestone and dolomitic limestone units, are demonstrated. The main hydrogeochemical processes are also discerned. For this purpose, a quad-fold approach is followed including: (1) nonparametric statistical tests, (2) concentration deviations from ideal conservative freshwater–seawater mixing, (3) a new parameter called Mixing Enrichment Factor (MEF) to quantify the mobilization of chemical constituents under mixing conditions, and (4) 1-D dual porosity reactive transport modeling with PHREEQC.

In chapter 4, SWI in the poorly karstified Damour aquifer is simulated in various ways and compared to measurements. Time series analysis of rainfall and aquifer response is recommended to decide whether quickflow through conduits can be safely ignored. This aids in justifying the selection of the exemplified EPM model. The results of a coupled discrete-continuum (CDC) approach are compared to the EPM model to examine the improvement of SWI representation when discrete features (DFs) are embedded in model domain. The simulation efforts utilized the SEAWAT code since it is density dependent and public-domain, and it enjoys widespread application.

In chapter 5, a coupled strategy of 'Integrated Fresh-Keeper' (IFK) wells and a high recovery (HR) brackish water reverse osmosis (BWRO) system is formulated. It is a double sourcing application, in which fresh-keeper wells are installed at the bottom of a deepened borehole of selected salinized wells, and then supported by high recovery RO desalination. The HR-RO design introduced here, has a very low reject percentage (92% to 96% permeate, 4-8% concentrate) during normal operation. It is also characterized by reduced energy consumption and low propensity of membrane fouling by precipitates, making it superior to other widespread commercial designs. This coupled strategy is proposed as an effective localized remedy in karstic or fractured aquifers, usually characterized by anisotropy, high transmissivities and complex dynamics. A detailed feasibility study of the proposed strategy is presented by taking a salinizing, brackish well (TDS ~1600 mg/L) in the Damour coastal aquifer as an example. It serves 3 purposes: production of high quality drinking water, financial gain, and mitigation of water stress by overpumping. A full

technical description of the water treatment facility is provided, together with a detailed economic feasibility assessment of the production unit of desalinated water.

In chapter 6, the thesis is summarized, and the potential of MAR and in particular RBF is explored, for Lebanon in broad lines, and for the study area, as a karst example. In addition, a structured multi-faceted approach to analyze and manage SWI in coastal aquifers from detection to remediation is provided. It is expanded here based on the overall outcome of this research. A list of challenges is added at the end of this chapter.

Chapter 7 covers the acknowledgements, and the final chapter 8 lists all bibliographic citations for the whole thesis.

Chapter 2

Separating baseline conditions from anthropogenic impacts: example of the Damour coastal aquifer (Lebanon)

This chapter was published as:

Khadra, W.M., Stuyfzand, P.J., 2014. Separating Baseline Conditions from Anthropogenic Impacts: example of the Damour coastal aquifer (Lebanon). *Hydrological Sciences Journal* 59, 1872-1893.

Abstract

A new structured approach is presented to derive groundwater baseline conditions, in this case for a dolomitic limestone aquifer suffering from salinization and other anthropogenic impacts. It builds on the HydroChemical System Analysis (HCSA) to map different groundwater bodies (hydrosomes) and hydrochemical zones within them, each of which show significant differences in baseline conditions. It also comprises a rigorous elimination scheme for samples affected by bias or pollution. The method is applied to the Damour coastal aquifer system, south of Beirut (Lebanon). Concentrations of Cl, Cl/Br, ^{2}H, ^{18}O and Ca/Sr were used to discern five hydrosomes and to determine mixing ratios. The dominant hydrochemical facies was (sub)oxic, calcareous and salinized, indicating a very low reduction capacity of the aquifer system, strong dissolution of dolomitic limestone and clear traces of seawater encroachment. The method proposed was capable of filtering out baseline conditions for 16 main constituents, 59 trace elements and two isotopes.

2.1 Introduction

Coastal aquifers are gaining a special interest in hydrogeology due to their hydraulic complexity and overexploitation to supply water to urbanized coastal zones, where more than half of the world's population is living (Essink 2001; Post 2005; Bobba 2007). They are also known for their complex hydrochemical nature due to a wide spectrum of groundwater origins, salinity sources, alkalinity, redox potential, the extent of cation exchange, and anthropogenic causes of contamination (Stuyfzand 1993a). In general, the future of coastal aquifers is not so bright, and water-resource managers are under a real challenge to protect their groundwater supplies (Sanford and Pope 2010).

This study focuses on a Mediterranean karstic, coastal aquifer of Cretaceous age, the Damour aquifer system, south of Beirut (Lebanon). This aquifer was chosen in the late 1970s as an alternative to the capital's main aquifer which was contaminated by seawater intrusion (Khadra 2003). A large amount of groundwater (≈13 Mm^3/year) is being extracted from the aquifer, most of which feeds part of the capital Beirut and its suburbs (Khadra 2003; CAMP 2004).

Karstified aquifers provide the main source of groundwater in many Mediterranean regions (El-Hakim and Bakalowicz 2007). Their multitude of water quality problems has generated many studies, for instance by Mandel et al. (1972), Kafri and Arad (1979), Stigter et al. (1998), Tulipano et al. (2005), Kempe et al. (2006), Abdul Rahman (2007), Weinstein et al. (2007), and El-Fiky (2010). Water quality problems also call for an assessment of baseline conditions of such aquifers, for several reasons (Edmunds and Shand 2008): (a) to be able to assess quantitatively whether or not anthropogenic pollution is taking place, (b) to improve groundwater monitoring systems, (c) to breach guidelines for potable water quality when the concentration of certain elements is quite natural, (d) to define zones of uncontaminated water and protect these areas better, and (e) to provide

guidelines for new policy, engagement with end users such as water utilities, and the general public. This need is even more acute for coastal karstic aquifers, because of their extreme vulnerability to salinization and other sources of pollution (Tulipano et al. 2005).

Hydrochemical studies of the Lebanese groundwaters (Arkadan 1999; Khadra 2003; Saad et al. 2004; Korfali and Jurdi 2007; Saadeh 2008; Korfali and Jurdi 2009) did not address their baseline conditions. The term "baseline" is defined in this study as "the range of concentrations of a given element, isotope or chemical compound in solution, derived entirely from natural, geological, biological or atmospheric sources, under conditions not perturbed by anthropogenic activity" (Edmunds and Shand 2008).

To date, the literature summarized by Edmunds and Shand (2008) lacks a standardized comprehensive methodology to establish groundwater baseline chemistry once a monitoring network has been defined and sampled. It covers a backward trend analysis of young groundwaters or, if available, the selection of a data subset from older monitoring networks that is assumed to reflect the natural composition, as evidenced by hydrological and geochemical tracers. However, it does not cover a scheme to fully eliminate data affected by bias or pollution (especially relevant for trace elements), and a method to define groundwater bodies and hydrochemical facies within them, each of which requires its own baseline chemistry. We therefore developed a new approach, consisting of a six-step procedure that incorporates:

1. an elimination scheme for data effected by bias or pollution;
2. the HydroChemical System Analysis (HCSA) as proposed by Stuyfzand (1999, 2005) to distinguish different groundwater bodies (hydrosomes) and hydrochemical zones (facies) within them;
3. historical data evaluation; and
4. statistical analysis.

2.2 Setting and methods

2.2.1 Geological and hydrogeological setting

The 60 km^2 study area belongs to the western flanks of the Lebanese range called the Mediterranean Province (Lebanese Ministry of Environment 2001). It lies along the coastal zone of Lebanon, at about 7 km south of the capital Beirut (Figure 2.1). It is characterized by two main topographical features. The first is a flat coastal plain in the west, which slopes very gently seaward, it is known as a cultivation strip. The second is a hilly, sloping terrain reaching a maximum elevation of about 550 m at the eastern boundary. The Damour River is the most important perennial river, whilst most other valleys are less deep and contain ephemeral streams (Figure 2.1).

The study area has a humid mesothermal Mediterranean climate characterized by dry summer and relatively mild moist winter with abundant sunshine. The wet season extends from November to April, with sparse precipitation events in May, September and October (Arkadan 2008). The northeast trending Lebanese mountain range acts as a barrier of humid westerly winds enhancing the effect of orographic precipitation to the west. Records between 1985 and 2009 (Meteorological Service 2010) show an annual precipitation between 352 and 1163 mm, with an arithmetic mean of 770 mm. A climatic cycle is expected at a recurrence interval of 14 years (Arkadan 2008).

Land-use patterns show 12% urbanized zones (including residential houses and transportation facilities), 14% agricultural lands (mainly banana plantations and vegetable gardening), while the remaining 74% form grass, vegetation and bare land cover. This has been the dominant area distribution over the last decades, although minor expansion of urbanization occurred in the mid-1990s, with high development at altitude zones exceeding 150 m that were only partially inhabited before (CAMP 2004). Industrial activities are scarce, apart from an important small area in Haret El Naameh village where floor tiles and refrigerators are manufactured.

Rock types are divided into eight main formations following the stratigraphic division in Lebanon. The exposed units range in age from the Cretaceous to recent (Figure 2.1). Six major and some minor faults dissect the area. They are sub-parallel and approximately east–west oriented (Khadra 2003). The general dipping of layers is westward, with some deviations due to faulting. The dip reaches its maximum inclination (55°) at the eastern part of the area. It decreases in a westward direction, reaching its minimum (8°) at the Maameltain-Chekka Formation boundary (Figures 2.1 and 2.2).

The Damour hydrological system (Figure 2.2 and Table 2.1), is made up of a main upper aquifer (C_{4c}–C_5), underlain by a semi-confining unit (C_{4b}) and a relatively thin lower aquifer (C_{4a}). The upper aquifer is covered by a minor small aquifer of very thin Quaternary deposits (Q). We assume that the middle semi-confining unit (C_{4b}) does not hinder the hydraulic connection between the two units whereas the Hammana formation (C_3), dominated by marly layers, forms an impermeable base of the system.

The Damour upper aquifer is only semi-confined in the west, while exposed to the surface in its greater part (Figure 2.1); it has few paved surfaces and, hence, is capable of receiving recharge from precipitation across a wide portion of its exposed parts. Recharge, as a percentage of precipitation, was estimated using a water balance approach (Khadra 2003). Neglecting storage changes, the average recharge to the upper aquifer (≈ 35 km^2 exposed in the study area) is estimated at 28% of gross precipitation (Table 2.2).

Figure 2.1 Geological map of the Damour area (modified after Khadra 2003).

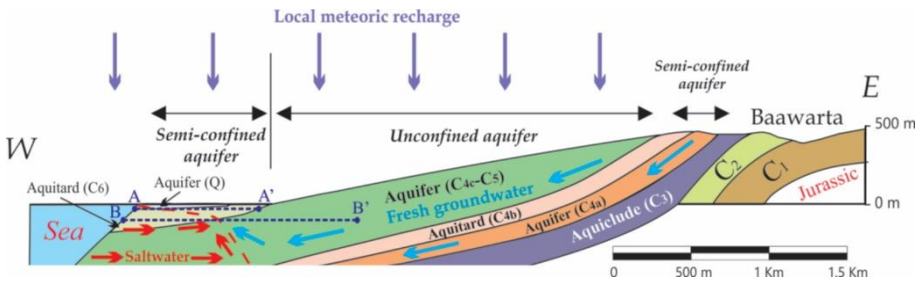

Figure 2.2 Hydrogeological cross section of the study area (modified after Khadra and Stuyfzand 2014). AA' and BB' are the simulated unidirectional flow paths from sea to land (*Section 3.3.5*). Symbols as shown in Figure 2.1.

Table 2.1 Generalized description of the hydrostratigraphic units in the Damour area (from surface to bottom).

Hydrogeologic Unit	Geologic Unit	Symbol	Approximate Thickness (m)	Description
Minor aquifer	Quaternary	Q	5	Gravel, sand and clay
Aquitard[a]	Chekka	C_6	160	Chalky to marly limestone
Aquifer	Upper Sannine-Maameltain	C_{4c}-C_5	400	Dolomitic limestone
Aquitard	Middle Sannine	C_{4b}	70	Marly limestone
Aquifer	Lower Sannine	C_{4a}	80	Dolomite and limestone
Aquiclude	Hammana	C_3	200	Marl and marly limestone

[a]: It behaves like a minor aquifer due to fractures, fissures and bedding planes.

Table 2.2 Water balance components estimated for the period April 2001 - March 2002 (modified after Khadra 2003).

Component	Value (mm/year)	Value (%)	Area[b] (km^2)	Value (Mm^3/yr.)
Precipitation	825	100	49	40
Evapotranspiration	327	40	49	16
Run-off	261	32	49	13
Recharge	237	28	49	11
Irrigation return flow[a]	900	Unknown	8	7
Pumped volume	417	25	24	10[c]

[a] Estimate based on land use and average weekly irrigation consumption. The Damour River provides major portion of this water, which is diverted through small canals. % of irrigation return flow out of total precipitation is unknown.
[b] The area excludes residential spots and transportation facilities.
[c] The Q and C_6 units have limited abstraction rates (ca. 0.006 Mm^3/year).

2.2.2 Data collection

A sampling campaign was launched in 2011/12 to collect 102 samples (Figure 2.3) from rainfall, pumping wells, the Damour River and the Mediterranean Sea, in order to build a reliable, homogeneous hydrochemical database covering a wide range of parameters (four physical, 72 chemical, and two isotopic). This dataset was added to the few data previously collected by others since 1979 (Ajam and Saa'd 1980a,b; Dar Al-Handasah 1999; Khadra 2003; Saad et al. 2004).

Two raingauges were installed at 1 km and 3.7 km from the shoreline (Figure 2.1) to collect rainfall on a daily basis. Cumulative samples were sent to the laboratory for detailed chemical analyses every two weeks. For groundwater, pumping wells were sampled because dedicated monitoring wells were absent (as in the whole of Lebanon and in many hardrock areas elsewhere). Wells were drilled by either percussion or rotary drill, and had 6 to 40 m long well screens, or none. Using pumping wells for water quality monitoring introduces specific problems, such as mixing of different water qualities (Mendizabal and Stuyfzand 2009). The recent sampling campaign tried to avoid other problems by pumping

the wells for a long time to ensure proper purging, requiring the evacuation of more than three standing volumes and a stable electrical conductivity (EC). Purging was not needed for government wells (20% of all wells), as they are continuously pumping for most of the year, nor for municipal wells (15% of wells) that run for most of the day. Pumping rates were 1000–4000 m^3/d for government wells, 150–650 m^3/d for municipal wells, and 5–20 m^3/d for private wells. Significant inflows of groundwater from shallow perched zones can probably be neglected in most cases, because it is common practice in Lebanon to stop drilling once groundwater appears.

Different sets of bottles were used for separate analyses: high-quality HDPE bottles for metals (100 mL) and for alkalinity, nitrate and ammonium (500 mL). Each bottle was cleaned in the laboratory and rinsed with distilled water, except for the 100-mL bottles that were rinsed in the laboratory 2–3 times with a small volume of 1:1 diluted HNO_3, followed by another rinsing with ultrapure water. The acid rinsed 100 mL PE bottles (for major and trace elements) were filled after filtration in the field using 0.45-µm syringe filters, and acidified in the laboratory, on the same day, by adding 65% suprapure HNO_3 to pH < 2 (0.7 mL of 65% HNO_3 to 100 mL of water). The 500-mL bottles were cooled to 4–8°C, and the more mineralized samples (EC > 1500 µS/cm), to be analysed by ICP-ES/ICP-MS, were diluted maximum 1:3 before delivery to the laboratory.

Most water samples were analysed for: (a) EC, pH and temperature, *in situ*, with a SevenGo Duo pro water quality meter (Mettler Toledo), (b) O_2 *in situ*, using a SX726 DO meter (Sanxin), (c) alkalinity by titration (HACH 8221), NO_3 by spectrophotometry (HACH 8039) and NH_4 by spectrophotometry (APHA 4500-C), in the American University of Beirut Core Lab, (d) main cations, Cl, Br, SO_4, Si, P and 58 trace elements (including heavy metals, rare earth elements and others), by ICP-ES/ICP-MS in AcmeLabs Vancouver, and (e) ^{18}O and ^{2}H by pyrolysis and mass spectrometry in the isotope laboratory of VU University Amsterdam.

The trace elements were analysed with a detection limit of 0.01–0.05 µg/L. Isotopes are reported as δ notation in per mil relative to Vienna-Standard Mean Ocean Water ($‰_{V\text{-}SMOW}$).

Duplicates, blanks and spikes showed acceptable results. Additional checks of the accuracy of the chemical analyses showed excellent ionic balances and measured ECs that closely matched the ECs calculated with Hydrogeochemcal (HGC 2.1, Stuyfzand 2012). Bird dropping correction was also applied to precipitation where necessary. This is a correction procedure to biogenic contributions from bird droppings, insect droppings, plant and animals debris, etc.

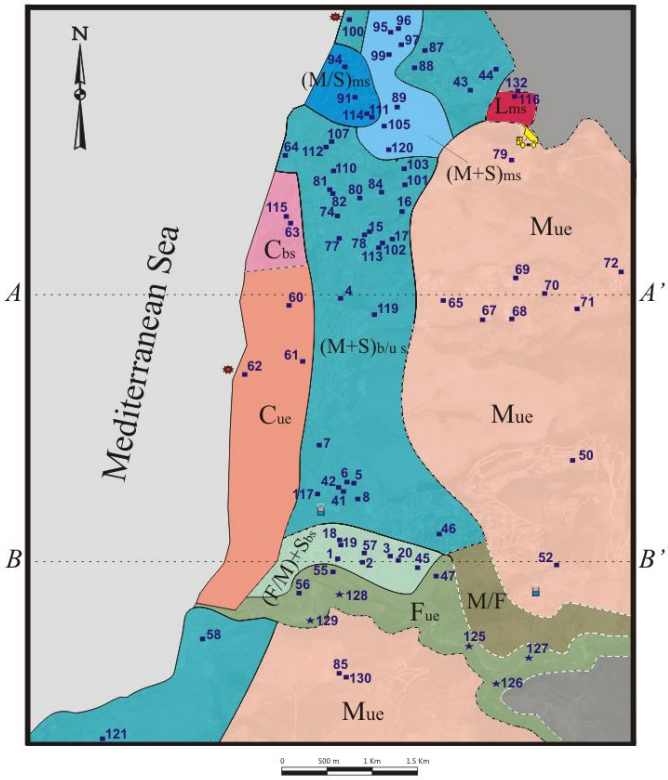

Legend

Mue	Mountainous Limestone Hydrosome (M) with an unpolluted, non-salinizing facies.
Fue	Damour River Filtrate Hydrosome (F) with an unpolluted, non-salinizing facies.
Cbs	Shallow Coastal Plain Water Hydrosome (C) with a slightly polluted, salinizing facies.
Cue	Shallow Coastal Plain Water Hydrosome (C) with an unpolluted, non-salinizing facies.
Lms	Landfill Leachate (L) with a moderately polluted, salinizing facies.
(M/S)ms	Mixed (M/S) Hydrosome with a moderately polluted, salinizing facies.
(M+S)ms	Mixed (M+S) Hydrosome with a moderately polluted, salinizing facies.
(M+S)b/us	Mixed (M+S) Hydrosome with a slightly polluted/unpolluted, salinizing facies.
(F/M)+Sbs	Mixed (F/M)+S Hydrosome with a slightly polluted, salinizing facies.
(M/F)	Mixed (M/F) Hydrosome (no recognizable facies).
	Unknown Hydrosome due to lack of wells.
	Boundary estimated by expert judgment.
■	Groundwater sample extracted via pumping well.
★	Surface water sample from the Damour River.
	Seawater sample from the Mediterranean Sea.
	Naameh Landfill.
	Rain gauge.

Figure 2.3 Hydrochemical map showing the spatial distribution of hydrosomes and their main hydrochemical facies. All mapped hydrosomes are calcareous and (sub)oxic. AA' and BB' refer to locations of cross-sections shown in Figure 2.5.

2.2.3 HydroChemical System Analysis

The HydroChemical System Analysis (HCSA; Stuyfzand 1999, 2005) is composed of a three-step approach starting with discriminating different water bodies of different origin (hydrosomes), then stepping down by characterizing hydrochemical zones (hydrochemical facies) within each hydrosome, and finally, if needed, identifying chemical water types. In this study, a hydrochemical map was constructed displaying the spatial distribution of hydrosomes and hydrochemical facies within them, and, in a next step, the baseline hydrochemistry for the different units was assigned.

2.2.3.1 Identification of hydrosomes via environmental tracers

A hydrosome is a coherent 3-D groundwater body with a specific origin. Hydrosomes can be identified and their boundaries established by combining information on geomorphology, groundwater flow, geophysics, hydrogeological structure, and water quality. The latter includes environmental tracers, which indicate the source water and water–rock interactions. Good tracers are couples such as δ^2H–$\delta^{18}O$ (Bouchaou et al. 2008), $\delta^{18}O$–Cl (Stuyfzand 1993a), Cl–Br (Stuyfzand 1993a; Alcalá and Custodio 2004; Cartwright et al. 2006; De Montety et al. 2008), Cl–SO_4 (Petelet-Giraud et al. 2007), Cl–HCO_3 (Lee and Song 2007) and Ca–Sr (Brenot et al. 2008), preferably in combination with major ions and less immobile trace elements such as B and Li to provide a full hydrochemical fingerprint.

2.2.3.2 Determination of hydrochemical facies

Hydrosomes can be subdivided into several characteristic zones, called hydrochemical facies, based on boundaries in chemical composition. Compositional variations are expected to occur along flow lines even within a single facies (Camp and Walraevens 2008). They are due to changes in recharge composition, flow patterns and the chemical interaction between the water and surrounding medium (Stuyfzand 1993a; 1999).

The hydrochemical facies is determined by combining four indices regarding redox state, water pollution, mineral saturation (normally calcite) and base exchange. These facies parameters and their codes are summarized in Table 2.3. The four indices were determined from the available water quality analyses, using Hydrogeochemcal (HGC 2.1, Stuyfzand 2012). Most samples (95%) clearly showed interaction with dolomitic limestone ($Ca_{0.7}Mg_{0.3}(CO_3)_2$), the composition of which was derived from their average Ca/Mg ratio corrected for seawater contribution (see *Section 2.2.3.4*). This justifies the use of the calcite saturation index in which, however, the log (solubility product) was raised by 0.3 to account for Mg solid solution (Morse and Mackenzie 1990). The omnipresence of dolomitic limestone also necessitated the use of the base exchange index (BEX) without including Mg (Table 2.3).

Table 2.3 Hydrochemical facies parameters (after Stuyfzand 2005).

Code	Facies Parameter	Description / Criterion
	pH classes	
c	calcareous	pH > 6.2
a	slightly acidic	5.0 < pH < 6.2
A	acid	pH < 5.0
	Redox Index[1]	Based on the major redox sensitive species in water (O_2, NO_3, SO_4, Fe-total, Mn-total, NH_4 and CH_4)
o	(sub)oxic	0-2
r	reduced (anoxic)	3-4
d	deeply anoxic	5-6
x	mixed	
	*Pollution Index (WAPI)**[1]	*
u	unpolluted	0-2
b	slightly polluted	2-6
m	moderately polluted	6-20
p	polluted	>20
	Base Exchange Index (BEX)	$BEX^2 = Na^+ + K^- + Mg^{2+} - 1.0716\ Cl^-$ $BEX^3 = Na^+ + K^- - 0.8768\ Cl^-$
e	equilibrium	0 (zero) / no BEX (e)
f	freshened	> +(0.5 +0.02 Cl) / positive BEX (+)
s	salinized	< -(0.5 +0.02 Cl) / negative BEX (-)

[1]: Redox index and WAPI are calculated following rigorous criteria explained in details in Stuyfzand 2012.
* WAPI is determined on the basis of maximum 10 quality indices (Stuyfzand 2012): esthetics, acidity (#), oxidation/reduction capacity (#), nutrients (#), total salt content (#), organic and inorganic micropollutants (#), pesticides, radioactivity and microbiology. The available data in this study permitted to base WAPI on 5 indices labeled with #.
[2]: After Stuyfzand 1986; for aquifers without dolomite.
[3]: After Stuyfzand 2008; for aquifers containing dolomite or dolomitic limestone.

2.2.3.3 Determination of chemical water type

The chemical water type is determined following the scheme of Stuyfzand (1989). This method combines in one code consecutively the chlorinity, the alkalinity, the dominating member of the strongest pair of cations and anions within a geohydrochemical family, and the BEX (set in dolomitic limestone mode), which can indicate freshwater or saltwater intrusion (Table 2.3). As an example, water type F4CaHCO$_3$+ means fresh, high alkalinity, freshened calcium bicarbonate water. The spectrum of water type parameters observed in the study area is shown in Table 2.4.

Table 2.4 Spectrum of chemical water type parameters observed in the study area, combining into a code like F4CaHCO$_3$+.

Code	Parameter	Description / Criterion
	Chlorinity (main type)	Chloride concentration in sampled water [mg/L]
g	Oligohaline-fresh	5-30
F	Fresh	30-150
f	Fresh-brackish	150-300
B	Brackish	300-1,000
b	Brackish-salt	1,000-10,000
S	Salt	10,000-20,000
H	Hypersaline	> 20,000
	Alkalinity (type)	Alkalinity as HCO$_3$ [mg/L]
*****	Very low	< 31
0	Low	31-61
1	Moderately low	61-122
2	Moderate	122-244
3	Moderately high	244-488
4	High	488-976
	Dominant Cation and Anion (Subtype)	Most important cation and anion
Ca	Calcium	The strongest family members discovered to date are placed in the appropriate fields inside two triangles constructed for this purpose (Stuyfzand 1989c)
Mg	Magnesium	
Na	Sodium	
HCO$_3$	Bicarbonate	
Cl	Chloride	
Mix	No anion family > 50% of anions sum	
	Base Exchange Index BEX (freshening/salinizing tendency)	Explained in Table 2.3
o	No base exchange	Marine cation equilibrium
+	Freshened	Marine cations surplus
-	Salinized	Marine cations deficit

2.2.3.4 Determination of mixing ratios

The mixing ratio in a water sample from different hydrosomes needs to be determined for: (a) mapping purposes, (b) identifying geochemical processes and likely source(s) of pollution, including salinization, and (c) calculating the chemical composition of one of the end-members when the composition of the other end-member(s) and the mixing ratio are known. The latter is useful to correct concentrations for seawater admixing.

In our case, the most likely two or three end members to mix in the sampled pumping wells are infiltrated local rain water (either in mountains or in coastal plain), infiltrated Damour River water, and/or intruded Mediterranean Sea water. The solution for two end-members, for instance freshwater and saltwater, with a single tracer such as Cl is:

$$Cl_{MIX} = (1 - f_S)\, Cl_F + f_S\, Cl_S \tag{2.1}$$

$$f_S = (Cl_{MIX} - Cl_F) / (Cl_S - Cl_F) \tag{2.2}$$

in which: Cl_{MIX}, Cl_F and Cl_S are chloride concentration in mixture, freshwater and saline water, respectively (mg/L), and f_S is the fraction of saltwater (-).

By correcting for seawater admixing, any concentration of the freshwater end member (C_{FC}) becomes:

$$C_{FC} = (C_{MIX} - f_S\, C_S) / (1 - f_S) \tag{2.3}$$

where C_{FC} is the concentration of freshwater end member (mg/L), C_{MIX} is the concentration in mixture (mg/L), C_S is the concentration in saline water (mg/L), and f_S is calculated using Cl according to equation 2.2.

For a mixture composed of three end-members, we need two independent tracers, for instance Cl and ^{18}O, according to the following formulas (modified after Stuyfzand and Stuurman 2006):

$$c = \frac{(\delta^{18}O_R - \delta^{18}O_L)(Cl_{MIX} - Cl_L) + (Cl_R - Cl_L)(\delta^{18}O_L - \delta^{18}O_{MIX})}{(\delta^{18}O_R - \delta^{18}O_L)(Cl_O - Cl_L) + (\delta^{18}O_L - \delta^{18}O_O)(Cl_R - Cl_L)} \tag{2.4}$$

$$b = \frac{\delta^{18}O_{MIX} - \delta^{18}O_L + c(\delta^{18}O_L - \delta^{18}O_O)}{\delta^{18}O_R - \delta^{18}O_L} \tag{2.5}$$

$$a = 1 - b - c \tag{2.6}$$

where *a*, *b*, *c* are fractions of infiltrated ocean, river and local rain water, respectively, in mixture (-); subscripts *O*, *R*, *L*, MIX are the component in groundwater deriving from ocean, river, local rain and the sampled mixture, respectively; Cl is chloride concentration (mg/L), $\delta^{18}O$ is ^{18}O content expressed as relative deviation from Standard Mean Ocean Water (‰ $_{SMOW}$).

In the above approach, conservative behavior is assumed during mixing and the quality of all end members should be well known. As pointed out by Mendizabal et al. (2010), the simultaneous use of various tracers helps to reduce uncertainties in the calculated mixing ratio and in the assumed end-member compositions. Equation 2.3 can also be used to trace recharge zones prior to salinization once salinized and/or contaminated zones are discerned.

2.2.4 Determination of groundwater baseline composition

A new comprehensive approach to establish groundwater baseline composition in six steps is presented in Figure 2.4 and described below:

1. Eliminate samples with a bad Ionic Balance (IB < 4 if ΣC + ΣA > 8 meq/L, IB < 6 if ΣC + ΣA = 2–8 meq/L, and IB < 10 if ΣC + ΣA < 2 meq/L, where: IB = 100 (ΣC – ΣA)/(ΣC + ΣA) with ΣC, ΣA = sum of cation and anions, respectively), and discard trace element data if affected by either filtration bias (raised Al ≥ 20 µg/L as indicator of suspended clay at 5.5 < pH < 8.5, Stuyfzand 1987), or well corrosion inputs (high Ni + Mo + (V, Cr) from stainless steel or high Cu from copper or brass well screens, raised if Ni > 50 µg/L, Mo > 10 µg/L, V or Cr > 5 µg/L and pH > 6.2, raised if Cu > 50 µg/L at pH > 6.2).
2. Apply HCSA to discern hydrosomes and hydrochemical facies, each of which requiring the determination of its Natural Background Concentration (NBC). HCSA also helps to exclude those samples which show mixing of hydrosomes, a mixed redox or a specific pollution level (WAPI > 2). Knowing the sample's position in the normal downgradient hydrochemical evolution and the geochemistry of the aquifer system (dolomitic limestone in our case), assists in detecting anthropogenic anomalies and in selecting the right mineral saturation index on which pH corrections may be based in Step 6.
3. Use NO_3, Cl/Br, Cl, TOC (or COD) as more specific chemical indicators of pollution (NO_3 > 13 mg/L, Cl/Br depends on type of influence (e.g. 500–600 in domestic sewage, see Alcala and Custodio 2004), Cl > 250 mg/L, and TOC > 1.4 mg/L), in addition to WAPI, and discard polluted samples from the "natural background" population.
4. Refer to historical data to define significant hydrochemical trends. In case a significant trend existed for the sampled location, then Natural Backgrounds Levels (NBLs) are the minimum values, otherwise take the average of oldest data as representative of NBLs. Data extending to pre-pumping periods is preferable, although data prior to excessive pumping might suffice. In some cases, notably when minimum values refer to a salinized facies, some further elimination might be required. Expert judgment remains needed to decide whether natural shifts in background quality are taking place, such as in the case of: (i) the natural leaching of soil organic material which leads to a lowering of for instance Fe(II) and NH_4 base line levels, (ii) natural shifts in coastline position due to sea level fluctuations with an impact on baseline levels for atmospheric Cl, Na and Mg, and (iii) natural vegetation succession which impacts on the evapo-concentration factor F (see equation 2.8). This judgment cannot be easily included in any algorithm, but it should make part of Step 4.

5. (a) Do statistical analyses (e.g. correlation matrix, cluster analysis, frequency distribution) to answer three main questions: (i) are there other sample clusters within the facies discerned, indicating a subfacies for which a separate "Natural Background Concentration" (NBC) is needed? (ii) are there any outliers as indicated by the frequency distribution? (iii) are there any good correlations with Cl, SO_4 or NO_3 which can help to trim down the NBC in the next step (Step 6)? The latter is useful when there is any correlation between Cl, SO_4 or NO_3 (as pollution indicators) and other parameters. In that case, finding the natural background of one of them (e.g. Na) would benefit from the Na–Cl relationship in extrapolating via the Cl background value.
   (b) Discard the upper 10% of the frequency distribution by taking values below the 90th percentile as representative. Note that these percentages are a matter of dispute and hence other values could be also justified (Edmunds and Shand 2008). For some parameters, notably those mobilized in (deeply) anoxic environments such as Fe, Mn, NH_4 and CH_4, the higher values could better represent the NBLs if their concentration decreased in response to an anthropogenic NO_3 intrusion or a lowering of groundwater tables by pumping.
6. After getting an impression of NBLs via data without and with trend, three final actions are needed: (a) deciding which NBL value to take, (b) checking whether those parameters that strongly correlate with Cl need to be adjusted, and (c) gluing together all NBLs into an NBC for facies X of hydrosome Y. This gluing together requires an accuracy check to ensure that the resulting composition (NBC) shows a correct IB and a pH in accordance with the dominant mineral saturation index (SI_{MIN}) for the aquifer system. If not, then estimate the major constituents with least confidence via IB, and adjust the pH so as to obtain the right SI_{MIN}.

2.3 Results

2.3.1 Identified hydrosomes and their facies

The following hydrosomes were identified using multi-tracing: mountainous limestone water (M), Damour River bank-filtrate (F), coastal plain water (C), landfill leachate (L), and intruded Mediterranean seawater (S). Relatively pure intruded seawater (presumably > 65% current Mediterranean seawater) has not been observed because of mixing with fresh groundwater. This seawater is suspected to occur in the deeper parts of Naameh and Damour coastal strip close to the shoreline. In addition, the mixing ratios for two and three end members aided in further identification of three mixed hydrosomes: M+S, M/S and (F/M)+S. The coding of the mapped hydrosomes and their origins and recharge mechanisms are listed in Table 2.5. Median values of major constituents are shown in Table 2.6.

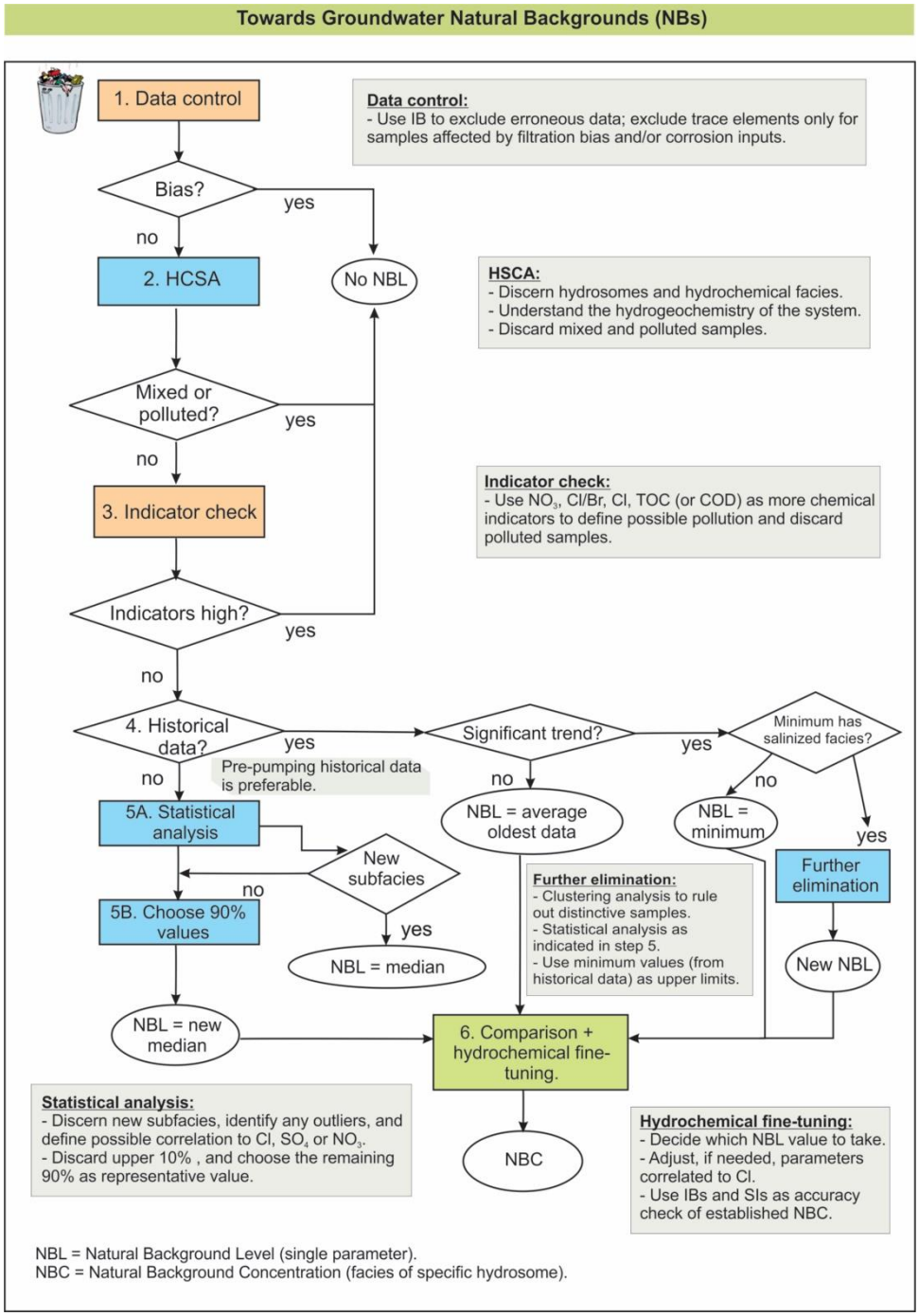

Figure 2.4 Flow chart of the new approach proposed for natural background (NB) determination.

Table 2.5 The hydrosomes identified in the study area.

Code	Name	Origin	Main Recharge Mechanism	% End-member
M	*Mountainous Limestone*	Local meteoric	Local precipitation	> 99.9%
F	*Damour River Bank-Filtrate*	Local meteoric	Remote precipitation, pumping	> 67%
C	*Coastal Plain Water*	Local meteoric	Local precipitation	> 99.9%
L	*Landfill Leachate*	Leachate, local meteoric	Local precipitation	--
S	*Intruded Mediterranean Sea Water*	Seawater	Pumping	> 67%
M/S	*Mixed M/S*	Mixture	Precipitation, pumping	10% < S < 67%
M+S	*Mixed M+S*	Mixture	Precipitation, pumping	0.1% < S < 10%
(F/M)+S	*Mixed (F/M)+S*	Mixture	Precipitation, pumping	33% < F< 67% & 33% < M< 67%

NB: The M hydrosome taps the C_{4c}-C_5 aquifer (dolomitic limestone) whereas the C hydrosome taps the C_6-Q coastal units (limestone).

All samples are calcareous and 95% is (sub)oxic. They are close to dolomitic calcite saturation and contain relatively high concentrations of oxidants (O_2, NO_3, SO_4) and very low concentrations of reductants (Fe, Mn, NH_4). Only 5% of all samples showed a mixed redox index due to the coexistence of sufficient Fe(II) and O_2 or NO_3. This does not translate into little mixing, but in the lack of reduced aquifer compartments. The relative uniformity in redox and pH justified the exclusion of redox level and pH classes as mappable facies parameters, i.e. it was redundant to give any designation since all samples were (sub)oxic and calcareous. However, the pollution index WAPI and base exchange index, BEX, showed enough variation for mapping two other groundwater qualifiers: pollution and salinization. WAPI was distributed as follows: 30% unpolluted, 52% slightly polluted and 18% moderately polluted. BEX showed 3% positive, 23% neutral and 74% negative. The spatial distribution of hydrosomes and their facies is shown in planar view in Figure 2.3 and in two cross-sections in Figure 2.5.

Table 2.6 Median composition of groundwater in the study area, grouped on the basis of hydrosomes and hydrochemical facies. Mediterranean Sea water, flux weighted average composition of bulk precipitation, and established baseline chemistry for the three major hydrosomes are also shown.

	# of samples	HCSA code	Chemical water type	EC 25ºC	Temp.	pH	Cl^-	SO_4^{2-}	HCO_3^-	NO_3^-	P	Na^+	K^+	Ca^{2+}	Mg^{2+}	Fe	Mn	NH_4^+	SiO_2	O_2	δ^2H	$\delta^{18}O$
				µS/cm	ºC	-	mg/L														‰	
Detection limit							1	1	1	1	0.02	0.05	0.05	0.05	0.05	0.01	5×10^{-5}	0.1	0.04	0.01		
Mountainous L.S. (M)	**12**	**M_{coue}**	**g3CaHCO30**	**539**	**20.2**	**7.13**	**27.4**	**16.5**	**337**	**2.0**	**0.103**	**11.7**	**1.5**	**80.50**	**29.9**	**<0.01**	**0.001**	**<0.1**	**11.8**	**4.7**	**-26.36**	**-5.84**
Damour River Bank-Filtrate (F)	**3**	**F_{coue}**	**F2CaHCO30**	**515**	**19.4**	**7.18**	**30.2**	**44.9**	**250**	**5.6**	**0.095**	**15.4**	**2.3**	**78.88**	**10.5**	**<0.01**	**0.000**	**<0.1**	**8.1**	**5.8**	**-29.25**	**-6.44**
Coastal Plain Water (C)	**5**		**F3CaHCO3+**	**803**	**22.1**	**6.89**	**86.2**	**92.9**	**328**	**7.0**	**0.089**	**57.7**	**3.5**	**119.36**	**15.3**	**<0.01**	**0.001**	**<0.1**	**37.2**	**4.5**	**-25.06**	**-5.53**
	3	C_{couf}	F3CaHCO3+	**759**	**22.1**	**6.94**	**85.1**	**71.9**	**312**	**7.0**	**0.089**	**37.7**	**3.8**	**115.39**	**12.7**	**<0.01**	**0.001**	**<0.1**	**21.5**	**3.7**	**-25.63**	**-5.53**
	2	C_{cobs}	f3CaMix-	1094	22.0	**6.75**	**177.0**	**100.4**	**336**	**6.4**	**0.375**	**66.5**	**2.4**	**187.00**	**15.9**	**<0.01**	**0.001**	**<0.1**	**38.4**	**4.7**	**-24.71**	**-5.43**
Landfill Leachate (L)	**1**	**L_{coms}**	**b3NaCl-**	**3947**	**18.2**	**6.58**	**1293.0**	**206.7**	**275**	**3.9**	**0.220**	**580.2**	**18.4**	**161.37**	**122.1**	**0.075**	**0.001**	**<0.1**	**11.4**	**6.3**	**-23.81**	**-5.42**
Mixed M/S	**4**	**$(M/S)_{coms}$**	**b3NaCl-**	**4561**	**21.9**	**7.05**	**1412.0**	**209.7**	**305**	**6.4**	**0.318**	**640.5**	**28.5**	**160.65**	**131.6**	**0.018**	**0.002**	**<0.1**	**15.3**	**4.5**	**-22.10**	**-4.95**
Mixed M+S	**70**		**B3CaCl-**	**1069**	**21.0**	**7.14**	**240.0**	**49.4**	**285**	**8.9**	**0.110**	**86.9**	**4.7**	**113.82**	**42.6**	**<0.01**	**0.001**	**<0.1**	**11.7**	**4.4**	**-24.30**	**-5.43**
	12	$(M+S)_{cous}$	F3CaHCO3-	802	20.9	7.20	141.9	19.9	255	11.3	0.089	31.5	2.9	112.50	34.8	0.213	0.005	<0.1	36.5	3.8	-25.55	-5.57
	58	$(M+S)_{com/bs}$	B3CaCl-	1452	21.2	7.10	359.0	61.5	290	9.0	0.118	147.3	5.6	119.80	45.7	<0.01	0.001	<0.1	11.7	4.4	-24.28	-5.41
Mixed (F/M)+S	**15**		**F3CaMix-**	**760**	**18.7**	**7.20**	**140.0**	**36.0**	**257**	**5.6**	**0.095**	**40.2**	**2.4**	**86.29**	**28.4**	**<0.01**	**0.001**	**<0.1**	**9.0**	**3.9**	**-28.89**	**-6.29**
	9	$(F/M)+S_{cous}$	F2CaHCO3-	691	18.4	7.30	120.0	8.6	240	4.6	0.095	22.5	2.0	76.00	26.0	<0.01	0.007	<0.1	8.6	3.9	-29.04	-6.30
	6	$(F/M)+S_{cobs}$	B3CaCl-	1359	18.7	7.16	308.3	80.1	259	6.2	0.101	141.5	5.6	92.94	39.8	<0.01	0.000	<0.1	9.1	4.6	-28.67	-6.27
Mediterranean Sea	**2**		**H2NaCl**	**45600**	**-**	**7.93**	**20400**	**3200**	**165**	**4.0**	**0.510**	**11600**	**470**	**460.00**	**1300**	**0.13**	**0.002**	**-**	**0.06**	**5.0**	**7.61**	**0.95**
Damour River	**5**		**g2CaHCO3**	**370**	**18.0**	**7.94**	**22.8**	**36.6**	**210**	**3.9**	**0.144**	**9.4**	**2.1**	**76.00**	**11.3**	**0.04**	**0.004**	**0.07**	**6.9**	**6.1**	**-31.2**	**-6.7**
Precipitation	**22**		**g*CaMix**	**99**	**-**	**7.14**	**11.2**	**8.1**	**24**	**10.0**	**0.100**	**4.9**	**0.2**	**8.00**	**0.7**	**<0.01**	**0.003**	**-**	**0.3**	**-**	**-**	**-**
							Established Natural Backgrounds (NBs)															
Mountainous L.S. (M)		**M_{coue}**	**g3CaHCO30**	**519**	**-**	**7.20**	**24.1**	**12.0**	**337**	**1.2**	**0.100**	**11.2**	**1.3**	**64.0**	**28.1**	**<0.01**	**0.001**	**<0.1**	**11.8**	**4.7**	**-26.36**	**-5.95**
Damour River Bank-Filtrate (F)		**F_{coue}**	**F2CaHCO30**	**505**	**-**	**7.29**	**30.2**	**43.4**	**239**	**5.7**	**0.086**	**15.4**	**2.0**	**75.1**	**10.5**	**<0.01**	**0.000**	**<0.1**	**8.1**	**5.5**	**-29.25**	**-6.44**
Coastal Plain Water (C)		**C_{couf}**	**F3CaHCO3+**	**757**	**-**	**7.05**	**82.1**	**71.9**	**292**	**5.5**	**0.084**	**37.7**	**2.4**	**97.1**	**12.7**	**<0.01**	**0.000**	**<0.1**	**28.5**	**3.6**	**-25.35**	**-5.53**

Table 2.6 (continued)

	HCSA code	*Al*	*As*	*B*	*Ba*	*Br*	*Cr*	*Cu*	*Ge*	*La*	*Li*	*Mo*	*Ni*	*Pb*	*Pd*	*Rb*	*Sb*	*Sc*	*Sr*	*U*	*V*	*Zn*
												µg/L										
Detection limit		1	0.5	5	0.05	5	0.5	0.1	0.05	0.01	0.1	0.1	0.2	0.1	0.2	0.01	0.05	1	0.01	0.02	0.2	0.5
Mountainous L.S. (M)	M_{coue}	**2**	**<0.5**	**30**	**9.5**	**100**	**0.6**	**0.9**	**<0.05**	**<0.01**	**1.5**	**0.3**	**0.3**	**0.3**	**<0.2**	**0.6**	**<0.05**	**1.0**	**107**	**0.57**	**1.2**	**7.6**
Damour River Bank-Filtrate (F)	F_{coue}	**1**	**<0.5**	**27**	**34.7**	**120**	**0.7**	**0.7**	**<0.05**	**<0.01**	**2.0**	**0.3**	**0.3**	**0.3**	**<0.2**	**0.6**	**<0.05**	**<1**	**136**	**0.50**	**0.3**	**3.8**
Coastal Plain Water (C)		**5**	**1.3**	**104**	**82.0**	**1255**	**0.9**	**3.1**	**0.200**	**0.01**	**2.3**	**3.4**	**3.1**	**0.3**	**<0.2**	**1.9**	**0.2**	**2.8**	**459**	**1.98**	**1.5**	**96.0**
	C_{couf}	3	1.5	50	54.2	382	0.7	1.1	0.120	<0.01	1.5	2.6	4.6	0.3	<0.2	2.1	0.14	2.0	510	1.75	1.5	173.2
	C_{cobs}	3	1.1	161	110.2	1996	1.2	6.1	<0.05	0.023	1.8	0.4	2.4	0.4	<0.2	1.0	0.15	3.5	379	2.71	2.0	37.5
Landfill Leachate (L)	L_{coms}	**12**	**3.1**	**372**	**27.0**	**5255**	**0.6**	**4.4**	**0.100**	**0.15**	**8.7**	**0.5**	**0.3**	**1.9**	**0.3**	**4.6**	**0.3**	**1.5**	**590**	**0.62**	**4.5**	**1159.6**
Mixed M/S	$(M/S)_{coms}$	**3**	**5.8**	**551**	**135.0**	**6203**	**1.0**	**5.6**	**0.100**	**0.03**	**13.7**	**3.0**	**4.4**	**0.4**	**0.4**	**10.3**	**0.4**	**1.9**	**1203**	**2.14**	**6.0**	**413.6**
Mixed M+S		**2**	**1.4**	**156**	**41.7**	**1572**	**0.8**	**2.1**	**0.050**	**<0.01**	**3.7**	**0.4**	**0.7**	**0.3**	**0.2**	**1.9**	**0.09**	**1.0**	**277**	**0.75**	**2.4**	**14.6**
	$(M+S)_{cous}$	1	0.8	63	79.4	494	0.5	0.8	0.120	<0.01	2.6	6.2	1.3	0.2	<0.2	1.8	0.06	4.0	641	1.51	0.6	13.0
	$(M+S)_{com/bs}$	2	1.4	160	40.8	1690	0.9	2.1	0.050	0.010	3.8	0.4	0.7	0.3	0.2	2.0	0.10	1.0	276	0.74	2.7	16.0
Mixed (F/M)+S		**2**	**0.9**	**74**	**30.6**	**1110**	**0.9**	**1.1**	**<0.05**	**<0.01**	**3.2**	**0.3**	**0.1**	**0.3**	**<0.2**	**1.6**	**<0.05**	**<1**	**206**	**0.56**	**1.8**	**3.5**
	$(F/M)+S_{cous}$	3	<0.5	35	20.8	348	1.0	1.1	<0.05	<0.01	1.8	0.4	0.5	0.4	<0.2	0.9	<0.05	<1	133	0.51	1.3	3.1
	$(F/M)+S_{cobs}$	2	1.0	92	34.8	1132	0.8	1.2	<0.05	<0.01	3.3	0.3	0.2	0.3	<0.2	1.6	0.05	<1	213	0.56	2.0	6.1
Mediterranean Sea		**21**	**61.6**	**3750**	**7.5**	**82200**	**5.2**	**12.5**	**0.25**	**0.07**	**143.0**	**10.6**	**3.9**	**0.5**	**1.0**	**125.0**	**0.22**	**5.0**	**7200**	**2.55**	**72.0**	**18.5**
Damour River		**53**	**0.2**	**29**	**5.5**	**63.2**	**1.0**	**0.6**	**0.0**	**0.0**	**2.1**	**0.5**	**0.5**	**0.4**	**0.1**	**0.7**	**0.1**	**0.5**	**115**	**0.5**	**0.6**	**1.9**
Precipitation		**8**	**<0.5**	**6**	**5.4**	**35**	**0.7**	**6.1**	**<0.05**	**0.01**	**0.1**	**0.2**	**0.7**	**0.9**	**<0.2**	**0.3**	**0.35**	**<1**	**15**	**0.02**	**0.4**	**7.2**
										Established Natural Backgrounds (NBs)												
Mountainous L.S. (M)	M_{coue}	**2**	**<0.5**	**30**	**8.4**	**83**	**0.6**	**0.9**	**<0.05**	**<0.01**	**0.7**	**0.2**	**0.3**	**0.3**	**0.10**	**0.5**	**<0.05**	**1.00**	**78**	**0.50**	**1.2**	**4.1**
Damour River Bank-Filtrate (F)	F_{coue}	**2**	**<0.5**	**27**	**23.6**	**120**	**0.7**	**0.7**	**<0.05**	**<0.01**	**2.0**	**0.4**	**0.3**	**0.2**	**0.10**	**0.6**	**<0.05**	**<1**	**136**	**0.50**	**0.3**	**3.2**
Coastal Plain Water (C)	C_{couf}	**2**	**<0.5**	**42**	**51.1**	**254**	**0.6**	**0.9**	**<0.05**	**<0.01**	**1.1**	**0.2**	**0.2**	**0.3**	**0.10**	**1.0**	**<0.05**	**2.00**	**236**	**0.84**	**0.3**	**3.3**

For all hydrosomes,

- Ce, Cs, Dy, Er, Eu, Gd, Ho, In, Lu, Nb, Nd, Pr, Pt, Re, Rh, Tb, Tl, Tm, Y, Yb < 0.01 µg/L.
- Co, Hf, Sm, Ta, Zr < 0.02 µg/L, Ag, Au, Be, Bi, Cd, Ga, Ru, Sn, Te, Th, W < 0.05 µg/L.
- Hg < 0.1 µg/L.
- Ti < 10 µg/L.

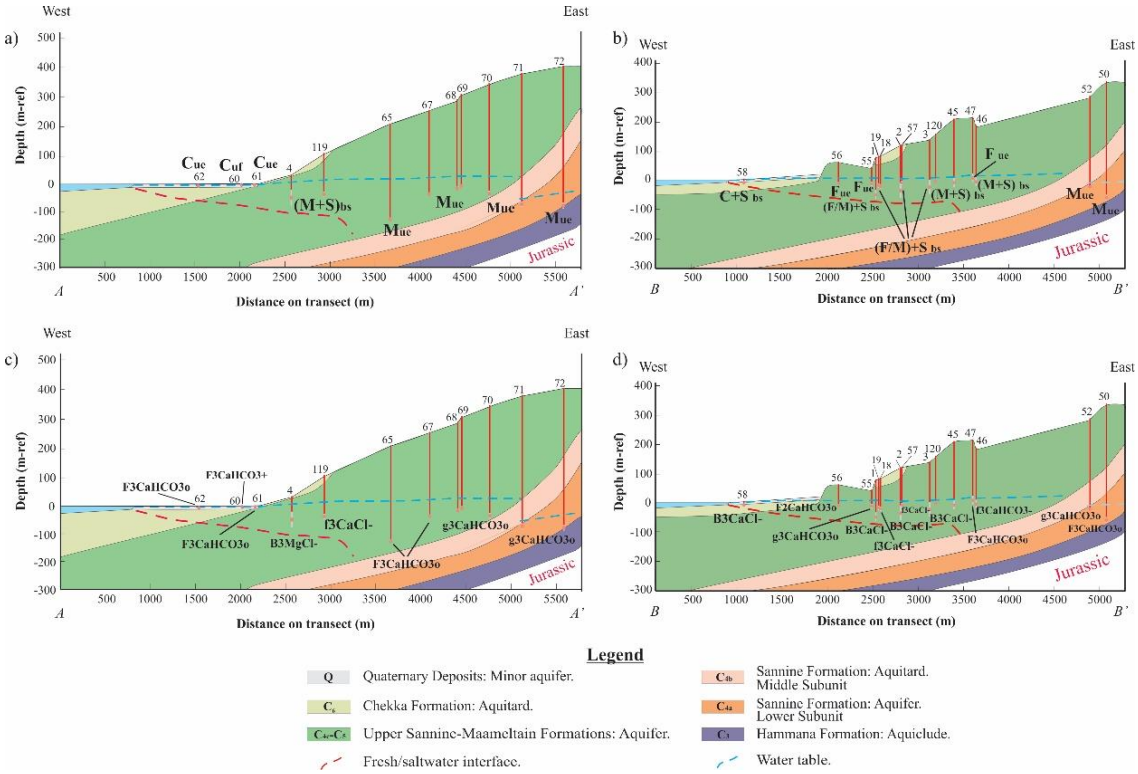

Figure 2.5 Hydrogeological cross-sections east–west through Baawarta village (a and c) and Mechref village (b and d) showing the spatial distribution of hydrosomes (a and b) and the water type at depth (c and d). Codes are explained in Tables 2.3, 2.4 and 2.5. The freshwater–saltwater interface (≈300 mg Cl/L) is based on a geophysical survey in the mid-1960s (Geofizika 1965), and updated using the Glover solution (Cooper 1964; Charmonman 1965). Locations of sections (AA' and BB') are as shown in Figure 2.3.

2.3.1.1 Mountainous limestone water (M)

This hydrosome is characterized by the best water quality, showing lowest concentrations of Na, Cl, Br, SO_4, NO_3, K and many trace elements. It shows relatively high HCO_3 and Mg contents, reflecting contact with dolomitic limestone. It occurs in the eastern part of the study area more than 2500 m away from the shoreline, where it is recharged by precipitation feeding the dolomitic limestone aquifers C_{4c}–C_5 (phreatic) and C_{4a} (semi-confined). Water quality is best there, thanks to hardly any saltwater intrusion, lower sea spray inputs, less agriculture, less population and a much thicker unsaturated zone (30–400 m). There is little difference in hydrochemistry between the phreatic and semi-confined aquifers, probably due to mixing in the wells and lack of confinement. Nevertheless few samples from the semi-confined aquifer showed slightly higher Fe, SiO_2, Li and Sr concentrations, testifying of a longer residence time and passage of the clayey, semi-confining C_{4b} layer.

The facies is in general unpolluted, leading to the code M_{ue}. The Mg-calcite saturation index is close to zero, BEX close to equilibrium, and the dominating water type is g3CaHCO$_3$o.

2.3.1.2 Damour river bank-filtrate (F)

This hydrosome is characterized by the lowest HCO_3, Ca, SiO_2, ^2H and ^{18}O concentrations, with relatively low Cl and SO_4 concentrations (< 50 mg/L), and a relatively high NO_3 content (5–15 mg/L). It occurs within 200 m from the Damour River channel, within ~1.5 km from the shore where heavy pumping from aquifer C_{4c}–C_5 forced the river to infiltrate. The facies is unpolluted, and BEX is neutral, leading to the code F_{ue}. The calcite saturation index is close to zero, and the water type is F2CaHCO$_3$o.

2.3.1.3 Coastal plain water (C)

The hydrochemical conditions of this hydrosome are variable, mainly due to high geochemical heterogeneities from one location to another and small thickness of the Quaternary deposits. It occurs close to the shoreline, within 900 m. The boundary between M and C is located where limestone hardrock is rising up from the coastal plain and not covered by Quaternary deposits.

This hydrosome is characterized by the lowest Cl:SO_4 and Cl:Br ratios, and the highest Ca:Mg ratio and SiO_2 concentration. This corresponds with calcite/aragonite domination of carbonate clastics in the Quaternary deposits (very low Mg content), the presence of highly soluble diatoms in the silty marine parts of the Quaternary deposits, and specific SO_4 and Br sources in the area. The latter could consist of oxidizing pyrite or agrichemicals (SO_4) and soil disinfectants (Br from methylbromide applications). The facies is slightly polluted in some parts and varies between freshening/equilibrium conditions to salinizing. Samples having low chloride content are freshening or at equilibrium (C_{uf} or C_{ue}) whereas others having higher chloride are salinizing (C_{bs}). The chemical water type is F3CaHCO$_3$+(o) and f3CaMIX-. Sample no. 58 showed a mixed C+S hydrosome with salinizing conditions.

2.3.1.4 Landfill leachate (L)

This presence of landfill leachate is highly probable, but its extension is uncertain due to lack of wells. One well (no. 116) could tap this hydrosome, because of its elevated concentrations of chloride (1293 mg/L), boron (372 µg/L), lead (1.9 µg/L) and zinc (1160 µg/L). This sample is plotted below the B/Cl reference line constructed for the salinized samples, which reflects higher chloride content compared to the corresponding boron. The anomalous Pb and Zn concentrations may indicate well corrosion, but the high salinity is surprising given the relative shallowness of the well, the regional depth to the fresh/salt interface, and the fact that the extracted water had high salinity since its construction.

Different origins could explain the elevated salinity, for instance deep circulations where old water is involved (Emblanch et al. 2005a; Yuce 2007), proximity of the well to the Naameh fault, which favours upconing, or a non-marine origin. The last possibility

could indeed involve leachate from the Naameh landfill (Figure 2.3) which is only 1500 m eastward. Additional wells were sampled 700 m and 40 m to the south and north, respectively, but both showed freshwater with F3CaHCO$_3$o type. However, the closest well showed raised chloride (121 mg/L) and exceptionally high zinc (2900 µg/L). In conclusion, further hydrochemical research is needed to identify the true salinity source of well no. 116, and to delineate the leachate's hydrosome. If this were to really exist, then it would reveal the violation of strict regulations that was supposed to keep this landfill safe. Over the last years, no evidence has been collected to confirm any landfill leakage to the groundwater.

2.3.1.5 Mixed M/S

This hydrosome is characterized by moderately high HCO_3 (average of 323 mg/L) with high chloride (> 1000 mg/L) and sulphate (> 200 mg/L). Nitrate ranges between 2 to 14 mg/L. The facies is in general moderately polluted and salinized, leading to the code $(M/S)_{ms}$. The calcite saturation index is close to zero, and the water type is b3NaCl– except for one sample having b3MgCl–, with higher Cl content and doubled Ca and Mg. It could reflect more salinization with ion exchange (Mg replacing Na), or high magnesium due to presence of dolomite in the freshwater–saltwater mixing zone.

2.3.1.6 Mixed M+S

This hydrosome characterizes the majority of water samples in the study area. It is characterized by variable HCO_3 from 200 to 455 mg/L with chloride exceeding 300 mg/L for most samples, a value that corresponds to the freshwater–saltwater mixing zone (Kresic 2007). The few samples with < 300 mg Cl/L have salinizing conditions although the recent sampling campaign was conducted in April, a month of high recharge. They are expected to become more salinized in dry periods. This agrees with time series data available for some wells that showed a difference exceeding 100 mg Cl/L between wet and dry periods.

The facies is in general slightly to moderately polluted with a salinized facies leading to the general code (M+S)b/ms. The dominating water type is B3CaCl– for samples in the mixing zone and F3CaHCO3– for samples temporarily on the freshwater side of the interface.

2.3.1.7 Mixed (F/M)+S

This hydrosome is characterized by a moderate HCO_3 (average of 238 mg/L) with chloride sometimes exceeding 250 mg Cl/L. It is an extension of the M+S hydrosome with river filtrate contribution. Sulphate concentration mostly exceeds 60 mg/L whereas nitrate is <10 mg/L. The facies is unpolluted to slightly polluted and salinized, leading to the code (F/M)+Su/bs. The water type is F2CaHCO3– for unpolluted samples, and B3CaCl– for the slightly polluted.

2.3.2 Establishing baseline hydrochemistry for discerned units

Following the procedure outlined in *Section 2.2.4*, samples with bad ionic balance, filtration bias, and well corrosion inputs were eliminated *a priori*. HCSA revealed three main hydrosomes: M, F and C, for which the Natural Background Levels (NBLs) were determined (Table 2.6). Mixed hydrosomes, for instance M/S and M+S, and polluted samples, as indicated by WAPI, were also discarded. By putting an upper limit of NO_3 at 13 mg/L one other sample of the filtered population had to be removed.

Historical data (1979–2011) for the M hydrosome showed a significant increase in most parameters. Ca, Mg and SO_4 were doubled, Cl and Na increased by 2–5 times, whereas NO_3 recorded negligible changes. The minimum values detected in 1979 (prior to excessive pumping) for the major elements were as follows (mg/L): Na (31.4), K (1.5), Ca (64), Mg (28.8), Cl (63.8), SO_4 (27.1), HCO_3 (256) and NO_3 (5). However, this sample was classified as having a salinized facies, and hence could only be used as an upper boundary for the M hydrosome NBLs. Hierarchical clustering analysis (using Ward's method for clustering, and squared Euclidean Distance for distance calculation or similarity measure) of the M hydrosome showed two distinctive clusters, of which the higher salinity cluster was discarded. Clustering was needed because a salinized facies is inherently biased and hence cannot be indicative of natural conditions. The upper 10% of the frequency distribution of the least salinized cluster was also eliminated, and the median for the remaining 90% was taken as its representative chemistry. However, some fine tuning of Ca was required, by taking the historical value. For the F and C hydrosomes, no historical data was available, and hence after applying steps 1 to 3 of the proposed methodology, statistical analysis rendered NBL determination possible by taking the median of the 90% values as representative of NBLs.

The established NBLs for hydrosomes M, F and C were checked for their IB and SI_{MIN}, and the latter necessitated a minor adjustment of pH. The C hydrosome required further fine tuning by choosing the minimum values for trace elements. This way, the Natural Background Concentration (NBC) produced for the three hydrosomes showed a calcareous, oxic, unpolluted facies, freshening for the C hydrosome while at equilibrium for the M and F.

2.3.3 Salinization sources

2.3.3.1 Sea spray and evapo(transpi)ration

The fresh end members receive marine inputs via atmospheric deposition of sea spray, which normally shows an inland decrease. The flux weighted average chloride concentration recorded in bulk precipitation (Cl_P) in the study area during the wet winter season of 2011/12 was 12.9 mg/L at 1 km from the sea shore, and 9.5 mg/L at 3.7 km. This winter had a gross precipitation only 20% higher than the average for the last 30 years while wind speeds and wind directions closely approached the normal values for 9 years

(Hassan 2011). The above mentioned concentrations should therefore approach long-term average values.

Sea spray had a significant impact on rainfall composition. On average, it contributed to about 21% of SO_4, 27% of Sr, 33% of Rb and B, 73% of Li, 77% of Cl, 97% of Mg and 100% of Na, K and Br whereas for Ca and Mo the contribution was < 3%. These values were derived by taking:

$$\%X_M = 100\alpha_X \, Cl_P/X_P \tag{2.7}$$

where $\%X_M$ is the marine contribution of constituent X (%), X_P is the concentration of X in the rainfall sample (mg/L), Cl_P is the chloride concentration in the rainfall sample (mg/L), and α_X is (X/Cl) in Mediterranean seawater (mg/L basis).

In this approach, it is assumed that: (a) fractionation of the constituents of seawater during spray formation can be ignored, and (b) there are no significant Cl sources other than the sea (Duce and Hoffman 1976; Stuyfzand 1993a). The relationships of different elements with Cl were not linear because of ion exchange (Na, K, Ca, Mg, B, Li, Mo, Rb and Sr), and dissolution/precipitation reactions (Ca, Mg and Sr).

Evapo(transpi)ration further raised the concentrations of all constituents of bulk precipitation. Open water evaporation did not contribute much, as can be deduced from the ^2H–^{18}O plot in Figure 2.6, showing that most groundwater samples plotted on either the mixing line with Mediterranean seawater or the Lebanese meteoric water line. The evapoconcentration factor (F) was derived by comparing the mean chloride content of baseline groundwater (Cl_{BG}) with the flux weighted mean concentration expected in rain water (Cl_P) multiplied by a factor (I) to account for the higher interception of aerosols by vegetation compared to a bulk rainfall collector (Stuyfzand 1993a):

$$F = Cl_{BG} / (I Cl_P) \tag{2.8}$$

In coastal areas, the value of I is 1.1 for surfaces with vegetation up to 0.1 m high, about 2 for dense, tall shrubs and the interior parts of forests, and 3 for the seawind facing borders of forests (Stuyfzand 1993a). This yields for coastal plain water, with Cl_{BG} = 82.1 mg/L (Table 2.6), I = 2 and Cl_P = 12.9 mg/L, an evapoconcentration factor (F) of 3.2, which translates into 69% evapotranspiration. For the mountainous region we obtain, with Cl_{BG} = 24.1 mg/L (Table 2.6), I = 1.1 and Cl_P = 9.5 mg/L, a value of F = 2.3 and 56% evapotranspiration.

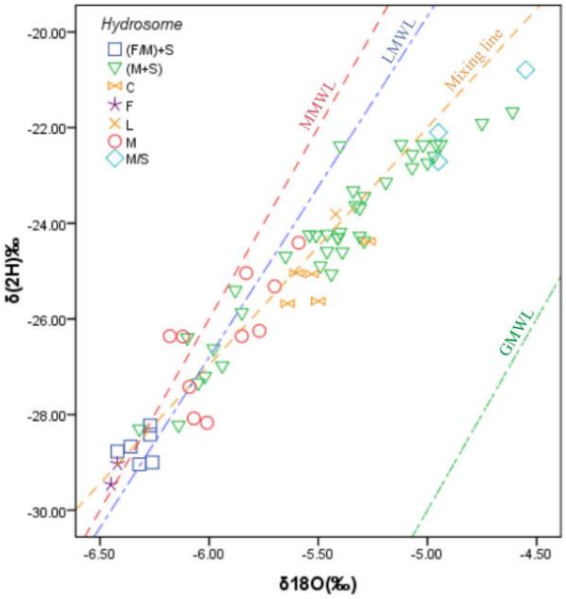

Figure 2.6 δ^2H vs $\delta^{18}O$ values of groundwater samples in the study area. They are compared to the Global Meteoric Water Line (GMWL, Craig 1961), the Mediterranean Meteoric Water Line (MMWL, Gat and Carmi 1970), and the Lebanese Meteoric Water Line (LMWL, Saad et al. 2005). The seawater–freshwater mixing line is also shown (dashed/orange).

2.3.3.2 Saltwater intrusion

The main source of salinization that created most of the chemical differences in the study area is saltwater intrusion. It raised the concentration of many dissolved constituents and contributed to the origin of the M/S, (M+S) and (F/M)+S hydrosomes. This was confirmed by an average Cl/Br ratio of 255 (mg/L basis), which matched saline groundwater ratio (Cartwright et al. 2006) and the Mediterranean Sea ratio (249).

Cumulative frequency plots of the freshwaters of M and F hydrosomes and the salinized samples of the M+S, M/S, (F/M)+S hydrosomes show the extent of shift from pristine conditions (Figure 2.7). Concentrations of Ca, Mg, Na and K show a significant increase in salinized hydrosomes with one order of magnitude. This is due to saltwater intrusion and cation exchange associated with salinizing processes. In contrast, fresh waters show limited variation for these ions consistent with their baseline concentrations. Distributions of Cl and Br display a clear positive skew with two orders of magnitude, due to stronger salinization at high abstraction spots and closer to the shore. Also, SO_4 shows one order of magnitude increase in salinized samples. This matches with intruding saline water, since lithogenic sources such as gypsum are lacking. Anthropogenic sources may also contribute to a fraction of this variation. Variations in B, Sr, Li, Rb and Mo do not exceed one order of magnitude. Note that the shape of Na, Mg, K, Sr, B, Li and Rb curves closely follows that of chloride, which confirms a similar salinity origin. In contrast, Ca and HCO_3 show a different shape controlled by carbonate dissolution. The shapes of NO_3 and Mo are also different, probably reflecting anthropogenic inputs.

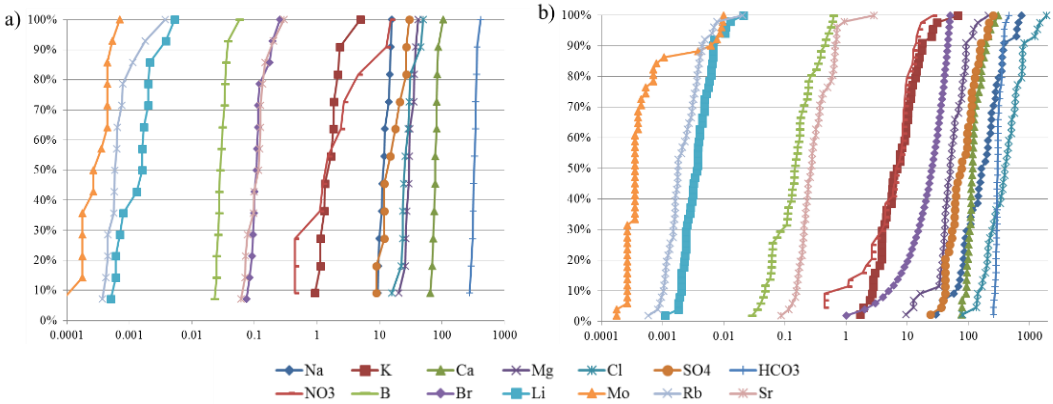

Figure 2.7 Cumulative frequency (log–probability) plots for selected major elements in the freshwaters of (a) the M and F hydrosomes and (b) the salinized samples of the M+S, M/S, (F/M)+S hydrosomes.

2.3.4 Anthropogenic inputs

WAPI was used as a preliminary index for identifying polluted samples, and then confirmed by higher than baseline concentrations. However, HCSA showed that most samples are of mixed origin with saltwater contribution (M+S and M/S); hence, the count on anthropogenic impact was exclusively given to relevant tracers with low or no contribution to Cl. Few wells showed nitrate values > 13 mg/L, a threshold indicating human impact (Babiker et al. 2004), since the surrounding wells had low nitrate values. Bivariate plots and correlation matrices of NO_3 against EC, Cl, Ca and Mg showed no correlation except for a few samples that showed Cl enrichment supported by a positive Cl–NO_3 relationship. This reveals the existence of limited agricultural inputs from fertilizers and/or manure. These spots spread in the vicinity of agricultural fields surrounding the Damour River, in the eastern part of Haret El Naameh, in the valley of Baal El Naameh, and in the north of Dawha. According to isotopic signatures most of the samples did not show a combined increase of nitrate and $\delta^{18}O$, and Cl *versus* $\delta^{18}O$ (corrected for seawater) did not show significant variation. These observations testify that agricultural return flow was negligible.

Moreover, the same spots in Naameh and Dawha villages recorded phosphorous concentration close to or above 0.1 mg/L, suggesting contributions by sewage effluent. Hierarchical agglomerative clustering analysis of molybdenum and uranium revealed a distinctive cluster overlapping with the same spots in Naameh, and suggesting imprints of urbanization. Mo also combined with Ni disclosing a possible stainless steel interaction. In contrast, vanadium as one possible indicator of industrial origin (Moskalyk and Alfanti 2003; Wright and Belitz 2010), showed no distinctive clusters. This matched with the limited industrial activity in the area that seems to have no impact on groundwater as yet.

Consequently, anthropogenic impacts other than saltwater intrusion are still at an early stage in a few spots only. Sewage effluents and agricultural processes constitute the two major sources. It is worth noting that cesspits were widely used for sewage disposal in the study area, but since 2011 a central system is in service that dumps its wastes, after local treatment, outside the studied aquifer. This should reduce the chances of future contamination. However, Dawha is not covered yet, which justifies an anticipated higher anthropogenic input.

2.4 Discussion

2.4.1 Spatial patterns

Three spatial patterns of the studied aquifer are outlined here: (1) the distribution of salinization, (2) the downgradient evolutionary trends, and (3) the altitude of recharge zones.

2.4.1.1 Salinization pattern

The highest salinities in the study area were recorded in Dawha and its vicinity where the $(M/S)_{ms}$ and $(M+S)_{ms}$ hydrosomes dominate (Figure 2.3). This spot has low groundwater abstraction which is less than one tenth of the central zone (Damour, Naameh and Haret El Naameh), nevertheless, its enhanced salinity is explained by the direct exposure of the main aquifer (C_{4c}–C_5) to the Mediterranean Sea contrary to the central zone protected by the Chekka Formation (C_6) (Figure 2.1), acting as a partial barrier for saltwater intrusion. The central zone revealed a consistent salinity pattern as going seaward, an exception occurred in parts of Mechref village where the Damour River filtrate played an adjusting role to salinity. Going further south to Delhamiye, saltwater has not significantly advanced yet since low urbanization and very few private wells with low consumption characterize this spot.

2.4.1.2 Evolutionary trends

In calcareous porous media, it is expected that groundwater becomes more reduced and less polluted as it flows from recharge to discharge areas due to elimination of dissolved constituents such as oxygen, sulphate, nitrate and heavy metals (Stuyfzand 1999; Edmunds and Shand 2008). However, this pattern does not apply to the Mountainous limestone hydrosome (M) or the slightly mixed M+S hydrosome, both of which show little hydrochemical differentiation with either depth or distance downgradient. This is explained by: (a) fissure flow in a relatively thick unsaturated zone, (b) a relatively shallow depth below the groundwater table from which the majority of wells tap groundwater, (c) little if any contact with aquitards, (d) consequently short residence times for elimination processes

to become important, (e) in-well mixing, and (f) reduced downward flow connected to overexploitation.

This lack of evolutionary trends is confirmed by a rather stable strontium maturity index (SMI). The index is defined as follows:

$$SMI = [(Sr_M - Sr_0) / Sr_0] / [(Ca_M + Mg_M - Ca_0 - Mg_0) / (Ca_0 + Mg_0)] \quad (2.9)$$

where X_M is the measured concentration of X corrected for seawater contribution (meq/L), X_0 is the minimum concentration of X in the hydrosome (at a starting point of flow close to the groundwater table), corrected for seawater contribution (meq/L).

Evolutionary trends downgradient would be reflected in SMI increasing in a downgradient direction because strontium (Sr^{2+}) in carbonate rocks forms with initial formation and not from consecutive precipitation processes occurring later, i.e. it does not form in re-precipitated calcite. Therefore, a comparison of Sr^{2+} to (Ca^{2+}+Mg^{2+}) contents is a useful tool to groundwater maturity from which relative dating, residence time or flow direction can be also inferred (Emblanch et al. 2005b; Tulipano et al. 1990). In this study, the saturation index calculated for gypsum showed a negative value for all samples confirming no existence of gypsum minerals to disturb the Ca:Sr ratio.

2.4.1.3 Recharge zones

Altitudes of recharge areas were revealed by $\delta^{18}O$, which testifies to the existence of localized recharge. A bivariate plot of land surface altitude versus $\delta^{18}O$ corrected for seawater contribution shows that most wells were recharged from altitudes between 100 and 400 m, which is the area of aquifer exposure to surface (Figure 2.8). This estimate of altitude effect is based on an average $\delta^{18}O$ depletion of 0.28 ‰ per 100 m, and –4.8 ‰ as an initial value at sea level, which were both derived from several stations spread in Lebanon (Saad et al. 2005). Accordingly, no input from higher eastern mountains outside the study area existed. The broad range of $\delta^{18}O$ for the M+S hydrosome with relatively depleted values recorded in low altitude wells (–6.1 ‰ ± 0.1) supports the conclusion that water infiltrated at about

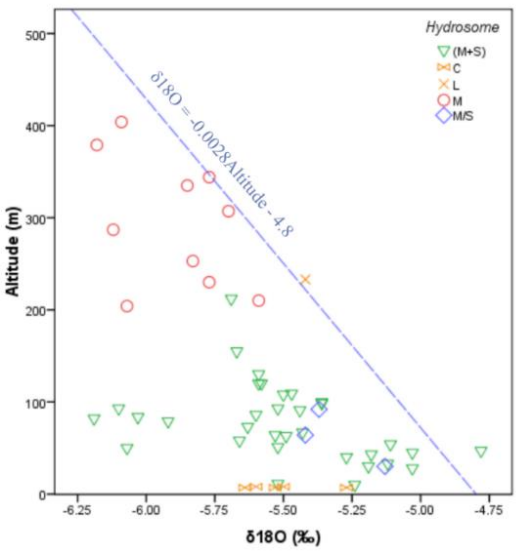

Figure 2.8 Land surface altitude (m) vs $\delta^{18}O$ (‰) corrected for seawater contribution for recent groundwater samples collected in the study area. Samples are grouped according to hydrosome.

400 m, and then made its trip downgradient. This result matches the hydrogeology of the system (Figures 2.1 and 2.2), where the steeply inclined Hammana Formation (C_3) acts as a barrier for outside lateral groundwater flow.

2.4.2 Comparison with natural backgrounds elsewhere

The current groundwater quality status of the Damour aquifer was compared with four European reference aquifers having similar limestone lithology and/or dominant hydrochemical processes, notably carbonate dissolution and saline mixing (Edmunds and Shand 2008) (Figure 2.9). These included: the Razlog Aquifer in Bulgaria (BUL), the Chalk Aquifer in Denmark (DN), the Devonian Aquifer in Estonia (ES), and the Wessex Basin in the UK (UK).

The Damour aquifer showed an intermediate position with respect to most dissolved constituents compared to the four EU reference aquifers. Its most elevated Mg and lowest Sr concentration are remarkable, probably due to the dolomitic character of the Mg bearing limestone. In addition, its groundwater had the lowest concentrations of K, Fe, Mn, As, Ba, Mo and Sc.

Denmark showed the highest concentrations of Cl, Na, SO_4, Br, Mo, Fe, Mn, SiO_2 and Sc. This may reflect higher sea spray inputs, more anoxic conditions and more contact with Si-minerals in overburden or in marly beds. Estonia displayed the lowest Cl, Na and Zn concentrations, and highest levels of HCO_3, K, Ba, Li, Mn and Rb. Bulgaria showed the highest NO_3, Cr and U concentrations, and UK the highest Cu levels. These differences are hard to interpret and may be even biased due to different methods of selecting water samples that reflect baseline conditions.

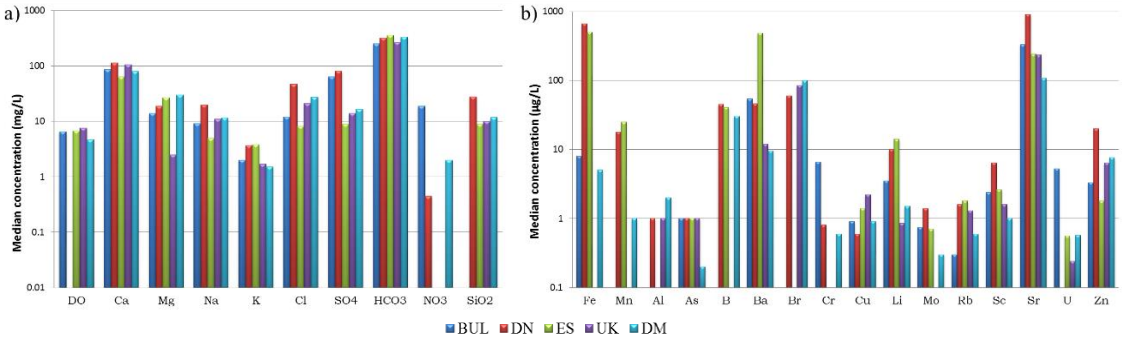

Figure 2.9 Bar plots of (a) major chemical constituents and (b) main trace elements of groundwater in the M (DM) hydrosome of the Damour aquifer and four other European reference aquifers in Bulgaria (BUL), Denmark (DN), Estonia (ES), and UK (UK).

2.4.3 Future outlook on salinization

It is evident that the studied hydrological system is facing salinization although still at a relatively early stage. Water authorities are trying to control groundwater discharge by banning the drilling of new wells, but without putting restrictions on the amount of groundwater extracted from currently running wells. Consequently, the future of this aquifer does not seem bright, unless optimized management strategies are pursued.

In addition, climatic factors will likely stress the system on the long-term, resulting in groundwater recharge reduction, water level decline and sea-level rise. The temperature and precipitation values predicted for West Asia by the Intergovernmental Panel on Climate Change (IPCC) show warmer conditions with lower precipitation in the next 100 years (Cruz et al. 2007). This will reduce groundwater recharge, and thereby add to the impact of urbanization and land use change. The global average sea-level rise estimated (for different emission scenarios) is about 34 cm (IPCC 2007), which will enhance salinization processes and enlarge the freshwater–saltwater mixing zone.

2.5 Conclusions

Hydrochemical System Analysis (HCSA) of the Damour aquifer system revealed the spatial distribution of groundwater bodies (hydrosomes) and hydrochemical zones (facies) within them. Concentration gradients might occur even in the same facies generating significant spatial trends, however, they were ignored here due to lack of relevant information. The following hydrosomes were identified and shown on a hydrochemical map: (1) Mountainous limestone water, (2) shallow coastal plain water, (3) Damour River bank-filtrate, and (4) mixed hydrosomes composed of freshwater from the limestone mountains, fresh river bank-filtrate and intruded saltwater of the Mediterranean Sea. This discrimination facilitated an easier hydrochemical analysis of the system, including salinization sources, anthropogenic inputs and evolutionary trends, by filtering relevant samples to be included in intended applications.

It is hypothesized that no recharge contribution exists via lateral groundwater flows from inland higher mountains, contrary to what was previously thought by others. In addition, the lack of typical downgradient hydrochemical patterns (in oxidants, pollutants and strontium maturity index) confirms the local origin of recharge to the system. This fact stresses the importance to keep current urbanization limited (≈12%), and to refrain from intensification of agriculture, which would significantly affect groundwater potentials.

The baseline groundwater quality as established for the above mentioned three unmixed hydrosomes is typical for a coastal dolomitic limestone aquifer showing fresh, (sub)oxic $CaHCO_3$ water without base exchange due to fresh or salt water intrusion. After dropping salinized and polluted facies in determining Natural Background Concentrations (NBCs), no diversity was revealed in hydrochemical facies, and hence the determined

baseline was the same at both the hydrosome and facies levels. Most dissolved constituents have an intermediate position compared to four European Union reference aquifers. Closer to the shoreline, saltwater intrusion (from the Mediterranean Sea) yields a salinized facies with mostly B3CaCl– water type. However, the fraction of seawater has not exceeded 10–20% yet, which classifies the system as being at an early stage of salinization. This can be explained by a relatively late start of excessive pumping (since 1991), high productivity of the karstic aquifer system, and the role of the Damour River in providing induced recharge to its nearby wells, especially the Mechref village. A limited anthropogenic input, mainly from urban influences and agrochemical applications, also affects the system, but its minor influence is overruled by the impact of saltwater intrusion.

Complexities in assessing groundwater baseline conditions arise, in particular where: (a) historical data of pristine water is lacking, (b) the hydrological system under investigation is facing anthropogenic influences, or (c) groundwater bodies of different origins interfere. A procedure is introduced in this paper, based on the following 6 steps: (1) eliminate biased data, (2) apply HCSA to discern groundwater bodies, each of which requiring the determination of its NBC precluding salinized samples, mixed redox and intermixed hydrosomes, (3) eliminate data showing signs of pollution, (4) define significant hydrochemical trends, (5) do statistical analysis to discern new subfacies, identify any outliers, and choose representative values, and (6) do a final check of the accuracy of the established NBC, and adjust some parameters if necessary. The subdivision of the population following HCSA warrants a detailed determination of natural background concentrations by revealing the appropriate diversity for each hydrosome and its facies. To date, this distinction is a unique outcome of HydroChemical System Analysis incorporation. It is noteworthy that NBCs for trace elements below detection limit (e.g. Fe, As, Ge, La and Sb) might be criticized against accuracy, however, this does not harm the proposed methodology. Such discrepancy arises from the precision of the analytical tests, which are improved over time toward better detection.

Acknowledgements We would like to thank all citizens who were cooperative with the sampling campaign. Special thanks goes to the municipalities of Mechref, Naameh, Baawerta and Damour for providing all needed support. We are also grateful for Beirut Water Authority which made all government wells in the study area accessible. The constructive comments of reviewer Kristine Walraevens and an anonymous reviewer contributed to some essential improvements of the manuscript.

Chapter 3

Hydrochemical effects of saltwater intrusion in a limestone and dolomitic limestone aquifer in Lebanon

This chapter was published as:

Khadra, W.M., Stuyfzand, P.J., van Breukelen, B.M., 2017. Hydrochemical effects of saltwater intrusion in a limestone and dolomitic limestone aquifer in Lebanon. *Applied Geochemistry* 79, 36-51.

Abstract

This study demonstrates groundwater quality differences between a limestone and a dolomitic limestone, (sub)oxic coastal aquifer in the Eastern Mediterranean (Lebanon), with and without ongoing moderate salinization since the last decades. For this purpose, 8 major and 50 trace elements (TEs) were analyzed in 80 water and 65 rock samples, and interpreted with a quad-fold approach utilizing: (1) nonparametric statistical tests, (2) concentration deviations from ideal conservative freshwater–seawater mixing lines, (3) a new parameter called Mixing Enrichment Factor to assess the mobilization of chemical constituents under salinizing conditions, and (4) 1-D dual porosity flow path modeling with PHREEQC. Dissolution/precipitation of $Ca_xMg_ySr_zCO_3$ and cation exchange were the main disclosed hydrogeochemical processes besides minor signs of organic matter oxidation. In the dolomitic limestone aquifer, less carbonate dissolved as compared to the limestone aquifer, partly because of lower pCO_2 in addition to seawater inflow triggering Mg-calcite precipitation by cation exchange. Saltwater intrusion led to mobilization of As, Ba, Cu, Ni, Rb, Sr and U in both aquifers, sometimes likely by cation exchange (e.g. Ba and Sr). Some of these TEs (notably Cu and Ni) recorded higher concentrations in the dolomitic limestone regardless of salinization. Other elements such as Al, Be, Ce, Cr, Nb, Pb, V, Y and Zr revealed no or a low mobilization tendency. The concentration of all TEs in groundwater remained below drinking water limits notwithstanding moderate salinization. This classifies carbonate rocks as a weak geogenic source of TEs, whereas encroaching seawater appears to be a more important source.

3.1 Introduction

Coastal aquifers are known for their complex hydrochemical nature due to (1) different inputs from precipitation, infiltrating rivers, intruding seawater, irrigation return flow, and wastewater infiltration (Stuyfzand 1999; Post 2002); (2) additional or intensified processes in the saltwater-freshwater mixing zone such as dissolution/precipitation, ion exchange, and oxidation/reduction (Herman et al. 1985; Magaritz and Luzier 1985; Stuyfzand 1993a); (3) changes in permeability and porosity due to enhanced karstification or dolomitization of carbonate aquifers (Wicks and Herman 1995; Emblanch et al. 2005a) or clay mobilization in clastic aquifers (Bradford and Kim 2010); and (4) urbanization of coastal zones (Porter et al. 1996). Approaches to interpret the hydrochemical evolution of groundwater bodies can be subdivided into 3 main groups: (1) mapping (including the use of water typologies and quality indices (e.g. Matthess 1982; Stuyfzand 1999), (2) mass balancing (Plummer and Back 1980; Plummer et al. 1994; Dai et al. 2006; Stuyfzand 2011; Parkhurst and Appelo 2013), and (3) 1-D (Appelo 1994), 3-D (Prommer et al. 2003) reactive transport or variable-density groundwater flow and solute transport modeling (e.g. Sanford and Konikow 1989; Simmons et al. 2010).

Studying the behavior of trace elements (TEs) in coastal groundwater flow systems is important because they need to be tested against maximum permissible concentrations (MPCs) of drinking (e.g. Mondal et al. 2010; Al Kuisi et al. 2015; Fiket et al. 2015) or

irrigation water (e.g. Shi et al. 2013), and some can be utilized as tracers of either infiltration water, pollution or geochemical processes (e.g. Stuyfzand 1993b; Gonneea et al. 2014; O'Connor et al. 2015; Stuyfzand 2015a; Sun et al. 2015). The behavior of TEs is initially affected by the geochemistry of hosting rocks, but saltwater intrusion and mixing with freshwater may trigger further hydrogeochemical processes, notably dissolution/precipitation and adsorption/desorption. For instance, a carbonate-philic element like Sr is significantly mobilized upon limestone dissolution (Shand and Edmunds 2008; Lin et al. 2013; Gonneea et al. 2014). Other elements such as As, U and Zn have less bonding affinity to carbonates (Shand and Edmunds 2008; Gonneea et al. 2014), but they may be mobilized by increased O_2 concentrations (for instance due to leakage of oxygenated water via multi-aquifer wells) in limestone and clastic (sandstone, shale, and alluvium) aquifers (Ayotte et al. 2011). Several studies in salinizing sandy aquifers confirm the affinity of TEs to become mobilized, e.g. Ba (Stuyfzand 1993b), Pb and Hg (Sun et al. 2015), or immobilized, e.g. F, Mo, Rb, V and U (Stuyfzand 1993b). In carbonate coastal aquifers with varying Ca/Mg host rock composition, the behavior of TEs has not yet been thoroughly tackled, except for a study of the Italian Dolomite Mountains (Frondini et al. 2014); however, salinization was not an issue there.

This paper focuses on water quality differences between limestone and dolomitic limestone aquifers with and without salinization. A (sub)oxic coastal system in the Eastern Mediterranean (Lebanon) is chosen for this purpose. The selected system has been subject to excessive pumping since 1991. This has intensified saltwater encroachment. It is yet at a moderate salinizing stage with maximum seawater fraction < 20%. Such carbonate aquifers are inherently complex due to their karstic nature. Many authors have addressed the hydrochemistry of Mediterranean coastal aquifers, e.g. Price and Herman (1991); Pulido-Leboeuf (2004); Tulipano et al. (2005); MED-EUWI (2007); De Montety et al. (2008); Sola et al. (2013); Zghibi et al. (2014); Ben Ammar et al. (2016). In Lebanon, however, hydrochemical studies have applied classical approaches only, like (a) Piper, Schoeller, Durov, and Radial plots (Arkadan 1999; Khadra 2003; Korfali and Jurdi 2007; Saadeh 2008; Korfali and Jurdi 2009), or (b) simple water quality indices (Khadra 2003; Saadeh 2008; El-Fadel et al. 2014). Recently, Khadra and Stuyfzand (2014) presented a detailed hydrochemical study of the (dolomitic) limestone Damour coastal aquifer system to the south of Beirut. It included a discrimination scheme to define different groundwater bodies (hydrosomes) and their interbedded hydrochemical zones (facies) in addition to the derivation of baseline quality for main constituents, stable isotopes, and many TEs.

The emphasis in this manuscript is given to the hydrochemical effects induced by saltwater intrusion (SWI) on various major constituents and trace elements in conjunction with potential geochemical differences between limestone and dolomitic limestone units. Four lines of research are followed for this purpose, in logical order of increasing complexity: (1) statistics on 4 water groups (limestone vs. dolomitic limestone with and without salinization); (2) shifts in concentrations of major ions from ideal seawater and freshwater mixing lines; (3) use of Mixing Enrichment Factor (*MEF*), which is introduced here as a new parameter to assess mobility of chemical constituents when mixing (including

salinization) occurs; and (4) 1-D flow path PHREEQC modeling with dual porosity formulation. Lines 1 and 3 analyze many species including TEs, whereas lines 2 and 4 are limited to Na, K, Ca, Mg, SO_4, TIC (or alkalinity), and occasionally Sr. 50 TEs (including metals, metalloids, lanthanoids, and actinoids) are considered. Their total amount in groundwater is < 0.3% of the total dissolved solids for all analyzed samples. 15 elements provide meaningful indications, whereas the others have concentrations constantly below their minimum detection limit (MDL).

3.2 Setting and methods

3.2.1 Site description

The study area spans an area of 60 km^2 along the coastal zone of Lebanon in the Eastern Mediterranean (Figure 2.1). It has a humid mesothermal Mediterranean climate characterized by dry summers and relatively mild, moist winters with sunshine abundance. The annual precipitation record over the last 25 years showed a range between 352 and 1163 mm, with an average of 770 mm (Meteorological Service 2010). Orographic precipitation is enhanced on the western side of the Lebanese mountain range due to humid westerly winds from above the Mediterranean Sea. A climatic cycle with extreme conditions of rainfall or partial drought is expected at a return period of ca. 14 years (Arkadan 2008).

The geology of the area is shown in Figures 2.1 and 2.2, and the hydrostratigraphic units are described in Table 2.1. The two main hosting units are the C_{4c}-C_5 dolomitic limestone and the coastal C_6-Q limestone. Their exposed parts have few paved surfaces only, and they are considered as major recharge zones for rainfall. Groundwater then flows westward to discharge in low areas at the sea excluding intercepted volumes by pumping wells. Groundwater recharge of local origin was confirmed by the downgradient hydrochemical patterns in oxidants, pollutants, and the strontium maturity index (Khadra and Stuyfzand 2014). Water budget components are summarized in Table 2.2.

The baseline groundwater quality of the main (C_{4c}-C_5) aquifer is typical for dolomitic limestone showing oligohaline-fresh, (sub)oxic, calcareous $CaHCO_3$ water. Hydrochemical conditions in 1979-1980 (i.e. 11 years before excessive pumping started) at Naameh-Haret El Naameh villages in the C_{4c}-C_5 aquifer recorded fresh $CaHCO_3$ water type with 115 mg Cl/L at 1200 m from the shoreline (Khadra 2003). Water quality has been deteriorating westward due to saltwater intrusion. Salinizing NaCl and $CaCl_2$ waters have been recently recorded at about 1000-1500 m inland (Khadra and Stuyfzand 2014). The C_6 unit (with ca. 1 m/d hydraulic conductivity) plays a partial role in retarding SWI; however, due to fractures saltwater penetrates and reaches the underlying dolomitic limestone aquifer.

The focus in this study is on the groundwater bodies hosted by the dolomitic limestone (C_{4c}-C_5) and the limestone (C_6-Q) units, which are either fresh (without SWI) or salinized (with SWI). Their mean composition is provided in Table S3.1 (*Appendix S3*).

3.2.2 Data collection

Detailed hydrochemical data on groundwater and seawater is available from Khadra and Stuyfzand (2014). A campaign was also launched to collect rock samples from the different geologic units.

3.2.2.1 Hydrochemical data

During a campaign in April 2011 Khadra and Stuyfzand (2014) collected 102 samples from pumping wells, the Damour River and the Mediterranean Sea. They cover a broad salinity range, from freshwater (TDS = 350 mg/L) in the east, via brackish groundwater close to the coastline (TDS = 2,900 mg/L) to hypersaline water of the Mediterranean Sea (TDS = 38,500 mg/L). They were all analyzed on 4 physical, 72 chemical, and 2 isotopic parameters. The hydrochemical data of 80 samples collected from groundwater in the limestone and the dolomitic limestone units, and the Mediterranean Sea are used for the sake of this study. Information on well purging and data quality control are given by Khadra and Stuyfzand (2014).

3.2.2.2 Geochemical analyses

Sixty five samples of fresh rock cuttings were collected from different formations in the study area including aquifers and aquitards at different stratigraphic levels (lower, middle and upper). No preservation was needed because of total elemental analysis. Sampling took into consideration facies variation within the same formation (matrix, fractures and veins). It was not feasible to collect core samples from the current mixing zone because drilling was banned in the area during the study period. The samples were analyzed at AcmeLabs Vancouver on bulk organic matter by LOI, main elemental composition using $LiBO_2$ fusion followed by XRF, 32 rare earth and refractory elements by ICP-MS following a Lithium metaborate/tetraborate fusion and nitric acid digestion, and 14 precious and base metals by ICP-MS after digestion in Aqua Regia. A table including (1) analyzed elements and oxides, (2) relevant methods of analyses, and (3) MDLs, is provided in the *Appendix S3* (Table S3.2).

3.2.3 Statistical methods

Kruskal Wallis H Test and *Mann-Whitney U Test* are two nonparametric tests selected to uncover significance of correlations between independent and dependent variables. The *Kruskal Wallis* is applicable to a group of two and more independent variables, whereas the *Mann-Whitney* tests two population distributions only (Hinkle et al. 2003). They are applied here to check the effect of: (1) saltwater intrusion, and (2) limestone vs. dolomitic limestone compositional contrast on TEs and major chemical constituents in groundwater. Statistically significant difference is assumed when asymptotic significance is ≤ 0.1, i.e., the null hypothesis is rejected at the 10% significance level. The relatively low stringent level aims at accounting for more possibly affected elements. No concern on mistakenly

endorsing a false response because the statistical outcome complements other approaches utilized for the same purpose.

3.2.4 Sea water input and correction procedure

According to Khadra and Stuyfzand (2014) saltwater intrusion is the main source of salinization in the studied aquifer, and an average Cl/Br ratio of 255 (on mg/L basis) matching the Mediterranean Sea ratio (249) excludes halite dissolution as a potential source of salinization. Hence, the initial step in analyzing the hydrogeochemistry of the mixing zone is to determine the percentage of admixed seawater since geochemical reactivity may vary depending on the extent of salinity and the type of mineral. The solution for 2 end-members, for instance fresh and saltwater, with a single tracer like Cl is given in Eqs. 2.1 and 2.2.

The theoretical composition of each salinized groundwater sample as expected for conservative ideal mixing between seawater and freshwater was subsequently quantified and related to the observed composition by using (Fidelibus et al. 1993; Appelo and Postma 2005):

$$C_{\mathrm{TMix}} = (1 - f_S)\times C_{\mathrm{F}} + f_S\times C_{\mathrm{S}} \tag{3.1}$$

$$\Delta C = C_{\mathrm{OBS}} - C_{\mathrm{TMix}} \tag{3.2}$$

where C_{TMix} = concentration of ions in a theoretical mixed sample [mg/L]; C_{S} = ditto in saline water (presumably seawater) [mg/L]; C_{F} = ditto in freshwater [mg/L]; C_{OBS} = ditto in observed sample [mg/L].

Ionic delta (denoted by ΔC) reveals whether hydrogeochemical processes other than saltwater mixing contribute to the observed depletion or enrichment (Fidelibus 2003; Pulido-Leboeuf 2004; Slama 2010; Sola et al. 2013; Zghibi et al. 2014; Habtemichael and Fuentes 2016). This approach is straightforward, provided that end-members can be easily defined. Therefore,

1. it needs to be proven that seawater is the saline end-member. This was accomplished by multi-tracing, e.g., using Eqs. 2.1 and 2.2 for more potential tracers such as Br and B to confirm seawater origin.
2. the coastal seawater quality needs to be established because it may have changed due to environmental pollution. Knowing the age of seawater intrusion, determined for instance by ^{3}H-^{3}He dating or travel times on the basis of a hydrological model, can guide whether the ancient (usually unpolluted) or the recent (possibly polluted) seawater should be used. When historical data is lacking, the ancient seawater quality can be deduced from SMOW corrected by an evapo-concentration factor to the recently measured chloride levels in seawater, and the outcome is then compared for both waters. In this study, the comparison shows only slightly higher Na, As, Ba, Cr, Cu, Ni and V concentrations, having a

minor effect on their Mixing Enrichment Factor except for V. Hence, the recent Mediterranean Sea water chemistry is selected.

3. it is not always valid to assume that all freshwaters have the same chemistry (as in previous studies, e.g. Slama 2010; Habtemichael and Fuentes 2016; Bouderbala et al. 2016) because different groundwater bodies may exist with large differences in among others Cl, Ca, Mg and HCO_3. Hence, separate freshwater end-members are assigned throughout this study following the two discriminated groundwater bodies in the limestone and dolomitic limestone units. The 100% mean freshwaters are set to concentrations as derived for the Baseline Groundwater Concentrations (BGCs) of the two aforementioned waters (Khadra and Stuyfzand 2014).

3.2.5 Mixing Enrichment Factor

Assuming no other anthropogenic sources to groundwater, Perelman (1972) suggested a migration coefficient "Mig" to assess the mobility of inorganic constituents in groundwater in relation to their concentration in the earth's crust. And recently, Frondini et al. (2014) and Koh et al. (2016) defined and applied an enrichment factor (*EF*; Eq. 3.3) to assess the relative mobility of an element based on the ratio to a reference element in the liquid and solid phases; however, EF does not account for groundwater mixing conditions.

$$EF = (C_T/C_R)_L / (C_T/C_R)_A \tag{3.3}$$

where C_T = trace element concentration, C_R = reference element concentration (Ca for limestone and Mg for dolomitic limestone), L = liquid phase, and A = hosting aquifer (solid phase).

A new, more versatile coefficient called *MEF* is proposed here to assess the mobility of TEs when mixing with seawater occurs. It is also applicable to main chemical constituents (e.g. Ca, Mg, Na and K), and it can likewise be used to mixing of surface waters (for instance in an estuary) where C_A is applied to suspended material.

$$MEF = 1000\ \Delta C_{MIX} / C_{MAX} \tag{3.4}$$

with: $$\Delta C_{MIX} = (1 - f_S)(C_F - BGC_F) + f_S(C_S - BGC_S) \tag{3.5}$$

$$C_{MAX} = C_A\, \rho\, (1 - \varepsilon)/\varepsilon \tag{3.6}$$

Following Eq. 3.3, $$C_F = [(C_{MIX} - (C_S\, f_S))/(1 - f_S)] \tag{3.7}$$

We assume $C_S = BGC_S$, so that *MEF* becomes after inserting Eqs. 3.5 to 3.7 into Eq. 3.4:

$$MEF = \frac{C_{\mathrm{MIX}} - (C_{\mathrm{S}} \times f_S) - BGC(1 - f_S)}{C_{\mathrm{A}} \times \left(\rho \times \frac{1-\varepsilon}{\varepsilon}\right)} \times 1000 \tag{3.8}$$

where *MEF* is the Mixing Enrichment Factor [‰] at a specific salinity fraction $f_S < 1$ (as in Eq. 2.2); C_{MIX} = concentration of mixed sample [mg/L]; BGC_{F}, BGC_{S} = baseline groundwater concentration of fresh and salt end-member respectively [mg/L]; C_{S} = concentration of seawater [mg/L]; C_{A} = content of hosting aquifer [mg/kg]; ρ = specific density of aquifer matrix [kg/L]; and ε = porosity [-].

$[(C_{\mathrm{MIX}} - (C_{\mathrm{S}} \times f_S))/(1-f_S)]$ is the freshwater end-member extracted from the mixed sample based on Eq. 2.1; $\rho \times (1 - \varepsilon)/\varepsilon$ converts the total content in the aquifer matrix into the maximum theoretical concentration in water when the aquifer matrix would completely dissolve. Therefore, the *MEF* represents the ratio of the mobilized concentration to the maximum theoretical concentration if the aquifer matrix would completely dissolve into the same volume of water. It accounts for the baseline groundwater concentrations, which should be excluded from the impact of (im)mobilization possibly stimulated by SWI because they are entirely natural.

MEF facilitates a quantitative comparison of the behavior of TEs and other constituents in subsurface water. *MEF* ≥ 0.01‰ indicates additional mobilization from solid hosting rocks to groundwater solution; *MEF* between -0.01‰ and 0.01‰ indicates that mixing with seawater and natural backgrounds form the exclusive sources of chemical elements in groundwater solution; and a *MEF* ≤ -0.01‰ indicates immobilization (loss from solution). The selected ±0.01‰ thresholds are empirical, based on the observed values and their variation. Same thresholds are also applicable to the enrichment factor (*EF*).

The enrichment factors (*EF* and *MEF*) are needed here to complement the statistical methods introduced in *Section 3.2.3*. They are capable of: (1) defining the behavior of elements (whether mobilized or immobilized), and (2) quantifying the degree of mobilization, unlike the statistical methods that can only discover an interlink between the dependent and the independent variables.

3.2.6 Forward reactive transport modeling

Forward reactive transport modeling is applied as a predictive approach to simulate the consequences of seawater incursion. PHREEQC-2 (Parkhurst and Appelo 1999) was used to construct 1-D flow path transport models. The flow is unidirectional from sea to land. One-dimensional simulation was preferred due to limited data and unknown heterogeneities of the aquifer. The major studied aquifer (C_{4c}-C_5) and the overlying C_6 unit are considered dual porous, due to fractures, fissures, bedding planes, and micro-porous rock matrices. Previous studies on karst aquifers showed that the dispersion model is a good representation of fissured karst systems especially when the mean transit time exceeds 2-3 years (Maloszewski and Zuber 1985; Maloszewski et al. 2004; Einsiedl et al. 2009). Exchange

between the matrix and the semi-stagnant water is assumed to occur via diffusion and reactive transport only (i.e., ignoring advection) unlike for mobile conduits where advection dominates. The simulation then utilizes a first-order exchange approximation with implicit mixing factors mixf_m and mixf_{im}. They are calculated according to the following equations (Parkhurst and Appelo 1999; Parkhurst and Appelo 2013):

$$\mathrm{mix}f_{im} = \frac{\varepsilon_m}{\varepsilon_m + \varepsilon_{im}} \times \left(1 - \exp\left(-\frac{\omega t(\varepsilon_m + \varepsilon_{im})}{\varepsilon_m \times \varepsilon_{im}}\right)\right) \tag{3.9}$$

$$\mathrm{mix}f_m = \mathrm{mix}f_{im}\frac{\varepsilon_{im}}{\varepsilon_m} \tag{3.10}$$

where ε_m is the porosity of mobile zone [-], ε_{im} is the porosity of immobile zone [-], ω is the exchange factor accounting for the exchange between immobile and mobile cells [s^{-1}], and t is the time step [s].

Half of the cells along a flow path (e.g. 300 cells out of 600) are used for mobile groundwater with uniform distribution of stagnant porosity and mixing conditions. An equivalent number + 1 cell (i.e. 301) is introduced as an associate in the immobile zone. Each mobile cell (x) exchanges with the immobile cell numbered 300 + 1 + x since cells 302 to 601 are the immobile ones (Parkhurst and Appelo 2013). The exchange factor is estimated in this study at 1.4e-8 s^{-1} assuming spherical stagnant zone with diffusion coefficient = 6.4e-13 m^2s^{-1}, ε_{im} = 0.08 to 0.12, and a shape factor = 0.21 (Van Genuchten 1985). Sensitivity of the exchange factor checked for one order magnitude showed minor impact.

Dispersivity estimate relied on the following empirical power law (Schulze-Makuch 2005):

$$\alpha_L = c(L)^k \tag{3.11}$$

where α_L = longitudinal dispersivity [m]; k is a scaling exponent; c is a parameter based on type of geological media [m^{1-k}]; L = flow tube length [m]; k is 0.4 and c is 0.8 for consolidated rocks based on extensive data sets compiled by Schulze-Makuch (2005).

Constraints on time steps and grid size are considered in order to minimize numerical dispersion in fractured bedrock. An advective diffusive flux ratio (ψ) is introduced as a guide in choosing grid spacing and model time steps according to the following equation (Lipson et al. 2007):

$$\psi = \frac{v \times b \times \Delta z}{D_f \times \varepsilon_{\mathrm{im}} \times \Delta x} \tag{3.12}$$

where ψ in a fracture is supposed to be > 10; v = average linear groundwater velocity [m^2s^{-1}]; D_f = diffusion coefficient across fracture wall [m^2s^{-1}]; b = fracture aperture [m]; $\varepsilon_{\mathrm{im}}$

= porosity of immobile zone, i.e. bedrock matrix [-]; Δx = the mobile cell length [m]; Δz = the immobile cell (or macro-pore) length [m], assumed here as 0.001 m (Yan et al. 2015).

The model setup including initial conditions (water chemistry and geochemistry), inflow solution chemistry, and geochemical reactions utilized are explained in *Section 3.3.5*.

3.3 Results

3.3.1 Geochemistry of hosting rocks

Results of the geochemical analyses of the discerned geological formations are summarized in Table 3.1, and a graphical output from a Pearson linear correlation matrix is provided in Figure S3.1 (see *Appendix S3*) where main clusters are recognized based on their so-called correlation score plot (Stuyfzand 2015b). The Lower Sannine Formation (C_{4a}) is enriched in magnesium approaching a dolomite like composition ($Ca_{0.58}Mg_{0.42}Sr_{0.0002}CO_3$) as deduced from major elements; strontium is assumed here as a solid solution impurity. The Middle Sannine Formation is conversely Ca-enriched with $Ca_{0.96}Mg_{0.04}Sr_{0.0002}CO_3$ principal mineralogical composition. It has higher Al, Fe and K content indicating more clay deposition. Lower Al correlation score (Figure S3.1) points to its marine origin as also confirmed by clustering of Ca, Mg and Sr; the latter indicates an environment supposedly rich in aragonite and low Mg-calcite.

The C_{4c}-C_5 carbonate rock aquifer, most dominant in the study area, shows high Mg content with $Ca_{0.70}Mg_{0.30}Sr_{0.0003}CO_3$ composition (Table 3.1). Few samples, however, at mid-levels have Ca-rich micritic limestone, with lowest Si, Al, K and trace elements such as Nb, Rb, Ga, La and Y, which is attributed to lack of non-carbonate impurities (Nader et al. 2006). More traces of silicon appeared at the bottom, upper levels and closer to the sea. Visual inspection of rocks reveals minor coatings and veins of quartz in addition to secondary deposition of chert nodules, and some intercalations of clay. The quite low Fe content (0.1 wt. %) could be carbonate-bound or present as ferric hydrous oxide. The two dolomitic units (C_{4a} and C_{4c}-C_5) have the highest Mg content and lowest Ca, Fe, Al, As, Ba and many other TEs (Ce, Co, Cr, Cu, La, Nd, Ni, Sr, V, Y, Yb, Zn and Zr).

The Chekka Formation (C_6) (overlying the C_{4c}-C_5 unit) has calcite predominance (90%) with ca. 8% clayey composition. The higher level and correlation score of its Ba content (Table 3.1; Figure S3.1) is probably attributed to more illite and/or K-feldspar, and clustering of some TEs such as Co, Cu, V and Zn indicates more adsorption on clay minerals like kaolinite or on fine-grained heavy minerals. It also has highest Sr content. The topmost Q unit is characterized by a sequence of uncemented clastic deposits, 69% calcareous fragments ($Ca_{0.94}Mg_{0.06}Sr_{0.0007}CO_3$ composition), in addition to ca. 18% quartz and 10% kaolinite. Presence of some clay or heavy minerals with higher Al-Fe content is inferred from strong correlation between Al_2O_3 and Fe_2O_3 (r = 0.79).

The bulk of the As, Ce, Co, Cu, Ga, La, Nb, Nd, Ni, Rb, V, Y, Yb and Zr contents in the C_6-Q and C_{4c}-C_5 units is probably bound to clay minerals (e.g. kaolinite or illite) or fine-grained heavy minerals (e.g. ilmenite or biotite) as confirmed by the positive correlations these TEs have to Al, K, Fe and Ti ($r > 0.6$). Some small dark mineral inclusions are clearly visible in the admixtures of clay. These impurities could be remnants of direct weathering of volcanic rocks that occurred in the early Cretaceous (Dubertret 1955). In addition, volcanism during that episode could have enriched the level of some TEs in seawater (e.g. Ni, Y and Zr), from which the clays deposited later (Nader 2000).

Organic matter (OM) is also a well-known host for a range of trace elements (Tribovillard et al. 2004; Pichler and Mozaffari 2015); however, bivariate correlations of geochemical data show no relation between OM and TEs unlike a clear positive correlation with iron ($r > 0.6$ between Fe and Al, Be, Ce, Cr, Cu, Ga, Mo, Nd, Ni, U, V, Y, Yb, Zn and Zr). This excludes OM as an apparent source of TEs, and nominates hydrous ferric oxides to be the main traps in clays, since pyrite role is ignored under oxic conditions.

Table 3.1 Minimum, maximum and median composition of hosting rocks, and the main mineral phases as deduced from XRF and ICP-MS/ES results. The whole data set is provided in Table S3.3 (see *Appendix S3*).

				wt %								PPM		
Unit		**# of samples**	**BOM**	**Ca**	**Mg**	**Na**	**K**	**Si**	**Fe**	**Al**	**Mn**	**As**	**Ba**	**Be**
Q	*min*	5	0.6	24.0	0.3	0.01	0.05	8.3	1.3	0.8	0.02	2.7	35	1.0
	max		2.7	29.2	4.3	0.04	0.08	10.3	2.7	1.7	0.03	5.2	163	5.0
	median		2.1	28.2	0.4	0.02	0.05	9.6	1.7	1.1	0.02	3.6	39	5.0
C_6	*min*	8	0.6	33.7	0.2	0.01	0.00	1.1	0.3	0.4	<0.01	0.6	33	1.0
	max		1.9	38.3	0.3	0.05	0.02	4.1	0.8	1.3	<0.01	5.7	411	3.0
	median		1.2	36.3	0.2	0.02	0.00	2.2	0.5	0.9	<0.01	3.5	41	2.0
C_{4c}-C_5	*min*	28	0.0	2.1	0.3	0.01	0.00	0.1	0.0	0.0	0.01	0.5	2	1.0
	max		3.4	39.7	12.6	0.04	0.07	41.9	0.4	0.7	0.04	4.0	23	3.0
	median		0.1	24.5	10.4	0.02	0.02	0.5	0.1	0.1	0.01	1.0	7	3.0
C_{4b}	*min*	3	0.7	26.4	0.5	0.02	0.03	1.1	0.2	0.4	0.01	0.9	12	1.0
	max		6.6	38.2	1.4	0.02	0.59	7.7	1.7	2.8	0.01	8.6	46	3.0
	median		2.7	34.8	1.1	0.02	0.06	2.5	1.0	0.9	0.01	6.1	19	2.0
C_{4a}	*min*	21	0.1	15.2	5.2	0.01	0.00	0.1	0.0	0.0	0.01	0.5	2	1.0
	max		1.1	31.7	13.1	0.06	1.13	7.8	2.0	3.3	0.01	5.9	45	5.0
	median		0.1	21.9	12.3	0.02	0.02	1.0	0.3	0.3	0.01	2.4	7	2.5

Table 3.1 (continued)

Unit		PPM											
		Ce	**Co**	**Cr**	**Cu**	**Ga**	**La**	**Mo**	**Nb**	**Nd**	**Ni**	**Pb**	**Rb**
Q	*min*	9.7	3.9	34	4.4	1.3	5.7	0.2	2.9	4.2	8.4	1.4	4.5
	max	17.5	7.8	130	25.2	3.5	14.5	0.6	6.4	10.7	28.4	4.4	9.4
	median	11.6	4.4	34	6.7	2.4	7.8	0.4	4.5	7.6	11.0	1.9	6.5
C_6	*min*	4.9	0.8	34	11.2	0.6	7.4	0.1	0.7	4.8	5.4	0.9	2.0
	max	12.1	2.3	185	41.4	2.2	13.3	1.4	2.2	8.8	40.3	2.3	4.5
	median	8.4	2.0	85	30.1	1.8	10.4	0.3	1.6	6.9	16.2	1.9	3.8
C_{4c}-C_5	*min*	0.3	0.2	7	0.3	0.6	0.2	0.1	0.1	0.4	0.5	0.2	0.5
	max	8.4	2.4	68	7.1	0.9	5.0	3.5	2.2	3.2	8.4	29.7	9.8
	median	1.7	0.6	21	1.6	0.8	1.3	0.2	0.6	1.1	1.2	0.6	1.9
C_{4b}	*min*	2.5	1.3	27	2.3	1.8	2.1	0.2	0.9	1.5	11.0	0.3	4.0
	max	11.2	3.9	198	10.2	5.2	7.7	0.5	5.4	3.6	18.8	1.6	32.8
	median	3.8	2.8	82	10.2	3.5	2.3	0.4	3.7	1.6	14.9	1.0	16.4
C_{4a}	*min*	0.5	0.3	7	0.5	0.5	0.3	0.1	0.1	0.3	0.5	0.2	0.4
	max	22.9	4.8	123	11.3	7.7	12.8	5.0	13.4	11.2	39.2	1.5	38.8
	median	3.0	1.4	21	1.6	1.1	1.6	0.3	1.2	1.4	4.5	0.6	3.8

Table 3.1 (continued)

Unit		PPM							Deduced major mineral phases (wt %)		
		Sr	**U**	**V**	**Y**	**Yb**	**Zn**	**Zr**	**$Ca_xMg_ySr_zCO_3$**	**Quartz**	**Kaolinite***
Q	*min*	174	1.2	22	6.6	0.6	13.0	38.5			
	max	761	4.9	52	23.2	1.6	64.0	58.6			
	median	218	1.5	47	8.2	0.6	21.0	49.2	$Ca_{0.94}Mg_{0.06}Sr_{0.0007}CO_3$	17.7	9.5
C_6	*min*	824	1.2	20	10.9	0.5	13.0	11.6			
	max	1133	7.9	67	23.7	1.5	81.0	22.7			
	median	975	2.5	45	16.8	1.1	35.0	17.7	$Ca_{0.99}Mg_{0.01}Sr_{0.0018}CO_3$	2.7	8.9
C_{4c}-C_5	*min*	28	0.3	9	0.3	0.1	1.0	0.6			
	max	241	3.1	27	4.6	0.3	26.0	23.6			
	median	160	1.2	16	1.3	0.1	5.0	4.5	$Ca_{0.70}Mg_{0.30}Sr_{0.0003}CO_3$	0.6	1.4
C_{4b}	*min*	75	1.1	12	1.1	0.1	6.0	6.8			
	max	227	2.1	128	3.9	0.4	19.0	41.0			
	median	76	1.3	62	1.8	0.1	12.0	30.4	$Ca_{0.96}Mg_{0.04}Sr_{0.0002}CO_3$	3.4	8.1
C_{4a}	*min*	73	0.7	10	0.2	0.1	1.0	1.1			
	max	168	3.9	117	7.7	0.8	19.0	119.1			
	median	97	1.6	20	1.3	0.2	3.5	9.8	$Ca_{0.58}Mg_{0.42}Sr_{0.0002}CO_3$	1.6	2.5

* Al was assumed to derive from kaolinite, justified by low K content in Q, C_6 and C_{4c}-C_5 formations although small amounts could be attributed to other sources (like feldspars) probably existing in the C_{4b} and the C_{4a} units. Kaolinite took part of Si, and the remaining was attributed to quartz.

3.3.2 Statistical results

Using the statistical software package *SPSS*, the *Kruskal Wallis H Test* was utilized to determine whether 23 dependent variables (Na, K, Ca, Mg, SO_4, TIC, Fe, Si, Al, As, Ba, Be, Co, Cr, Cu, Mo, Ni, Pb, Rb, Sr, U, V and Zn) have statistically significant differences among 4 water groups hosted by: (1) limestone, (2) limestone with SWI, (3) dolomitic

limestone, and (4) dolomitic limestone with SWI. Results reveal statistical differences for the 6 main constituents (Na, K, Ca, Mg, SO_4 and Fe) and 10 TEs (As, Ba, Be, Co, Cu, Ni, Rb, Sr, U and V) indicating that salinization and/or geochemical contrast (between limestone and dolomitic limestone) do have an effect on their variance with different effect size (Table S3.4, *Appendix S3*). In contrast, Al, Cr, Mo, Pb, Zn, and TIC are not affected. The *Mann-Whitney U Test* then determines specifically which variable is responsible for the recorded difference (Is it SWI or compositional contrast?). In fact, Na, K, Si, SO_4 and some TEs (As, Ba, Cu, Rb, Sr and U) show variance between limestone and dolomitic limestone even under freshwater conditions whereas salinization poses an effect on Na, Ca, SO_4, U and V concentrations for both geochemistries. K, Mg, As, Ba, Cu, Ni, Rb and Sr are affected by SWI in the dolomitic limestone only (Table S3.5, *Appendix S3*). Be, Co and Fe are influenced by the dual impact of geochemistry and SWI; otherwise they are not affected separately.

3.3.3 Chemical equilibria

Most samples show undersaturation with respect to aragonite, dolomite, siderite, witherite, strontianite and barite; supersaturation of silicate minerals (e.g. kaolinite); and near equilibrium with calcite and Mg-calcite. Few samples on the western rim of Dawha village have (Mg)calcite, aragonite, and dolomite oversaturation. Halite and gypsum were not observed in the rock samples, while the water is strongly undersaturated. Average pCO_2 of fresh groundwater in the dolomitic limestone and limestone units record $10^{-1.7}$, and $10^{-1.4}$ atm, respectively. They show higher than average values mentioned for carbonate aquifers by Drever (1997) and Langmuir (1997) ($10^{-2.5}$ - 10^{-2} atm), but a similar range was observed elsewhere, e.g. East Anglia, U.K (Heathcote 1985), and Drahany Highlands, Czech Republic (Faimon et al. 2012). Worldwide patterns of pCO_2 depend on climatic conditions (temperature and rainfall), and according to Brook et al. (1983) the Eastern Mediterranean area has pCO_2 range on land from $10^{-2.6}$ to $10^{-2.2}$. Nevertheless, the discrepancy in pCO_2 observed in the studied groundwater points toward more uptake of CO_2 from root respiration and oxidation of organic matter probably buried with limestone weathering products (Faimon et al. 2012).

Ionic deltas (ΔC) were calculated for major ions (Na, Ca, Mg and SO_4), TIC and Sr (due to its incorporation into $CaCO_3$). Subsequently, the samples were discerned based on formations from which they derive, the limestone C_6-Q and the dolomitic limestone C_{4c}-C_5 units. Excellent correspondence of saltwater fraction calculated for chloride and with multi-tracing using Eqs. 2.1 and 2.2 for Br, B, Na and SO_4 confirm that the seawater is the saline end-member. On the other hand, two freshwater end-members were assigned separately for the second end-member as derived for the baseline groundwater concentrations in the limestone and the dolomitic limestone (the BGCs are provided in Table 3.2). Noteworthy that salt sources like halite dissolution, connate old sea water with altered composition, and recent irrigation return flows or sewage effluent are nearly absent as confirmed from bivariate plots and correlation matrices of NO_3 against EC, Cl, Ca and Mg (Khadra and Stuyfzand 2014).

Plots of ΔNa, ΔCa, ΔMg, ΔTIC and ΔSr (calculated using Eq. 3.2) versus seawater fraction (Figure 3.1) show different processes revealing departure from ideal seawater-freshwater mixing. ΔTIC exhibits a dominant enrichment in both aquifers pertaining to carbonate dissolution predominance. Simultaneously all samples are Na depleted with respect to the theoretical mixing line, and the depletion increases with salinity. Ca is conversely enriched for most samples with reasonable correlation to seawater fraction. This is a typical behavior in salinized groundwater and common for both formations (limestone and dolomitic limestone) conforming to Na/Ca cation exchange. However, the steeper slope of Na and Ca in the limestone samples testifies of more exchange with salinity owing to higher exchange capacity (see Table 3.4). In addition, part of Ca stronger increase pertains to more calcite dissolution in the limestone rocks, partly due to higher pCO_2, and subsequently lower pH and $SI_{calcite}$, in the coastal plain region compared to the mountains. pCO_2 relative rise is probably attributed to higher vegetation density and higher temperature. Mg records a different trend; it is mostly enriched in the dolomitic limestone aquifer, but depleted in most limestone samples (Figure 3.1). This is due to more Mg release by dissolution from Mg-rich hosting rocks, and occasional exchange of Na (and K) for Mg.

Sr shows a steeper slope in the limestone unit, which reflects the better Sr fit into pure $CaCO_3$ than in dolomitic limestone. This is also confirmed from the observed ascending trends of Ca, Sr and TIC in the limestone unit. SO_4 ionic deltas show dominance of near conservative mixing conditions for the C_{4c}-C_5 units, whilst enrichment prevails for the limestone samples. This latter anomaly is probably related to atmospheric inputs and/or some agrochemicals applied in the overlying quaternary sand unit, which is a main cultivation strip.

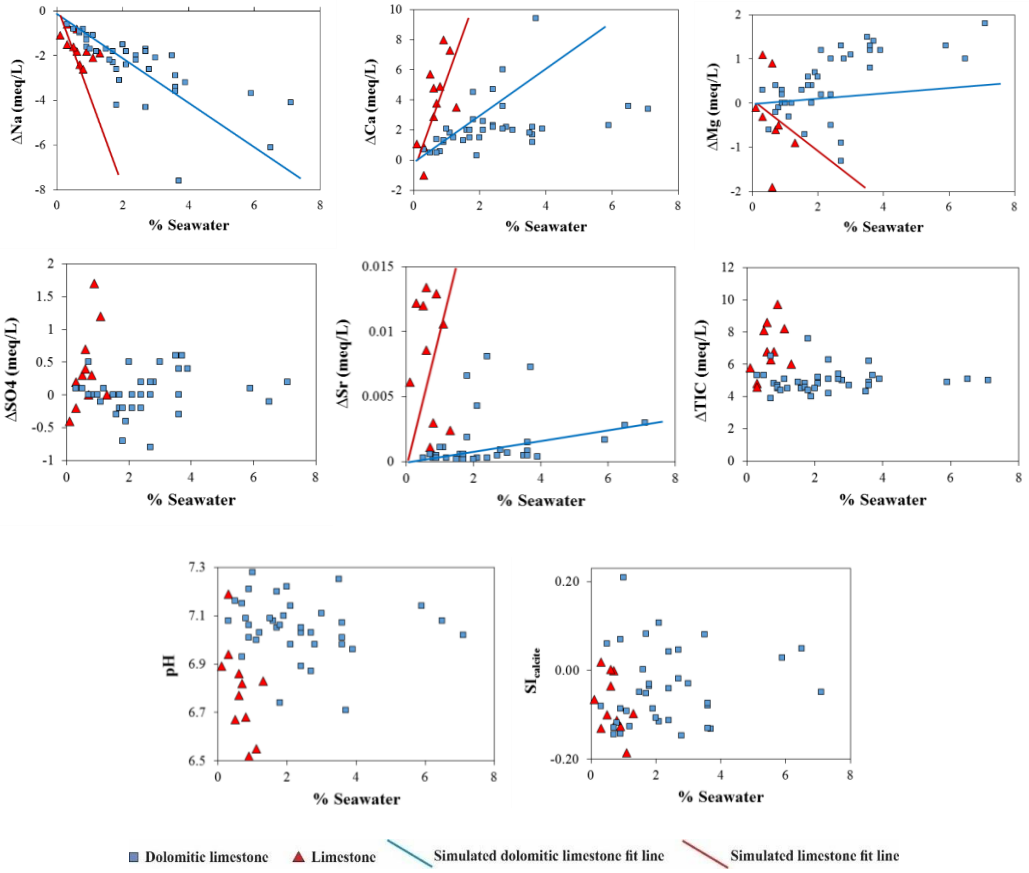

Figure 3.1 Ionic deltas (Δ) of Na, Ca, Mg, SO_4, Sr and TIC, pH and $SI_{calcite}$ vs. % of seawater. Samples are discerned based on formations from which they derive, the C_{4c}-C_5 aquifer (dolomitic limestone), and the C_6-Q units (limestone). The simulated (solid) lines are generated via PHREEQC (see "*Flow path reactive transport modeling results*" section).

3.3.4 Seawater mixing effect

The mixing between intruding seawater and ambient freshwater probably induced a new hydrochemical equilibrium affecting the behavior of major constituents and some trace elements. Few groundwater samples with Al > 10 µg/L in near pH neutral water were eliminated a priori due to probable filtration bias (Stuyfzand 1987). All major and trace elements are assessed here for calcareous salinized samples in the limestone (C_6-Q) and dolomitic limestone (C_{4c}-C_5) hosting units. The aim is to define: (1) the affinity of these elements toward (im)mobilization, and (2) the associated difference in mobilization degree between limestone and dolomitic limestone. This is done by calculating their Mixing

Enrichment Factor (*MEF*) via Eq. 3.8 (Table 3.2). Also listed are the predominant ionic forms in (sub)oxic environment, and the main aquifer sources/sinks.

MEF values of the major and trace elements including those statistically interlinked to SWI show the following results:

1. Ca is mobilized by salinization, Na and K are immobilized, and Fe maintains an equilibrium status. This applies to both limestone and dolomitic limestone, but with higher immobilization of Na and K in the latter.
2. Mg is immobilized for the limestone groundwater but mobilized for the dolomitic limestone.
3. Si is mobilized in the limestone unit only.
4. As, Ba, Cu, Ni, Rb, Sr, U and Zn are mobilized in both domains.
5. As, Mo, Rb and U show relatively higher mobilization in the salinized limestone unit.
6. Al, Be, Co, Cr, Pb and V reveal no affinity to mobilize due to SWI, and hence their slight increase in groundwater reflects admixing with seawater.

35 more TEs with < 0.05 µg/L in all groundwater samples could not be evaluated on their behavior (Table 3.2). Some of them such as Ce, Nb, Nd, Y and Zr have significant levels in the hosting rocks (median is 1 to 50 ppm) (Table 3.1), but reveal concentration levels below detection in all water samples. This is in harmony with their very weak mobilization potential at near pH neutral conditions (Janssen and Verweij 2003).

Table 3.2 Sources and behavior of TEs and major constituents in the 2 discerned geochemistries, limestone (C_6-Q) and dolomitic limestone (C_{4c}-C_5) for fresh and salinized groundwater.

TE	Predominant ionic form	Main aquifer source	Aquifer geochemistry		Seawater	Hydrochemistry of salinized groundwater		BGC[1]		*EF*, fresh groundwater (BGC)		*MEF*, salinized groundwater	
			mg/kg		µg/L					0% f_S	0% f_S	1% f_S	7.5% f_S
	(sub)oxic conditions		*C_6+Q (L.S)*	*C_{4c}-C_5 (Dol. L.S)*	*S*	*L.S*	*Dol. L.S*	*L.S*	*Dol. L.S*	*L.S*	*Dol. L.S*	*L.S*	*Dol. L.S*
Na	Na^+	$NaAlSi_3O_8$	300	200	11569000	67450	183600	37700	11200	278.67	95.95	-13.55	-54.06
K	K^+	$KAlSi_3O_8$	400	200	467000	4000	7600	2400	1300	13.31	11.14	-0.32	-1.74
Ca	Ca^{2+}	$CaCO_3$, $CaMg(CO_3)_2$	290500	259500	460000	131000	114000	97100	64000	0.74	0.42	0.012	0.010
Mg	Mg^{2+}	$CaMg(CO_3)_2$	7100	78300	1300000	20500	45700	12700	28100	0.10	0.61	-0.01	0.01
Fe	Fe^{2+}	$Fe(OH)_3$, FeS_2	11600	1500	132	6	63	5	5	0.00	0.00	0.00	0.00
Si	H_4SiO_4	SiO_2	57800	38500	28	16830	8789	13318	5514	0.51	0.25	0.01	0.00
Al	$Al(OH)^{4-}$	clay minerals	10250	1900	21	3.7	2.9	2.0	2.0	0.00	0.00	0.00	0.00
As	AsO_4^{3-}	$Fe(OH)_3$	3.4	1.3	61.6	1.7	1.8	0.3	0.3	0.16	0.33	0.03	0.04
Ba	Ba^{2+}	$BaSO_4$, feldspar	76	8	8	83	70	51	8	1.50	1.45	0.04	0.78
Be	Be^{2+}	clay minerals	2.9	2.2	0.3	0.03	0.04	0.03	0.03	0.02	0.02	0.00	0.00
Co	Co^{2+}	FeS_2	3.4	0.7	0.5	0.11	0.05	0.03	0.03	0.02	0.06	0.00	0.01
Cr	CrO_4^{2-}	clay & heavy minerals	70	20	5.2	0.80	1.2	0.6	0.6	0.02	0.05	0.00	0.00
Cu	Cu^{2+}	clay & heavy minerals	19	2	12.5	2.5	2.1	0.9	0.9	0.11	0.77	0.01	0.09
Mo	MoO_4^{2-}	$Fe(OH)_3$, FeS_2	0.5	0.5	10.6	4.5	1.5	0.2	0.2	0.93	0.69	0.78	0.20
Ni	Ni^{2+}	FeS_2, $CaCO_3$	17.4	2.1	3.9	5.1	2.5	0.2	0.3	0.03	0.24	0.02	0.09
Pb	Pb^{2+}	$CaCO_3$ & clay minerals	2.1	1.8	0.5	0.3	0.3	0.3	0.3	0.31	0.29	0.00	0.00
Rb	Rb^+	clay minerals	5.0	2.4	124.9	2.7	2.9	1.0	0.5	0.44	0.36	0.02	0.01

Table 3.2 (continued)

TE	Predominant ionic form	Main aquifer source	Aquifer geochemistry		Seawater	Hydrochemistry of salinized groundwater		BGC[1]		*EF*, fresh groundwater (BGC)		*MEF*, salinized groundwater	
			mg/kg		µg/L					0% f_S	0% f_S	1% f_S	7.5% f_S
	(sub)oxic conditions		*C_6+Q (L.S)*	*C_{4c}-C_5 (Dol. L.S)*	*S*	*L.S*	*Dol. L.S*	*L.S*	*Dol. L.S*	*L.S*	*Dol. L.S*	*L.S*	*Dol. L.S*
Sr	Sr^{2+}	$CaCO_3$	649	148	7216	555	345	236	78	0.81	0.79	0.04	0.20
U	UO_2^{2+}	$Fe(OH)_3$	2.6	1.4	2.5	2.0	1.4	0.8	0.5	0.72	0.61	0.04	0.05
V	VO_4^{2-}	$Fe(OH)_3$	43.2	15.8	71.8	1.7	3.0	0.3	1.2	0.02	0.13	0.00	0.00
Zn	Zn^{2+}	clay & heavy minerals	35	7	19	117	146	3	4	0.21	1.05	0.28	2.92

(M)EF ≥ 0.01 = mobilization, *(M)EF* ≤ -0.01 = immobilization, and else = mobilization equilibrium. *MEF* is calculated for salinized groundwater, *EF* for BGC quality.
Concentrations of Au, Bi, Cd, Ce, Cs, Dy, Er, Eu, Ga, Gd, Hf, Hg, Ho, In, La, Lu, Nb, Nd, Pd, Pr, Pt, Re, Rh, Ru, Sb, Sm, Sn, Ta, Tb, Te, Th, Tl, Tm, Y, and Zr were < 0.05 µg/L in salinized groundwater, and hence their behavior could not be established.

NB: A difference in the mobilization of some elements (e.g. V) may arise when utilizing ancient clean seawater (e.g. > 40 years ago). This is due to slightly different concentrations of some major and trace elements (see Table S3.6, *Appendix S3*).

[1] Baseline Groundwater Concentration (BGC) derived by Khadra and Stuyfzand (2014).

3.3.5 Flow path reactive transport modeling results

Reactive transport simulations were performed along two flow paths following presumed saltwater intrusion lines: flow path 1 across the cultivation strip of the Damour village in the coastal plain via the C_6 limestone unit, and flow path 2 across the Naameh-Haret El Naameh villages (an area heavily stressed by groundwater abstraction) in the dolomitic limestone aquifer (C_{4c}-C_5) (see Figures 2.1 and 2.2). Flowlines start with the Mediterranean Sea water offshore, and invade the coast initially filled with the average groundwater composition (fresh-brackish) as recorded in 2002. The simulations are then allowed to run for 9 years to generate the year 2011 conditions. The chemistry of ambient groundwater and intruded seawater is provided in Table 3.3; physical and geochemical PHREEQC-2 parameters are provided in Table 3.4. Simulations involved ideal intrusion assuming uniform pumping in wells along the two flow paths (Figure 2.1) although in reality non-uniform extraction may produce irregular patterns where salinity may rise and fall before it stabilizes with fresh-brackish water.

Table 3.3 Hydrochemistry of intruding seawater and initial ambient groundwater used in PHREEQC-2 modeling along path 1 (limestone) and path 2 (dolomitic limestone); ions in mmol/L.

		Ca	Mg	Na	K	HCO_3	Cl	SO_4	pH
Mediterranean Sea water		11.5	53.5	505	12.0	2.7	575	33.3	7.93
Onshore groundwater	**path 1**	3.0	0.5	1.1	0.1	5.4	1.4	0.6	6.89
	path 2	4.9	0.7	2.8	0.1	5.4	5.0	1.1	6.68

Table 3.4 PHREEQC-2 forward dual porosity modeling physical and geochemical parameters. L.S = limestone; Dol. L.S = dolomitic limestone.

Flow path	L (m)	Δt (year)	Δx (m)	# of transport steps	# cells	ε_m	ε_{im}	v (m/d)	α_L (m)
1	1200	2.7e-01	10	33	241	0.008	0.08	0.10	11
2	1500	2.3e-01	5	40	601	0.03	0.12	0.06	30

Table 3.4 (continued)

Flow path	*CEC* (mol/kg H_2O)		Rock density (kg/L)		Mole fractions $Ca_{(x)}Mg_{(y)}Sr_{(z)}CO3$		
	mobile cells	immobile cells	L.S	Dol. L.S	Ca	Mg	Sr
1	0.005	0.1	2.70	--	1.00	0.00	0.0018
2	0.005	0.02	--	2.85	0.75	0.25	0.0003

ε_m values were fine-tuned to get a reasonable description of the observed ΔNa, ΔCa, ΔMg and ΔSr patterns (Figure 3.1).
ε_{im} relied on literature values.

The literature lacks data describing Cation Exchange Capacity (*CEC*) in karstified limestone and dolomitic limestone. The *CEC* of rocks in meq/kg is estimated here as 7×% clay + 35×% organic carbon (Appelo and Postma 2005). This equation may apply for the bulk rock; however, the effective *CEC* is expected to be lower especially for the mobile (fractured) sections of the dual porosity medium. Therefore, immobile and mobile cells were assigned different values in the 1-D dual domain reactive transport model. The initial values of CEC_{immobile} (23 to 65 meq/kg) relying on clay and organic carbon content were in reasonable agreement with the scarce literature on limestone (e.g. Gillespie et al. 2001; Ertas and Topal 2008) and dolomitic limestone (e.g. Gillespie et al. 2001; Topal and Kaya 2016), as obtained in the lab for rock samples. The CEC_{mobile} was initially assigned one order of magnitude lower than CEC_{immobile}. Due to higher porosity, *CEC* is higher in the matrix than in the mobile domain as it is expressed in meq/L (i.e. the porosity difference sets the *CEC* difference between mobile and immobile). In addition, concentrated and sometimes turbulent flow in the mobile zones (fissures, large diameter solution channels) may reduce the *CEC* due to polishing effects (reducing surface area), and perhaps by selective erosion of fines and more oxidation of organic material. Later both *CEC*s were fine-tuned to lower values by model optimization supported by sensitivity analysis in order to better represent actual *CEC*s in the natural environment.

Applying a 1-D dual porosity formulation, both mobile and stagnant zones were initially filled with fresh-brackish water. Later the seawater was allowed to intrude through advection along the selected flow paths. A constant inland groundwater velocity was assumed, estimated at 0.10 m/d along path 1 based on available hydraulic head and aquifer conductivity data, and 0.06 m/d for flow path 2, as deduced from the landward movement of the 250 mg/L chloride isoline between 2002 (Khadra 2003) and 2011 (Khadra and Stuyfzand 2014). Dispersivity was estimated based on Eq. 3.11, and then fine-tuned during the calibration process where necessary. Molecular diffusion could be neglected.

The *wateq4f.dat* database was used in PHREEQC-2 simulations to account for Mg-calcite, which is thermodynamically treated as a calcite-magnesite solid solution. This is applied to path 2 only via the dolomitic limestone aquifer. Moles of calcite and magnesite were deduced from the hosting rocks geochemistry (Table 3.1). Activity coefficients and mole fractions (Table 3.4) were used to calculate the dimensional Guggenheim parameters necessary to determine the activities of components in a non-ideal binary solid solution (Glynn and Reardon 1990). Pure $SrCO_3$ was also allowed to equilibrate with aqueous solution for both flow paths. The *CEC* estimated in meq/kg was converted into mol/kg of water as required for PHREEQC calculations. Sensitivity analysis (with 2 times lower/higher values) was performed to check the impact of CEC_{immobile} on the response of major ions. It confirmed the minor impact of CEC_{mobile} (Figure S3.2 and S3.3, *Appendix S3*). The model was capable to generate: (1) a reasonable description of the observed ΔNa, ΔCa, ΔMg and ΔSr patterns (Figure 3.1), and (2) a close match between simulated and observed concentrations in wells along the two flow paths (Figure 3.2). The results of simulation runs without cation exchange are also added to the same plots to show the

significance of this process. Figure 3.2a shows clear differences even for the closest observation whereas Figure 3.2b generally shows less changes.

The 1-D transport model along flow path 1 (via the C_6 limestone unit) over a 9-year period (from 2002 to 2011) shows Ca surplus (43 meq/L), and simultaneous Na, Mg and K deficit (Figures 3.2a and 3.3a). This pattern is typical for cation exchange during salinization. At the shoreline, the intruding Mediterranean Sea water (Table 3.3), supersaturated with respect to $CaCO_3$, induces calcite precipitation by desorbing Ca, and at ca. 35 m calcite dissolves (Figure 3.4a). This dissolution is probably driven by the mixing of freshwater and saltwater, which leads to undersaturation. It tends to concentrate at the freshwater side of the mixing zone or near the saline side at the discharge areas (Rezaei et al. 2005). Sr shows a similar response to Ca along this flow path; however, the strontium maturity index (Khadra and Stuyfzand 2014) pleads for no coprecipitation of Sr with $CaCO_3$. The decrease is therefore attributed to Sr sorption on exchange surfaces, being more in the limestone unit.

Flow path 2 (dolomitic limestone) (Figure 3.2b) shows three features which are clearly different from flow path limestone: (i) the peak of Ca surplus at the start of the intrusion zone; (ii) Mg being the key counter cation (whilst it is Na at flow path limestone), and (iii) a nearly suppressed response of Sr. The model simulates the formation of calcite-magnesite solid solution (Figure 3.4b) as induced by the high Mg:Ca ratio of intruding seawater (see Table S3.1 for Mg:Ca ratios in seawater and fresh water) according to the following reaction:

$$Ca_xMg_{(1-x)}CO_3 + yMg^{2+} \rightarrow Ca_{x-y}Mg_{(1-x+y)}CO_3 + yCa^{2+}$$

As a result, Ca is added while Mg is removed from groundwater. This mineral-water interaction process intensifies the impact of cation-exchange (Ca surplus vs. Mg deficit) along flow path dolomitic limestone. Note that the Mg deficit induces Mg desorption, and causes a lower fraction of the exchangeable Mg in the salinized zone compared to the fresh water zone, whereas this situation is opposite at flow path limestone (Figure 3.3). Noteworthy to mention that path 1 shows a shorter exchange zone although it has higher *CEC*. This is because the groundwater flow velocity along path 1 is 1.6 times higher than along path 2.

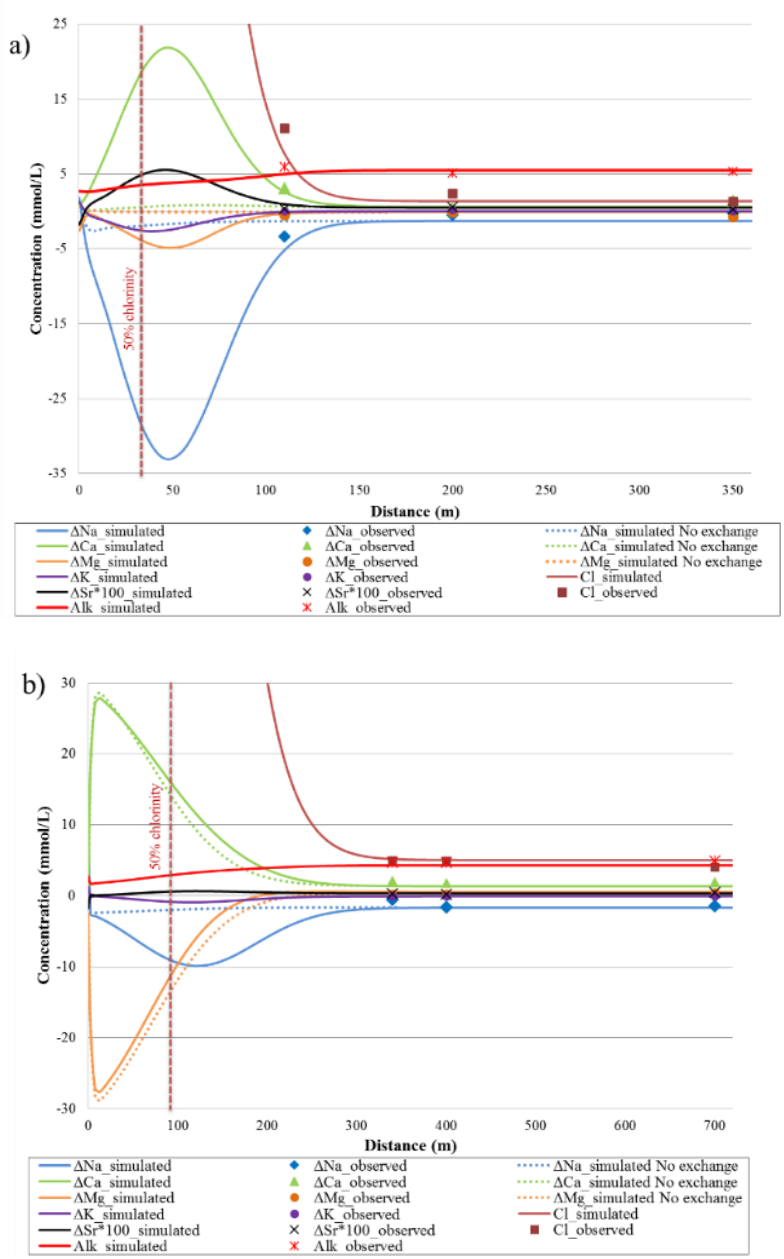

Figure 3.2 1-D dual porosity flow path simulations of the current (2011) conditions of advective transport of seawater along (a) path 1 into the C_6 unit (limestone), and along (b) path 2 into the C_{4c}-C_5 unit (dolomitic limestone). Path 2 considers a calcite-magnesite solid solution. Stagnant zones are modeled using first-order exchange approximations assuming dual-porosity medium. Negative values = depletion, positive values = enrichment; ΔNa, ΔCa, ΔMg, ΔK and ΔSr are calculated via Eq. 3.2. Vertical dashed red line is the 50% breakthrough point of seawater chlorinity. Dot-dashed lines show simulation results without cation exchange.

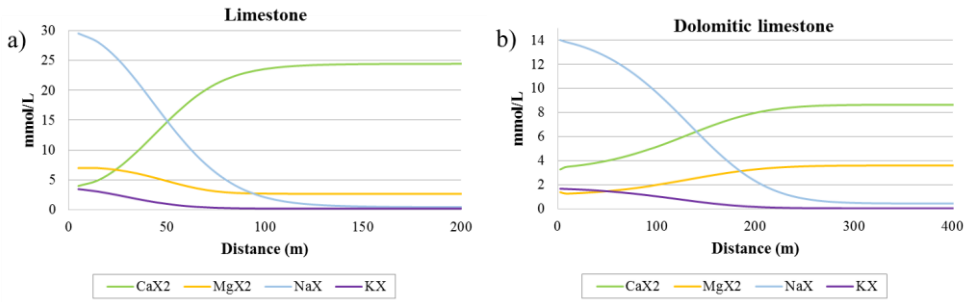

Figure 3.3 1-D dual porosity flow path simulations of the replacement of Na, Mg, Ca and K on the cation exchanger along (a) path 1 (limestone), and (b) path 2 (dolomitic limestone). Path 2 considers a calcite-magnesite solid solution.

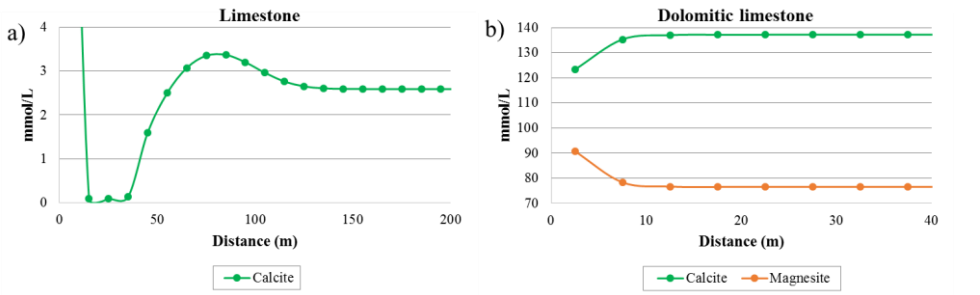

Figure 3.4 1-D dual porosity flow path simulations of calcite and magnesite along (a) path 1 (limestone), and (b) path 2 (dolomitic limestone), showing the spatial changes in the solid phase (e.g. the change of Ca in calcite and Mg in magnesite). Path 2 considers a calcite-magnesite solid solution.

3.4 Discussion

3.4.1 Hydrogeochemical disparities

The discussion here focuses on major hydrogeochemical differences between limestone and dolomitic limestone units in accordance to: (a) geochemical activity, and (b) salinity effects. This includes the main geochemical processes, and the response of major chemical constituents and trace elements in the salinized groundwater.

3.4.1.1 Main geochemical processes

The main discerned geochemical processes in the studied aquifers are carbonate ($Ca_xMg_ySr_zCO_3$) dissolution/precipitation, and typical cation exchange reactions in the saltwater mixing zone. The primary hydrochemical difference between samples from

limestone and dolomitic limestone consists of the contrasting ratios of Ca:Mg and Ca:Sr, for both the aquifer rock and water samples. Salinization of groundwater in the limestone coastal plain leads to more Ca mobilization compared to the dolomitic limestone. This is evidenced by a higher positive ΔCa (average ΔCa = 10.5 and 4.6 meq/L) (Figure 3.1) and *MEF* values (0.012‰ and 0.010‰) (Table 3.2) for the limestone and dolomitic limestone, respectively. Carbonate dissolution and cation exchange both contribute to the recorded mobilization. This is due to more Ca in the limestone hosting unit (36.3 wt.%) and probably its adsorption complex than in the dolomitic limestone (24.5 wt.%), in addition to higher pCO_2 characterizing the coastal plain region compared to the dolomitic limestone with less vegetation and a higher altitude of the recharge area.

On the other hand, seawater intrusion triggers a further Ca substitution by Mg of the dolomitic limestone, or the precipitation of a more dolomitic limestone, driven by the high Mg concentration compared to Ca, in the intruding seawater. Dolomitization or high Mg-calcite precipitation has been observed elsewhere with different Mg:Ca molar ratios (e.g. Whitaker and Smart 1993; Sacks and Tihansky 1996). This response at high salinity in the dolomitic limestone overwhelms cation exchange unlike the limestone unit where pure calcite precipitation/dissolution is stimulated by Na/Ca exchange and mixing of two water bodies with different pCO_2, respectively. Under fresh-brackish water conditions, Mg is released to solution in the dolomitic limestone (*MEF* = 0.01‰) exchanging (besides Ca) with Na and K. This behavior is different for the limestone where Mg (*MEF* = -0.01‰), Na and K exchange for Ca.

The data also reveals higher mobilization of Sr under freshwater conditions in the limestone unit (Table 3.2), which is attributed to more incorporation of Sr into $CaCO_3$. However, the *MEF* scores, contrary to the 1-D reactive transport model, indicate that SWI stimulates higher mobilization in the dolomitic limestone despite Sr lower concentrations in the hosting rocks, a difference not easy to explain.

Silica (quartz or opal) dissolution with slightly higher mobilization in the limestone unit, is probably due to more silica weathering from the overlying quaternary (Q) sand. The zero *MEF* data for Fe indicate that reactions such as pyrite oxidation or reductive iron hydroxide dissolution do not take place, as expected.

3.4.1.2 Behavior of trace elements

Based on statistical variances and the enrichment factors, the response of 15 TEs to SWI, and to geochemical contrast between limestone vs. dolomitic limestone shows the following traits:

1. *TEs in fresh groundwater: limestone versus dolomitic limestone*

   The concentrations of Ba, Rb, Sr and U in fresh groundwater are significantly higher in limestone than in dolomitic limestone, which is in line with their differences in geochemistry (Table 3.2). On the other hand, significant differences in geochemistry between both units (limestone higher), are not reflected in differences in the concentrations of Al, As, Co, Cr, Cu, Ni and Zn in natural background groundwater

(Table 3.2). Only V shows a reverse trend, notwithstanding lower contents of dolomitic limestone, the concentration in its groundwater is higher.

It can therefore be concluded that Ba, Rb, Sr and U are relatively mobile in limestone and are probably dissolving from it, whereas the other TEs are not. *EFs* for the background groundwater qualities of both units (Table 3.2) show immobilization for Al, Co and Cr, which matches their insoluble behavior in neutral water (Fishbein 1981; Edmunds and Smedley 1996; Drever 1997). As, Cu, Ni and Zn however are more mobilized in the dolomitic limestone as indicated by their higher *EF* values. (Hydro)oxides sorption surfaces explain this discrepancy because they form the main substrates for adsorption, and they are less dominant in the dolomitic limestone unit.

Previous studies on trace element enrichment in (dolomitic) limestone aquifers are scarce. Frondini et al. (2014), observed in the Sassolungo and Sella dolomite aquifer in Italy that Ba, Sr and U, and to a smaller extent Rb were enriched in its groundwater, which is in line with this study.

2. *TEs in salinized groundwater: limestone versus dolomitic limestone*

Concentrations of As, Ba, Cu, Ni, Rb, Sr and U increase by SWI in both units. It is likely that the higher salinity stimulates both their desorption (through a higher expelling power) and the dissolution of hosting minerals (through the higher ionic strength reducing the activity coefficients and increasing ion complexation). In addition, part of the mobilization could be attributed to the lower pH induced by salinity (see salinized groundwater in Table S3.1), since the higher Ca (due to Na/Ca exchange) eventually leads to $CaCO_3$ precipitation.

As and U reveal more mobilization in the limestone unit whereas the others are more enhanced in the dolomitic limestone (Table 3.2). As and Ni are mobilized although they occur at low levels in natural background water (< 0.4 µg/L) (Table 3.2). This behavior of arsenic, contrary to observations in fresh groundwater, is attributed to arsenate species initially adsorbing on oxyhydroxides at neutral pH (Drever 1997), but SWI later facilitates more mobilization. SWI also stimulates Ba and Sr mobilization either by cation exchange or dissolution from carbonate rocks (Sr) and barite or feldspars (Ba). The positive correlation of As, Ba and Sr with seawater intrusion has been observed in other aquifers as well (e.g. Mondal et al. 2010; Stuyfzand and Mendizabal 2010). *MEF* scores reveal higher mobilization of Ba and Sr in the salinized dolomitic limestone aquifer despite their lower concentrations in the hosting aquifers.

The observed differences in the behavior of Cu, Ni, Rb and U between the two units is justified by the same reasoning of their recorded discrepancies in freshwater.

3. *TEs independent of salinity and (dolomitic) limestone geochemical contrast*

Al, Be, Co, Cr, Pb and V show no significant signs of (im)mobilization ($-0.01 \leq MEF \leq 0.01$) for both limestone and dolomitic limestone, independently of salinity.

This response is attributed to their insoluble behavior in neutral and alkaline pH conditions (Fishbein 1981; Edmunds and Smedley 1996; Drever 1997) in addition to the high affinity of Be (WHO 2001), Pb (Hem 1992) and V (Luengo-Oroz et al. 2014) to adsorb on sediment surfaces. V is statistically interlinked to SWI in both units, but its relationship with intruding seawater is not clear due to the big contrast between recent and ancient seawater.

Statistical analyses also show that Mo and Zn are independent of salinity and (dolomitic) limestone geochemical contrast. However, their *MEF* scores reveal high mobilization in both units. This contradicts the Mo immobilization observed in salinizing anoxic sandy aquifers (Stuyfzand 1993b). Mo is known to mobilize in anoxic environments where reductive Fe dissolution controls Mo release to the aqueous solution (Bennett and Dudas 2003; Smedley et al. 2014; Pichler and Mozaffari, 2015). However, this scenario is irrelevant here due to dominance of oxidizing conditions. In fact, Mo levels record a progressive increase down the flow gradient. In this case, the mobilization of Mo may be attributed to alkaline pH conditions and subsequent desorption from Mo-rich minerals (e.g. Fe or Al oxides). This response is due to low retention of Mo on solid surfaces at pH > 5 (Goldberg and Forster 1998; Carroll et al. 2006), and a function of groundwater residence time (Smedley et al. 2014). A similar behavior has been observed elsewhere (e.g. Smedley and Edmunds 2002). The higher Fe and Al content of the limestone hosting unit (Tables 3.1 and 3.2) explains its higher Mo mobilization compared to the dolomitic limestone.

The behavior of Zn could be related to bias due to its corrosion from wells with old galvanized iron pipes. Low levels of Pb in groundwater supports this hypothesis because of its affinity to adsorb on iron and form lead-iron scales (HDR 2009).

3.4.1.3 TEs permissible levels

TEs in groundwater normally occur at very low concentrations. They are harmful only when permissible levels are exceeded. In general, two main natural causes potentially raise TEs in coastal groundwaters: (1) water-rock interactions, and (2) saltwater intrusion. The latter has more versatile effect due to direct seawater mixing or enhanced mobilization. In this study, the collected data shows that TEs have increased by few µg/L only. All TEs including heavy metals (e.g. copper, lead and zinc) are still below permissible drinking water levels in accordance to the best recognized standards (EU 1998; US EPA 2008; WHO 2008) (Table S3.7, *Appendix S3*). They reveal satisfactory results even for the brackish water samples. Hence, it is obvious that the dissolution of (dolomitic) limestone carbonate rocks contributes very little to TEs in groundwater (Sr excluded, but there are no quality standards for Sr), and the impact of moderate SWI is not as bad as for some main constituents (e.g. Na, Cl and Ca). In the study area, TEs pose no health concern to date, but progressive salinization may lead to unfavorable shifts.

3.5 Conclusions

Four lines of research were followed in this paper to assess water quality differences between limestone and dolomitic limestone aquifers disturbed by saltwater intrusion (SWI) in coastal areas. These included: (1) nonparametric statistical tests on 4 water groups (limestone and dolomitic limestone with and without salinization); (2) ionic shifts of major chemical constituents from ideal freshwater-seawater mixing; (3) a new parameter called Mixing Enrichment Factor (*MEF*) to assess the (im)mobilization of trace elements (TEs) and main constituents under mixing conditions; and (4) 1-D dual porosity flow path PHREEQC reactive transport simulations. This multiple approach was applied to a moderately salinizing coastal aquifer system in Lebanon (Eastern Mediterranean) where main hydrochemical disparities between limestone and dolomitic limestone were revealed. The discussion focused on 8 major chemical constituents (Na, K, Ca, Mg, SO_4, TIC, Fe and Si), and 15 trace elements (Al, As, Ba, Be, Co, Cr, Cu, Mo, Ni, Pb, Rb, Sr, U, V and Zn). 35 other TEs were analyzed, but were excluded from the comparison because of very low concentrations (< 0.05 µg/L). Some of them such as Ce, Nb, Nd, Y and Zr had significant levels in the hosting rocks (1 to 50 ppm), but remained below detection in the salinized water samples preventing final conclusions about any (im)mobilization.

Two main chemical processes explained the non-conservative behavior of the major constituents in both limestone and dolomitic limestone units. These are the dissolution of $Ca_xMg_ySr_zCO_3$ and cation exchange spurred by saltwater intrusion. The dolomitic limestone unit showed less carbonate dissolution due to a lower unsaturated zone pCO_2 connected with less vegetation and a higher altitude of the recharge area, and a lower cation exchange capacity compared to limestone. The presence of high Mg-calcite raised the Mg levels in groundwater, and enhanced the Mg participation (besides Ca) in the exchange for Na and K. Fe revealed no difference between the two aquifers. Silica (quartz or opal) showed more mobilization in the limestone unit, which is probably dictated by more dissolution in the overlying quaternary sand-rich unit, and therefore does not contribute to the geochemical contrast between both aquifers.

As, Ba, Cu, Ni, Rb, Sr and U revealed the strongest mobilization among the investigated TEs during saltwater intrusion under calcareous (sub)oxic conditions. Zn is presumably biased by corrosion of well materials, and the apparent Mo mobilization is independent of SWI and (dolomitic) limestone geochemical contrast.

Besides the stimulating role of SWI, the geochemical contrast between limestone and dolomitic limestone proved to be an important factor explaining part of the observed variation in the concentration of TEs in fresh groundwater. For example, As, Cu and Ni recorded stronger mobilization in the freshwater dolomitic limestone, whereas Ba, Rb, Sr and U were more mobilized in the limestone unit. Other elements such as Al, Be, Co, Cr, Pb and V showed no (im)mobilization in either rock type. The observed TE discrepancy between the limestone and dolomitic limestone units is geochemically mainly linked to the higher Sr content of limestone, and higher content of clay minerals and iron (hydro)oxides in the limestone unit.

To conclude, it was demonstrated that: (1) the geochemical contrast between the limestone and dolomitic limestone aquifers do have an effect on the behavior of some major constituents and TEs, (2) carbonate rocks do not form a significant geogenic sources of TEs (Sr excluded), (3) the mobilization of TEs by salinization is small compared to the enhanced concentration rise produced by direct seawater mixing, and (4) the current TEs levels in the studied aquifer are far below the drinking water limits, thanks to a moderate salinization to date. Their current levels pose no concern nowadays, a situation that should not be taken for granted if excessive pumping persists.

Acknowledgements Prof. Dr. Thomas Pichler and one anonymous reviewer are highly appreciated for their constructive comments and suggestions that helped to improve this manuscript. We would like also to thank agricultural engineer Mr. Khaled Aoun for his continuous aid in data gathering. The unlimited cooperation of Mr. Abed El-Hadi Mezher, from the municipality of Naameh, is acknowledged as well.

Appendix S3: Supplementary Material

Table S3.1 Median composition of the groundwater bodies hosted by the dolomitic limestone (C_{4c}-C_5) and the limestone (C_6-Q) units, which are either fresh (without SWI) or salinized (with SWI) (adapted from Khadra and Stuyfzand, 2014).

	EC 25ºC	Temp.	pH	Cl^-	SO_4^{2-}	HCO_3^-	NO_3^-	P	Na^+	K^+	Ca^{2+}	Mg^{2+}	Fe	Mn	NH_4^+	SiO_2	O_2	δ^2H	$\delta^{18}O$
	µS/cm	*ºC*	-	*mg/L*														*‰*	
Detection limit				*1*	*1*	*1*	*1*	*0.02*	*0.05*	*0.05*	*0.05*	*0.05*	*0.01*	*5 × 10⁻⁵*	*0.1*	*0.04*	*0.01*		
C_{4c}-C_5 fresh	539	20.2	7.13	27.4	16.5	337	2.0	0.103	11.7	1.5	80.50	29.9	<0.01	0.001	<0.1	11.8	4.7	-26.36	-5.84
C_6-Q fresh	803	22.1	6.89	86.2	92.9	328	7.0	0.089	57.7	3.5	119.36	15.3	<0.01	0.001	<0.1	37.2	4.5	-25.06	-5.53
C_{4c}-C_5 salinized	4561	21.9	7.05	1412.0	209.7	305	6.4	0.318	640.5	28.5	160.65	131.6	0.018	0.002	<0.1	15.3	4.5	-22.10	-4.95
C_6-Q salinized	1304	21.8	6.75	248.6	98.9	351	8.4	0.315	93.8	5.1	189.1	24.0	0.006	0.002	<0.1	40.3	4.5	-23.93	-5.42
Mediterranean Sea	45600	-	7.93	20400	3200	165	4.0	0.510	11600	470	460	1300	0.13	0.002	-	0.06	5.0	7.61	0.95

Table S3.1 (continued)

	Al	As	B	Ba	Br	Cr	Cu	Ge	La	Li	Mo	Ni	Pb	Pd	Rb	Sb	Sc	Sr	U	V	Zn
	µg/L																				
Detection limit	*1*	*0.5*	*5*	*0.05*	*5*	*0.5*	*0.1*	*0.05*	*0.01*	*0.1*	*0.1*	*0.2*	*0.1*	*0.2*	*0.01*	*0.05*	*1*	*0.01*	*0.02*	*0.2*	*0.5*
C_{4c}-C_5 fresh	2	<0.5	30	9.5	100	0.6	0.9	<0.05	<0.01	1.5	0.3	0.3	0.3	<0.2	0.6	<0.05	1.0	107	0.57	1.2	7.6
C_6-Q fresh	5	1.3	104	82.0	1255	0.9	3.1	0.200	0.01	2.3	3.4	3.1	0.3	<0.2	1.9	0.2	2.8	459	1.98	1.5	96.0
C_{4c}-C_5 salinized	3	5.8	551	135.0	6203	1.0	5.6	0.100	0.03	13.7	3.0	4.4	0.4	0.4	10.3	0.4	1.9	1203	2.14	6.0	413.6
C_6-Q salinized	3	1.5	236	100	1880	1.1	5.2	0.033	0.01	2.9	0.6	5.2	0.4	0.1	2.0	0.2	3.7	469	2.6	2.4	28.4
Mediterranean Sea	21	61.6	3750	7.5	82200	5.2	12.5	0.25	0.07	143.0	10.6	3.9	0.5	1.0	125.0	0.22	5.0	7200	2.55	72.0	18.5

For all groundwater bodies,

- Ce, Cs, Dy, Er, Eu, Gd, Ho, In, Lu, Nb, Nd, Pr, Pt, Re, Rh, Tb, Tl, Tm, Y, Yb < 0.01 µg/L.
- Co, Hf, Sm, Ta, Zr < 0.02 µg/L, Ag, Au, Be, Bi, Cd, Ga, Ru, Sn, Te, Th, W < 0.05 µg/L.
- Hg < 0.1 µg/L.
- Ti < 10 µg/L.

Table S3.2 Analyzed elements and oxides, relevant methods of analyses, and minimum detection limits (MDLs). XRF = X-ray fluorescence; ICP-MS = inductively coupled plasma mass spectrometry; ICP-ES = inductively coupled plasma emission spectroscopy.

	MDL	Method		MDL	Method
SiO_2	0.01%	XRF	Pb	0.1 ppm	ICP-MS
Al_2O_3	0.01%	XRF	Rb	0.1 ppm	ICP-ES
Fe_2O_3	0.01%	XRF	Sb	0.1 ppm	ICP-MS
CaO	0.01%	XRF	Se	0.5 ppm	ICP-MS
MgO	0.01%	XRF	Sn	1 ppm	ICP-ES
Na_2O	0.01%	XRF	Sr	0.5 ppm	ICP-ES
K2O	0.01%	XRF	Ta	0.1 ppm	ICP-ES
MnO	0.01%	XRF	Th	0.2 ppm	ICP-ES
TiO2	0.01%	XRF	Tl	0.1 ppm	ICP-MS
P2O5	0.01%	XRF	U	0.1 ppm	ICP-ES
Cr_2O_3	0.00%	XRF	V	8 ppm	ICP-ES
Ba	0.01%	XRF	W	0.5 ppm	ICP-ES
LOI	0.10%	XRF	Y	0.1 ppm	ICP-ES
Au	0.5 ppb	ICP-MS	Zn	1 ppm	ICP-MS
Ag	0.1 ppm	ICP-MS	Zr	0.1 ppm	ICP-ES
As	1 ppm	ICP-MS	La	0.1 ppm	ICP-ES
Ba	1 ppm	ICP-ES	Ce	0.1 ppm	ICP-ES
Be	1 ppm	ICP-ES	Pr	0.02 ppm	ICP-ES
Bi	0.1 ppm	ICP-MS	Nd	0.3 ppm	ICP-ES
Cd	0.1 ppm	ICP-MS	Sm	0.05 ppm	ICP-ES
Co	0.2 ppm	ICP-ES	Eu	0.02 ppm	ICP-ES
Cs	0.1 ppm	ICP-ES	Gd	0.05 ppm	ICP-ES
Cu	0.1 ppm	ICP-MS	Tb	0.01 ppm	ICP-ES
Ga	0.5 ppm	ICP-ES	Dy	0.05 ppm	ICP-ES
Hf	0.1 ppm	ICP-ES	Ho	0.02 ppm	ICP-ES
Hg	0.1 ppm	ICP-MS	Er	0.03 ppm	ICP-ES
Mo	0.1 ppm	ICP-MS	Tm	0.01 ppm	ICP-ES
Nb	0.1 ppm	ICP-ES	Yb	0.05 ppm	ICP-ES
Ni	0.1 ppm	ICP-MS	Lu	0.01 ppm	ICP-ES

Table S3.3 The detailed chemical composition of all sampled rocks based on XRF and ICP-MS/ES results.

			wt %								PPM					
Unit	**Sample label**	**BOM**	**Ca**	**Mg**	**Na**	**K**	**Si**	**Fe**	**Al**	**Mn**	**As**	**Ba**	**Be**	**Ce**	**Co**	**Cr**
Q	3	2.1	28.16	0.37	0.02	0.08	10.33	1.74	1.11	0.031	2.7	39	<1	11.6	4.6	41
Q	4	2.4	29.24	0.54	0.01	0.05	8.32	2.74	0.87	0.023	5.2	35	<1	9.7	7.8	34
Q	5	2.7	28.21	0.40	0.01	0.08	9.58	1.92	1.38	0.031	3.6	49	1	13.7	4.4	34
Q	52	0.6	24.05	4.29	0.04	0.05	9.68	1.26	0.77	0.023	2.7	35	5	10.1	3.9	34
Q	53	2.1	28.60	0.34	0.04	0.05	8.42	1.44	1.72	0.015	3.6	163	5	17.5	4.4	130
C_6	1	1.1	37.10	0.16	0.02	0.02	1.68	0.34	0.67	<0.01	4.2	42	<1	6.7	0.8	68
C_6	2	1.0	36.85	0.16	0.03	0.02	1.96	0.38	0.77	<0.01	3.9	44	<1	7.9	1.2	55
C_6	10	1.4	36.51	0.25	0.01	0.00	2.10	0.52	0.88	<0.01	3.5	38	1	8	2	89
C_6	11	1.9	35.48	0.24	<0.01	0.00	2.48	0.77	1.03	<0.01	5.7	39	2	9.1	2	96
C_6	12	1.6	36.01	0.25	0.01	0.00	2.38	0.45	0.98	<0.01	1.5	38	<1	8.7	2	116
C_6	24	1.2	36.05	0.26	<0.01	0.01	2.52	0.59	0.98	<0.01	3.4	52	<1	8.9	2	82
C_6	26	0.7	38.27	0.19	<0.01	0.00	1.12	0.25	0.45	<0.01	0.6	33	<1	4.9	1.9	34
C_6	54	0.6	33.72	0.34	0.05	0.02	4.07	0.72	1.25	<0.01	2.6	411	3	12.1	2.3	185
C_{4c}-C_5	6	0.6	39.35	0.32	<0.01	0.00	0.23	0.24	0.14	<0.01	1	3	<1	1.4	<0.2	14
C_{4c}-C_5	7	0.5	39.59	0.34	<0.01	0.00	0.09	0.19	0.05	0.008	0.5	2	<1	1	0.7	14
C_{4c}-C_5	8	3.4	7.64	1.44	0.01	0.03	34.55	0.30	0.10	0.008	1.2	19	2	0.7	0.2	21
C_{4c}-C_5	9	0.1	23.37	11.69	0.02	0.02	0.84	0.15	0.26	<0.01	1.1	7	1	2.9	0.7	14
C_{4c}-C_5	13	0.1	24.00	11.44	0.02	0.02	0.47	0.10	0.20	<0.01	0.5	10	1	2.4	<0.2	21
C_{4c}-C_5	14	0.1	26.75	9.54	0.02	0.02	0.42	0.13	0.17	<0.01	1.7	23	<1	2.1	1.1	41
C_{4c}-C_5	15	0.4	24.35	11.39	0.01	0.00	0.47	0.12	0.21	<0.01	1.1	4	<1	2	<0.2	34
C_{4c}-C_5	16	0.1	22.57	12.56	<0.01	0.00	0.56	0.12	0.24	<0.01	0.7	5	<1	2.8	0.3	68
C_{4c}-C_5	17	0.1	35.52	2.97	0.01	0.02	0.65	0.10	0.19	<0.01	0.6	8	<1	2.3	0.6	14
C_{4c}-C_5	18	0.1	36.33	2.58	<0.01	0.00	0.47	0.08	0.13	<0.01	<0.5	4	<1	2.1	0.7	7
C_{4c}-C_5	19	0.2	25.15	3.83	0.01	0.04	10.89	0.08	0.13	<0.01	0.6	14	<1	1.7	<0.2	14
C_{4c}-C_5	20	0.1	23.99	11.37	0.02	0.02	0.89	0.10	0.17	<0.01	<0.5	7	<1	2.2	0.6	<1
C_{4c}-C_5	21	2.4	2.09	0.96	0.04	0.03	41.89	0.17	0.12	<0.01	<0.5	9	3	0.9	0.5	14
C_{4c}-C_5	22	0.1	24.56	11.31	<0.01	0.00	0.19	0.09	0.10	<0.01	<0.5	3	1	1	0.4	<1
C_{4c}-C_5	23	0.1	24.69	11.28	<0.01	0.00	0.19	0.06	0.08	<0.01	<0.5	4	<1	1	0.4	21
C_{4c}-C_5	25	0.4	25.94	10.02	0.03	0.01	0.28	0.03	0.05	<0.01	<0.5	11	<1	1.1	0.5	14
C_{4c}-C_5	27	0.1	24.05	11.48	<0.01	0.00	0.19	0.05	0.08	<0.01	<0.5	4	<1	1	0.8	<1
C_{4c}-C_5	28	0.1	30.11	7.17	0.01	0.02	0.47	0.13	0.20	<0.01	<0.5	8	<1	1.4	0.8	27
C_{4c}-C_5	48	0.1	24.28	11.41	0.01	0.02	0.23	0.06	0.10	<0.01	<0.5	4	<1	1	0.4	<1

Table S3.3 (continued)

			wt %								PPM					
Unit	**Sample label**	**BOM**	**Ca**	**Mg**	**Na**	**K**	**Si**	**Fe**	**Al**	**Mn**	**As**	**Ba**	**Be**	**Ce**	**Co**	**Cr**
C_{4c}-C_5	49	0.1	24.15	11.38	0.02	0.03	0.42	0.08	0.20	<0.01	<0.5	6	3	1.7	0.5	7
C_{4c}-C_5	50	0.1	25.61	10.80	<0.01	0.00	0.09	0.06	0.04	<0.01	<0.5	3	<1	0.3	0.2	27
C_{4c}-C_5	51	0.1	39.70	0.40	<0.01	0.00	0.09	0.02	0.03	<0.01	<0.5	3	3	0.8	0.3	<1
C_{4c}-C_5	55	0.1	23.50	11.58	0.01	0.01	0.42	0.08	0.16	<0.01	0.7	12	<1	2.3	0.5	14
C_{4c}-C_5	56	0.0	25.88	9.08	0.03	0.03	1.26	0.42	0.32	0.008	4	15	<1	3.6	1.9	21
C_{4c}-C_5	57	0.1	21.23	9.90	0.01	0.02	6.26	0.13	0.13	0.008	1	4	<1	1.7	1.1	21
C_{4c}-C_5	58	0.1	21.99	10.85	0.04	0.07	2.76	0.40	0.74	0.039	3.5	13	3	8.4	2.4	34
C_{4c}-C_5	59	0.1	36.70	0.65	0.04	0.02	2.01	0.42	0.69	<0.01	1.7	12	<1	4.3	1	34
C_{4c}-C_5	65	0.1	23.52	11.53	0.01	0.02	0.51	0.13	0.18	0.008	0.6	6	3	2.3	0.9	14
C_{4b}	29	2.7	34.85	1.10	0.02	0.06	2.48	0.96	0.93	<0.01	8.6	19	1	3.8	2.8	198
C_{4b}	63	6.6	26.39	1.36	0.02	0.59	7.67	1.65	2.78	0.008	6.1	46	<1	11.2	3.9	82
C_{4b}	64	0.7	38.16	0.48	0.02	0.03	1.12	0.20	0.38	<0.01	0.9	12	3	2.5	1.3	27
C_{4a}	30	0.1	21.85	12.27	0.02	0.02	1.31	0.50	0.46	0.008	3.5	5	<1	3.8	2.8	123
C_{4a}	31	0.1	22.19	12.60	<0.01	0.00	0.47	0.15	0.20	<0.01	1.3	7	<1	2.8	1.6	21
C_{4a}	32	0.1	22.42	12.64	<0.01	0.00	0.42	0.08	0.16	0.008	0.7	6	1	1.7	0.6	14
C_{4a}	33	0.1	22.87	12.42	<0.01	0.00	0.14	0.08	0.06	0.008	0.7	2	<1	1.2	0.9	<1
C_{4a}	34	0.1	20.75	12.27	0.01	0.02	1.82	0.72	0.64	0.008	2.5	7	2	5.1	1.7	27
C_{4a}	35	0.1	21.78	12.81	0.01	0.02	1.03	0.29	0.28	0.008	0.5	5	<1	3.2	1.2	21
C_{4a}	36	0.1	21.56	12.69	0.01	0.02	1.03	0.30	0.29	0.008	<0.5	5	3	3.4	1.6	<1
C_{4a}	37	0.1	21.89	11.87	0.02	0.02	1.17	0.44	0.43	0.008	0.9	9	<1	3.1	1.7	41
C_{4a}	38	0.1	21.11	12.48	0.01	0.05	1.31	0.44	0.53	<0.01	2.4	4	<1	4.5	1.5	27
C_{4a}	39	0.1	20.34	11.92	0.04	0.25	2.34	0.78	0.97	<0.01	4.7	14	<1	8.2	3.2	21
C_{4a}	40	1.1	15.23	9.19	0.06	1.13	7.81	2.04	3.26	0.008	5.9	45	5	22.9	4.8	75
C_{4a}	41	0.1	21.89	12.96	<0.01	0.01	0.47	0.10	0.15	<0.01	<0.5	4	<1	1.6	0.9	<1
C_{4a}	42	0.1	24.37	11.66	<0.01	0.00	0.09	0.02	0.04	<0.01	<0.5	4	2	0.5	0.3	<1
C_{4a}	43	0.1	22.31	13.12	<0.01	0.00	0.14	0.03	0.04	<0.01	<0.5	3	<1	0.6	0.6	48
C_{4a}	44	0.1	30.01	6.77	<0.01	0.00	0.98	0.11	0.17	<0.01	0.9	11	<1	1.6	1.4	14
C_{4a}	45	0.1	21.99	12.65	0.01	0.02	0.89	0.14	0.29	<0.01	0.7	7	<1	2.4	1.5	14
C_{4a}	46	0.1	22.24	12.96	<0.01	0.00	0.42	0.10	0.16	<0.01	1.6	4	<1	1.3	1	<1
C_{4a}	47	0.1	31.74	5.22	0.02	0.02	0.89	0.34	0.39	<0.01	3.8	18	<1	3	1.8	<1
C_{4a}	60	0.1	22.73	12.17	0.02	0.02	0.61	0.18	0.22	0.008	2.6	8	3	2.5	0.4	7
C_{4a}	61	0.1	21.26	11.95	0.04	0.15	1.87	0.37	0.73	<0.01	2.7	20	<1	5.6	0.7	34
C_{4a}	62	0.1	21.84	11.75	0.04	0.13	1.59	0.41	0.64	<0.01	3	20	<1	6.3	1.1	21

Table S3.3 (continued)

		PPM															
Unit	**Sample #**	**Cu**	**Ga**	**La**	**Mo**	**Nb**	**Nd**	**Ni**	**Pb**	**Rb**	**Sr**	**U**	**V**	**Y**	**Yb**	**Zn**	**Zr**
Q	3	6.6	2.4	7.9	0.6	5.2	7.6	11	1.5	7.1	224	1.2	41	9.2	0.63	18	49.2
Q	4	6.7	1.8	6.8	0.4	3.5	5.7	17.4	1.4	5.3	200	1.2	52	7.7	0.56	33	38.5
Q	5	8.5	3.2	7.8	0.4	6.4	7.8	10.4	1.9	9.4	218	1.5	49	8.2	0.86	21	52
Q	52	4.4	1.3	5.7	0.3	2.9	4.2	8.4	4.4	4.5	174	1.8	22	6.6	0.64	13	58.6
Q	53	25.2	3.5	14.5	0.2	4.5	10.7	28.4	3.2	6.5	761	4.9	47	23.2	1.59	64	49.1
C_6	1	11.2	1.5	11.3	0.2	1.3	7	5.8	2.3	3.7	978	1.9	38	16.6	0.95	32	14.5
C_6	2	21.8	1.7	10.1	0.2	2.2	5.8	8.4	1.8	3.8	1133	2.3	36	15	1.05	32	17.7
C_6	10	28.9	1.8	8.8	0.6	1.3	6.5	25.5	1.9	3.2	824	2.6	53	15.8	1.08	37	17.5
C_6	11	41.4	2.1	10.4	1.4	1.5	6.7	40.3	2	3.9	972	3.3	67	17.3	1.13	56	19.6
C_6	12	31.3	1.7	10.3	0.3	1.9	8.1	14	1.7	3.9	903	3	50	17	1.06	33	17.6
C_6	24	37.5	2	12.2	0.3	1.7	8.6	18.4	1.4	4.5	1017	2.3	46	18.4	1.14	41	21.3
C_6	26	11.8	0.6	7.4	0.1	0.7	4.8	5.4	0.9	2	929	1.2	20	10.9	0.53	13	11.6
C_6	54	34.9	2.2	13.3	1.3	1.9	8.8	40.1	2	2.8	1100	7.9	44	23.7	1.51	81	22.7
C_{4c}-C_5	6	0.7	<0.5	1.6	0.3	0.4	1.5	<0.1	0.4	1	179	1.1	16	1.4	<0.05	8	5.3
C_{4c}-C_5	7	0.3	<0.5	1.1	0.2	0.4	0.5	<0.1	0.3	0.5	199	1.3	14	1.2	0.06	3	2.3
C_{4c}-C_5	8	3.2	<0.5	0.7	0.1	0.6	0.5	1.3	29.7	0.9	31	0.4	<8	0.6	<0.05	26	3.7
C_{4c}-C_5	9	2	<0.5	1.9	<0.1	0.8	1.8	1	2.7	4.5	142	1	16	1.8	0.16	9	7.8
C_{4c}-C_5	13	3.5	<0.5	2.1	0.1	0.7	0.9	4.1	0.9	3.2	189	2.7	12	1.8	0.16	12	4.4
C_{4c}-C_5	14	5.6	<0.5	1.9	0.1	0.1	1.3	4.9	1.2	2.6	194	2.6	19	2.5	0.15	19	4.4
C_{4c}-C_5	15	2.7	<0.5	1.4	0.2	0.7	0.9	0.6	0.5	3.2	87	1.1	12	1.1	0.12	4	5.7
C_{4c}-C_5	16	1.7	<0.5	1.9	<0.1	1.2	1.8	1.6	0.4	3.7	95	1	13	1.8	0.12	10	7
C_{4c}-C_5	17	1.4	<0.5	1.6	<0.1	0.7	1.2	<0.1	0.8	3	223	0.8	10	1.5	0.17	4	5.6
C_{4c}-C_5	18	0.9	<0.5	1.3	<0.1	0.2	1.1	<0.1	0.4	2.2	241	1.2	11	1.3	0.13	3	5.1
C_{4c}-C_5	19	2.2	<0.5	1	<0.1	1.1	0.5	1.1	0.3	1.7	72	0.5	<8	0.8	<0.05	3	7
C_{4c}-C_5	20	1.2	<0.5	1.6	<0.1	0.3	1.6	0.5	0.6	3.1	156	0.4	<8	1.2	0.1	6	6.2
C_{4c}-C_5	21	0.6	<0.5	0.6	<0.1	0.9	0.7	1.1	0.2	1	28	0.3	<8	0.6	0.06	1	5.6
C_{4c}-C_5	22	1.1	<0.5	0.6	0.2	0.2	0.7	1.2	0.6	1.1	167	3.1	20	0.5	0.09	6	2.1
C_{4c}-C_5	23	0.9	<0.5	0.6	0.2	0.1	0.5	1.1	0.4	1.3	167	2.4	20	0.4	0.05	4	1.2
C_{4c}-C_5	25	1.9	<0.5	1.3	<0.1	0.4	0.8	0.6	0.5	0.6	168	2.4	9	1.7	0.13	5	10.6
C_{4c}-C_5	27	1	<0.5	0.7	<0.1	0.1	0.4	1.1	0.5	1.1	171	0.6	<8	0.7	<0.05	4	2.2
C_{4c}-C_5	28	2.8	<0.5	1	<0.1	0.2	1.1	2.2	0.7	1.9	107	0.7	11	0.9	0.09	6	4.4
C_{4c}-C_5	48	0.7	<0.5	0.7	1.1	<0.1	0.4	1.3	0.3	1.4	159	2.7	11	0.5	0.07	3	2.1
C_{4c}-C_5	49	1.5	<0.5	0.9	3.5	0.4	0.5	0.8	0.6	3	161	2.8	23	0.6	<0.05	2	3.4
C_{4c}-C_5	50	1.2	<0.5	0.2	0.1	<0.1	<0.3	0.6	2.4	0.5	143	2.8	17	0.3	<0.05	5	1.5
C_{4c}-C_5	51	0.6	<0.5	0.3	<0.1	<0.1	<0.3	<0.1	1.5	0.5	175	1.6	18	0.3	0.07	2	0.6

Table S3.3 (continued)

		PPM															
Unit	**Sample #**	**Cu**	**Ga**	**La**	**Mo**	**Nb**	**Nd**	**Ni**	**Pb**	**Rb**	**Sr**	**U**	**V**	**Y**	**Yb**	**Zn**	**Zr**
C_{4c}-C_5	55	1.5	<0.5	2.8	0.1	0.3	1.8	1.7	0.4	1.8	169	1.3	21	2.3	0.06	5	4.5
C_{4c}-C_5	56	7.1	<0.5	3	0.1	0.7	2.4	6.2	1.7	3	129	0.8	19	3.2	0.16	8	8.5
C_{4c}-C_5	57	3	<0.5	1.2	<0.1	1.3	1.1	3.1	0.8	1.2	115	0.8	12	1.4	<0.05	9	3.4
C_{4c}-C_5	58	4.5	0.9	5	<0.1	2.2	3.2	8.4	1.3	9.8	147	1.5	22	4.6	0.33	9	23.6
C_{4c}-C_5	59	1.7	0.6	2.4	<0.1	1.1	2.5	0.7	0.5	7.5	204	1.9	27	1.8	0.22	5	10.7
C_{4c}-C_5	65	1.6	<0.5	1.6	<0.1	0.8	1.2	2.9	0.7	2.3	121	0.7	10	1.8	0.1	7	4
C_{4b}	29	10.2	1.8	2.3	0.5	3.7	1.5	18.8	1.6	16.4	76	1.3	62	1.1	0.14	12	30.4
C_{4b}	63	10.2	5.2	7.7	0.2	5.4	3.6	11	1	32.8	75	1.1	128	3.9	0.44	19	41
C_{4b}	64	2.3	<0.5	2.1	<0.1	0.9	1.6	<0.1	0.3	4	227	2.1	12	1.8	0.14	6	6.8
C_{4a}	30	3.5	<0.5	1.9	0.5	1.7	1.8	10	0.6	6.4	107	2.1	37	1.3	0.15	7	13.6
C_{4a}	31	1.3	<0.5	1.5	0.5	0.6	1.1	4.1	0.4	2.9	124	1.6	12	1.4	0.1	3	6.1
C_{4a}	32	1.6	<0.5	1	0.5	0.3	1	2.7	0.3	2.6	127	2.3	18	0.5	0.08	2	4.6
C_{4a}	33	1	<0.5	0.7	0.5	<0.1	0.7	2.5	0.3	0.8	168	2.1	10	0.6	0.05	2	2.5
C_{4a}	34	3	1.3	2.5	0.2	2.2	2.2	7	1.5	6.8	81	1	27	2.2	0.22	5	20.7
C_{4a}	35	1.2	<0.5	1.6	0.3	1.2	1.4	4.5	0.8	3.8	73	0.8	12	1.2	0.2	4	19.8
C_{4a}	36	1.3	<0.5	2.3	0.2	1.6	1.9	4.4	1.1	4.2	76	1	16	1.6	0.21	5	21.7
C_{4a}	37	1.5	0.5	1.7	0.1	1.7	1.2	5.7	0.8	6.4	129	0.7	20	1.3	0.22	3	14.3
C_{4a}	38	2.6	0.6	2.3	0.2	1.9	3.4	7	0.7	4.3	76	1.6	29	2	0.17	4	15.1
C_{4a}	39	3.2	1.6	3.7	0.2	3.3	4.2	17.4	0.8	11.4	102	1.8	52	3.2	0.32	10	29.5
C_{4a}	40	11.3	7.7	12.8	0.2	13.4	11.2	39.2	1.4	38.8	85	3.9	117	7.7	0.84	19	119.1
C_{4a}	41	0.6	<0.5	0.8	0.1	0.4	0.7	1.9	0.4	2	98	1.6	15	0.7	0.07	2	5.3
C_{4a}	42	0.5	<0.5	0.3	<0.1	<0.1	0.3	0.5	0.2	0.4	97	0.7	<8	0.2	<0.05	<1	1.4
C_{4a}	43	0.5	<0.5	0.5	<0.1	<0.1	0.3	0.6	0.4	0.5	92	0.8	<8	0.2	<0.05	1	1.1
C_{4a}	44	1.8	<0.5	1	0.3	<0.1	0.4	4.7	0.7	2.1	84	1	10	0.7	0.11	3	4.4
C_{4a}	45	1.4	<0.5	2	0.3	0.8	1.7	4.9	0.5	3.7	86	1.9	24	0.9	0.12	3	9.8
C_{4a}	46	0.8	<0.5	0.9	5	0.1	0.7	4.2	0.3	2.1	84	2.2	20	0.6	0.09	2	4.1
C_{4a}	47	3.3	<0.5	1.6	0.5	0.6	1.5	11	0.7	5.7	85	1.4	22	0.8	0.16	4	8.9
C_{4a}	60	1.7	<0.5	1.6	0.3	3	1	1.5	0.4	2.8	106	1.5	12	1.7	0.11	4	6.1
C_{4a}	61	1.9	0.9	4.2	0.2	1.1	2	3	0.7	10.6	104	1.4	52	1.9	0.36	3	12.8
C_{4a}	62	1.7	<0.5	6.4	0.4	1.2	2.8	5.1	0.6	9.9	151	3.9	52	3.3	0.16	5	14

Table S3.4 The *Kruskal Wallis H Test* results for the 4 groups of water (independent variables) hosted by: limestone, limestone with SWI, dolomitic limestone, and dolomitic limestone with SWI.

	Al	As	Ba	Be	Co	Cr	Cu	Mo	Ni	Pb	Rb
Asymp. Sig.[a]	0.314	**0.008**	**0.011**	**0.006**	**0.072**	0.167	**0.009**	0.144	**0.065**	0.715	**0.011**
Chi square	3.553	11.876	11.117	12.341	6.982	5.064	11.558	5.415	7.220	1.359	11.230
Effect size[b]	0.25	0.85	0.79	0.88	0.50	0.36	0.83	0.39	0.52	0.10	0.80

[a] Statistically significant difference (bold numbers) is assumed when Asymptotic Significance (Asymp. Sig.) is ≤ 0.1 (10% significance level).
[b] Effect size is a measure of degree of association in the population deduced from the Chi square, e.g. 0.85 for As means that 85% of the recorded difference is due to variation over the 4 independent variables.

Table S3.4 (continued)

	Sr	U	V	Zn	Na	K	Ca	Mg	SO_4	TIC	Si	Fe
Asymp. Sig.	**0.170**	**0.013**	**0.008**	0.324	**0.05**	**0.014**	**0.009**	**0.017**	**0.005**	0.258	0.043	0.055
Chi square	10.143	10.763	11.919	3.479	13.050	10.621	11.569	10.143	12.978	4.036	8.167	7.599
Effect size	0.72	0.77	0.85	0.25	0.93	0.76	0.83	0.72	0.93	0.29	0.58	0.54

Table S3.5 The *Mann-Whitney U Test* Asymptotic Significance for the 5 main constituents and the 10 TEs discerned in Table S3.4. Statistically significant difference (bold numbers) is assumed when Asymp. Sig. is ≤ 0.1 (i.e. 10% significance level).

	As	Ba	Be	Co	Cu	Ni	Rb	Sr	U	V	Na	K	Ca	Mg	SO_4	Si	Fe
AB	0.827	0.127	0.317	0.121	0.146	0.827	0.275	0.827	**0.050**	**0.046**	**0.050**	0.376	**0.050**	0.275	**0.077**	0.127	0.317
AC	**0.051**	**0.025**	1.000	0.439	**0.085**	0.285	**0.050**	**0.053**	**0.025**	0.291	**0.025**	**0.100**	**0.100**	**0.100**	**0.024**	0.101	0.439
AD	**0.034**	0.077	**0.022**	**0.026**	**0.032**	0.721	**0.034**	0.289	1.000	**0.032**	**0.034**	**0.034**	**0.034**	**0.034**	**0.032**	0.289	**0.022**
BC	**0.010**	**0.025**	0.197	0.232	**0.022**	**0.024**	0.097	**0.025**	**0.025**	**0.024**	**0.025**	0.101	**0.025**	0.297	**0.024**	**0.025**	0.845
BD	**0.034**	0.724	**0.026**	0.714	0.593	0.476	**0.034**	**0.077**	0.289	**0.034**	**0.034**	**0.034**	0.289	**0.034**	**0.032**	0.157	**0.026**
CD	**0.007**	**0.014**	**0.006**	**0.053**	**0.013**	**0.014**	**0.014**	**0.014**	**0.014**	**0.014**	**0.014**	**0.014**	**0.014**	**0.014**	**0.014**	**0.086**	0.118

A = limestone, B = limestone with SWI, C = dolomitic limestone, D = dolomitic limestone with SWI

Table S3.6 Behavior of TEs and major constituents in the 2 discerned geochemistries, limestone (C_6-Q) and dolomitic limestone (C_{4c}-C_5) for fresh and salinized groundwater assuming ancient clean seawater.

TE	Ancient Seawater (SMOW × F-evap.)	*MEF*, salinized groundwater	
	µg/L	1 % f_S	7.5 % f_S
	S#	*L.S*	*Dol. L.S*
Na	11351073	-13.13	-50.20
K	420258	-0.25	-0.91
Ca	434678	0.01	0.01
Mg	1361717	-0.01	0.00
Fe	2	0.00	0.00
Si	2118	0.01	0.00
Al	5.15	0.00	0.00
As	2.58	0.04	0.20
Ba	30.90	0.04	0.77
Be	0.001	0.00	0.00
Co	0.10	0.00	0.01
Cr	0.21	0.00	0.00
Cu	0.93	0.01	0.11
Mo	10.30	0.78	0.20
Ni	0.72	0.02	0.09
Pb	0.03	0.00	0.00
Rb	123.61	0.01	0.01
Sr	8343	0.04	0.17
U	3.40	0.04	0.05
V	1.96	0.00	0.01
Zn	2.06	0.28	2.93

S# is clean mean standard ocean water (SMOW) evapo-concentrated to measured Cl (e.g. > 40 years ago).

Table S3.7 Trace elements drinking water standards according to WHO guidelines (WHO 2008), EU Water Directive 98/83/EC (EU 1998) and U.S. Environmental Protection Agency (US EPA 2008).

Element	WHO (µg/L)	EU (µg/L)	US EPA
Al	100	200	200
As	10	10	10
Ba	700	*	2000
Be	*	*	4
Co	*	*	*
Cr	50	50	100
Cu	2,000	2,000	1,300
Mo	70	*	
Ni	70	20	
Pb	10	10	15
Rb	*	*	*
Sr	*	*	*
U	15	*	30
V	*	*	*
Zn	3,000	*	5,000

*: No standard guideline.

(a)

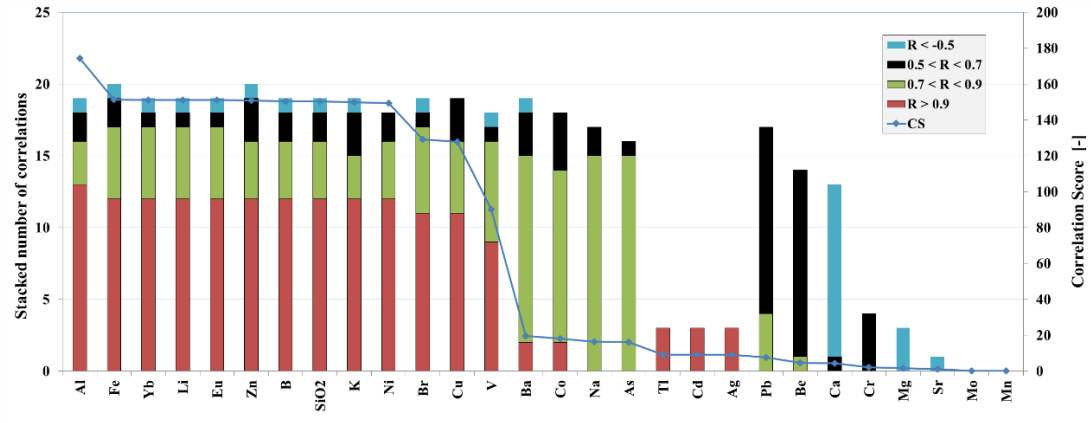
Stacked number of correlations
Correlation Score [-]
R < -0.5
0.5 < R < 0.7
0.7 < R < 0.9
R > 0.9
CS
Al Fe Yb Li Eu Zn B SiO2 K Ni Br Cu V Ba Co Na As Tl Cd Ag Pb Be Ca Cr Mg Sr Mo Mn

(b)

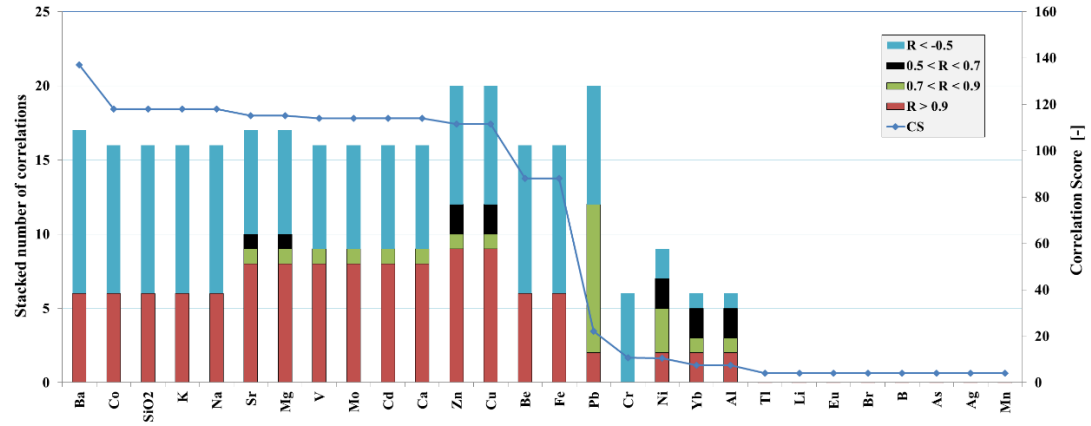
Stacked number of correlations
Correlation Score [-]
R < -0.5
0.5 < R < 0.7
0.7 < R < 0.9
R > 0.9
CS
Ba Co SiO2 K Na Sr Mg V Mo Cd Ca Zn Cu Be Fe Pb Cr Ni Yb Al Tl Li Eu Br B As Ag Mn

(c)

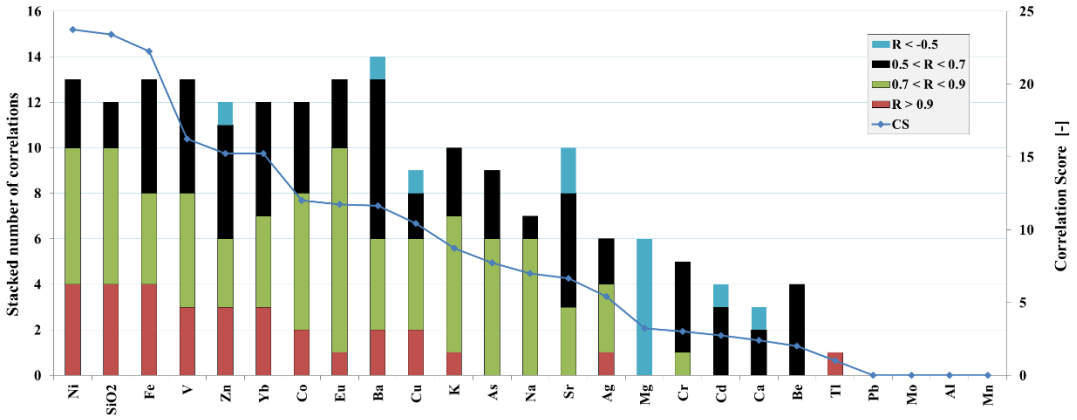
Stacked number of correlations
Correlation Score [-]
R < -0.5
0.5 < R < 0.7
0.7 < R < 0.9
R > 0.9
CS
Ni
SiO2
Fe
V
Zn
Yb
Co
Eu
Ba
Cu
K
As
Na
Sr
Ag
Mg
Cr
Cd
Ca
Be
Tl
Pb
Mo
Al
Mn

(d)

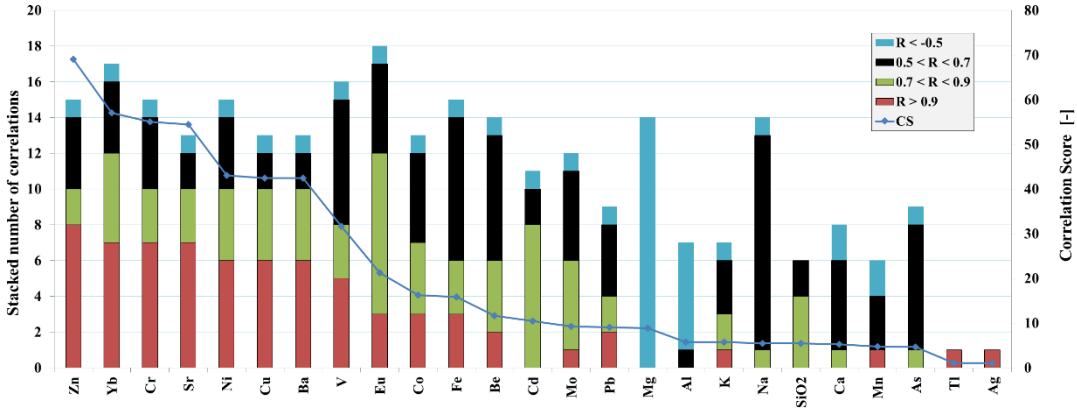
Stacked number of correlations
Correlation Score [-]
R < -0.5
0.5 < R < 0.7
0.7 < R < 0.9
R > 0.9
CS
Zn
Yb
Cr
Sr
Ni
Cu
Ba
V
Eu
Co
Fe
Be
Cd
Mo
Pb
Mg
Al
K
Na
SiO2
Ca
Mn
As
Tl
Ag

(e)

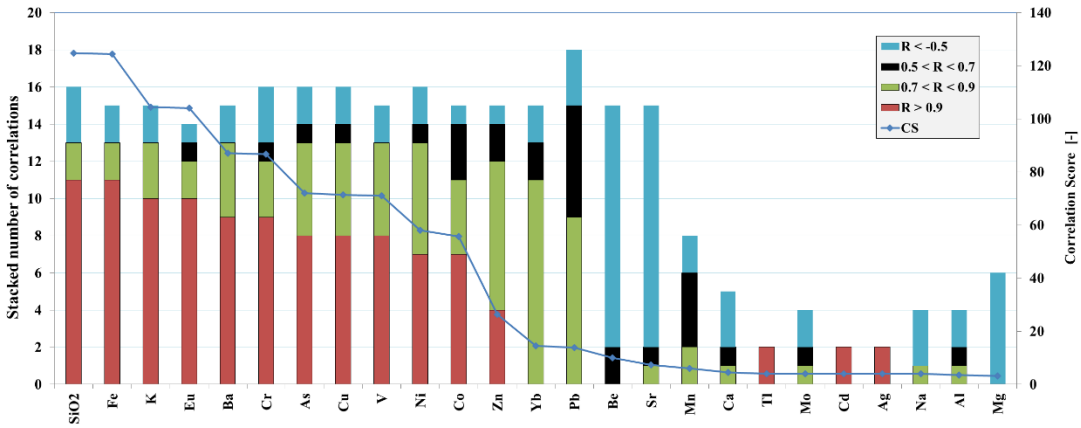

Figure S3.1 Correlation score (CS) plots of the main geochemical elements in (a) C_{4a} (dolomite and limestone), (b) C_{4b} (marly limestone), (c) C_{4c}-C_5 (dolomitic limestone), (d) C_6 (chalky to marly limestone) and (e) Q (gravel, sand and clay) geologic units. They show potential clusters of highly correlating elements. The stacked number of correlations (>0.5 or <-0.5) of each element are plotted with respect to all other elements, and then ranking follows a descending order from highest to lowest CS. The number of samples for each unit is provided in Table 3.4.

CS = $n^2_{0.9} + n_{0.7} + \sqrt{n_{0.5}}$, where: $n_{0.9}$ = number of parameters with R>0.9 and R<-0.9; $n_{0.7}$ = number of parameters with R=0.7 to 0.9 and R=-0.9 to -0.7; $n_{0.5}$ = number of parameters with R=0.5 to 0.7 and R=-0.7 to -0.5. (Stuyfzand 2015).

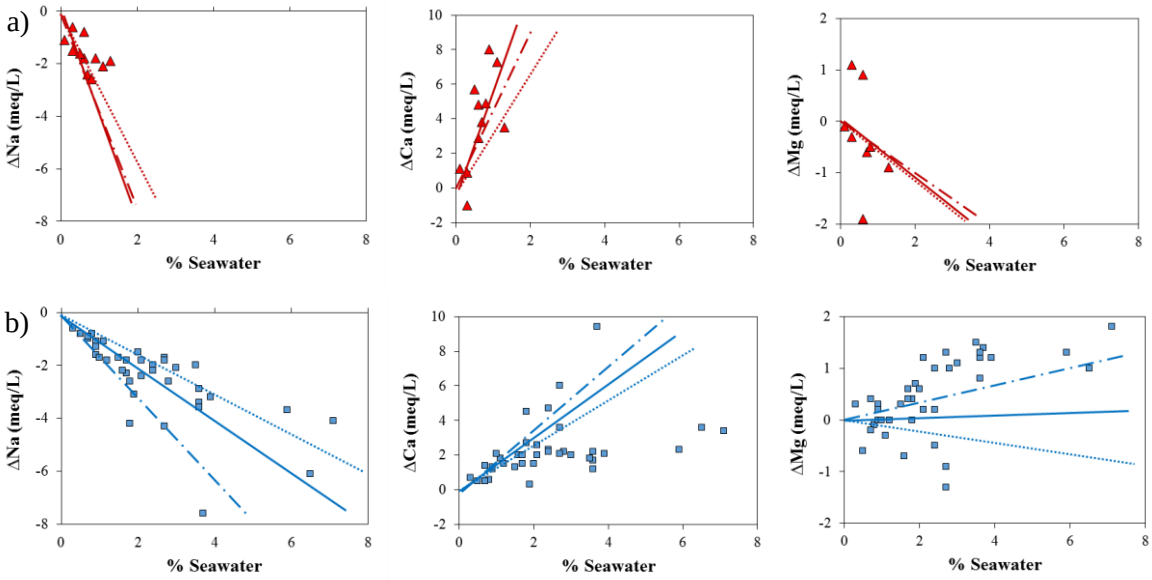

Figure S3.2 Sensitivity analysis of Na, Ca and Mg predicted by the 1-D dual porosity reactive transport models to lower/higher $CEC_{immobile}$ values at (a) path 1 (via the C_6 limestone unit) and (b) path 2 (via the C_{4c}-C_5 dolomitic limestone unit). *CEC* values of round dot, solid and long dash dot lines are 0.05, 0.1 and 0.2 mol/kg H_2O for red color and 0.01, 0.02 and 0.04 mol/kg H_2O for blue color, respectively.

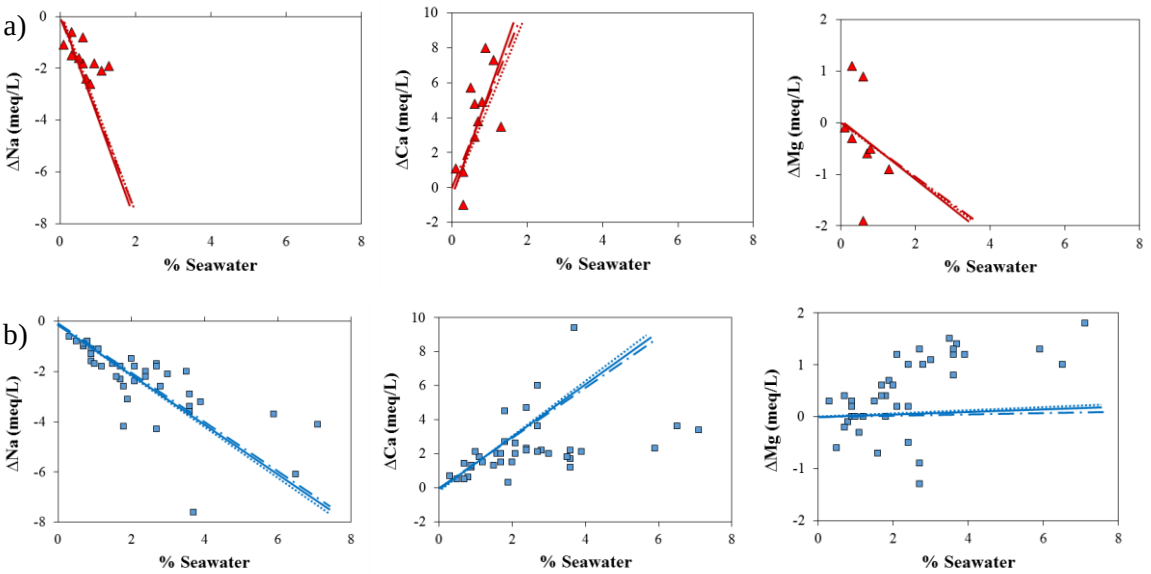

Figure S3.3 Sensitivity analysis of Na, Ca and Mg predicted by the 1-D dual porosity reactive transport models to lower/higher CEC_{mobile} values at (a) path 1 (via the C_6 limestone unit) and (b) path 2 (via the C_{4c}-C_5 dolomitic limestone unit). *CEC* values of round dot, solid and long dash dot lines are respectively 0.01, 0.005 and 0.0025 mol/kg H_2O for red and blue colors.

Chapter 4

Simulation of saltwater intrusion in a poorly karstified coastal aquifer in Lebanon (Eastern Mediterranean)

This chapter is based on:

Khadra, W.M., Stuyfzand, P.J., under review. Simulation of saltwater intrusion in a poorly karstified coastal aquifer in Lebanon (Eastern Mediterranean). *Hydrogeology Journal*.

Abstract

To date, there is no agreement on the best way to simulate saltwater intrusion (SWI) in karst aquifers. An equivalent porous medium (EPM) is usually assumed without justification of its applicability. In this paper, SWI in a poorly karstified aquifer in Lebanon is simulated in various ways and compared to measurements. Time series analysis of rainfall and aquifer response is recommended to decide whether quickflow through conduits can be safely ignored. This aids in justifying the selection of the exemplified EPM model. The results of a coupled discrete-continuum (CDC) approach are compared to the EPM model to examine the improvement of SWI representation when discrete features (DFs) are embedded in model domain. The two approaches yielded reasonable patterns of hydraulic head and groundwater salinity, which seem trustworthy enough for management purposes. The CDC model, however, was also capable to reproduce some local anomalous chloride patterns thanks to more freedom in adapting to the measurements. It improved the overall accuracy of salinity at wells and resulted in a better representation of the fresh-brackish water interface. Therefore, the CDC approach can be beneficial in modeling SWI in poorly karstified aquifers, and should be compared with the results of the EPM method to decide whether the difference in the outcome at local scale warrants its more complicated application. The simulation efforts utilized the SEAWAT code since it is density dependent and public-domain, and it enjoys widespread application. Including DF's necessitated manual handling because the selected code has no built-in option for such features.

4.1 Introduction

Most hydrogeological applications consider water as a constant-density fluid due to its minor or negligible variation in space and time; however, salinized environments necessitate the use of more coupled formulations to account for variable-density flow (Bachu 1995; Post 2005). Saltwater intrusion (SWI) models that include density-dependent flow have been widely used in porous media (e.g. Shoemaker and Edwards 2003; Dausman and Langevin 2005; Kihm et al. 2007; El Yaouti et al. 2008; Kopsiaftis et al. 2009; Monti et al. 2009; Dentoni et al. 2015; Soupios et al. 2015; Gopinath et al. 2016), but in fractured and karstic domains SWI is more intricate due to possible non-Darcian flow, i.e. turbulent dynamics generated by concentrated flow pathways. Hybrid codes that couple Darcian groundwater flow in porous medium with turbulent flow in conduits have been developed, e.g. MODFLOW-CPFM1 (Shoemaker et al., 2008), and CFPv2 (Reimann et al., 2014) in addition to coupling of EPM and discrete features (DFs) in the so-called coupled discrete-continuum (CDC) or hybrid EPM-DF approach (e.g. Kavouri et al. 2017). Some codes account for 1-D solute transport in conduits (e.g. Spiessl et al. 2007), but codes with density-dependent flow, which are essential for SWI and salt transport, are still scarce. So choosing a robust modeling approach to tackle SWI models in karstic aquifers remains a challenge.

Different approaches have been implemented, which shows a certain disagreement on a common method. Popular approaches are: (1) equivalent porous medium (EPM) (e.g.

Langevin 2003; Nocchi and Salleolini 2013; Steiakakis et al. 2016), (2) dual-porosity (DP) continuum (e.g. Blessent et al. 2014), and (3) discrete fracture networks (DFN) (e.g. Quinn et al. 2006; Papadopoulou et al. 2010; Dokou and Karatzas 2012). The impact of a configuration of vertical, horizontal or inclined fractures on the distribution and the shape of the freshwater-saltwater interface was examined by Sebben et al. (2015). Their findings show that vertical fractures close to the seawater wedge increase the width of the mixing zone whereas horizontal fractures in the lower part of the aquifer can push the wedge seaward. Nevertheless, the ambiguity of where and how large the fractures and/or conduits actually are in the field always limits the efforts to reach a comprehensive understanding, notably where the fracture sets are irregular. Xu (2016) developed a 2-D model (called VDFST-CFP) to simulate SWI in karstic aquifers, but it is limited to confined aquifers, ignores mechanical dispersion and, to our knowledge, has still not been applied to any field study. Wang et al. (2016) proposed using inverse hydraulic tomography to describe the transmissivity field of fractures and conduits. The discerned network may then be embedded in a DFN groundwater flow model. However, this approach requires: (1) intensive field investigations, and (2) further research to consider salinity in establishing the inverted transmissivity values.

Due to the aforementioned inherent complexity, modelers generally lean toward applying the EPM approach. The EPM models have been applied successfully in fractured and karstic domains for 2-D/3-D groundwater flow (e.g. Dafny et al. 2010; Polemio and Romanazzi 2014; Archontelis and Ganoulis 2015; Maihemuti et al. 2015; Neukum et al. 2015) and SWI (e.g. Langevin 2003; Nocchi and Salleolini 2013; Romanazzi et al. 2015; De Filippis et al. 2016; Steiakakis et al. 2016; Zhao et al. 2016). Yet, its underlying simplification is not always valid (e.g. Teutsch 1993; Ghasemizadeh et al. 2012), making its use for every case questionable. EPM is usually adequate for large-scale problems where and when homogenous overall behavior may be assumed (Scanlon et al. 2003). It is also meaningfully applicable in systems with high-frequency orthogonal fractures where EPM can properly describe dispersivity values and groundwater flow patterns (Sebben et al. 2015). Other constraints that justify relevant use of EPM have not been encountered in the literature.

In this paper, the EPM and the CDC approaches are used to simulate SWI in a poorly karstified system, called the Damour coastal aquifer in Lebanon (Eastern Mediterranean), and their results are compared to check the overall improved accuracy of SWI representation when discrete features are embedded in the model domain. This answers the question of whether bothering with discrete features to model SWI in a poorly karstic aquifer like the Damour is needed or not. A prior step is time series analysis to investigate the overall hydrodynamic behavior of the system, and to decide beforehand whether conduit quickflow anticipated in karst systems can be safely ignored. This should provide a reasonable ground to select either the EPM or the CDC in such media because poorly to moderately karstified aquifers, called ‘merokarst’ (Ford and Williams 2007), are usually dominated by baseflow obeying Darcy’s law (Panagopoulos and Lambrakis 2006; Panagopoulos 2012). Several merokarstic aquifers span the Mediterranean region, for

instance in Italy (Angelini 1997), Spain (Padilla and Pulido-Bosch 1995), Greece (Panagopoulos 2012), and the West Bank (Abusaada and Sauter 2013). Their EPM groundwater flow models showed reliable results, but simulating SWI was not an issue there.

4.2 Setting and methods

4.2.1 Site description

The Damour coastal aquifer in Lebanon is part of the Eastern Mediterranean basin at about 7 km to the south of the capital Beirut (Figure 2.1). It has crucial importance because it supplies one third of the domestic water needs for a population exceeding one million people in part of the capital and its suburbs. Although it is a major national water resource suffering from ongoing salinization, it still lacks a reliable SWI model.

The main hydrostratigraphic units are shown in Table 2.1 and Figure 2.1. It is assumed that the upper major unit (C_{4c}-C_5) and the lower subunit (C_{4a}) are hydraulically connected due to severe fracturing of the middle formation (C_{4b}) whereas the C_3 formation is assumed to form an impervious base of the system. The area is dissected by six major and many minor faults. Layers dip westward steepening to a maximum inclination of 55° (with the horizontal) in the east due to what is known as the Mount Lebanon Flexure (Figure 2.2).
The area has a humid mesothermal Mediterranean climate, which is characterized by dry summers and mild moist winters with considerable sunshine. The annual precipitation records over the last decades showed a range between 352 and 1163 mm (Figure S4.1, *Appendix S4*) with 770 mm average (Meteorological Service 2010). The large variation is part of a climatic cycle, which showed a 14-year recurrence interval over the last 50 years (Arkadan 2008). A major perennial river, called the Damour River, and other ephemeral streams intersect the study area (Figure 2.1).

According to field observations, the main aquifer (C_{4c}-C_5) lacks high-grade karst features, notably ponors, dolines, epikarst, and springs. One small spot south of Baawarta has pure limestone outcrops with *karren* (limestone with small-scale solutional forms) karstic features. Very few small caves exist (Awad 1983), and well logs disclosed fractures without signs of karstic features (Khadra 2003).

The general direction of groundwater flow is from the east with minor northward and southward deviations. Groundwater extraction was estimated in a thorough survey in 2011 conducted for the purpose of this study. The extraction comprises 78 private, 22 governmental and 5 municipal wells. Governmental and municipal wells have been pumping with known rates throughout the years; the total estimated discharge was about 13 Mm^3/year. Minor quantities, totaling about 0.5 Mm^3/year are also extracted from private wells. The former estimate is quite accurate as it is based on water authority records whereas the latter relied on interviews with well owners and farmers about pump capacities,

water consumption and its usage. Therefore, the discharge of private wells is likely inaccurate, but it can be safely ignored compared to the high discharge of public wells.

The hydrochemistry of the system was thoroughly discussed by Khadra and Stuyfzand (2014, 2016), and Khadra et al. (2017b). Originally, the groundwater is fresh typical of dolomitic limestone hosting rocks. It deteriorates close to the shoreline by saltwater encroachment. Doming of chloride at Naameh and to a lower extent at Mechref villages indicates upconing due to overpumping (Figure 4.1). The maximum seawater fraction of groundwater as abstracted by wells is still < 20%.

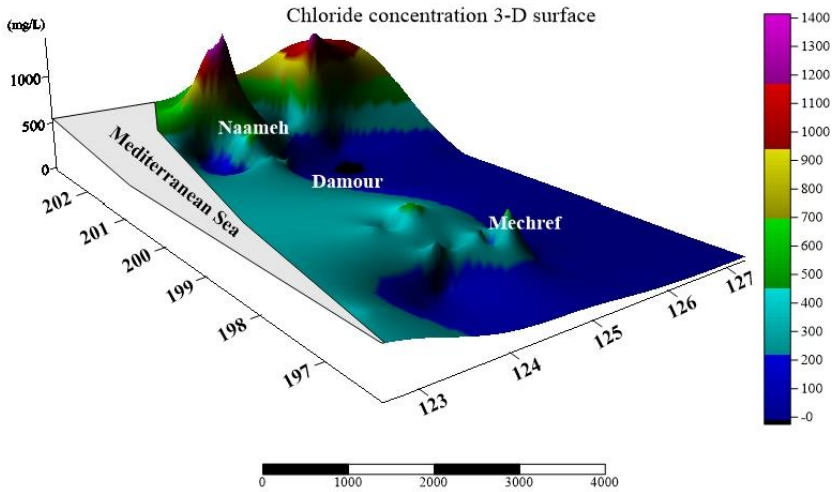

Figure 4.1 3-D surface of chloride concentration (mg/L). Data acquired in year 2011 at a depth of 0-30 m below the water table. Dark blue delineates freshwater whereas other zones are salinized.

4.2.2 Description of aquifer hydrodynamics

One way to describe the overall hydrodynamic response of an aquifer is to analyze time series data (Padilla et al. 1994; Kovács and Sauter 2007). Water level fluctuations and variations of spring discharge with rainfall can indicate the magnitude of water reserves in the aquifer, and may show how fast the reserve declines. A fast response usually indicates a well-developed karst drainage system (high karstification degree) dominated by conduit quickflow. In contrast, slower responses are indicative for baseflow, which characterizes poorly developed karst and absence of karst networks (Panagopoulos and Lambrakis 2006). Factors related to the unsaturated zone may have strong impacts as well, for instance to delay the effective recharge signal and eventually the aquifer response (Kovács 2003; Kovács and Sauter 2007). Therefore, whenever a slow response is recorded, time series

analysis should be supported by field observations to confirm the absence of mature karst features or epikarst.

Autocorrelation analyses of water level or spring discharge and cross-correlation between them are two recognized statistical methods that aid in understanding the response of the system to recharge (Padilla et al. 1994). Their interpretation is well documented in the literature for many old and recent case studies (e.g. Mangin 1994; Padilla and Pulido-Bosch 1995; Angelini 1997; Larocque et al. 1998; Jemcov and Petric 2009; Lee and Lee 2000; Panagopoulos and Lambrakis 2006; Kovačič 2010; Russo et al. 2015; Fu et al. 2016; Lafare et al. 2016). Further elaboration on these and other methods is provided below:

1. The autocorrelation function quantifies the memory effect of the system, which is determined by the decorrelation lag time, usually predefined at an autocorrelation (r_k) value of 0.1 or 0.2 (Benavente et al. 1985). Uncorrelated data discloses steep slopes, i.e. the autocorrelation value is lower than 0.2 over short lag time. In contrast, correlated interdependent series vary smoothly with gentle slopes over a longer period, i.e. maintaining a longer memory effect expressed by an autocorrelation value above 0.2 over longer lag time (Lee and Lee 2000; Panagopoulos and Lambrakis 2006).
2. The cross-correlation function is useful to show the time delay between input and output. This delay is inferred from sharp peaks in the time series shown on the curve; for instance, the lag time associated with a positive maximum cross-correlation indicates the time after which a certain response was attained. The time lag strongly depends on how fast the system drains. A mature karst system with a well-developed network of conduits drains quickly, and hence shows a shorter lag time unlike poorly karstified aquifers, which show longer periods (i.e. opposite behavior). Also, the cross correlogram for mature karst has steep ascending and descending slopes (indicative of shorter response time) while the poorly developed karst has negligible or gentle slopes. In general, a poorly karstified and drained system with high storage has a response time of > 60-70 days compared with few days for mature and well-drained systems (Mangin 1994; Padilla and Pulido-Bosch 1995). Two intermediary classes may fall in between, with small (10-15 days) and large memory effects (50-60 days) respectively (Mangin 1994).
3. Other statistical methods that may be useful are coherency, gain and cross-amplitude functions, (Kovács 2003; Panagopoulos and Lambrakis 2006). The coherency function reveals the linearity between inputs and outputs (merokarst shows a non-linear response with low values of the coherence function); the gain function complements the cross-correlation function by expressing the delay in aquifer response (merokarst has < 1 ratio of output to input signal); and the cross-amplitude indicates the signal filtering and attenuation characteristics of poorly karstified aquifers (Padilla and Pulido-Bosch 1995).

4.2.3 Defining major geological (geo-)lineaments

Geo-lineaments are mappable rectilinear or slightly curvilinear features of a surface that reflect subsurface phenomena (O´Leary et al. 1976). They include: (1) faults, (2) fold axes, (3) photo lineaments, and (4) conduits. Geological maps usually reveal main faults and folds while photo lineaments are extracted manually or automatically from aerial photography or satellite imagery where they show up in a different tonal contrast (LINE module of *PCI Geomatica* (www.pcigeomatics.com) could be one alternative for automatic lineament extraction). Delineation of more faults may also be accomplished by transient electromagnetic (TEM) sounding (Kourgialas et al. 2016). Any information on conduit patterns should be inspected as it comes from tracer tests or speleological investigations. In deep aquifers, there is a chance that the effect of surface fractures alter with depth, and that the role of conduits changes as well.

4.2.4 Accounting for geo-lineaments in the model mesh

Accounting for geo-lineaments in the model mesh is possible by incorporating them discretely (as discrete features in the CDC approach) or by using dual-porosity (DP) formulations. The former has wider applications as there is still no consensus on the value of DP to improve model accuracy (Blessent et al. 2014).

Recent studies have combined the EPM models with discrete features (DFs) by representing the embedded DFs by the Hagen-Poiseuille law (e.g. Quinn et al. 2006; Papadopoulou et al. 2010; Dokou and Karatzas 2012). This approach is convenient for sparsely distributed features. However, very few commercial codes (e.g. FEFLOW, Diersch 2014; HydroGeoSphere, Therrien et al. 2010) are now available to handle 3-D variable-density flow in discrete fractures or a dual-continuum. An alternative is to represent faults by higher or lower hydraulic conductivity values depending on whether they act as barriers or preferential flow paths (Bense et al. 2003). This way to handle DFs is recommended for most common codes that do not address discrete features (e.g. SEAWAT from the USGS). The values for the hydraulic conductivities of the DFs should only follow from the calibration process. The literature offers some general hints to set initial values, but these may not apply in all given cases.

Strike-slip and dip-slip faults promote infiltration of water, but the latter have higher storage (Bhuiyan 2015). The initial hydraulic conductivities of faults may be assigned aquitard conditions of carbonate aquifers (Celico et al. 2006). For example, a 0.1 m/d is a reasonable initial value (Bredehoeft 1997; Bense et al. 2003), which is about 3-5 orders of magnitude lower than the surrounding material as also suggested by Mayer et al. (2007). On the other hand, conduits are always represented by extremely high hydraulic conductivity and porosity. Dispersivity is to be significantly lowered (e.g. $\leq$ 1 m) to neglect dispersion and favor advection. The initial hydraulic conductivity of conduits may be estimated by combining Darcy's equation (Eq. 4.1) for a continuum model and the Hagen-Poiseuille equation (Eq. 4.2) for a discrete-continuum model.

$$q = -K\frac{\partial h}{\partial x} \tag{4.1}$$

$$q = -\frac{gd^2}{32\mu}\frac{\partial h}{\partial x} \tag{4.2}$$

Combination of Eqs. 4.1 and 4.2, yields the following formula for K provided that Reynolds number (qd/μ) is < 2000 to ensure laminar flow.

$$K = \frac{gd^2}{32\mu} \tag{4.3}$$

K is hydraulic conductivity [L/T], d is discrete feature diameter assumed equal to aperture in this study [L], μ is kinematic viscosity of water [L^2/T], g is gravitational constant [L/T^2], and q is specific discharge (L/T).

At this stage, a finer grid may be required at DFs to avoid numerical instability in the solute transport, which might be induced by advection-dominated flow at or near the DFs. The Peclet number (P_e) is one quantitative measure that can aid on this decision. A value of $P_e \leq 4$ is recommended for a stable solution (Zheng and Bennett 2002).

$$P_e = \frac{vL}{D} \tag{4.4}$$

or

$$P_e = \frac{L}{\alpha} \tag{4.5}$$

where v is the seepage velocity [L/T]; L is the cell width [L]; D is the dispersion coefficient [L^2/T]; α is dispersivity [L].

4.3 Model development

4.3.1 Numerical code and discretization

The USGS SEAWAT code (Guo and Langevin 2002), which is a combination of MODFLOW (McDonald and Harbaugh 1988) and MT3DMS (Zheng and Wang 1999), was used to build the numerical model for this study. SEAWAT utilizes a finite-difference mesh to solve 3-D variable-density flow and solute transport even in heterogeneous and anisotropic media. The code is widely used, and was proven and verified for porous media. It was also tested and evaluated against many variable-density benchmarks (Langevin et al. 2003), such as the modified Henry and saltpool problems (Langevin and Guo 2006).

SEAWAT is utilized in this study because it is: (1) a density dependent code, (2) public-domain, and (3) has widespread applications as it builds on the popular MODFLOW code (i.e. more people can follow).

The mesh extended from the Mediterranean Sea to about 7 km eastward (inland) and from 2 km south of the Damour River to the Dawha village northward, covering the whole hydrologic system. Grid orientation granted that cells are parallel to the strike of the bedding and at the same time roughly parallel to the shoreline. Transverse hydraulic conductivity (K_y) is parallel to the strike of the bedding (NNE-SSW) whereas longitudinal conductivity (K_x) is parallel to the dip (nearly perpendicular to the shoreline). The deepest point of the model is 750 m underground, reaching the top of the impervious Hammana formation (C_3), which constitutes the system base (Figure 2.2). The various geologic units were discretized based on the hydrostratigraphy (Table 2.1): 6 layers × 27 m for the C_6 formation, 18 layers × 20 m for the C_{4c}-C_5 formation, 2 layers × 20 m for the C_{4b} formation, and 2 layers × 35 m for the C_{4a} formation. This refinement aimed at better representing the saltwater-freshwater interface. All layers had uniform thicknesses except the topmost, which followed the topographic surface imported from a digital elevation model. The shallow coastal quaternary unit (Q) overlying the C_6 formation was ignored because of its minor thickness (an average of ca. 5 m) compared to the others.

A custom horizontal grid was used to obtain more detail in certain parts of the model with a larger interest. The grid was refined near pumping wells and to model discrete features, with 35 m width parallel to strike for faults (assuming the coexistence of fault zones) and 10 m for other lineaments. A still finer refinement was avoided to prevent excessive computation times. The grid had 163 rows, 55 columns, and 28 layers, i.e. a total of 251,020 cells; minimum size was 10 × 65 m^2 and maximum 170 × 170 m^2. Inactive cells included the Mediterranean Sea and some of the permanently dry cells with no chance of ever being wetted.

4.3.2 Boundary conditions

The conceptualized model was surrounded by the following boundaries (Figure 4.2): (a) general head boundary (GHB) to the north, south and west, and (b) no-flow boundary at the east where the C_3 impermeable unit extends with a steep inclination. Selecting GHB at the Mediterranean Sea boundary to the west aims to account for submarine groundwater discharge (SGD) as a result of the simulation rather than forcing the model into a fixed behavior via the constant head and concentration packages (Abarca et al. 2007; Mulligan et al. 2011). SEAWAT automatically corrects for equivalent freshwater heads. The uppermost active cells of the top layer formed a specified flux boundary that was represented by the recharge package (RCH) in SEAWAT. The vertical flux through this boundary was estimated as the product of rainfall and an infiltration coefficient over different zones, based on type of exposed hydrostratigraphic unit, land cover and dipping of layers (Table 4.1). The calibrated value of recharge for a major portion of the aquifer was estimated at 28%, similar to previous records (Khadra 2003). An annual average precipitation of 770 mm all over the steady-state phase was set as an initial guess, but a variable amount, as

recorded over the last 20 years (Figure S4.1, *Appendix S4*), was then assigned to the transient simulation. Salinity of rainfall was set constant at 30 mg/L as deduced from average chloride in rainfall (11 mg/L) and average evapo-concentration factor in the study area (Khadra and Stuyfzand 2014).

The Damour River was simulated by the RIV package. This type of boundary was assigned to the layers that intersect the river. Finally, groundwater withdrawal from pumping wells was simulated using the WEL package. Each well was assigned an average annual rate, since major wells pumped continuously for most of the year. The discharge of only a few wells varied over the last years; this was accounted for in wells' input data.

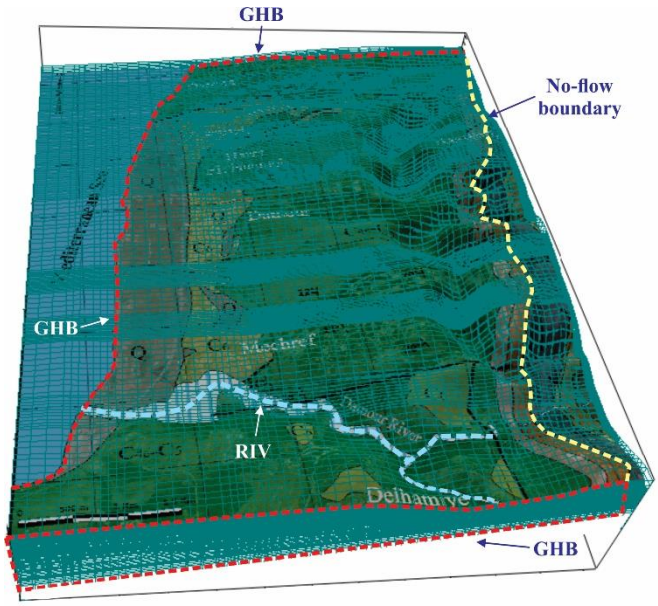

Figure 4.2 Grid of the Damour aquifer 3-D model showing the major boundary conditions. GHB is general head boundary, and RIV is the river package in SEAWAT.

Table 4.1 Zonations of recharge rate distribution over the study area.

Zone	Area (km^2)	Infiltration Coefficient (%)	Mean Recharge (mm)	Description
I	0.5	5	38	Naameh village characterized by high urbanization.
II	7.5	20	154	Quaternary deposits and C_6 formation.
III	45	28	216	Exposed outcrops of the C_{4c}-C_5 formation with gentle dips.
IV	7	40	308	Exposed outcrops of the C_{4b}, C_{4a} and C_{4c}-C_5 formations with steep dips (east of study area) in addition to part of Mechref village.

4.3.3 Hydraulic properties

Twenty detailed drilling logs are available for the study area; however, all wells tap the major aquifer (C_{4c}-C_5) only, which rendered them useless in providing a detailed description of the whole geologic sequence. So hydraulic conductivity of the matrix was assumed vertically uniform, but given different values for horizontal distribution according to 15 pilot points deduced from the results of pump tests (Khadra 2003).

A heterogeneous pattern was generated via statistical interpolation utilizing Inverse Distance Squared method. It significantly improved the model outputs compared to uniform value. The distribution array was created using the logarithmic values of hydraulic conductivity estimated from pump tests at the pilot points, which are visualized as data nodes, in the C_{4c}-C_5 unit. The interpolation scheme covered all nodes of the model domain, and had 0.01 and 1500 m/d as the minimum and the maximum interpolation data bounds, respectively. The lower aquifer (C_{4a}) was assigned similar hydraulic characteristics as C_{4c}-C_5 whereas other layers (with no pump test data) were initially assigned constant values from the literature (Schwartz and Zhang 2003), including storage values.

Geostatistical simulation via the inverse modeling code PEST (Doherty 1994) was then applied to get better optimized values (Table 4.2). PEST was run in estimation mode to estimate the *K* and storage values required to optimize the objective function. Hydraulic heads and chloride concentrations measured at several wells were used as observation objectives. *K* and specific yield were log transformed, and the values assigned initially for cells were used as the initial parameter values constrained by the minimum and maximum expected bounds.

The average effective porosity was initially estimated based on electrical resistivity (Geofizika 1965) using Archie's law (Archie 1942) (Table 4.2). It cannot be very accurate, but it could be a good a priori estimate. The values showed close agreement with calibration results for the C_{4c}-C_5 unit, but were overestimated for the C_6 unit.

Table 4.2 Final values of hydraulic properties after calibration.

Unit	*Kx*	*Ky*	*Kz*	*Storage* [-]	*Porosity* [-][c]
	[m/d]				
C_6	1.1-1.8	1.1-1.8	0.8	0.07[a]	0.08
C_{4c}-C_5	7 - 900	7 - 900	0.7 - 16	0.06[a]	0.12-0.19
C_{4b}	3	1.8	0.3	5×10^{-3} [b]	0.08
C_{4a}	7 - 900	7 - 900	0.7 - 16	7.3×10^{-6} [b]	0.12

[a]: Specific Yield (S_y)
[b]: Specific storage (Ss)
[c]: Porosity was initially estimated for C_6 and C_{4c}-C_5 based on electrical resistivity values (Geofizika 1965) using Archie's law (Archie 1942): $\rho_r = a\ \rho_w \phi^{-m}$, where ρ_r is the resistivity of a saturated porous medium [Ohm-m]; ρ_w is ditto for pore fluid [Ohm-m]; ϕ is porosity [-]; a and m are empirical factors assumed as 1 and 1.52, respectively (Hamada et al. 2013). Estimated values (0.09-0.14) closely matched calibrated values for C_{4c}-C_5, but were higher (0.3) than calibrated for C_6.

NB: A 10:1 horizontal/ vertical anisotropy ratio applied initially to all units, but was adjusted locally by inverse modeling where necessary.

4.4 Results

4.4.1 Time series analysis

Two loggers were installed between 2012 and 2015 in two wells in northern and southern parts of the study area, at Dawha and Mechref villages respectively (Figure 2.1), recording the water level at 15 minutes interval over the whole period. A barometer logger in the vicinity of a rain logger was used for barometric compensation (Figure 2.1). The rain logger measured the precipitation over the intended period.

Total daily rainfall values and the water level at the end of the day provided input and output time series, respectively. Their correlograms show gentle slopes at both sites with 0.2 autocorrelation estimate (r_k) after 76 and 82 days at Merchref and Dawha, respectively (Figure 4.3a). This relatively long response time is indicative of absence of high transmissivity conduits and thus reflects poor karstification with significant storage. An immediate drop of the autocorrelation function over the first 3-4 days appears at both wells, which indicates quickflow via larger conduits compared to the slower and delayed baseflow that dominates this system, in which water drains slowly from the aquifer. This bimodal response reveals a probable low karstification degree.

Similarly, the cross-correlation function of Mechref shows a gentle slope with a very small r_k value (maximum 0.1) (Figure 4.3b), which indicates baseflow dominance in agreement with a low karstification degree, as was confirmed by field observations. This applies to Dawha as well, although the r_k value there shows a wider variability, which we attribute to minor local karstic features. The delay time, calculated as the difference between lag = 0 and maximum cross-correlation, is ca. 70 days at both sites. These values are in line with porous (non-karst) media aquifers having comparable catchment sizes, e.g. > 50 days for Quaternary deposits in the Italy North-Western Alp (Russo et al. 2015), and 45-85 days from the St Bees Sandstone aquifer, UK (Lafare et al. 2016).

Accordingly, poor karstification is the general description that fits the hydrodynamic behavior of the studied aquifer. This result is in agreement with field observations showing that high grade karstic features are missing, which also excludes the possibility that selected wells are by chance far away from larger conduits. It is, therefore, concluded that baseflow dominates this groundwater flow regime, and the role of quickflow in it is minor. This response is also indicative of a high storage capacity, as was confirmed previously by the small water level drawdowns that were observed during pump tests (Khadra 2003).

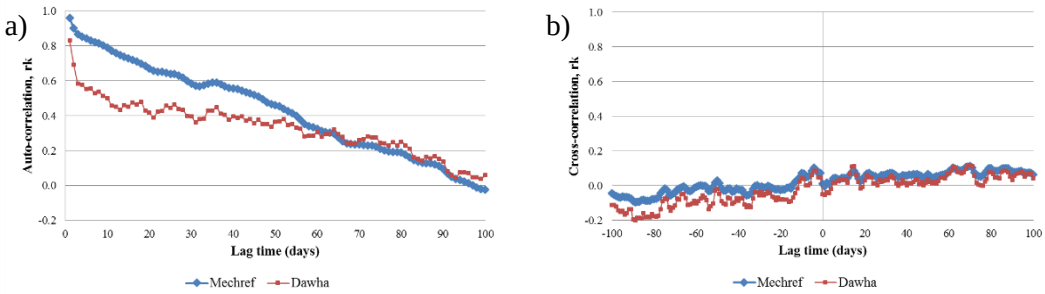

Figure 4.3 Correlograms drawn from (a) autocorrelation and (b) cross-correlation functions at two wells in Mechref and Dawha villages located respectively at the northern and southern parts of the study area. The used r_k is 0.2 and 0.1, respectively.

4.4.2 Discrete features

The geological map of the study area (Figure 2.1) shows major faults, and confirms the absence of main folds. Photo lineaments were delineated (Figure 4.4) based on automated extraction using the *LINE* module of *PCI Geomatica* (input parameters are provided in Table S4.1, *Appendix S4*). The input parameters of this extraction are to some extent subjective, and hence the output was manually checked to remove non-natural linear features (e.g. roads). The remaining lineaments matched the overall E-W lateral shearing that has structured the area (Yassine Hajj Chehadeh 2015). Four major underground conduits were extrapolated to the shoreline based on the location of submarine springs discovered in early seventies (FAO 1973) and an active littoral spring that the authors recently came across (Figure 4.4). This network matches the general pattern of the karst system that was generated for the same aquifer via a pseudo-genetic stochastic model by Borghi et al. (2012).

All extracted geo-lineaments were subsequently included in the model; they extend vertically to all layers assuming they formed after deposition. Assigned hydraulic conductivities varied between faults and other lineaments (notably conduits). The initial guess of the conductivity of faults was set at 0.1 m/d (horizontal) and 0.01 m/d (vertical) over the cells thicknesses, but later corrected during the automated calibration process. The initial conductivity of geo-lineaments was selected according to Eq. 4.3, at 7000 m/d, assuming an aperture of 0.5 mm. The aperture width is the average value that Masciopinto (2013) calculated stochastically based on the experimental variogram of aperture covariance estimated from pump tests. This value is assumed constant over the entire aquifer depth, so any reduction due to higher stresses with depth is ignored. For transport purposes, longitudinal and transverse dispersivities were assumed uniform over each lineament length with 10:1 vertical anisotropy. The initial values for all DFs were lowered to ≤ 1 m.

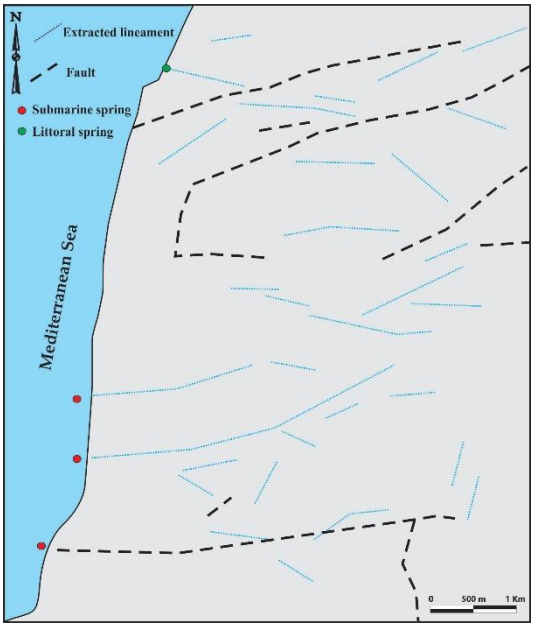

Figure 4.4 Geo-lineaments extracted from Landsat image acquired in 2006, and superimposed by major faults in the area. Submarine springs were delineated based on FAO (1973) thermal infrared (TIR) survey.

4.4.3 Simulation results

The numerical simulation was carried out in two phases: pre-development (1941-1991) and post-development (1991-2011). Automatic parameter optimization was done using PEST to adjust hydraulic conductivity, the anisotropy ratio and the storage coefficients. The stresses imposed on the system were first estimated. Then the observed hydraulic head and chloride concentration for different wells since 1980 and the position of the fresh-brackish water interface, were used for calibration.

The first runs of the pre-development phase assumed steady-state flow to provide initial conditions of the system in addition to some refinement of hydrologic boundaries, although there is doubt that steady-state conditions will ever be reached in karst aquifers (Scanlon et al. 2003). The post-development situation under transient conditions was then simulated to modify the zonal distribution of hydraulic conductivity and boundary conditions. Salinity conditions were thereafter generated with longitudinal dispersivity of 20 m all over the study area in addition to porosity modification to reach a realistic representation of the brackish water wedge. Calibration ceased when: (a) Root Mean Square (RMS) error of hydraulic head and chloride concentration reached 1 m (Figure 4.5a) and 250 mg/L (Figure 4.5b), respectively, and (b) the position and shape of the simulated fresh-brackish water interface (300 mg Cl/L isoline) in years 1965 and 2011 closely matched the observed wedge at 3 different cross-sections (Figure 4.6).

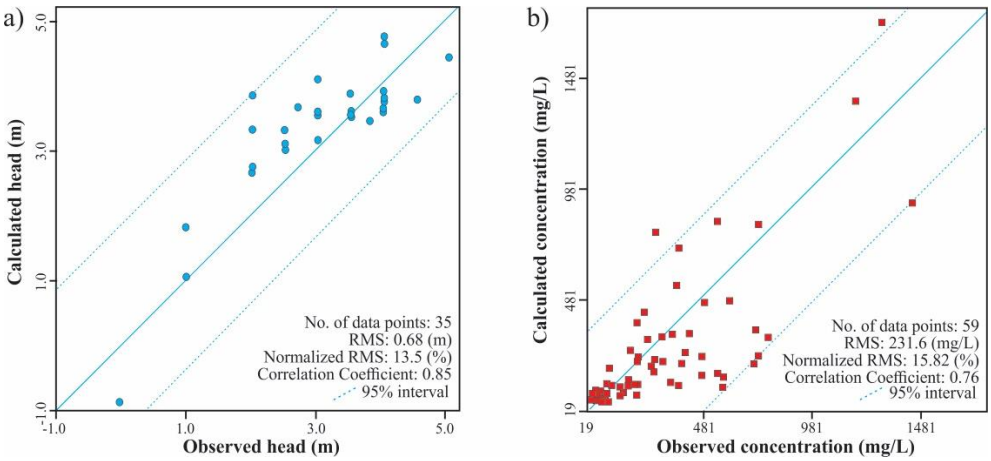

Figure 4.5 Calculated vs. observed (a) hydraulic head and (b) chloride concentration in year 2011. Data acquired at a depth of 0-30 m below the water table. RMS is the Root Mean Square.

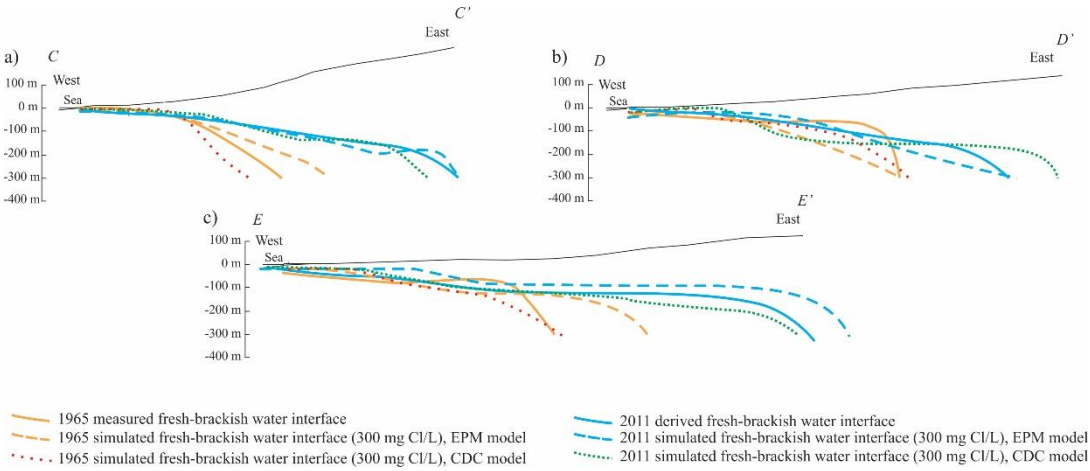

Figure 4.6 Calculated and observed fresh-brackish water interface in years 1965 and 2011 at 3 cross-sections (a) north of Naameh, (b) Naameh and (c) Damour. Position of sections indicated in Figure 2.1. Observed position of 1965 relied on electrical resistivity data (Geofizika 1965) whereas 2011 approximate position was analytically derived using the Glover solution (Cooper 1964; Charmonman 1965) assuming a homogeneous medium and a density of 1005 kg/m^3 for brackish-salt water (> 300 mg Cl/L) typifying the simulated salinized conditions. The 2011 interface lines matched measured chloride concentrations at different wells.

Special attention was paid to the role of the geo-lineaments and the plausibility of the CDC model after their insertion. Discrete features were assigned different initial values of hydraulic conductivity, porosity and dispersivity in line with the aforementioned methodology, and then they were optimized during the same calibration process. The determination of *K* and storage values solely relied on automatic calibration via PEST. Main hydraulic parameters were then supported by sensitivity analysis (see *Section 4.4.4*). The final values are listed in Table 4.3.

Table 4.3 Final values of DFs hydraulic properties after the corrections of the calibration process.

Type	*Kx*	*Ky*	*Kz*	σ_{Kx}	σ_{Ky}	σ_{Kz}	*Storage*	*Porosity*	*Dispersivity*
	[m/d]						[-]	[-]	[m]
Conduit/fracture	6050	15000	3	445	1100	0.2	0.004	0.7	0.5
Fault	0.5	4	0.01	0.1	1	0.002	0.001	0.05	1

σ_K: The standard deviation of uncertainty associated with *K* as estimated by the parameter optimization process of PEST.

Groundwater flow and salt transport conditions were computed by the model over a 70-year period, from 1941 to 2011. The pre-development phase allowed the simulation of aquifer conditions including the mixing zone (defined by the 300-10,000 mg Cl/L isolines) prior to significant pumping in 1991, whereas the post-development stage simulated salinity conditions after excessive pumping started. Heavy pumping after 1991 increased seawater intrusion at an average rate of ca. 25 m/year as indicated by the evolution of the brackish water wedge. The simulated extent of lateral intrusion by 2011 varied across the study area; in descending order: Mechref (400 m), Damour (300 m), Naameh (200 m) and Dawha (maintained same conditions). This order and the observed differences are mainly related to groundwater extraction rates being maximum at Mechref and minimum at Dawha.

The zone budget computed with SEAWAT showed that the volume of water extracted from the system prior to 1991 was only 0.057 Mm^3/year, and that ca. 71.9 Mm^3/year crossed the coastline inland. After post-development, about 3% more of seawater volume got into the system. This SWI was associated with more induced recharge from the Damour River, and inflows across the northern and southern boundaries (Figure 4.7), which indicates a volume compensation between the deep inflow of saltwater and the shallow freshwater outflow. In this mass balance, the aquifer recharge form rainfall matched the estimate of Khadra (2003), and the Damour river leakage matched the river bank infiltration induced since 1991 by the following extractions: 2 governmental (4900 m^3/d), 2 municipal (240 m^3/d) and very few private wells (6 m^3/d) in the Mechref village at 300-450 m from the river. In fact, using the double tracers $\delta^{18}O$ and chloride (Khadra and Stuyfzand 2014), these wells have 52 to 76% river interception, summing up to about 1.2 Mm^3/year.

It is speculated that 60% of the groundwater discharge to the sea (i.e. ca. 45 Mm^3/year) is fresh water. This value is only an estimate containing errors because it depends on

groundwater density as estimated from simulated salt concentrations (Eq. 4.6; Langevin 2003), which is not necessarily calibrated at the shoreline.

$$Q_f = Q_t(\rho_s - \rho)/(\rho_s - \rho_f) \quad (4.6)$$

where Q_f is simulated fresh groundwater discharge [m^3/d], Q_t is simulated total groundwater discharge [m^3/d], ρ_s is density of seawater [kg/m^3], ρ_f is density of freshwater [kg/m^3], ρ is the simulated density of groundwater discharging to the sea as recorded in the last active cell adjacent to the constant head boundary [kg/m^3].

Part of the fresh groundwater exits in the form of submarine groundwater discharge (SGD). A thermal infrared survey in early seventies delineated three submarine springs at tens of meters from the shoreline and at a depth of < 30 m (FAO 1973). In 2011, a survey was carried out by the author to check their persistence, and define their discharge and quality. It covered the main spots where submarine springs previously existed based on old thermal images and the statements of local citizens. Several transects measuring electrical conductivity (EC) and temperature of seawater showed no indicators of SGD existence. Hence, two divers working simultaneously at the same spots did a thorough scanning of the seafloor, and confirmed no presence of the springs. On the other hand, one new littoral spring was discovered; it had a very small discharge (ca. 5 m^3/d) in October with chloride concentration of 1700 mg/L. It is therefore hypothesized that submarine groundwater discharges at depth or in seepage zones spreading all over the shoreline, which is also an indication that there are no significant conduits. The recent absence (in 2011) of the three SGDs needs further investigation, but one possible explanation is that they have very low discharge (expected to be not much higher than the newly discovered one) making them difficult to locate, especially where terrigenous sediments cover the continental shelf.

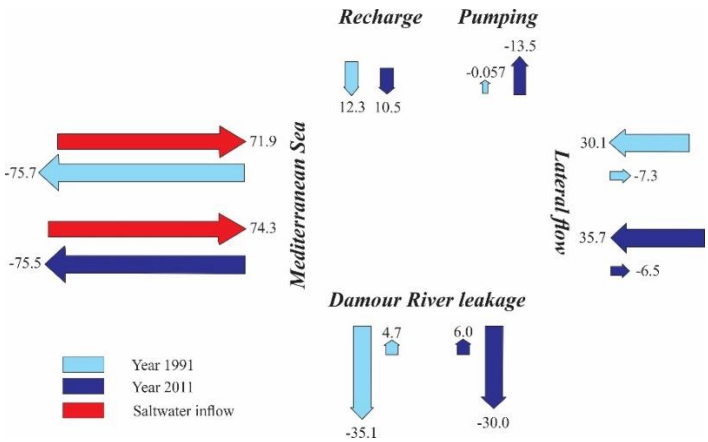

Figure 4.7 Summary of groundwater flow zone budget. Values are in million cubic meters per year (Mm^3/year).

4.4.4 Sensitivity analysis

The sensitivity of the hydraulic conductivity, porosity and dispersivity of the porous medium and its discrete features (DFs) on the salinity distribution is assessed based on the position of the freshwater-saltwater interface (10,000 mg Cl/L) in an E-W cross section in the middle of the study area (Figure 4.8). K_z of the main aquifer was shown to slightly affect the depth of the fresh-brackish water interface, enhancing it landward with higher K_z (Figure 4.8a). The impact of the vertical hydraulic conductivity of C_6 on the chloride concentration was tested for one order range, but it only showed minor effects. The decrease of porosity for all units from 0.3 to 0.1 did enhance salt transport, and advanced the interface about 300 m landward (Figure 4.8b). The decrease of longitudinal dispersivity over the whole domain from 60 m to 20 m improved the overall chloride concentration accuracy and pushed the interface back by about 250 m (Figure 4.8c). In contrast, increasing the vertical over horizontal dispersivity ratio from 0.01 to 0.3 showed a negligible impact on the interface position (Figure 4.8d).

The GHBs were sensitive to hydraulic head rather than to the specified concentration but had local effects only. Similarly, varying the Damour River bed thickness had negligible effect. Salinity variations of the river were neglected due to minor changes of surface water chloride levels (< 25 mg /L) throughout the year. Recharge variation had a minor effect on water levels, especially when compared to the impact of the uncertainty of hydraulic conductivity, but it directly affects the water budget.

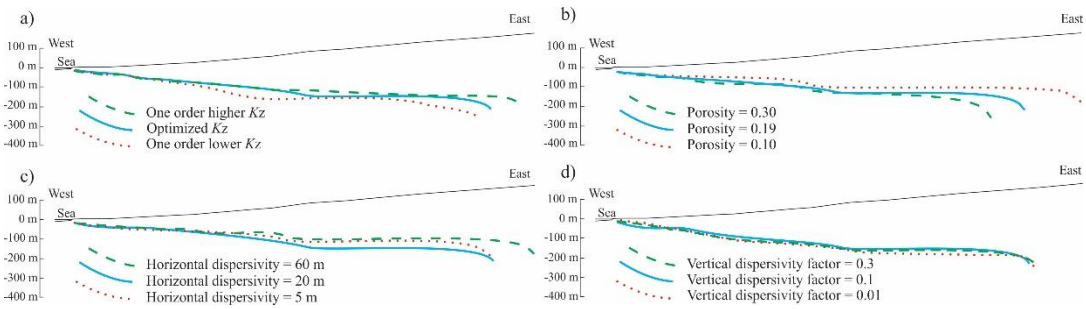

Figure 4.8 Variation of the freshwater-saltwater interface position in the middle of the study area (at EE') by different (a) vertical hydraulic conductivity (*K*z), (b) porosity, (c) longitudinal dispersivity and (d) vertical dispersivity factor of the main aquifer.

The results of the sensitivity analysis of the DFs are also shown in Figure 4.9. One order of magnitude higher horizontal hydraulic conductivity of the DFs advanced the toe of the interface by around 450 m (Figure 4.9a). This is attributed to more advection and eventually SWI in the DFs. Similarly, one order of magnitude higher vertical hydraulic conductivity (*K*z) or longitudinal dispersivity advanced the toe by ca. 200 m (Figure 4.9c and d). Conversely, higher porosity pushed the interface position back landwards (Figure 4.9b).

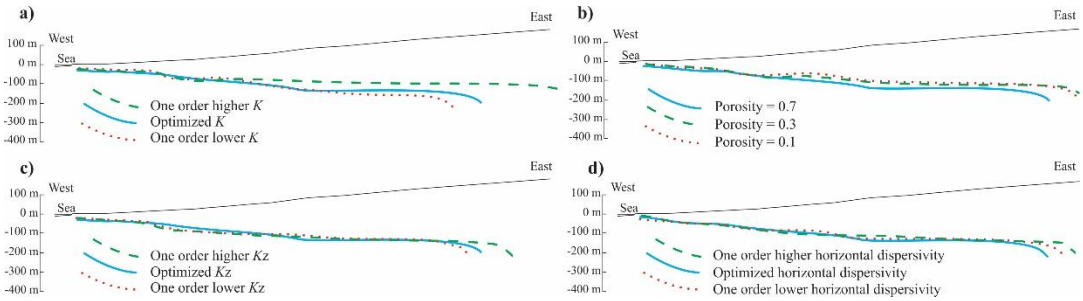

Figure 4.9 Variation of the freshwater-saltwater interface position in the middle of the study area (at EE') by different (a) horizontal hydraulic conductivity, (b) porosity, (c) vertical hydraulic conductivity (*K*z), and (d) longitudinal dispersivity of the discrete features.

4.5 Discussion

4.5.1 EPM vs. CDC resemblance

The adequacy of the EPM approach (without DFs) and the CDC approach (with DFs) was assessed based on the RMS and the normalized RMS error of salinity, the correlation coefficient, and the match of the simulated saltwater-freshwater interface with the data in 1965 and 2011. A comparison of the performance of the models after a clearly defined automatic parameter optimization showed reasonable results for both as is shown in (Figure 4.10). However, the CDC approach reduced the overall model error (RMS of salinity) by ca. 28% (Figure 4.10), and reduced the error of the chloride concentrations at most wells (Fig. 4.11) relative to the EPM method. The two models were also compared using the Akaike Information Criterion (AIC; Akaike 1974) and the Bayesian Information Criterion (BIC; Schwarz, 1978), which are two relative measures for the goodness-of-fit (Mooi and Sarstedt 2011). Statistical results performed in *SPSS Statistics 17.0* confirm that the CDC model has a better fit than the EPM model as reflected by lower AIC and BIC values (Table 4.4).

The EPM model in the study area overestimated the position of the toe of the fresh-brackish water interface for the years 1965 and 2011, at which it was checked (Figure 4.6). With the CDC model, the discrepancy in the position of the toe was reduced, which is in agreement with the recent experimental findings of Sebben et al. (2015) for a Henry problem embedding continuous orthogonal fractures. At some locations no positive response was obtained. The same phenomenon was found for the Madison aquifer of western South Dakota (USA) where a comparison of flow with and without discrete conduits showed that model calibration with Conduit Flow Package (CFP) improved at some spots only (Saller et al. 2013).

Table 4.4 Comparison of the EPM and the CDC models according to 5 statistical measures to goodness-of-fit.

Model	RMS (mg/L)	Normalized RMS (%)	Correlation Coefficient	AIC	BIC
EPM	319.9	21.85	0.66	236	477
CDC	231.6	15.82	0.76	233	474

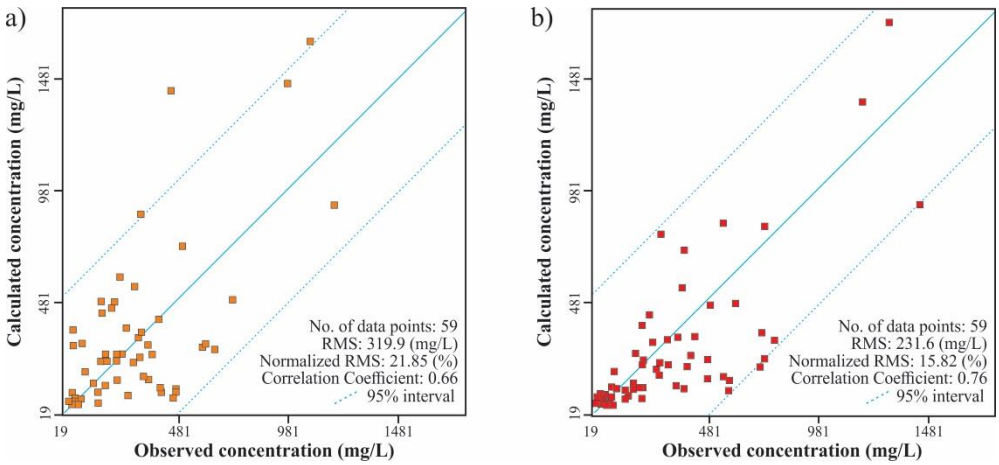

Figure 4.10 A comparison between observed vs. simulated chloride concentrations in year 2011 utilizing (a) the EPM, and (b) the CDC models.

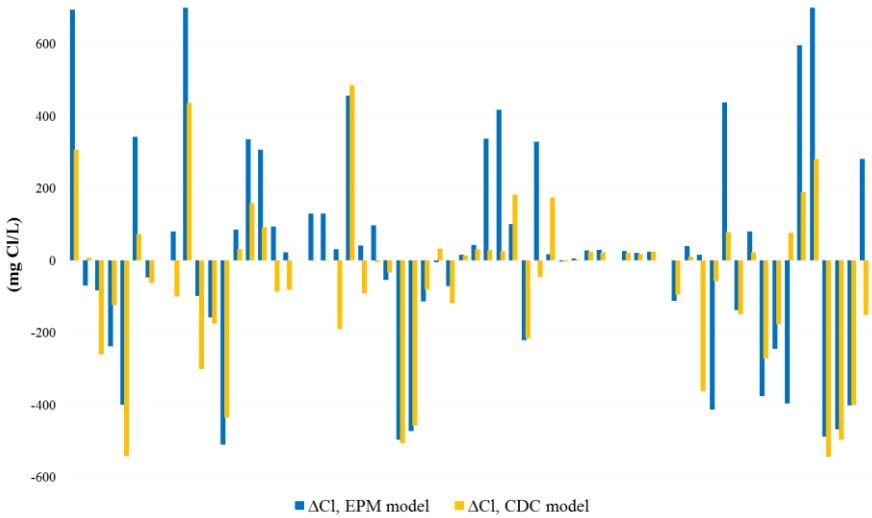

Figure 4.11 A bar plot comparing ΔCl values at all wells in year 2011, for EPM and CDC models. ΔCl = $Cl_{simulated}$ - $Cl_{observed}$.

4.5.2 Options for mature karst

Analyses of time series for highly developed (mature) karst aquifers elsewhere showed short-memory effects indicating fast response, like for instance < 20 days in the French Pyrenees (Padilla and Pulido-Bosch 1995), and < 8 days in Greece (Panagopoulos and Lambrakis 2006), southwestern Slovenia (Jemcov and Petric 2009), and southwest China (Fu et al. 2016). Such strongly karstified aquifers are examples of cases for which the EPM approach is not valid (e.g. Teutsch 1993; Kovács 2003; Fattahi et al. 2010) due to turbulent dynamics that are controlled by dominance of conduit flow. In these cases a trial of the CDC approach is worthy because it may work in accounting for some local heterogeneities that improve model output.

Uncertainty analysis is also suggested as a possible check of the EPM or CDC adequacy, for instance by Monte Carlo simulation with different realizations of hydraulic conductivity fields yielding probability maps of heads and chloride concentrations. This would allow dividing the investigated area into different zones according to their degree of uncertainty, which eventually helps to judge the suitability of the model for specific sub-areas or purposes, or to delineate zones that need a more detailed investigation. If unsatisfactory, then other options are sought. Options are: (a) a dual 1-D/2-D continuum approach, (b) a lumped parameter "black box" (although only suitable to assess the global response of the system), or (c) a dedicated complex model that accounts for several factors that have been ignored in the current study: recharge, epikarst, vadose zone conditions, and more detailed information on conduits (Chen and Goldscheider 2014; Pardo-Igúzquiza et al. 2015).

4.6 Conclusions

Modeling fractured and karstic aquifers is a challenge due to the dominance of non-Darcian flow and the scarcity of codes with formulations that account for turbulent behavior, more so when simulating saltwater intrusion (SWI) requiring variable-density flow and solute transport. To date, there is no agreement on the best way to simulate SWI in karstic media. Modelers lean toward assuming an equivalent porous medium (EPM) even though it is not always justified because the assumptions underlying such codes are rarely met.

This paper suggests two steps to simulate SWI in poorly karstic aquifers: (1) start with time series analysis to discover the hydrodynamic response of the system and decide whether ignoring quickflow is justifiable, and (2) try a coupled discrete-continuum (CDC) approach to check whether it warrants better results at the desired scale than an EPM model. These methods were successfully applied to a poorly karstic dolomitic limestone aquifer in Lebanon (the Eastern Mediterranean). Time series analysis revealed a relatively long response time of groundwater levels to rainfall inputs. This indicates that conduit quickflow is scarce, justifying the initial use of the EPM simplification. Information on geo-lineaments (main fractures, faults, and discerned conduits) was then used to embed discrete features into the 3-D continuum to obtain a more karst-representative CDC model.

Inserting discrete features aimed at reducing uncertainty of salinity patterns. The precise conduit network is almost never known, and hence the delineated geo-lineaments constitute at most a fraction of a wider web, so higher resolution data is necessary where more detail is required.

Comparison of the two approaches showed that the CDC had less difference between measured and computed salinity values than the EPM. This comparison relied on: (a) 5 statistical measures of salinity or hydraulic head goodness-of-fit (root mean square (RMS) and normalized RMS error of salinity, correlation coefficient, Akaike Information Criterion, and Bayesian Information Criterion), and (b) the match of the simulated saltwater-freshwater interface with available data from 1965 and 2011. The CDC model improved the local-scale salinity values for the majority of wells including the position of the fresh-brackish water interface, and reduced the overall model error (RMS of chloride) by ca. 28%. For the EPM method, 26 simulated wells out of 59 were more than 200 mg/L off, whereas the count being 16 for the CDC model; only at a few wells CDC scored worse than EPM. Therefore, it is assumed that the CDC is better warranted for modeling SWI in the poorly karstic Damour aquifer, which is worth its more complicated application, as is the case with any model seeking higher accuracy at local scale.

More efforts are still needed to test the performance of the CDC approach including a prior time series analysis of rainfall and water table response in other systems, also in mature karst, in an attempt to come up with additional conclusions and recommendations that can reduce the confusion of modeling SWI in all types of karstic aquifers.

Acknowledgements Dr. Vincent Post (BGR, Germany) is acknowledged for his time to evaluate the merits of the first draft of this manuscript and provide useful suggestions. The reviews of Prof. Dr. Adrian Werner (Flinders University, Adelaide) and Prof. Dr. Theo Olsthoorn (TU Delft) contributed to substantial improvements that focused the outcome of this work. We are also grateful to agricultural engineer Mr. Khaled Aoun for his aid in installing a multi-set monitoring system in the vicinity of Damour (Lebanon), and to the Mechref Village Company for helping us to collect necessary water level data over several years.

Appendix S4: Supplementary Material

Table S4.1 Input parameters of geo-lineaments automated extraction using *LINE* module of *PCI Geomatica*.

Parameter	Value
Filter radius	10 pixels
Edge gradient threshold	80
Curve length threshold	100 pixels
Line fitting error threshold	50 pixels
Angular difference threshold	30°
Linking distance threshold	20 pixels

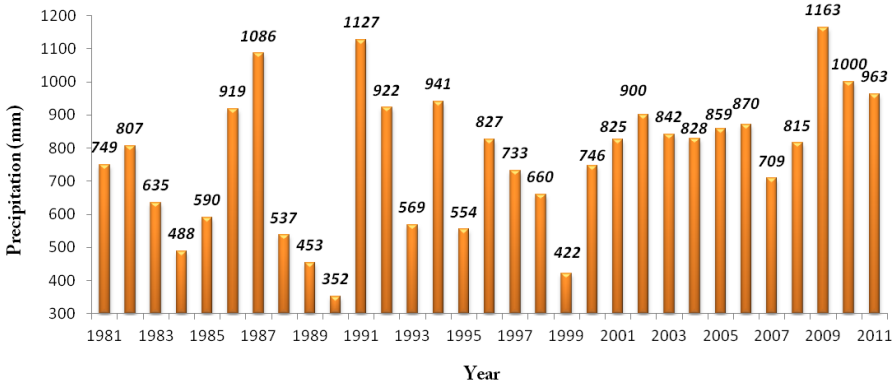

Figure S4.1 Annual precipitation record between 1981 and 2011 at Beirut Airport station, 7 km to the north of the Damour coastal aquifer.

Chapter 5

Mitigation of saltwater intrusion by 'integrated fresh-keeper' wells combined with high recovery reverse osmosis

This chapter was published as:

Khadra, W.M., Stuyfzand, P.J., Khadra, I.M., 2017. Mitigation of saltwater intrusion by 'integrated fresh-keeper' wells combined with high recovery reverse osmosis. *Science of the Total Environment* 574, 796-805.

Abstract

Most countermeasures to mitigate saltwater intrusion in coastal, karstic or fractured aquifers are hindered by anisotropy, high transmissivities and complex dynamics. A coupled strategy is introduced here as a localized remedy to protect shallow freshwater reserves while utilizing the deeper intercepted brackish water. It is a double sourcing application where fresh-keeper wells are installed at the bottom of a deepened borehole of selected salinized wells, and then supported by high recovery RO desalination. The RO design has < 1 kWh/m^3 energy consumption, and up to 96% recovery in addition to low scaling propensity without use of any anti-scalant. A feasibility study is presented as an example for a salinizing, brackish well (TDS ~1600 mg/L) in the Damour coastal aquifer in Lebanon. The concept is expected to produce ca. 1000 m^3/d of freshwater from this well by pumping 250 m^3/d of fresh groundwater from the top well screen and 800 m^3/d of brackish groundwater (to be later desalinized) from the fresh-keeper well screen below. Cost analysis shows that the capital cost could be returned back in 1 to 4 years depending on the choice of produced water (bottled or tap) and available market. As an alternative, water from the RO plant could be blended with lower quality water, for instance untreated brackish groundwater (if unpolluted), to supply 3 more volumes for domestic use. The usage of brackish groundwater from integrated fresh-keeper wells thus serves 3 purposes: production of high quality drinking water, financial gain and mitigation of water stress by overpumping.

5.1 Introduction

Planning of coastal aquifers requires special attention due to proximity and direct interaction with seawater. Wells close to the shoreline often encounter a rapid increase in salinity deteriorating water quality and making it of less suitability. Many sources of saltwater exist (Stuyfzand and Stuurman 2006; Bobba 2007), such as: (1) direct seawater encroachment, (2) connate seawater from the past geologic time, (3) saltwater concentrated in enclosed areas like tidal lagoons and playas, (4) return flow from irrigation, (5) halite dissolution, and (6) anthropogenic salty wastes. The first source is the most dominant and imminent, due to steeply increasing water demands and ineffective management strategies (Datta et al. 2009). The situation worsens where alternative water resources are scarce or absent, leading to rapid exhaustion of groundwater reserves.

In many instances groundwater extraction cannot be reduced, which necessitates strategies to simultaneously prevent saltwater intrusion and provide other resources. These have been considered as major challenges to coastal hydrologists. Replenishment of already deteriorated water is expensive and sometimes ineffective, and prevention is hampered by the need to provide enough substitutes of chemically suitable water. Therefore, this issue has attracted much attention over the last decades, and several countermeasures have been proposed (see *Section 1.2*).

This paper formulates a coupled strategy of 'Integrated Fresh-Keeper' (IFK) wells, and a high recovery (HR) brackish water reverse osmosis (BWRO) system. An IFK well is installed at some vertical distance below the fresh water pumping well to be secured, within

the same borehole. It creates a vertical hydraulic barrier that intercepts upconing brackish water below the upper well screen before it reaches the overlying freshwater body. This concept was first introduced by KWR Watercycle Research Institute (The Netherlands) as a remedy to salinizing well fields (Grakist et al. 2002; Kooiman et al. 2004; Stuyfzand and Raat 2010). Abandoned or intentionally drilled saline wells could be exploited to provide new volumes of freshwater; this is achieved by (a) protecting freshwater at shallower depths (i.e. keeping it fresh) where additional amounts may be safely extracted, and (b) desalting pumped saltwater. Collected water is then distributed as high quality potable water or lower quality for domestic use. This in lieu delivery of groundwater can also aid efforts to reduce pumping rates at heavily exploited spots which subsequently reduces saltwater encroachment. Nevertheless, waste disposal has created an environmental problem against wider adoption of the desalting process, which encouraged efforts towards higher recoveries. The HR-BWRO design introduced here follows a modified Type A Zero Liquid Discharge (ZLD) scheme (Pérez-González et al. 2012) characterized by a very low percentage of reject, sometimes reaching 4% during normal operation. It is also characterized by reduced energy consumption and low propensity of membrane fouling by precipitates making it superior to other widespread commercial designs.

The proposed strategy is tested here as an example to utilize brackish water extracted from a salinizing well at the Damour coastal aquifer (Lebanon). This aquifer is one of the major water resources of Beirut city (the Lebanese capital) and its suburbs, and has been facing saltwater intrusion since the 1960s. Masciopinto (2013) proposed the use of well barriers via artificial recharge along the Damour coastline to reduce seawater intrusion. The IFK approach is another management option with a more localized remedy. It is presumably more convenient than creating larger scale hydraulic barriers, especially in settings where a precise understanding of system dynamics is not possible, as in karstic or fractured aquifers.

5.2 Methods

5.2.1 Selection of proper vertical barrier

The decision on the proper depths and simultaneous fresh/brackish pumping rates at an individual site is a critical step in planning for IFK wells. Local scale numerical modeling is needed to define the proper layout of wells and warrant a stable saltwater interface with suitable feed volume and quality. For this purpose, two alternatives exist: (a) 3-D models with fine discretization around wells of interest (Anderson and Woessner 1992), or (b) axisymmetric (radial) profile models (Langevin 2008). The finite-difference code SEAWAT (Guo and Langevin 2002) could do the job; however, 3-D formulations require lengthy runtimes and computational costs. Hence, faster radial axisymmetric 2-D simulation is desirable provided that some input parameters are adjusted and the proper weighting scheme is chosen (Langevin 2008; Louwyck et al. 2012). Parameter scaling

seems to be sometimes awkward, but it is a worth effort because the axially symmetric models require significantly less execution times and are capable of producing reliable solutions to complex problems involving reactive or nonreactive transport (Wallis et al. 2013).

5.2.2 Design of high recovery RO system

After deciding on location and flux of the IFK wells or the vertical negative barrier, the RO system specifications and the fate of membrane concentrate should be considered. RO recovery usually varies between 35% and 85% depending on feedwater, scaling propensity and reject quality (Greenlee et al. 2009). This paper aims at introducing a high recovery BWRO system at up to 96% recovery during normal operation. The proposed design is illustrated in Figure 5.1 and Table 5.1; it is a HR-RO tandem following modified Type A Zero Liquid Discharge (ZLD) scheme (Pérez-González et al. 2012), where main foulants and scalants are reduced in a pre-treatment multi-stage facilitating more efficient desalination with higher recovery (Henthorne and Boysen 2015). Such tandem designs have been recently introduced by several authors as promising options aiming at high recoveries and reduced effluents (e.g. Ning and Troyer 2009; Rahardianto et al. 2010), in addition to their successful application at different sites, for instance, El Paso (Texas), Kifan (Kuwait), Ehime (Japan), Mas Palomas (Spain) and Laayoune (Morocco).

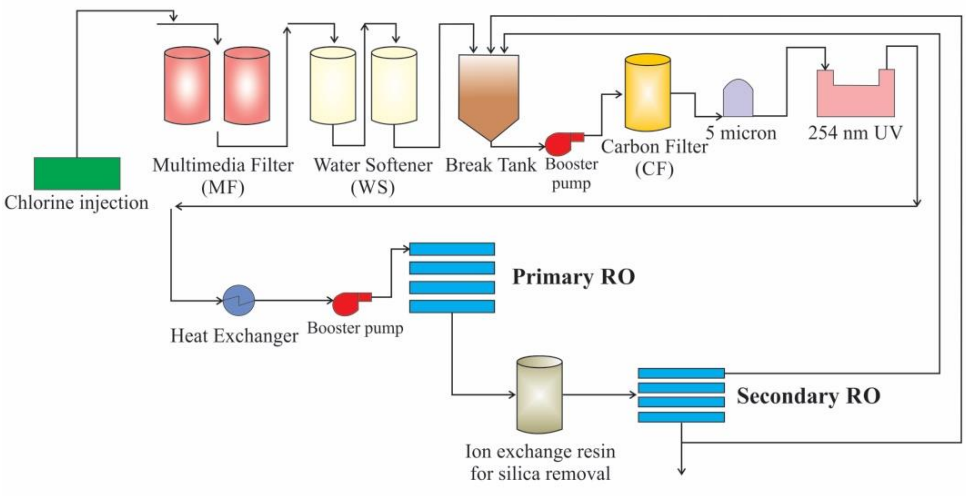

Figure 5.1 Process flow diagram of the proposed treatment system design. The intermediate treatment stage (silica removal ion exchange resin) is optional depending on SiO_2 concentration.

Feedwater initially enters a pre-treatment phase where: (a) chlorine injection at the beginning keeps microorganisms down, (b) multimedia filter with dual parallel units minimizes instantaneous water flow and drain requirements, and removes particles > 25 μm (further elimination is usually not needed in BWRO due to low turbidity in groundwater), (c) filtered water is then supplied to downstream dual series softeners (primary and polisher) to strongly reduce the hardness of feedwater after which (d) non-back washable carbon filter (CF) removes impurities, chlorine (introduced in the beginning because it should not go through the ROs) and some contaminants notably humic acids to avoid potential organic foulants, then (e) water enters a 5 micron filter to catch any particles that fall off the carbon filter before (f) it is exposed to 254 nm UV light (germicidal light) to disinfect any possible microbial growth (carbon beds may be a breeding ground for bacteria, and uncontrollable microbial growth would ultimately affect the RO membranes by forming thin biofilms). The water subsequently goes through a heat exchanger to regulate its temperature at the RO inlet (best is 19–20 °C).

Pre-treated water then enters a primary RO of several units. The system re-circulates part of the membrane reject through the same configuration, which improves recovery without significant increase in energy consumption. The reject is then sent to a secondary RO system to provide higher recoveries. Two booster pumps (centrifugal pumps) are needed to allow for acceptable flow rates through the CF and RO. High recovery reject goes to drain during operations, and when there is no demand on the system (i.e. no request to make water) the reject follows a recirculation operational mode. It goes back to the break tank to repeat the loop via carbon filter, 5 micron, 254 nm UV, primary and secondary RO (Figure 5.1). This mode achieves nearly 100% recovery; it is advantageous to avoid halting the system during no demand because stagnant water creates unwanted effects such as micro-contamination and clogging. Another purpose of the heat exchanger and the recirculation loop is Hot Water Sanitization (HWS). From a maintenance perspective, HWS is an essential step done once or twice a month in order to kill any microbial growth in the entire system (including the CF and the ROs). It is a temporary mode (30–60 min) where production of water is stopped, a small volume is alternatively heated to 80–85 °C, and then allowed to go through the circulation loop back to the break tank and consequently via the RO membranes (Figure 5.1).

Table 5.1 RO tandem design and implementation (example for 400 m^3/d).

Multimedia filter
- Back-wash and rinse based upon ΔP
- Dual / Parallel units to minimize instantaneous water flow and drain requirement
- Always filtered water supplied to downstream softeners

Water softener
- Dual Series Softeners (Primary / Polisher)
- Regenerate based on total hardness
- Final (fast) rinse controlled by conductivity (compare inlet to outlet)
  - Optimized chemical cost
  - Reduced service water
  - Reduced waste stream
  - High water quality

Carbon filter
- Non – back-washable carbon
- Replace carbon every 6 months to 1 year (manual valves provided to facilitate change out)
- Continuous circulation over bed
- Sanitized twice a month (No need for carbon regeneration in case of CF annual replacement)

5 micron
- Cartridge filter
- Natural or synthetic yards
- Disposable and replaced when clogged

254 nm UV
- UV lamp is replaced every 1 year

Primary RO configuration
- Membrane Material: Polyamide Composite
- Membrane Configuration: Full Fit / Loose –wrap
- Membrane Size: 8'' diameter x 40'' Length
- Membrane Manufacturer: FILMTEC™
- Design Membrane Flux: 34 m^3/d

Secondary RO configuration
- Membrane Material: Polyamide Composite
- Membrane Configuration: Full Fit/ Loose –wrap
- Membrane Size: 4'' diameter x 40'' Length
- Membrane Manufacturer: FILMTEC™
- Design Membrane Flux: 9.5 m^3/d

The system could be improved further by adding membrane pretreatment to replace conventional pre-treatment. This may further improve feedwater quality and avoid fluctuations in notably turbidity and TDS. Economically, this option is more expensive; however, costs are counteracted by the expected reduced costs of the RO system and life extension when operating under better quality feedwater. In case of potential SiO_2 precipitation, an intermediate treatment stage (Figure 5.1) with ion exchange resins for silica removal could be installed between the primary and secondary ROs.

Designing the RO system with proper configuration of membranes could rely on different commercial softwares. Reverse Osmosis System Analysis (ROSA) from Dow Water and Process Solutions (www.dowwaterandprocess.com) is one famous alternative using DOW FILMTEC™ elements. ROSA is capable of defining system configuration and

chemistry of permeate/concentrate once feedwater composition is selected, and its results have been proven to be of high reliability and in agreement with experimental tests at different sites (e.g. Moudjeber et al. 2014).

5.3 Application to the Damour aquifer - Lebanon

The Damour aquifer is a major coastal aquifer in Lebanon lying south of the capital Beirut (Figure 2.1). It is a main source of water providing one third of Beirut and its suburbs demands, and has been extensively pumped since 1991 with a total abstraction rate of about 13.5 Mm^3/year. A description of the hydrogeological setting of this area is available from Khadra and Stuyfzand (2014). Upconing was recorded at different spots. The increase of population and water demands forced water authorities to continue pumping at the expense of water quality. One major governmental well, known as D1 to the water authorities (Figure 2.1), previously pumping at 2880 m^3/d in Naameh village was shut down in 2009 due to high salinity (Cl > 1000 mg/L). Salinization is foreseen to slowly progress in the coming decades, and hence water authorities are expected to lose other wells close to the shoreline if no further action is taken.

Another governmental well, known as D5, located between the villages of Damour and Mechref at a distance of 1370 m from the shoreline (Figure 2.1) was chosen here as an example site for possible IFK installation. It has been pumping continuously since 1991 at a constant rate of 1680 m^3/d. It taps the current saltwater mixing zone, and it is anticipated that continued pumping at shallower depths will result in more deterioration of water quality due to upconing of saltwater. Its groundwater chemistry is presented in Table S5.1 (*Appendix S5*) for wet and dry seasons.

5.4 Results and discussion

5.4.1 IFK pumping layout

For the purpose of choosing the proper pumping layout of the vertical barrier, a radial axisymmetric numerical model was built using SEAWAT (Guo and Langevin 2002). A radius of 100 m was chosen to represent the well domain for one year, which was assumed a safe assumption with no flow interference based on the following formula:

$$r = \sqrt{\frac{Qt}{\pi bn}} \tag{5.1}$$

where r is the radial distance [m]; Q is discharge rate [m^3/d]; t is the time [d]; b is the thickness of flow domain [m] based on borehole logs; n is the porosity [−].

A radially symmetric 2-D model approach was adopted following Langevin (2008). Logarithmic mean was assigned for interblock conductivity calculation (option 2 in the LPF package of SEAWAT). The negative vertical barrier was located at one edge of the model (left side in Figure 5.2), and cells representing the borehole were assigned high vertical hydraulic conductivity. Parameters at each cell were adjusted to account for the increase in aquifer volume away from it. As a function of radial distance, each parameter on cell to cell basis became:

$$X_i^* = r_i 2\pi X_i \tag{5.2}$$

where X_i^* is the adjusted input parameter at the ith column (hydraulic conductivity, specific storage, porosity and recharge); r_i is the radial distance from model edge to center of cell of the ith column; X_i is the measured parameter at the ith column.

A 1 m horizontal discretization was assigned in the first 25 m surrounding the well, and then allowed to increase at 1.5 factor reaching a maximum of 2.5 m at the edge. Vertical discretization was set at 5 m to a total depth of 170 m from ground level (Figure 5.2). Local vertical hydrostratigraphy relied on well-logs (Figure 5.3), but lateral heterogeneities were ignored. The sub-layers were given different hydraulic conductivities (K), which were generated using a stochastic approach (Kerrou et al. 2013). Vertical lithological variation was sorted into 3 main lithotypes: limestone with marl and/or marly limestone, partially fractured limestone, and highly fractured limestone (Figure 5.3). Lithotypes were then converted into different hydraulic conductivities assuming log-normal distribution. Fifteen values estimated from pump tests in the studied aquifer (Khadra 2003) were utilized for this purpose. Their cumulative distribution function CDF was plotted against ln(K) in order to sort the samples into different groups (Figure 5.4), which were represented by their geometric means. The smaller (20 m/d), intermediate (105 m/d) and larger (235 m/d) values were later assigned to the three aforementioned facies, respectively (Figure 5.3).

A constant-head boundary (−90.5 m) was assigned to one edge of the model (right side in Figure 5.2) in agreement with hydraulic head values in the well's vicinity. The constant-head over the simulation period was justified by minor water level fluctuations recorded in most pumping tests due to high transmissivity of the aquifer (Khadra 2003). The topmost layer had recharge boundary assigned to upper active cells (Figure 5.2). Recharge to the aquifer was variable on monthly basis according to rainfall data (Table S5.2, *Appendix S5*) (Meteorological Service 2010) with a 40% infiltration coefficient; chloride concentration of recharge water was assigned a constant value of 30 mg/L as deduced from average chloride in rainfall (11 mg/L) and average evapo-concentration factor in the study area (Khadra and Stuyfzand 2014). Noteworthy that SEAWAT sets the recharge to the upper-most active (wet) layer. So no need to account for water flow in the unsaturated zone including the soil moisture characteristics. A constant-concentration (1000 mg Cl/L) was assigned to the layer directly overlying the no-flow boundary at the bottom. Its value was deduced after several trials to maintain a good match between observed and simulated salinity values, including seasonal variations, recorded over a one year period in 2009 (Figure 5.5). The constant

boundary assumption is also justified by stable conditions revealed from chloride time-series collected over the last decade during continuous prolonged pumping at a rate higher than the intended by the IFK installation.

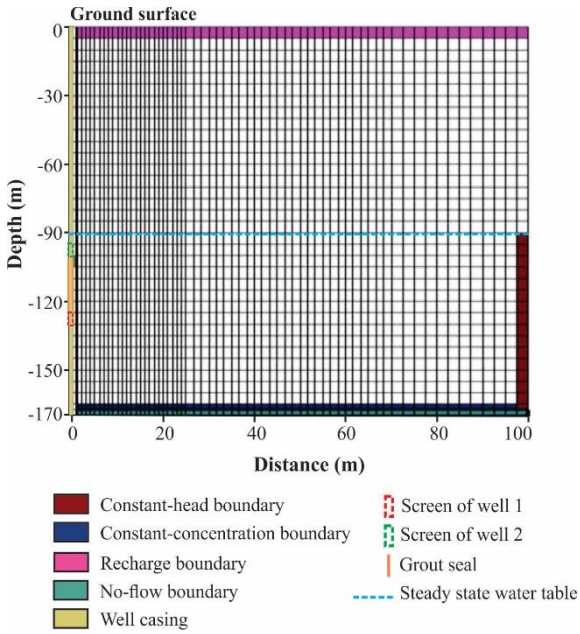

Figure 5.2 Discretization mesh of the 2-D radial axisymmetric model. X-axis represents distance (in meters) from well D5 located at the left corner; y-axis represents depth (in meters) from land surface; vertical dimension was suppressed to 50%. Initial salt concentration= 200–400 mg/L.

After the 1-year period satisfactory representation (Figure 5.5), another shallower well was added (Figure 5.3), and the pumping of the main well was reduced from 1680 m^3/d to 800 m^3/d. A second simulation was then run for different scenarios using both wells in order to choose the proper pumping rates to obtain a stable vertical fresh-saltwater interface. This was assessed based on the breakthrough of chloride in the shallower well. Results showed that pumping 800 m^3/d at the fresh-keeper (main) well for 10 years could warrant a salinity of ca. 200 mg Cl/L in the shallower well (Figure 5.6), which was allowed to pump at 250 m^3/d. This way the IFK installation provided local protection against saltwater upconing and simultaneously supplied additional freshwater reserves. Theoretically, the behavior of the new array might differ from the historical attitude over the last decade due to separation of flow via a shallow and a deep well. Therefore, the response was checked for both arrangements (one and two screens). Numerical results showed that the deeper screen will not be stressed more than before especially when the pumping rate is lower (800 m^3/d vs. 1680 m^3/d).

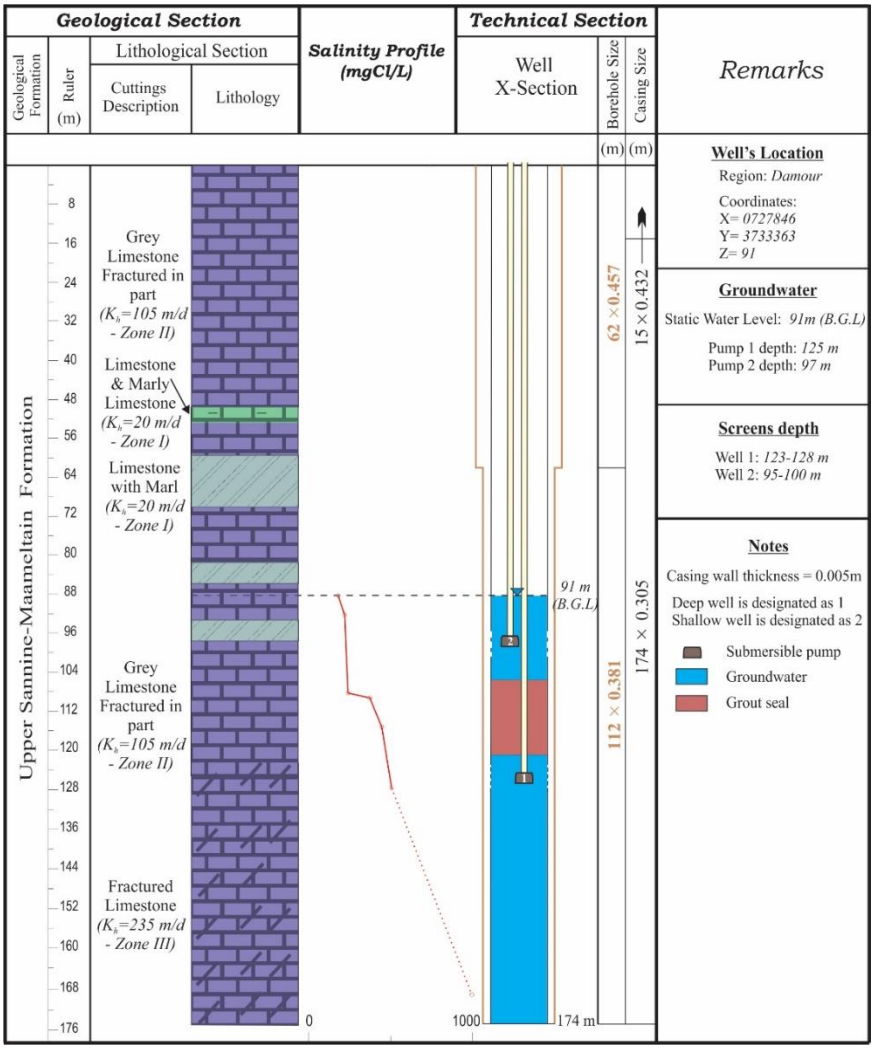

Figure 5.3 Geological and technical cross-section of well D5 in the Damour area (south of Beirut, Lebanon) modified for IFK installation. Salinity profile relied on data collected in 2011 at different depths in the same well and the close vicinity. The dotted line is extrapolated from modeling outcome. Zones (I, II and III) of K_h are generated in Figure 5.4.

Figure 5.4 Cumulative distribution function (CDF) of the Gaussian *ln(K)* distribution generated using a variance and mean of 85 m/d and 65 m/d, respectively. Values are sorted then discriminated into three zones (I, II and III), which are subsequently attributed to the corresponding lithofacies (higher values to more permeable lithofacies).

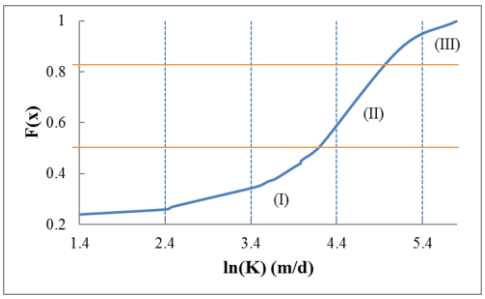

Figure 5.5 Observed and simulated salinity concentration versus time at well D5 utilizing a time-series over a 1-year period in 2009. After 300 days salinity drops as a result of recharge increase in the Fall season.

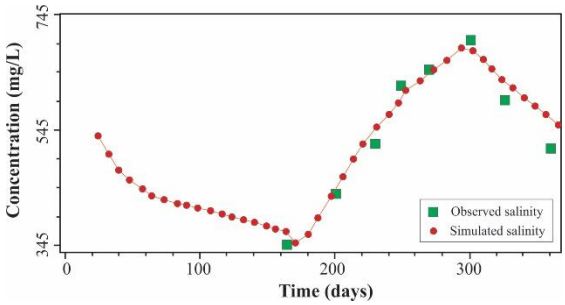

Figure 5.6 Predicted chloride distribution of the IFK installation after 10 years of continuous pumping at well D5.

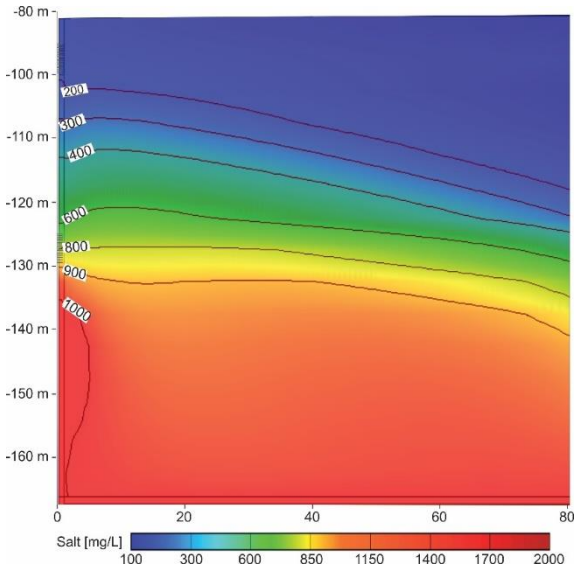

The diminution of the extraction rate will increase the total fresh groundwater outflow at the shoreline by 680 m^3/d (i.e. 3.4 m^3/d/m assuming that well domain is represented by a radius of 100 m), which may subsequently push back the seawater/freshwater interface position by about 70 m. This estimate contains some uncertainty, and hence should be later corroborated by the outcome of numerical models. It assumes Dupuit and Ghyben-Herzberg approximations according to the following formula (Masciopinto 2006, 2013),

$$L = K\frac{B^2 - H^2}{2\delta \times Q} \tag{5.3}$$

where L is the distance between the shoreline and the seawater/freshwater interface toe [m]; Q is the freshwater discharge into the sea per unit of coast length [m^3/d/m], estimated at 40 m^3/d/m as deduced from hydraulic heads in the vicinity but raised later by 3.4 m^3/d/m; K is the hydraulic conductivity [m/d], 20 m/d; B is aquifer saturated thickness [m], 370 m; H is the depth of the interface at the outflow section [m], assumed here to be at shoreline; δ is freshwater/seawater specific ratio [-], assigned a value of 39.

5.4.2 Design of the HR-RO system

The proposed multi-stage HR-RO tandem design is preceded by different pre-treatment steps as displayed in Figure 5.1 improving the overall quality of feedwater. An overview of the HR-RO design is explained in Figure 5.7 and Table 5.2. The first pass utilizes HSRO-390-FF membranes from FILMTEC™ 8 in. in diameter and 40 in. long. It has 4 stages with 2 pressure vessels in the first stage and 1 vessel in the three others; each having 3 elements per vessel. This array is favored because equal membrane elements reduce production between vessel inlet and outlet (Fritzmann et al. 2007). About 40% of reject is re-circulated (path 4 in Figure 5.7a) for further treatment and higher recovery. The second pass utilizes LC HR-4040 4 in. diameter × 40 in. long membranes with same number of stages; the first two have two vessels whereas the others have one (Table 5.2). A booster interstage pump is added before the first stage to counteract for reduced driving force on the feed side induced by higher concentration and pressure loss. pH is adjusted using ion exchange softening to maintain neutral conditions.

The quality and quantity of permeate water rely solely on ROSA calculations. It is assessed for two feedwaters anticipated during wet and dry seasons (Table S5.1). For the dry season, pass 1 has 71% recovery whereas pass 2 has 72% summing to a cumulative recovery of 92% (Table 5.3). The evolution of water quality from raw conditions via primary and secondary ROs to final permeate and concentrate quality is summarized in Table 5.4. When utilizing wet season groundwater chemistry the total recovery reaches 96%. The system produces a total feed flow of 367 and 33 m^3/d for permeate and concentrate, respectively in the dry period. The permeate has a TDS of 39 mg/L collected from first pass (70%) and second pass (30%) (Table 5.3). The concentrate (33 m^3/d) is brackish-salt with TDS of 19,584 mg/L including 2,930 mg/L HCO_3, 7,022 mg/L Na, 8211

mg/L Cl and 1,007 mg/L SO_4. This overall process leads to a total power consumption of 0.96 kWh/m^3. However, in the wet season, the system consumes 0.89 kWh/m^3 to produce 384 m^3/d of permeate and 16 m^3/d of concentrate with 18 mg/L and 24,791 mg/L TDS, respectively.

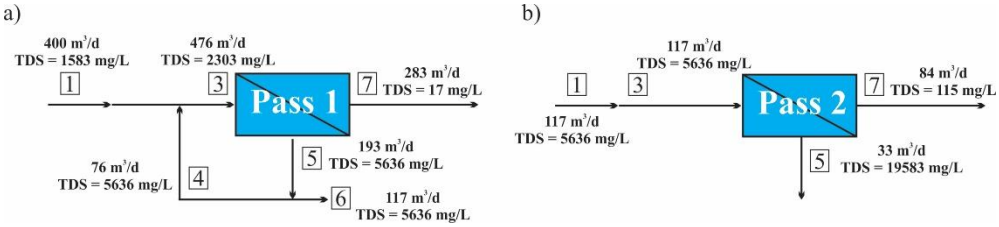

Figure 5.7 (**a**) Primary (pass 1) and (**b**) secondary (pass 2) RO tandem system configuration. Numbers and associated conditions are for the dry season; they are explained in Table 5.3. Stream 1 in pass 2 comes from stream 6 in pass 1. Streams 2, 4 and 6 are not displayed in case of no recirculation.

Table 5.2 Technical specifications of primary (pass 1) and secondary (pass 2) HR-RO tandem system operated for a groundwater sample representing the dry conditions of well D5 in the Damour aquifer, Lebanon. The flux unit *lmh* is liter/m^2/h.

Pass #	**Pass 1**				**Pass 2**			
Stage #	1	2	3	4	1	2	3	4
Element Type	HSRO-390-FF				LC LE-4040			
Pressure Vessels per Stage	2	1	1	1	2	2	1	1
Elements per Pressure Vessel	3	3	3	3	3	3	3	3
Total Number of Elements	6	3	3	3	6	6	3	3
Pass Average Flux	21.67 lmh				22.24 lmh			
Stage Average Flux	27.54 lmh	22.80 lmh	17.58 lmh	12.92 lmh	37.54 lmh	21.51 lmh	10.52 lmh	4.83 lmh
Permeate Back Pressure	4.14 bar	4.14 bar	4.14 bar	4.14 bar	0.00 bar	0.00 bar	0.00 bar	0.00 bar
Booster Pressure	17.24 bar	0.00 bar	0.00 bar	0.00 bar	17.24 bar	0.00 bar	0.00 bar	0.00 bar
Chemical Dose	-				-			
Energy Consumption	**1.01 kWh/m³**				**0.83 kWh/m³**			

Table 5.3 HR-RO tandem system results for a groundwater sample at well D5 representing the dry season conditions.

	Stream #	**Flow (m³/d)**	**Pressure (bar)**	**TDS (mg/L)**	**Permeate TDS (mg/L)**	**Permeate Volume (m³/d)**	**Concentrate TDS (mg/L)**	**Concentrate Volume (m³/d)**	**Recovery (%)**
Pass 1	1	400.00	0.00	1583.12	17	283	5636	117	71
	3	476.31	17.24	2303.25					
	4	76.31	12.18	5636.38					
	5	193.63	12.18	5636.38					
	6	117.31	12.18	5636.38					
	7	282.69	-	16.59	**39**	**367**	**19583**	**33**	**92**
Pass 2	1	117.00	0.00	5635.94	115	84	19583	33	72
	3	117.00	17.24	5635.94					
	5	33.10	13.47	19583.82					
	7	83.90	-	115.09					

Table 5.4 Evolution of water quality from raw conditions at well D5 via primary RO (pass 1) and secondary RO (pass 2) to final permeate and concentrate quality. Results represent the dry season conditions.

	Feedwater (mg/L)	Pass 1		Pass 2	Final Outcome	
		Permeate (mg/L)	*Concentrate (mg/L)*	*Permeate (mg/L)*	*Concentrate (mg/L)*	*Permeate (mg/L)*
TDS	1594	17	5636	115	19584	39
Cl	700	56	2005	41	8211	14
SO_4	84.0	0.5	286.9	2.8	1007.3	1.0
HCO_3	260.0	2.5	872.8	25.4	2930.4	7.8
NO_3	18.0	1.9	57.0	5.3	188.1	2.7
Na	330	5	2015	40	7023	13
K	1.9	0.2	6.2	0.3	21.1	0.2
Ca	124.3	< 0.1	0.3	< 0.1	0.3	< 0.1
Mg	62.9	< 0.1	< 0.1	< 0.1	< 0.1	< 0.1
SiO_2	10.9	0.1	37.0	0.2	130.3	0.2
B	0.1	< 0.1	< 0.1	< 0.1	< 0.1	< 0.1
Ba	0.03	< 0.1	< 0.1	< 0.1	< 0.1	< 0.1
Sr	0.19	< 0.1	< 0.1	< 0.1	< 0.1	< 0.1
pH	7.50	5.61	7.8	6.4	7.8	5.8

5.4.3 Assessment of permeate/concentrate quality and volume

There is usually a call for trade-off between low recovery producing small freshwater volumes with moderately brackish concentrate and high recovery producing more fresh water but more saline concentrate, eventually with higher chance of membrane fouling and more difficult disposal (due to legislative restrictions or well clogging). Scale precipitation in the concentrate stream of some minerals, for instance calcite, gypsum, barite and SiO_2 limits recovery rates. It is a major limitation in high recovery applications, which reduces the mass transfer coefficient of membranes (Wolthek et al. 2013). The pre-treatment process is capable of reducing the fouling propensity and thereby minimizes membrane scaling; however, in this study it was not quantified and thereby scaling estimates demonstrated here represent the worst case scenario by skipping pre-treatment stage, i.e. it is kept as a safety margin.

The proposed design was advantageous in its efficient performance with low scaling propensity under high recovery conditions. The thermodynamic ion association model PHREEQC-2 (Parkhurst and Appelo 1999) was used to calculate the Saturation Index (SI) of the relevant minerals.

$$SI = \log (IAP/K_S) \tag{5.4}$$

where IAP = the ion activity product, K_S = the solubility product of the mineral.

SIs of different susceptible minerals thus showed a scaling potential for SiO_2 only (Table 5.5). Other potential mineral such as $CaSO_4$, $BaSO_4$ and $SrSO_4$ had no risk of scaling, because Ca was removed in the hardness reduction step, while Ba and Sr were

already nearly absent in the source water. Silica removal is usually problematic due to the lack of reliable anti-scalants although there is a chance for scaling not to occur at all because crystallization is slow. Anyway, it is customary to try limiting SiO_2 content to about 120–220 mg/L to ensure a proper operation of the RO desalination system (Fritzmann et al. 2007). In addition, the design could be modified by adding an intermediate treatment between primary and secondary ROs (Figure 5.1) in case of problematic performance of the system.

Table 5.5 Scaling propensity of concentrate water produced by the proposed HR-RO tandem system. Higher concentration of wet season reject is due to higher recovery.

		Wet season	Dry season
	pH	7.75	7.81
	Langelier Saturation Index	-0.66	-1.09
	TDS (mg/L)	24791	19584
	HCO_3 (mg/L)	6324	2930
	SiO_2 (mg/L)	224	130
		PHREEQC-2	
Saturation Index	Calcium carbonate ($CaCO_3$)	-0.91	-1.25
	Gypsum ($CaSO_4$)	-3.71	-3.85
	Barium sulfate ($BaSO_4$)	-0.29	-0.29
	Strontium carbonate ($SrCO_3$)	-0.86	-1.04
	Strontium sulfate ($SrSO_4$)	-2.39	-2.37
	Silica amorphous (SiO_2)	0.36	0.09

Boron was also checked since it is a very critical component in RO systems. The feedwater extracted at well D5 in the Damour aquifer had ca. 0.18 mg/L, which is lower than drinking water limits. So no threat is posed by its presence in the permeate water, but in case of higher values (> 1.0 mg/L) further modifications to the RO design become essential. One alternative is to back up the RO system with boron-specific ion exchange (Jacob 2007) although the cost may rise significantly especially due to frequent replacement of exhausted ion exchange bottles. Another alternative is to use ultra-filters (UF) in the pre-treatment phase. In addition, some special FILMTEC™ membranes currently exist for boron removal (e.g. BW30-380, BW30-400, BW30 LE-400); however, they have overall lower recovery rates.

5.4.4 Options of concentrate disposal

A major environmental dilemma in any RO system is the disposal of concentrate, which is usually included in the feasibility assessment of the treatment facility. An innovative design should reduce the volume of reject and eliminate the use of chemicals in the treatment process as much as possible to avoid problematic disposal. Several alternatives (though not ideal) exist: (a) disposal to surface water (oceans or rivers), sewer, deep well injection, evaporation/salt ponds, or waste water treatment facilities, which either digest the low

concentrate volume amidst the main stream or which are supplemented with e.g. electrodialysis reversal (EDR) treatment (Turek et al. 2009) or eutectic freeze crystallization (Hasan et al. 2017); (b) irrigation of plants tolerant to high salinity (e.g. halophytes) (Ahmed et al. 2001); or (c) manufacturing of different by-products (e.g. fertilizers). EDR is recommended for reject having high $CaSO_4$ and $CaCO_3$, which eventually crystallizes facilitating a zero liquid discharge technology. Sending the reject to a wastewater treatment facility is expensive (transport costs) and thereby necessitates increasing recovery rates to reduce the reject volume.

The easiest and least expensive option of reject disposal is discharging it to the sea. For instance, in United Arab Emirates (UAE) reject brine is disposed either directly to the sea or via creeks (Ahmed at al. 2001). The environmental impact of this choice depends on many factors including: (a) salinity of reject, (b) chemical composition, (c) point of discharge and (d) type of marine life around the discharge point. However, all these drawbacks could be overcome when only a very small volume is disposed especially when efficient dispersion in the sea is possible due to the dynamic conditions of the sea shore (waves, tides, currents … etc.). In south eastern Spain, a brine of 80,028 mg/L TDS was disposed, which is 4 times higher than in our case. But the chosen site was already contaminated by the expansion of Alicante Harbor and large sewage disposal. At a later time, more diffusers were added to improve dispersion or dilute the water before disposal (Fernández et al. 2005).

A safer step is post-treating reject water before discharge, for instance by removing dissolved gases and adjusting pH level. Evaporation and crystallization could be also considered to recover salts like magnesium hydroxide ($Mg(OH)_2$), sodium chloride (NaCl), calcium carbonate ($CaCO_3$), sodium sulfate (Na_2SO_4) and calcium chloride ($CaCl_2$) (Pérez-González et al. 2012). In addition, deep-well injection into confined aquifers more saline than the RO concentrate was recently proposed as another alternative of concentrate disposal (Stuyfzand and Raat 2010). Unfortunately suitable aquifers do not exist everywhere, and fractured and karstic confined aquifers might not be convenient due to high risks of leakage. For example, the deep well disposal at the North District Wastewater Treatment Plant in Miami-Dade County (Florida) turned out to contaminate the upper aquifer several months after injection onset (Walsh and Price 2010).

In the Damour area, a wastewater treatment plant or disposal aquifer does not exist. Therefore, the reject water (or at least part of it) could be dumped directly into the sea as one viable choice. The Mediterranean Sea is ca. 1350 m away with seaward natural gradient, which reduces expenses of transport. Alternatively, the option of disposal to the Damour River (1 km away) (Figure 2.1) was assessed here. This river has a surface water discharge between 6×10^3 m^3/d and 215×10^4 m^3/d with 34 and 18 mg/L background chloride concentration, respectively. This results in a chloride load of 138 kg/d and 39 × 103 kg/d during low and high discharge periods. Assuming a reject chloride concentration of 8200 mg/L as released by the RO tandem system and 10% as the maximum permissible increase of chloride in the river (Nederlof and Hoogendoorn 2005), then the allowed disposal is, respectively, 2.5 m^3/d and 470 m^3/d in the lowest and highest discharge seasons,

which holds for other chemical constituents as well. This makes the Damour River a suitable alternative for safe disposal of reject water during the wet season. A disposal outlet may be selected close to the estuary or at a spot without downstream water users in order to avoid any (ecological) objections. In the remaining period of the year, the reject is either disposed to the sea or held in collection tanks (though more expensive option) to be released later during higher discharge.

5.4.5 Economic assessment

A cost analysis of the HR-RO tandem desalination plant was executed to evaluate the economic feasibility of the proposed strategy. It included the initial capital cost, operation and maintenance costs, pipelines for reject disposal in addition to a comparison to selling prices of potable and domestic water in Lebanon. The capital costs of the two RO passes were estimated at 550,000 US$ hosting 11 pressure vessels and 33 membrane elements. This is for a 400 m^3/d capacity plant, i.e. it is multiplied by two when a series of two plants is required (800 m^3/d). 200,000 US$ were separately added for the pre-treatment multi-stage components. Operation included energy consumption, labor, cleaning/replacement of system components (membrane and pre-treatment filters), and water quality monitoring. The detailed description is provided in Table S5.3 (*Appendix S5*).

The proposed design revealed low energetic demand of < 1 kWh/m^3. In Lebanon, the cost of each kWh electricity cannot be accurately estimated. This country has been facing electricity shortages since the civil war in the 1970s. Reliance is on the official electricity provider, Électricité du Liban, and local generation facilities. The former has lower prices, but since electricity outages are unpredictable the energy costs required for desalination remain dynamic. In this study, the assessment assumed 50% local electricity generation. Each 1 kWh worth maximum 0.17 US$, which is equivalent to 0.16 US$/$m^3$ assuming a 0.96 kWh/m^3 in the dry season. Maintenance costs included cleaning of primary and secondary ROs every 6 and 4 months, respectively, which was estimated annually at 30,500 US$ (Table S5.3). This also includes 500 US$ as the annual cost of energy consumption (0.02 kWh/m^3) required to run HWS (Hot Water Sanitization) twice a month. It is recommended that cleaning of membranes from fouling takes place on regular basis or when rejection of the system increases by 10% (FilmTec's Technical Manual 2014). All membranes are then replaced every 5 years.

Moreover, the operation costs accounted for labor; one full time employee (operator) would suffice to support the plant 5 days a week (8 h per day), and the rest of the time automation and remote access to monitor the system could do the job in addition to a second employee for water quality monitoring.

Therefore, the total cost of the HR-RO tandem system over a 10-year life span was estimated at 0.99 US$/$m^3$. This value included 0.59 US$/$m^3$ for operation and maintenance. Accounting for the total intended freshwater production of the system (735 m^3/d), post-treatment, bottling and marketing, and then comparing it to the commercial selling prices of potable and domestic water in Lebanon reveals an annual profit of 4.3 and 0.3 million US$,

respectively (Table 5.6). This means that the capital cost could be returned back in 1–4 years if proper marketing plans are implemented. It is noteworthy that the price of water in Lebanon is relatively high due to improper management. The average price of untreated tap water is ca. 10 US$/m^3 whereas the certified drinking water costs 105–210 US$/m^3. The viability of the project is partly dictated by the high price of domestic water in Lebanon when intention is to sell tap water only. The price is comparable to that in water scarce countries, e.g. 15 US$/m^3 in Somali and 10 US$/m^3 in Nigeria. Failure on the market may always pose a financial risk to the profitability of the project.

It may be argued that aquifer storage and hydraulic barriers are generally less expensive options than the proposed IFK installation (e.g. 0.3–0.6 US$/m^3 for AR (Maliva 2014), and 0.16–0.2 US$/m^3 for PHB (Ortuño et al. 2012)); however, they are only feasible under specific local hydrologic conditions usually not met in karstic aquifers due to complex dynamics and most often the lack of proper recharge and/or storage basins (see cons of "*hydraulic barriers*" in Table 1.1). Therefore, despite relatively higher costs, IFK still appeals as a main alternative in karstic media in comparison to other countermeasures.

Table 5.6 Cost of water production by the proposed HR-RO tandem design and the selling prices of water in Lebanon. This assessment is for a series of two units of the skid design (i.e. 800 m^3/day capacity).

	HR-RO tandem (US$)	Selling price in Lebanon	
		Potable bottled water[a] (US$)	Domestic tap water (US$)
Cost of water ($/m^3)	0.99	100	10
Post-treatment[b] ($/m^3)	0.10		
Total price (RO plant/day)	800	73,500	7,350
Bottling/distribution[c] ($/year)		0.1 million	--
Marketing and promotion ($/year)		1 million	0.2 million
Profits (RO plant/year assuming 25% selling)[d]		4.3 million	0.3 million[e]

[a] This price is the least provided for certified potable water in the Lebanese market; it exceeds 180$/m^3 for some distinguished trademarks.
[b] The desalted brackish groundwater should be polished to some extent in order to gain some buffer capacity against pH fluctuations. This could be done by admixing a small portion of brackish or fresh groundwater.
[c] It includes bottle washing, packaging, distribution and consumable items.
[d] This estimate assumes 300 working (business) days per year.
[e] This estimation assumes that oligohaline water (Cl < 30 mg/L) is sold for domestic use, but blending it with brackish water (maximum TDS of ca. 1500 mg/L) could supply 3 more volumes of water tripling the value of estimated profits.

5.5 Conclusions

A major challenge in managing water resources is to control saltwater intrusion in coastal aquifers. This is done by testing specific scenarios to select the best scheme. One option consists of a planned pumping strategy through hydraulic controls applying negative barriers via a row of vertical wells between sea and freshwater wells. However, the efficiency of this system depends on among others anisotropy and thickness of the aquifer,

which may render it unreliable. This applies in particular to karstic and fractured aquifers, where simulation results carry more uncertainty about salt transport and location of the transition zone. In areas where relatively small volumes of water (extracted by 2–3 wells) would suffice to bridge the gap in water demand, Integrated Fresh-Keeper (IFK) wells form a more secure option than larger scale barriers. IFKs are less complicated, cheaper, and more effective with a lower chance of failure.

This paper proposes a coupled strategy of IFK and high recovery (HR) Reverse Osmosis (RO). The IFK will sustainably produce 2 water types via its 2 separated well screens within the same borehole: freshwater from the shallow screen and brackish or slightly brackish water from the deeper one. The brackish water is treated to demineralized bottled water by utilizing a HR-RO tandem desalination plant. The RO design provides high recovery with low scaling propensity without use of anti-scalants.

Application of the aforementioned strategy to a single pilot well in the Damour aquifer (south of Beirut, Lebanon) provides ca. 250 m^3/d of freshwater by vertical hydraulic interception. In addition, a desalination plant composed of a series (two units) of the proposed skid design could be adequate to treat the extracted brackish water of a pilot well (known as D5) at a capacity of 800 m^3/d. Consequently, the IFK installation coupled with the HR-RO system may supply in a sustainable way a total of about 985 m^3/d of freshwater. This reduces future salinization risks when fresh groundwater abstraction would continue. About 735 m^3/d of this water is suitable for drinking purposes after a slight post-treatment to meet drinking standards, e.g. liming or blending with small portion of brackish or fresh groundwater to stabilize the water and increase its alkalinity and TDS. The other 250 m^3/d of fresh water is good enough to supply as domestic water or to polish up the RO-permeate. The total expense of the desalting process was estimated at 0.99 US$/$m^3$ for a 10-year period life span, which could return back the plant capital cost in the first 1 to 4 years depending on the choice of selling bottled or tap water.

Brackish water has large compositional variation depending on mixing ratios and chemical reactions (e.g. cation exchange, dissolution and precipitation). Under prolonged pumping, there is a chance that salinity in the deeper well might rise. However, (1) the recommended pumping rate is half the current rate which is expected to relieve part of the ongoing stress on the system, and (2) the numerical simulations of the proposed IFK installation conforms to suitable conditions over the 10-year period (salinity may rise by about 20% only). Hence, this strategy necessitates installing a monitoring system to control water levels and groundwater quality from both well screens. A combined pressure and electrical conductivity (EC) sensor could do the job, while the EC can also be used to keep water quality constant for the HR-RO unit by adding more or less fresh water from the shallow well screen. Anyway, the proposed system could safely handle 100% salinity increase (temporal or over long time), which may lower the total RO recovery by 9% and the profits by 11 % only. At this rate, the system maintains its profitability paying back in maximum 5 years when selling tap water.

Installing IFKs opens the door for re-exploiting some abandoned brackish wells, and thereby reduces pumping rates of other wells yielding an optimized scheme. For instance,

some wells in the Damour aquifer currently abandoned due to high salinity may be re-operated after IFK installation, and the extracted brackish water, or at least part of it, could be blended with permeate water of the primary HR-RO system without need for further desalination. This could provide significant volumes of tap water. The strategy formulated here can be extrapolated to other sites, and the proposed treatment system could be used for similar feedwater conditions or be adapted after minor modification for more brackish waters. It is efficient, feasible, easy, profitable and thereby economically attractive in addition to a further potential benefit anticipated, namely the reduction of seawater intrusion lateral extent due to diminution of extraction rates.

Acknowledgements The sincere cooperation of Mr. Riad Domiati from Beirut Water Authority – Damour Compound is greatly appreciated. The reviewers are also thanked for their time to revise this manuscript.

Appendix S5: Supplementary Material

Table S5.1 Chemistry of groundwater extracted at well D5 (Damour aquifer – Lebanon) for both wet and dry seasons. The well is cased to 83 m below groundwater level (BGL), slotted between 13 and 74 m BGL, and pump installed at 34 m BGL. Fresh top water is selected based on samples collected in the very close vicinity at 4 m BGL. Reliable observations deeper than 35 m BGL are not available.

	Season (mg/L)		Freshwater on top (mg/L)
	Wet	***Dry***	
TDS	1094	1587	792
Cl	373	700	209
SO_4	58	84	66
HCO_3	307	260	261
NO_3	4.3	5.5	6.3
PO_4	0.1	0.1	0.1
Na	156	340	93
K	5.6	5.9	4.1
Ca	101	128	86
Mg	57	65	34
Fe	0.007	0.008	0.005
Mn	0.003	0.003	0.001
NH_4	0.065	0.065	0.065
SiO_2	9.0	10.9	8.9
Barium	0.032	0.032	0.027
Boron	0.107	0.176	0.061
Strontium	0.207	0.207	0.174
pH	7.2	7.5	7.18

Table S5.2 Rainfall data in the Damour area over a 10-year period, variable on monthly basis for the first year (based on year 2009 available data) and annually averaged for the remaining 9 years.

Rate (mm/yr)	Start Time (day)	Stop Time (day)
660	0	31
852	31	58
660	58	89
84	89	119
72	119	150
0	150	180
0	180	211
0	211	242
504	242	272
312	272	303
1176	303	333
1272	333	365
825	365	720
825	720	3650

Table S5.3 Detailed cost analysis of a HR-RO tandem plant for a total capacity of 400 m³/d. Expansion of the system to higher volumes requires a series of the proposed skid design where the total cost is multiplied by the number of units involved.

Primary RO – Pass 1		Secondary RO – Pass 2		RO Tandem	
Unit set for economic evaluation	m³-m³/h-bar	Unit set for economic evaluation	m³-m³/h-bar	Unit set for economic evaluation	m³-m³/h-bar
System water production (m³/h)	11.8	System water production (m³/h)	3.5	System water production (m³/h)	15.3
System recovery (%)	71	System recovery (%)	72	System recovery (%)	92
Project Economic Variables		**Project Economic Variables**		**Project Economic Variables**	
Project Life (years)	10	Project Life (years)	10	Project Life (years)	10
Interest rate (%)	8	Interest rate (%)	8	Interest rate (%)	8
Power cost ($kWh)	0.17	Power cost ($kWh)	0.17	Power cost ($kWh)	0.17
Projection Results		**Projection Results**		**Projection Results**	
Pass 1 permeate production (m³/h)	11.8	Pass 2 permeate production (m³/h)	3.5	Tandem permeate production (m³/h)	15.3
Pass 1 feed pressure (bar)	17.2	Pass 2 feed pressure (bar)	17.2	Tandem feed pressure (bar)	17.3
Pass 1 concentrate pressure (bar)	12.2	Pass 2 concentrate pressure (bar)	13.5	Tandem concentrate pressure (bar)	12.6
Pass 1 recovery (%)	15.0	Pass 2 recovery (%)	15.0	Tandem recovery (%)	15.0
Pass 1 energy recovery efficiency (%)	50.0%	Pass 2 energy recovery efficiency (%)	50.0%	Tandem energy recovery efficiency (%)	50.0%
Capital Expense		**Capital Expense**		**Capital Expense**	
Pass 1 pressure vessels	5	Pass 2 pressure vessels	6	Tandem pressure vessels	11
Pressure vessel cost ($/vessel)	20,000	Pressure vessel cost ($/vessel)	20,000	Pressure vessel cost ($/vessel)	20,000
Pass 1 capital for pressure vessels	$100,000	Pass 2 capital for pressure vessels	$120,000	Tandem capital for pressure vessels	$220,000
Product	HSRO-390-FF	Product	LC LE-4040	Product	HSRO-390-FF + LC LE-4040
Pass 1 total elements	15	Pass 2 total elements	18	Tandem total elements	33
Element cost ($/element)	$10,000	Element cost ($/element)	$10,000	Element cost ($/element)	$10,000
Pass 1 capital for elements ($)	$150,000	Pass 2 capital for elements ($)	$180,000	Tandem capital for elements ($)	$330,000
Capital for pre-treatment ($)	$200,000			Pre-treatment capital	$200,000
Pass 1 capital ($)	$250,000	Pass 2 capital ($)	$300,000	Land acquisition [a] ($)	$0
Pass 1 capital($/m³)	$0.24	Pass 2 capital($/m³)	$0.98	Disposal pipelines ($)	$10,000
				Construction works ($)	$30,000
				HR-RO Tandem capital ($)	$790,000
				HR-RO Tandem capital($/m³)	$0.59

Table S5.3 (continued)

Primary RO – Pass 1		Secondary RO – Pass 2		RO Tandem	
Operating Expense		**Operating Expense**		**Operating Expense**	
Power		**Power**		**Power**	
Pass 1 pumping power (kW)	11.9	Pass 2 pumping power (kW)	2.9	Tandem pumping power (kW)	9.2
Pass 1 pump specific energy (kWh/m³)	1.01	Pass 2 pump specific energy (kWh/m³)	0.83	Tandem pump specific energy (kWh/m³)	0.96
Brine energy recovery (kWh/m³)	-26.8	Brine energy recovery (kWh/m³)	-26.8	Brine energy recovery (kWh/m³)	-26.8
Pass 1 net energy consumption (KWh/m³)	1.01	Pass 2 net energy consumption (KWh/m³)	0.83	Tandem net energy consumption (KWh/m³)	0.96
Pass 1 net energy cost ($/year)	$1,063	Pass 2 net energy cost ($/year)	$259	Tandem net energy cost ($/year)	$1310
Energy expense NPV ($)	$7,133	Energy expense NPV ($)	$1,740	Energy expense NPV ($)	$8,792
Pass 1 energy expense ($/m³)	$0.17	Pass 2 energy expense ($/m³)	$0.14	Tandem energy expense ($/m³)	$0.16
Membrane cleaning		**Membrane cleaning**		**Membrane cleaning**	
Pass 1 cleaning frequency (cycle/year)	2	Pass 2 cleaning frequency (cycle/year)	4	Tandem cleaning frequency (cycle/year)	6
Pass 1 Cleaning expense ($/cycle)	$5,000	Pass 2 Cleaning expense ($/cycle)	$5,000	Tandem Cleaning expense ($/cycle)	$5,000
Pass 1 cleaning expense ($/year)	$10,000	Pass 1 cleaning expense ($/year)	$20,000	Tandem cleaning expense ($/year)	$30,500
Pass 1 cleaning expense NPV ($)	$67,101	Pass 2 cleaning expense NPV ($)	$134,201	Tandem cleaning expense NPV ($)	$204,657
Pass 1 cleaning expense ($/m³)	$0.01	Pass 2 cleaning expense ($/m³)	$0.07	Tandem cleaning expense ($/m³)	$0.02
Labor (for both passes 1 and 2)				**Labor**	
Full time employee (FTE)	1			Full time employee (FTE)	1
Salary for each FTE ($/year)	$7,200			Salary for each FTE ($/year)	$7,200
Total labor ($/year)	$7200			Total labor ($/year)	$7,200
Total labor NPV ($)	$48,313			Total labor NPV ($)	$48,313
Labor expense ($/m³)	$0.02			Labor expense ($/m³)	$0.01
Membrane replacement cost		**Membrane replacement cost**		**Membrane replacement cost**	
Pass 1 replacement rate (%/year)	10	Pass 2 replacement rate (%/year)	10	Tandem replacement rate (%/year)	10
Replacement price ($/element)	$10,000	Replacement price ($/element)	$10,000	Replacement price ($/element)	$10,000
Pass 1 replacement cost for elements ($/year)	$15,000	Pass 2 replacement cost for elements ($/year)	$18,000	Tandem replacement cost for elements ($/year)	$33,000
Pass 1 replacement membrane NPV ($)	$100,651	Pass 2 replacement membrane NPV ($)	$120,781	Tandem replacement membrane NPV ($)	$221,432
Pass 1 membrane replacement expense ($/m³)	$0.15	Pass 2 membrane replacement expense ($/m³)	$0.59	Tandem membrane replacement expense ($/m³)	$0.25

Table S5.3 (continued)

Primary RO – Pass 1		Secondary RO – Pass 2		RO Tandem	
Pre-treatment elements replacement cost (for both passes 1 and 2)				**Pre-treatment elements replacement cost**	
Replacement cost ($/year)	$20,000			Replacement cost ($/year)	$20,000
Replacement cost NPV ($)	$134,202			Replacement cost NPV ($)	$134,202
Pre-treatment replacement expense ($/m³)	$0.19			Pre-treatment replacement expense ($/m³)	$0.15
				Water quality monitoring cost	
				Lab capital cost ($)	$5,000
				Full time employee (FTE) salary ($/year)	$7,200
				Consumable items ($/year)	$10,00
				Total monitoring ($/year)	$8,200
				Total monitoring NPV ($)	$60,023
				Water quality monitoring expense	$0.01
Operating expense subtotal		**Operating expense subtotal**		**Operating expense subtotal**	
Pass 1 operating expense NPV ($)	$223,197	Pass 2 operating expense NPV ($)	$256,723	Tandem operating expense NPV ($)	$539,862
Pass 1 operating expense per m³	$0.54	Pass 2 operating expense per m³	$0.79	Tandem operating expense per m³	$0.59
Pass 1 Total		**Pass 2 Total**		**Tandem Total**	
Pass 1 cost NPV ($)	$373,197	Pass 2 cost NPV ($)	$436,723	Tandem cost NPV ($)	$869,862
Life Cycle Cost ($/m³)	$0.36	Life Cycle Cost ($/m³)	$1.43	Life Cycle Cost ($/m³)	$0.65
Total System		**Total System**		**Total System**	
Capital	$250,000	Capital	$300,000	Capital	$790,000
Operating expense NPV ($)	$223,197	Operating expense NPV ($)	$256,723	Operating expense NPV ($)	$539,862
Cost of water NPV ($/m³)	$0.59	Cost of water NPV ($/m³)	$1.82	Cost of water NPV ($/m³)	$0.99

PV: The present value (*PV*) is the total amount that a series of future payments is worth now.

[a] *Land acquisition* is zero because the selected well (well D5 in the Damour aquifer – Lebanon) already owns enough space as part of its local territory.

Chapter 6

Synthesis and spin-off for water management

6.1 Summary of the findings

In **chapter 2**, a new structured approach is presented to derive groundwater baseline conditions. It builds on the HydroChemical System Analysis (HCSA) to map different groundwater bodies (hydrosomes) and hydrochemical zones within them, each of which showing significant differences in baseline chemistry. It includes an elimination scheme for biased data and data showing signs of pollution, the definition of significant hydrochemical trends, and statistical analysis to discern new subfacies, identify any outliers, and choose representative values. All water bodies requiring natural concentrations are assigned through HCSA, precluding salinized samples, mixed redox and intermixed hydrosomes. This step of subdividing the population warrants a detailed determination of natural background concentrations by revealing the appropriate diversity for each hydrosome and its facies.

The method was successfully applied to the Damour coastal aquifer system (Lebanon), which is a dolomitic limestone aquifer suffering from salinization and other minor anthropogenic impacts, such as inputs from sewage effluents and agricultural processes. It was capable of filtering out baseline conditions for 16 main constituents, 59 trace elements (TEs) and two isotopes. Concentrations of Cl, Cl/Br, ^{2}H, ^{18}O and Ca/Sr in combination with major ions and less immobile trace elements (e.g. B and Li) were used to discern and discuss different hydrosomes. The aforementioned discrimination of groundwater bodies facilitated an easier hydrochemical analysis of the system, including salinization sources, anthropogenic inputs, recharge zones, and evolutionary trends.

In **chapter 3**, groundwater quality differences between coastal limestone and coastal dolomitic limestone aquifers, both (sub)oxic and both with and without ongoing moderate salinization since the last decades, showed that: (1) the geochemical contrast between the limestone and dolomitic limestone aquifers do have an effect on the behavior of some major constituents and TEs, (2) carbonate rocks do not form a significant geogenic source of TEs (Sr excluded), (3) the mobilization of TEs by salinization is small compared to the enhanced concentration rise produced by direct seawater mixing, and (4) the current TEs levels in the studied aquifer are far below the drinking water limits, thanks to a moderate salinization to date. Data available from the Mediterranean Sea show that groundwater samples with seawater fraction > 17% are susceptible to arsenic levels exceeding drinking water limits.

Dissolution/precipitation of $Ca_xMg_ySr_zCO_3$ and cation exchange were the main disclosed hydrogeochemical processes besides weak signs of little organic matter oxidation. In the dolomitic limestone aquifer, less carbonate dissolved as compared to the limestone aquifer, partly because of lower pCO_2 in addition to seawater inflow triggering Mg-calcite precipitation by cation exchange. The presence of high Mg-calcite raised the Mg levels in

groundwater, and enhanced the Mg participation (besides Ca) in the exchange for Na and K. Fe revealed no difference between the two aquifers. Silica (quartz or opal) showed more mobilization in the limestone unit, which is probably dictated by more dissolution in the overlying quaternary sand-rich unit.

Saltwater intrusion (SWI) also led to mobilization of As, Ba, Cu, Ni, Rb, Sr and U in both aquifers, partly by cation exchange (e.g. Ba and Sr). The geochemical contrast between limestone and dolomitic limestone proved to be an important factor explaining part of the observed variation in the concentration of TEs regardless of SWI. For example, As, Cu and Ni recorded stronger mobilization in the freshwater dolomitic limestone, whereas Ba, Rb, Sr and U were more mobilized in the limestone unit. Other elements such as Al, Be, Co, Cr, Pb and V showed no (im)mobilization in either rock type. The observed TE discrepancy between the limestone and dolomitic limestone units is mainly linked to the higher Sr content of limestone and its higher content of clay minerals and iron (hydro)oxides.

In **chapter 4**, two steps are suggested to simulate SWI in poorly karstified aquifers: (1) start with time series analysis to discover the hydrodynamic response of the system and decide whether ignoring quickflow is justifiable, and (2) try a coupled discrete-continuum (CDC) approach to check whether it warrants better results at the desired scale than an equivalent porous medium (EPM) model. Time series analysis in the Damour aquifer revealed a relatively long response time of groundwater levels to rainfall inputs. This indicates that conduit quickflow is scarce, justifying an initial use of the EPM simplification. Information on geo-lineaments (main fractures, faults, and discerned conduits) was then used to embed discrete features into the 3-D continuum to obtain a more karst-representative CDC model.

Comparison of the two approaches showed that the CDC had less difference between measured and computed salinity values than the EPM. This comparison relied on: (a) 5 statistical measures of salinity or hydraulic head goodness-of-fit (root mean square (RMS) and normalized RMS error of salinity, correlation coefficient, Akaike Information Criterion, and Bayesian Information Criterion), and (b) the match of the simulated saltwater-freshwater interface with available data from 1965 and 2011. The CDC model improved the local-scale salinity values for the majority of wells including the position of the fresh-brackish water interface, and reduced the overall model error (RMS of chloride) by ca. 28%. It is assumed that the CDC is better suited for modeling SWI in the poorly karstified Damour aquifer, which is worth its more complicated application, as is the case with any model seeking higher accuracy at local scale.

More efforts are still needed to test the performance of the CDC approach, including a prior time series analysis of rainfall and water table response, also in mature karst. This will

hopefully lead to a more appropriate protocol for modeling SWI in all types of karstic aquifers.

In **chapter 5**, a coupled strategy is introduced as a localized remedy to protect shallow freshwater reserves in karstic or fractured aquifers while utilizing the deeper intercepted brackish water. It sustainably produces 2 water types via its 2 separated well screens within the same borehole: freshwater from the shallow screen and brackish or slightly brackish water from the deeper one. The brackish water is treated to demineralized bottled water by utilizing a HR-RO tandem desalination unit. The RO design has < 1 kWh/m^3 energy consumption, and up to 96% recovery in addition to low scaling propensity without use of any anti-scalant.

A feasibility study presented as an example to a single pilot well in the Damour aquifer shows that ca. 1000 m^3/d of freshwater can be produced from this well by pumping 250 m^3/d of fresh groundwater from the topwell screen and 800 m^3/d of brackish groundwater (to be later desalinized) from the fresh-keeper well screen below. Cost analysis shows that the capital cost could be returned back in 1 to 4 years depending on the choice of produced water (bottled or tap) and available market (selling prices of bottled or tap water in Lebanon are 100 and 10 US$/$m^3$, respectively). Several alternatives (though not ideal) exist for the disposal of concentrate, e.g. disposal to surface water (oceans or rivers), sewer, deep well injection, evaporation/salt ponds, or to waste water treatment facilities. The Damour River is a suitable alternative for safe disposal of reject water during wet season. In the remaining period of the year, the reject is either disposed to the sea or held in collection tanks to be released later during higher discharge.

Installing IFKs opens the door for re-exploiting some abandoned brackish wells, and thereby reduces pumping rates of other wells yielding an optimized scheme. For instance, some wells in the Damour aquifer that are currently abandoned due to high salinity, may be re-operated after IFK installation, and the extracted brackish water, or at least part of it, could be blended with permeate water of the primary HR-RO system without need for further desalination. This could provide significant volumes of tap water.

The usage of brackish groundwater from integrated fresh-keeper wells thus serves 3 purposes: production of high quality drinking water, financial gain and mitigation of water stress by overpumping. The formulated strategy can be extrapolated to other sites, and the proposed treatment system could be used for similar feedwater conditions or be adapted after minor modification for more brackish waters.

6.2 MAR in Lebanon

New options of water buffering are urgently needed in Lebanon. Managed aquifer recharge (MAR) is thought to be one viable choice. It is included in the national water sector strategy aiming to recharge up to 200 Mm^3 of water by 2020 (MoEW 2010). Thirty three locations spread over the country were recently nominated as suitable sites for recharge of surface or treated effluent water (Figure 6.1; MoEW and UNDP 2014); however, no (fully) functional pilot has been yet installed. Serious doubts are raised on MAR feasibility due to the following obstacles MAR may face in the Lebanese context:

1. Limited storage capacity of the most abundant aquifer type, being (karstic) limestone and dolomite, coupled with a very high transmission rate and unpredictable tunneled flow which hampers recovery. Daher et al. (2011) therefore developed a conceptual methodology for Aquifer Rechargeability Assessment in Karst – referred to as ARAK.
2. Limited availability of surface water which is related to the high natural infiltration rates on karstic terrains.
3. Limited space to build the required infrastructure (e.g. water intake, pretreatment, wells or tunnels). Lebanon is densely populated (ca. 6 M people on 10,452 km^2).
4. Lack of sufficient financial means and lack of expertise in dedicated drilling. Dams are still seen as the major solution, such as Bisri Dam for Beirut and its suburbs.
5. Lack of societal acceptation (no faith in MAR technology, so press releases are needed).

However, any plan to harvest lost amounts of surface, rain or storm water, and to store it underground for supply during the dry seasons is highly welcomed.

Artificial recharge was earlier tested by Daoud (1973) in Hazmieh area (south eastern suburbs of Beirut) to prevent saltwater intrusion in the surrounding vicinity. Four recharge attempts were carried out between April 1968 and May 1971; injection rates with water from a nearby irrigation canal varied between 11,650 and 15,000 m^3/d, with continuous operations for 10 to 210 days. This induced a 1.2 m groundwater level rise at an observation well 460 m away, with a simultaneous improvement of water quality (average salinity reduced by ca. 50%). Recharge continued till 1975, the onset of the Lebanese Civil War, during which recharge activities presumably ceased. Since 2000, intermittent injection with an average of 4,750 m^3/d has been resumed during short periods of the wet season. Neither proper monitoring nor reliable information is available, and salinization in the surrounding area is still ongoing (MoEW and UNDP 2014). Later efforts were devoted to evaluate the Hazmieh site and the chances of re-running the recharge wells there. For this purpose, a feasibility study, funded by the German Federal Ministry for Economic Cooperation and Development (BMZ) and commissioned by Deutsche Gesellschaft für

Internationale Zusammenarbeit (GIZ) GmbH as part of the regional program 'Adaptation to Climate Change in the Water Sector in the MENA region' (ACCWaM), suggested that implementing MAR in Hazmieh or elsewhere in Lebanon is a viable option (Prinz 2016).

Another potential site is in the Damour aquifer, south of Beirut. Its recharge is possible from the neighboring perennial Damour River. One pilot injection program was initiated in 1970's; however, operations also ceased in the mid-seventies (due to the Civil War), and all related information was lost (MoEW and UNDP 2014). Suggestions to remediate this aquifer were aroused later, for instance by Khadra (2003) and Masciopinto (2013) suggesting a set of injection wells parallel to the coastline to create a positive hydraulic barrier. Schepper (2010) and Daher et al. (2011) proposed diverting part of the Damour River water to a system of infiltration tunnels. These efforts remained at the desk level, and none has provided a full feasibility assessment. A rechargeability and feasibility assessment of the Damour main aquifer (dolomitic limestone) shows that MAR via infiltration ponds or injection wells is not a good choice (Daher et al. 2011). They suggested to apply sub-horizontal injection wells or two infiltration tunnels (each 1 km long), but they did not validate these ideas. Constructing a horizontal drain near the river mouth to recharge the quaternary (Q) unit is probably a more feasible option than recharging the karst aquifer. Meanwhile a project funded by the Dutch government is in progress to identify MAR systems fit for Lebanon, and to run a full pilot test and assess its overall performance. The project is part of a program aiming at strengthening the Lebanese water and agriculture sector (updates to the media are available at: https://www.facebook.com/dutchlebanesewaterprogramme/). One proposed site is in the Damour coastal strip; its details are provided in *Section 6.3.2.2*.

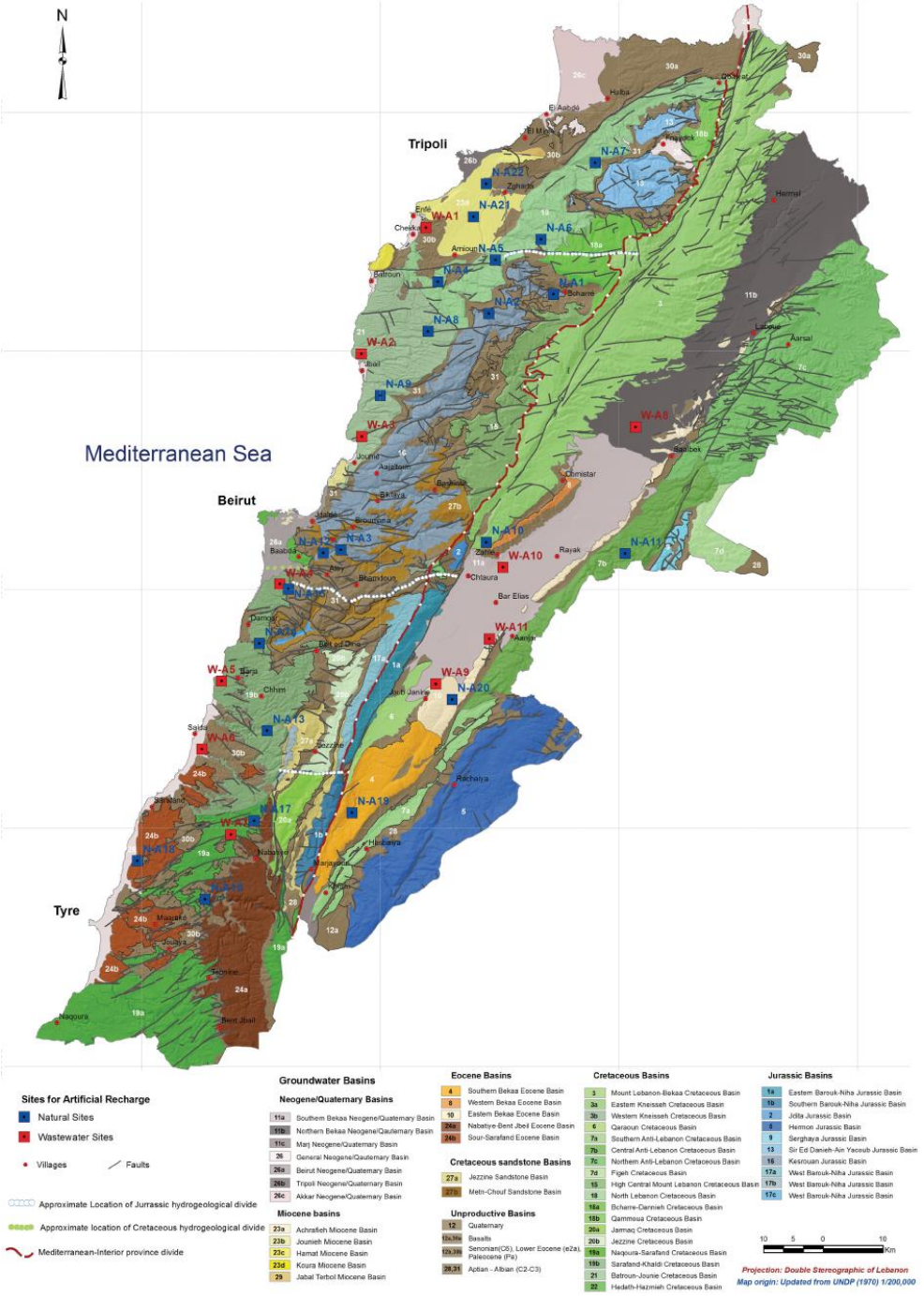

Figure 6.1 Geological map of Lebanon with the proposed sites to apply artificial recharge using either surface water (N-A1 to N-A22) or treated effluent water (W-A1 to W-A11) (MoEW and UNDP 2014).

6.3 Assessment of MAR potential in the Damour area

6.3.1 Introduction

MAR in the Damour area is generally problematic due to dominance of karstic media (see *Section 6.2*). Nevertheless, two major solutions are possible: (1) river bank filtration (RBF) along the Damour River to recharge the major dolomitic limestone aquifer, or (2) artificial recharge (AR) of the alluvial quaternary unit in the coastal strip, via surface water transported from the river. Several wells close to the Damour River are already intercepting bank filtrated water. This option can easily gain public support because of: (1) easy implementation, (2) low costs, (3) good investment of surface water that is lost otherwise, and (4) natural attenuation of river water during aquifer passage, resulting in lower concentrations of suspended material, pathogens and various chemical pollutants (Stuyfzand 1998; Medema and Stuyfzand 2002). AR in the Damour coastal strip is also a good solution, better than recharging the major karstic aquifer, thanks to its higher porosity (inherent to uncemented clastic sediments), more homogeneous character and lower permeability, together facilitating a high recovery efficiency. In addition, any site there can benefit from easy transport of the Damour River water for nearly no cost. This is done via irrigation canals that already dissect the coastal plain. Therefore, an aquifer storage recovery (ASR) site(s) could be a low cost method to store excess water in the wet season and extract it in dry periods.

Water quality concerns need to be seriously addressed, however, when applying either RBF or ASR, not only in the Damour area but anywhere. Firstly, there is the clogging potential of the source water. Clogging will reduce the efficiency of recharge/recovery facilities over time and may induce high labor costs to regenerate the infiltration capacity of the river bed or ASR well. The clogging mechanism is mainly (bio)physical during infiltration (e.g. sedimentation due to high turbidity and total suspended solids, or the growing of biofilms and algae), and (bio)chemical during recovery (e.g. iron oxides, manganese oxides, calcite and biofilms caused by mixing of water from various environments and high fluxes occurring near the well). Secondly, the chemical and microbiological quality of the source water (here river water) may be problematic due to disposal of effluents and solid wastes which may increase among others nitrate, heavy metals, total organic carbon (TOC), organic micropollutants (OMPs), bacteria and viruses, and radioactivity. Thirdly, there is a chance that infiltrating river water, by interacting with deposited muds and subsequently the aquifer matrix, will raise the levels of some chemical constituents (e.g. Fe, Mn, As, NH_4, Ca and HCO_3). This applies to RBF only.

6.3.2 Hydrological analysis

6.3.2.1 RBF north of the Damour River

The evaluation of the hydrodynamic interaction of the Damour River with the nearby interconnected aquifer in vicinity of Mechref village (Figure 2.1) shows attracting figures about the surface water supply potential. Analysis of double tracers (using Eqs. 2.4 to 2.6) for a mixture of three end-members (river, local rain and infiltrated ocean water) shows that wells close to the Damour River (within ca. 350 m from the channel) have > 50% river water contribution. This currently sums up to a total discharge of 3300 m^3/d, a value that was corroborated by 3-D numerical modeling (*Section 4.4.3*). This means that the Mechref village wells (Figure 2.3) receive river bank-filtrate from the south via fluvial gravel beds, before mixing with native groundwater. Information on the RBF periodicity or signs of flow reversals during dry periods are not available.

Modeling different scenarios with additional wells installed close to the Damour River shows a potential to increase induced river recharge, provided that exacerbation of SWI be avoided. The closer the wells are to the river the more surface water they intercept, but this will reduce the subterranean detention times. It is not clear whether this reduction will have a significant effect on water quality via filtration, adsorption, and elimination of heavy metals, OMPs, and bacteria and viruses (Stuyfzand et al. 2006), because the potential of natural attenuation in fractured karstic limestone is estimated to be low compared to the sedimentary inlay of the Damour valley. Therefore, further investigations are needed to decide on the best trade-off between quality and quantity of intercepted water when new RBF wells are to be installed.

6.3.2.2 ASR in the Damour coastal plain

Any ASR site in the Damour coastal plain can be recharged during the wet season by surface water of the Damour River using irrigation canals that transport water from the river down to the coastal strip. These canals (two separate ones operating since the French mandate in Lebanon) now distribute surface water all over the strip during the dry season, but supplying limited amounts only (once a week for each lot of land). During the wet season, water is not needed for irrigation, so these canals are closed, and all river water is then discharged to the sea through the Damour River itself. Therefore, the canals can be partially opened during the wet season to supply the required recharge water for any ASR site, in order to store it temporarily in the quaternary unit when there is no need for irrigation water, and then recover it in the dry season to supply water for irrigation and domestic use.

One of the plans of the recent Dutch foreign aid program is to install a small pilot site in the Damour coastal area with a capacity of ca. 30 m^3/d. This pilot is expected to run till late 2018 as a test of how it functions and hopefully also as a demonstration site for

replication. The expected cost of construction including 1 gravity recharge well, 4 piezometers for monitoring, a pretreatment plant (e.g. coarse pre-filter, sedimentation, rapid sand filtration and chlorination), and other logistical facilities is no more than 50,000 US$. Meanwhile no cost for water transport is required since the canals are already spreading all over the coastal strip for a fixed lump-sum charge. The success of this pilot may trigger local interests in installing more sites there to supply all farms, resorts, restaurants and café shops with their high water needs during the high demand season. In addition, there is national interest in installing similar ASR plants at other sites in Lebanon.

Khadra and Stuyfzand (2014) mapped the coastal plain water based on origin, so the water in the quaternary unit and the underlying C_6 unit was considered as one hydrosome. Hence, further efforts are needed to separate the two and assess the expected hydrogeochemical interactions when the alluvial unit is recharged with surface water. This is indeed one aspect of the overseen efforts of the Dutch pilot, as part of evaluating the viability of this plant and how it functions.

6.3.3 Hydrochemical analyses

Available data of the Damour River (e.g. Tables 2.6 and 6.1) shows slightly polluted CaHCO3 water characterized by low HCO_3, Ca, SiO_2, with relatively low Cl and SO_4 concentrations (< 50 mg/L). Iron and Mn are < 0.04 mg/L, ammonium is < 0.1 mg/L, and nitrate averages 4 mg/L. The Damour river bank-filtrate water mapped by Khadra and Stuyfzand (2014) (F hydrosome in Figure 2.3) mostly mimics the surface water source except for being much less polluted. It is also characterized by pH stabilization, and attenuation of phosphate and some trace elements (e.g. Al, Cr, La, Ni, Pb, Sb and V). This testifies of the efficacy of the bank filtration process. Ba, Br and Sr are however mobilized due to desorption and/or dissolution from hosting minerals. Ba shows the highest mobilization, in line with the results of Khadra et al. (2017b).

Table 6.1 Average BOD and coliform pollution of the Damour River in the dry season (MoE/UNDP/ECODIT 2011).

BOD (mg/L)	Thermotolerant coliform (c/100 mL)	E. Coli (c/100 mL)
21.3	490	15

BOD = Biochemical oxygen demand.

The increase of Na level in the bank-filtrate points to Ca/Na exchange. Redox reactions are negligible, as indicated by minor change in O_2, SO_4, NO_3 and NH_4. Dissolution of Mg-calcite and SiO_2 is very limited, and hence only a small TDS increase is recorded. This is confirmed by chemical mass balances, which show that the concentration change of major

elements is limited to the dissolution of 0.19 mmol/L Mg-calcite, 0.23 meq/L of cation exchange, and the dissolution of only 0.02 mmol/L of quartz or (biogenic) opal.

These reactions were quantified by inverse modeling of chemical mass balances. Two genetically linked points were chosen as an input (the Damour River) and output (the river bank-filtrate (Table 2.6), the effects of admixed native groundwater were eliminated, and then the chemical reactions supposedly responsible for generating the recorded output were (semi)automatically selected and quantified. REACTIONS+ (R+) program developed in Excel spreadsheet was used to draw up the mass balances (Stuyfzand and Timmer 1999; Stuyfzand et al. 2006; Stuyfzand 2011). It provides a handy option for inverse modeling with special subroutines to correct for admixed water, and to account for the unsaturated zone and salinization (Khadra and Stuyfzand 2016).

More concerns exist regarding the behavior of potential pollutants in the Damour River. Fractured/karstic limestone has a low natural attenuation, which could form a problem if OMPs, and bacteria and viruses reach the RBF wells. This necessitates post-treatment of the raw extracted groundwater.

6.3.4 Hydrogeochemical sustainability

The hydrogeochemical sustainability of the current ongoing RBF on the northern border of the Damour River, was checked based on the pollution level of: (1) the water of the river prior to infiltration, and (2) the river bank-filtrate. WAPI is a pollution index (Table 2.3) utilized for this purpose. It is > 20 (polluted) and between 1 to 4 (unpolluted to slightly polluted) for the Damour River water and the river bank-filtrate, respectively (analysis of OMPs was ignored due to missing data). The consumption rate of acid buffering capacity is extremely low compared to the aquifer's capacity, and the original reducing capacity of the aquifer is already close to zero. So, leaching of valuable aquifer constituents is not a matter of concern. Nothing is known about what happens in the river bed, such as the potential accumulation of muds there, due to lack of data.

A hydrogeochemical sustainability analysis is required as well for any future MAR in the Damour coastal plain. In general, the value of WAPI of the Damour River, as a main potential recharge source, confirms the need for pretreatment processes. Data on OMPs should be collected as well as an essential part of the overall assessment.

6.3.5 Conclusions

RBF forms a forgotten but strong MAR application candidate to be added to the Lebanese national water strategy. This is not only true for the Damour River with surrounding fractured, karstic (dolomitic) limestones, but also for other karstic aquifers in Lebanon in the vicinity of major perennial rivers, e.g. the Litani, the Awali, and the Ibrahim rivers. Dedicated studies are needed, however, to check their suitability for RBF application. Aquifer storage recovery (ASR) in alluvial aquifers having nearby recharge sources (e.g.

from rivers) also seem to be an attractive option in Lebanon. The foreseen Dutch pilot in the Damour coastal strip aims at assessing the overall applicability of this technique in the Lebanese context. It is expected to create additional faith in ASR application, which is needed to overshadow the failure of previous artificial recharge attempts in karst aquifers. In addition, further research is needed to investigate the feasibility of utilizing other sources for recharge, for instance by harvesting rainwater, urban stormwater, or even treated effluent water, where rivers are far away or have a too bad water quality.

6.4 Towards a structured multi-faceted approach to analyze and manage saltwater intrusion in coastal aquifers

Analysis of coastal aquifers is in many aspects similar to other inland (ground)water reservoirs; however, the interaction with seawater necessitates further steps to account for admixing. This requires special consideration of some physical and chemical aspects of groundwater, including the anticipated direct effect on water quality and its variable volumes. Therefore, from a management perspective, a thorough assessment of coastal reserves calls for a structured multi-faceted approach. Two start lines coupling hydrological and hydrochemical perspectives are suggested below to analyze and manage SWI in coastal aquifers. They are subsequently combined into a calibrated hydrological and/or hydrochemical model, which is used to model future scenarios based on predicted impacts and to select remediation schemes (Figure 6.2). The proposed steps are not new; nevertheless, part of the detailed handling contains original contributions elaborated in relevant sections throughout this thesis as developed by the author over the last years with emphasis on karstic carbonate aquifers.

1. *Line 1: Hydrological System Analysis (HSA)*
    a. Collect basic hydrological data from wells, springs, rivers and lakes, including pump tests and geophysical surveys (e.g. electrical and seismic surface methods).
    b. Evaluate the hydrogeological structure (spatial distribution of groundwater and its interrelation with the hosting rocks regarding their water bearing properties).
    c. Construct hydrogeological maps and cross-sections (wells and their depths are to be displayed).
    d. Determine the configuration of the water table (or potentiometric surface).
    e. Present the main groundwater flow patterns.
    f. Build groundwater flow models.
    g. Analyze the water budget.

2. *Line 2: HydroChemical System Analysis (HCSA)*
   a. Collect hydrochemical data with wide range of parameters from groundwater, surface water, rainfall and the neighbouring sea.
   b. Construct hydrochemical maps and cross-sections showing hydrosomes and facies.
   c. Identify salinization and recharge sources.
   d. Define groundwater baseline concentrations (BGCs) for main constituents, trace elements and isotopes.
   e. Define main hydrogeochemical reactions, and assess their impact on water quality.
   f. Build reactive transport and/or variable-density and solute transport models.

3. *Apply calibrated/validated numerical model(s)*
   a. Model future scenarios.
   b. Formulate remediation schemes.

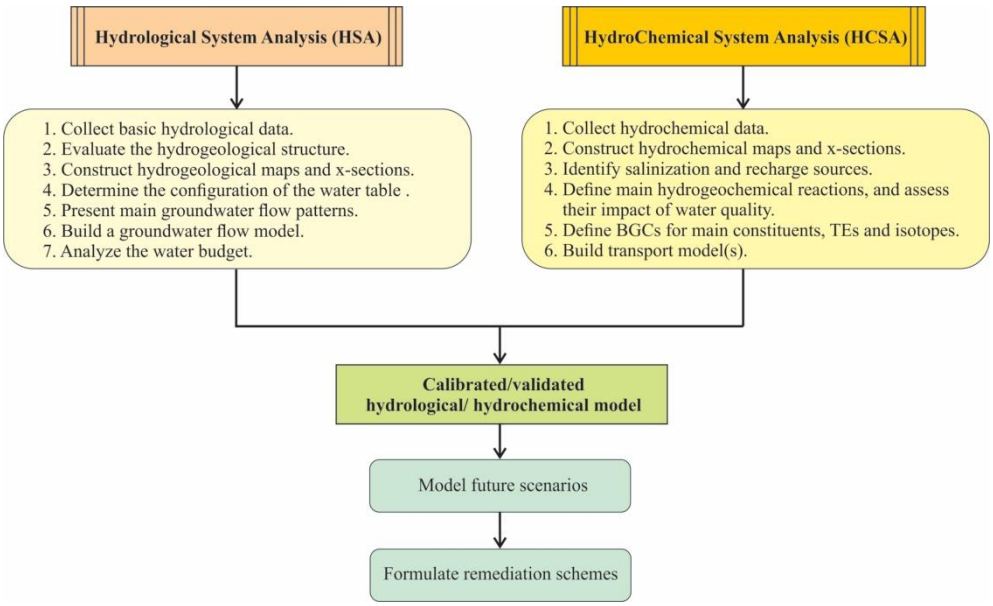

Figure 6.2 A structured multi-faceted approach to analyze and manage saltwater intrusion (SWI) in coastal aquifers. BGC = Baseline Groundwater Concentration.

6.5 Future challenges

Research on saltwater intrusion (SWI) in coastal aquifers during the past century disclosed many of its hydrological and hydrochemical features, but several fundamental challenges remain (Werner et al. 2013). Hence, it is recommended to devote more future efforts to different aspects, summarized here according to 4 main groups:

1) Scientific issues re hydrology:
   i. Explore the mechanisms that affect the thickness of the freshwater-seawater mixing zone including the role of fractures.
   ii. Discern the settings where simplified homogeneous models do not suffice in reproducing SWI behavior.
   iii. Study the effects of dispersive processes and their variation in heterogeneous fractured and karstic domains.
   iv. Estimate the residence time of groundwater in salinized karst aquifers, preferably by recognizing fresh and salt water end-member ages separately.

2) Scientific issues re hydrogeochemistry:
   i. Assess the magnitude and qualitative effects of irrigation return flow and its (dis)similarity to intruding seawater.
   ii. Evaluate the effects of hosting rock geochemistry on aquifer hydraulics of the mixing zone.
   iii. Characterize the hydrodynamic aquifer properties via artificial tracers such as artificial DNA loaded nanoparticles.

3) Practical issues re mapping and monitoring:
   i. Install short or dedicated well screens for better water sampling.
   ii. Acquire water and rock samples from the mixing zone and from the intruded Mediterranean seawater below this zone.
   iii. Explore the recent distribution of SWI and monitor its temporal changes via new geophysical investigations.
   iv. Collect more data on salinity stratifications.
   v. Conduct new campaigns to capture concentrated submarine groundwater discharge or recharge along the shoreline.
   vi. Conduct a new inventory of organic micropollutants (OMPs) in various surface and groundwaters.
   vii. Explore deeper parts of aquifer system, also looking for very deep flows that are recharged further inland or up in the mountain.

4) Practical issues re management:
   i. Build SWI models with finer discretization to capture larger scale variations (this necessitates more computational power).
   ii. Discern smaller lineaments, and assess their effects on SWI models.
   iii. Predict the effect of future climate change, sea level rise, and urbanization on groundwater quality.
   iv. Apply simulation-optimization methods for better planning of current groundwater extraction arrays.
   v. Assess the chances of success of MAR pilots, including ASR, RBF and canal recharge using urban runoff.
   vi. Apply a pilot of an 'integrated fresh-keeper' well combined with high recovery reverse osmosis.

Chapter 7

Acknowledgements

I would like to express my warmest feelings and deep gratitude to prof. dr. Pieter J. Stuijfzand for his unlimited assistance and honest support. What I learnt from him is indescribable; he is a great man who I will never forget. Special thanks goes to dr. Vincent Post who played a crucial role to get me accepted to the Ph.D. program initiated at VU University Amsterdam. I also acknowledge dr. Boris van Breukelen for his critical reviews and support especially on hydrochemical modeling. Dr. Koos Groen is thanked for his discussions, and dr. Maarten Waterloo is recognized for his comments and suggestions to install a multi-faceted hydrological monitoring network in the study area. I am also thankful to my colleagues at the American University of Beirut especially prof. dr. Abdel Fattah Abdel Rahman and dr. Ata Elias for their support. Two graduate students are also acknowledged for their help in some field activities. Finally, I am very grateful to my parents, beloved wife and my children for their endurance of my crowded calendar over the last years.

Wisam M. Khadra
TU Delft, the Netherlands

Chapter 8

Bibliography

Abarca, E., Carrera, J., Sánchez-Vila, X., Dentz, M., 2007. Anisotropic dispersive Henry problem. Adv. Water Resour. 30 (4), 913-926. http://dx.doi.org/10.1016/j.advwatres.2006.08.005.

Abd-Elhamid, H.F., Javadi, A.A., 2011. A Cost-Effective Method to Control Seawater Intrusion in Coastal Aquifers. Water Resour. Manage. 25, 2755–2780. http://dx.doi.org/10.1007/s11269-011-9837-7.

Abdoulhalik, A., Ahmed, A., Hamill, G.A., 2017. A new physical barrier system for seawater intrusion control. J. Hydrol. 549, 416–427. http://dx.doi.org/10.1016/j.jhydrol.2017.04.005.

Abdul Rahman, A.C., 2007. Environmental isotopic and hydrochemical study of water in the karst aquifer and submarine springs of the Syrian coast. Hydrogeol. J. 15, 351–364. http://dx.doi.org/10.1007/s10040-006-0072-x.

Abusaada, M., Sauter, M., 2013. Studying the Flow Dynamics of a Karst Aquifer System with an Equivalent Porous Medium Model. Groundwater 51(4), 641–650. http://dx.doi.org/10.1111/j.1745-6584.2012.01003.x.

Acra, A., Raffoul, Z., Karahogopian, N., 1983. Long-term investigation of sea water infiltration and ground water quality in Greater Beirut. MESAEP, Proc. 2nd International Meeting on Environmental Pollution in the Mediterranean Region, Iraklion, Crete.

Adnan, MS, Hendrayana, H., Ekaputra, DP., 2013. Groundwater model as a tool for sustainable groundwater management. Int. J. Integr. Eng. 5(1), 46-57.

Afonso, M.D., Jaber, J.O., Mohsen, M.S., 2004. Brackish groundwater treatment by reverse osmosis in Jordan. Desalin. 164 (2), 157–171.

Ahmed, M., Sayya, W.H., Hoey, D., Al-Handaly, J., 2001. Brine disposal from reverse osmosis desalination plants in Oman and the United Arab Emirates. Desalin. 133, 135–147. http://dx.doi.org/10.1016/S0011-9164(01)80004-7.

Ajam, N. and Saa'd, H., 1980a. Technical report on four drilled wells in Damour area, Lebanon. Beirut: Ministry of Water and Electric Resources.

Ajam, N. and Saa'd, H., 1980b. Technical report on six drilled wells in Haret en Naame-Mechrif area, Lebanon. Beirut: Ministry of Water and Electric Resources.

Akaike, H., 1974. A new look at the statistical model identification. IEEE Transactions on Automatic Control 19 (6), 716-723. http://dx.doi.org/10.1109/TAC.1974.1100705.

Alcalá, F., Custodio, E., 2004. Use of the Cl/Br ratio as tracer to identify the origin of salinity in some Spanish coastal aquifers. Proc. 18th Salt Water Intrusion Meeting, Cartagena, Spain.

Al Kuisi, M., Abed, A.M., Mashal, K., Saffarini, G., Saqhour, F., 2015. Hydrogeochemistry of groundwater from karstic limestone aquifer highlighting arsenic contamination: case study from Jordan. Arab J. Geosci. 8, 9699–9720. http://dx.doi.org/10.1007/s12517-015-1919-z.

Al-Zubari, W.K., 2003. Assessing the sustainability of non-renewable brackish groundwater in feeding an RO desalination plant in Bahrain. Desalination 159, 211–224.

Anderson, M., Woessner, W., 1992. Applied Groundwater Modeling: Simulation of Flow and Advective Transport. Academic Press, USA.

Angelini, P., 1997. Correlation and spectral analysis of two hydrogeological systems in central Italy. Hydrol. Sci. J. 42 (3), 425–438. http://dx.doi.org/10.1080/02626669709492038.

Appelo, C.A.J., 1994. Cation and proton exchange, pH variations, and carbonate reactions in a freshening aquifer. Water Resour. Res. 30(10), 2793-2805. http://dx.doi.org/10.1029/94WR01048.

Appelo, C.A.J., Postma, D., 2005. Geochemistry, groundwater and pollution, 2nd edition, Balkema Publishers, the Netherlands.

Archie, G.E., 1942. The electrical resistivity log as an aid in determining some reservoir characteristics. Trans. Am. Inst. Min. Metall. Pet. Eng. 146:54–61.

Archontelis, A., Ganoulis, J., 2015. Comparison between hydrodynamic simulation and available data in a karst coastal aquifer: The case of Almyros Spring, Crete Island, Greece. In: Andreo et al. (eds) Hydrogeological and Environmental Investigations in Karst Systems, Environmental Earth Sciences 1, Springer-Verlag Berlin Heidelberg, p 303-311. http://dx.doi.org/10.1007/978-3-642-17435-3_30.

Arkadan, A., 1999. The geology, geomorphology and hydrogeology of the Damour-Awali area coastal and hinterland. MS Thesis. American University of Beirut, Beirut, Lebanon.

Arkadan, A. 2008. Climatic changes in Lebanon, predicting uncertain precipitation events—Do climatic cycles exist? In Zereini and Hötzl (eds.), Climatic changes and water resources in the Middle East and North Africa. Berlin: Springer, Environmental Science and Engineering, 59–74.

Awad, H.M., 1983. Geomorphology, stratigraphy and hydrogeology of the Doha-Damour area and hinterland. MSc Thesis, American University of Beirut, Lebanon.

Ayotte, J.D., Szabo, Z., Focazio, M.J., Eberts, S.M, 2011. Effects of human-induced alteration of groundwater flow on concentrations of naturally-occurring trace elements at water-supply wells. Appl. Geochem. 26, 747–762. http://dx.doi.org/10.1016/j.apgeochem.2011.01.033.

Babiker, I., Mohamed, M., Terao, H., Kato, K., Ohta, K., 2004. Assessment of groundwater contamination by nitrate leaching from intensive vegetable cultivation using geographical information system. Environ. Int. 29, 1009–1017.

Bacchus, S.T., Bernardes, S., Xu, W., Madden, M., 2015a. What Georgia can learn from aquifer storage and recovery (ASR) in Florida. In McDowell et al. (eds.), Proc. 2015 Georgia Water Resources Conference, University of Georgia, Athens.

Bacchus, S.T., Bernardes, S., Xu, W., Madden, M., 2015b. Fractures as preferential flowpaths for aquifer storage and recovery (ASR) injections and withdrawals: Implications for environmentally sensitive near-shore waters, wetlands of the Greater Everglades Basin and the regional karst Floridan aquifer system. J. Geography and Geology 7(2), 117-155.

Bachu, S., 1995. Flow of variable-density formation water in deep sloping aquifers: review of methods of representation with case studies. J. Hydrol. 164, 19-38. http://dx.doi.org/10.1016/0022-1694(94)02578-Y.

Badon Ghyben, W., 1888. Nota in verband met de voorgenomen putboring nabij Amsterdam (A note in connection with the proposed wellbore near Amsterdam). Tijdschrift Van Koninklijk Instituut Van Ingenieurs (Magazine of Royal Institute of Engineers) 9, 8–22 (in Dutch).

Barcelona, M.J., Kim, M., Masciopinto, C., La Mantia, R., 2006. A Gypsum-Barrier Design to Stop Seawater Intrusion in a Fractured Aquifer at Salento (Southern Italy). Proc. 1st SWIM-SWICA Joint Saltwater Intrusion Conference, Cagliari-Chia Laguna, Italy, 263-272.

Bartak, R., Grischek, T., Ghodeif, K., Ray, C., 2012. Beach Sand Filtration as Pre-Treatment for RO Desalination. Int. j. water sci. 1(2), 1-10.

Basri, M.H., 2001. Two new methods for optimal design of subsurface barrier to control seawater intrusion. PhD thesis, University of Manitoba, Manitoba.

Bear, J., Dagan, G., 1964. Some exact solutions of interface problems by means of the hodograph method. J. Geophys. Res. 69(8), 1563–1572. http://dx.doi.org/10.1029/JZ069i008p01563.

Bear, J., Cheng, A.H.-D., 1999. Introduction. In Bear et al. (eds.), Seawater intrusion in coastal aquifers: concepts, methods and practices. Kluwer Academic Publishers, the Netherlands.

Bear, J., Cheng, A., 2010. Modeling Groundwater Flow and Contaminant Transport, Theory and Applications of Transport in Porous Media, vol. 23. Springer Science+Business Media B.V., 834p.

Bear, J., Zhou, Q., 2007. Sea Water Intrusion into Coastal Aquifers. In Delleur (ed), The Handbook of Groundwater Engineering, 2nd edition. CRC Press, USA, 12.1–12.29.

Ben Ammar, S., Taupin, J.D., Zouari, K., Khouatmia, M., 2016. Identifying recharge and salinization sources of groundwater in the Oussja Ghar el Melah plain (northeast Tunisia) using geochemical tools and environmental isotopes. Environ. Earth Sci. 75, 606. http://dx.doi.org/10.1007/s12665-016-5431-x.

Benavente, J., Pulido-Bosch, A., Mangin, A., 1985. Application of correlation and spectral procedures to the study of the discharge in a karstic system (Eastern Spain). In: Karst Water Resources, Ankara-Antalya, p. 67–75.

Bennett, B., Dudas, M.J., 2003. Release of arsenic and molybdenum by reductive dissolution of iron oxides in a soil with enriched levels of native arsenic. J. Environ. Eng. Sci. 2, 265–272. http://dx.doi.org/10.1139/s03-028.

Bense, V.F., Van Balen, R.T., De Vries, J.J., 2003. The impact of faults on the hydrogeological conditions in the Roer Valley Rift System: an overview. Netherlands J. Geosci. 82 (1), 41-54.

Bhattacharjya, R.K., Borah, T., 2016. Coastal aquifer management models: A comprehensive review on nodel development. In Sarma et al. (eds.), Urban hydrology, watershed management and socio-economic aspects, Water Science and Technology Library 73, http://dx.doi.org/10.1007/978-3-319-40195-9_8.

Bhuiyan, C., 2015. Hydrological characterization of geological lineaments: a case study from the Aravalli terrain, India. Hydrogeol. J. 23: 673–686. http://dx.doi.org/10.1007/s10040-015-1239-0.

Blessent, D., Jørgensen, P., Therrien, R., 2014. Comparing discrete fracture and continuum models to predict contaminant transport in fractured porous media. Groundwater 52(1), 84–95. http://dx.doi.org/10.1111/gwat.12032.

Bobba, A.G., 2007. Groundwater development and management of coastal aquifers (including island aquifers) through monitoring and modeling approaches. In Thangarajan (ed.), Groundwater Resource Evaluation, Augmentation, Contamination, Restoration, Modeling and Management. Springer, India, pp. 283–333.

Borghi, A., Renard, P., Jenni, S., 2012. A pseudo-genetic stochastic model to generate karstic networks. J. Hydrol. 414–415, 516–529. http://dx.doi.org/10.1016/j.jhydrol.2011.11.032.

Bouchaou, L., Michelot, J., Vengosh, A., Hsissou, Y., Qurtobi, M., Gaye, C., Bullen, T., Zuppi, G., 2008. Application of multiple isotopic and geochemical tracers for investigation of recharge, salinization, and residence time of water in the Souss-Massa aquifer, southwest of Morocco. J. Hydrol. 352, 267–287. http://dx.doi.org/10.1016/j.jhydrol.2008.01.022.

Bouderbala, A., Remini, B., Saaed, Hamoudi A., Pulido-Bosch, A., 2016. Application of multivariate statistical techniques for characterization of groundwater quality in the

coastal aquifer of Nador, Tipaza (Algeria), Acta Geophysica 64 (3), 670-693. http://dx.doi.org/10.1515/acgeo-2016-0027.

Bouwer, H., 2002. Artificial recharge of groundwater: hydrogeology and engineering. Hydrogeol. J. 10, 121–142. http://dx.doi.org/10.1007/s10040-001-0182-4.

Bradford, S.A., Kim, H., 2010. Implications of cation exchange on clay release and colloid-facilitated transport in porous media. J. Environ. Qual. 39, 2040–2046. http://dx.doi.org/10.2134/jeq2010.0156.

Bredehoeft, J.D., 1997. Fault permeability near Yuca Mountain. Water Resour. Res. 33(11), 2459-2463.

Brenot, A., Baran, N., Petelet-Giraud, E., Négrel, P., 2008. Interaction between different water bodies in a small catchment in the Paris basin (Brévilles, France): tracing of multiple Sr sources through Sr isotopes coupled with Mg/Sr and Ca/Sr ratios. Appl. Geochem. 23, 58–75. http://dx.doi.org/10.1016/j.apgeochem.2007.09.006.

Brook, G.A., Folkoff, M.E., Box, E.O., 1983. A world model of soil carbon dioxide. Earth Surf. Proc. 8, 79–88.

Cai, J., Taute, T., Schneider, M., 2015. Recommendations of controlling saltwater intrusion in an inland aquifer for drinking-water supply at a certain waterworks site in Berlin (Germany). Water Resour. Manag. 29 (7), 2221–2232. http://dx.doi.org/10.1007/s11269-015-0937-7.

CAMP, 2004. Coastal Area Management Programme (CAMP) Lebanon. Beirut: UNEP, National Project of the Mediterranean Action Plan (MAP) of UNEP.

Camp, M.V., Walraevens, K., 2008. Identifying and interpreting baseline trends. In Edmunds and Shand (eds.), Natural groundwater quality. Oxford: Blackwell Publishing Ltd, pp. 131–154.

Carlston, C.W., 1963. An early American statement of the Badon Ghyben-Herzberg principle of static fresh-water-salt-water balance. Am. J. Sci. 261 (1), 88-91. http://dx.doi.org/10.2475/ajs.261.1.88.

Carroll, K.C., Artiola, J.F., Brusseau, M.L., 2006. Transport of molybdenum in a biosolid-amended alkaline soil. Chemosphere 65, 778–785. http://dx.doi.org/10.1016/j.chemosphere.2006.03.044.

Cartwright, I., Weaver, T., Fified, L., 2006. Cl/Br ratios and environmental isotopes as indicators of recharge variability and groundwater flow: an example from the southeast Murray Basin, Australia. Chem. Geol. 231, 38–56. http://dx.doi.org/10.1016/j.chemgeo.2005.12.009.

Celico, F., Petrella, E., Celico, P., 2006. Hydrogeological behaviour of some fault zones in a carbonate aquifer of Southern Italy: an experimentally based model. Terra Nova 18, 308–313. http://dx.doi.org/10.1111/j.1365-3121.2006.00694.x.

Charmonman, S., 1965. A solution of the pattern of fresh-water flow in an unconfined coastal aquifer, J. Geophys. Res. 70(12), 2813–2819. http://dx.doi.org/10.1029/JZ070i012p02813.

Chen, Z., Goldscheider, N., 2014. Modeling spatially and temporally varied hydraulic behavior of a folded karst system with dominant conduit drainage at catchment scale, Hochifen–Gottesacker, Alps. J. Hydrol. 514, 41-52. http://dx.doi.org/10.1016/j.jhydrol.2014.04.005.

Cooper, H.H., 1964. Sea water in the coastal aquifers. Washington, DC: U Geological Survey Water-Supply Paper 1613-C.

Craig, H., 1961. Isotopic variations in meteoric waters. Sci. 133, 1702–1708.

Cruz, R.V., Harasawa, H., Lal, M., Wu, S., Anokhin, Y., Punsalmaa, B., Honda, Y., Jafari, M., Li, C., Huu Ninh, N., 2007. Asia. Climate change 2007: impacts, adaptation and vulnerability. Contribution of Working Group II to the fourth assessment report of the Intergovernmental Panel on Climate Change. In Parry et al. (eds.), An assessment of the Intergovernmental Panel on Climate Change. Cambridge: Cambridge University Press.

Dafny, E., Burg, A., Gvirtzman, H., 2010. Effects of Karst and geological structure on groundwater flow: The case of Yarqon-Taninim Aquifer, Israel. J. Hydrol. 389, 260–275. http://dx.doi.org/10.1016/j.jhydrol.2010.05.038.

Daher, W., Pistre, S., Kneppers, A., Bakalowicz, M., Najem, W., 2011. Karst and artificial recharge: Theoretical and practical problems: A preliminary approach to artificial recharge assessment. J. Hydrol. 408 (3–4), 189–202. http://dx.doi.org/0.1016/j.jhydrol.2011.07.017.

Dai, Z., Samper, J., Ritzi Jr, R., 2006. Identifying geochemical processes by inverse modeling of multicomponent reactive transport in the Aquia aquifer. Geosphere 2(4), 210–219. http://dx.doi.org/10.1130/GES00021.1.

Daoud A., 1973. Groundwater Recharge in the Beirut Area. MS Thesis. American University of Beirut, Beirut, Lebanon.

Dar Al-Handasah, 1999. Beirut southern suburbs rehabilitation Lot VIII-Doha Aramoun Damour water wells, progress report. Beirut: Council for Development and Reconstruction (CDR), 125.

Datta, B., Vennalakanti, H., Dhar, A., 2009.Modeling and control of saltwater intrusion in a coastal aquifer of Andhra Pradesh India. J. Hydro-environ Res. 3, 148–159. http://dx.doi.org/10.1016/j.jher.2009.09.002.

Dausman, AM., 2008. Saltwater/Freshwater Interface Movement in Response to Deep-Well Injection in a Coastal Aquifer. 20th Salt Water Intrusion Meeting, Naples, Florida, USA.

Dausman, A.M., Langevin, C.D., 2005. Movement of the saltwater interface in the Surficial Aquifer System in response to hydrologic stresses and water management practices, Broward County, Florida. U.S. Geological Survey Scientific Investigations Report 2004-5256.

De Filippis, G., Foglia, L., Giudici, M., Mehl, S., Margiotta, S., Luigi Negri, S., 2016. Seawater intrusion in karstic, coastal aquifers: Current challenges and future scenarios in the Taranto area (southern Italy). Sci. Total Environ. 573, 1340–1351. http://dx.doi.org/10.1016/j.scitotenv.2016.07.005.

De Montety, V., Radakovitch, O., Vallet-Coulomb, C., Blavoux, B., Hermitte, D., Valles, V., 2008. Origin of groundwater salinity and hydrogeochemical processes in a confined coastal aquifer: Case of the Rhône delta (Southern France). Appl. Geochem. 23, 2337–2349. http://dx.doi.org/10.1016/j.apgeochem.2008.03.011.

Dentoni, M., Deidda, R., Paniconi, C., Qahman, K., Lecca, G., 2015. A simulation/optimization study to assess seawater intrusion management strategies for the Gaza Strip coastal aquifer (Palestine). Hydrogeol. J. 23, 249–264. http://dx.doi.org/10.1007/s10040-014-1214-1.

Diersch, H.J.G., 2014. Finite element modeling of flow, mass and heat transport in porous and fractured media. 1st ed., Springer, Verlag Berlin Heidelberg. http://dx.doi.org/10.1007/978-3-642-38739-5.

Doherty, J., 1994. PEST Model-independent parameter estimation. User's manual. Watermark Numerical Computing, Australia.

Dokou, Z., Karatzas, G., 2012. Saltwater intrusion estimation in a karstified coastal system using density-dependent modelling and comparison with the sharp-interface approach, Hydrol. Sci. J., 57(5), 985-999. http://dx.doi.org/10.1080/02626667.2012.690070.

Drever, J., 1997. The Geochemistry of Natural Waters, 3rd edition, Prentice Hall, New Jersey.

Dubertret, L., 1955. Carte Géologique du Liban au 1/200000 avec notice explicative. République Libanaise, Ministère des Travaux Publiques, Beirut, Lebanon.

Duce, R.A., Hoffman, E.J., 1976. Chemical fractionation at the air/sea interface. Annu. Rev. Earth Planet. Sci. 4, 187–228.

ECODIT, 2015. Strategic environmental assessment for the new water sector strategy for Lebanon, Final SEA report, Plan Bleu and the Ministry of Energy and Water, Beirut, Lebanon.

Edmunds, W.M., Smedley, P.L., 1996. Groundwater geochemistry and health: an overview. In Appleton et al. (eds.), Environmental geochemistry and health: with special reference to developing countries. London: Geological Society of London Special Publication no.113.

Edmunds, W.M., Shand, P., 2008. Groundwater baseline quality, In Edmunds and Shand (eds.), Natural groundwater quality. Blackwell Publishing Ltd, 1–21.

Einsiedl, F., Maloszewski, P., Stichler, W., 2009. Multiple isotope approach to the determination of the natural attenuation potential of a high-alpine karst system. J. Hydrol. 365, 113–121. http://dx.doi.org/10.1016/j.jhydrol.2008.11.042.

El-Fadel, M., Rachid, G., Alameddine, I., Abu Najm, M., 2014. Saltwater Intrusion in karst aquifers along the Eastern Mediterranean. 23rd Salt Water Intrusion Meeting, Husum, Germany, 311-314.

El-Fiky, A., 2010. Hydrogeochemical characteristics and evolution of groundwater at the Ras Sudr-Abu Zenima area, Southwest Sinai, Egypt. Earth Sci. 21(1), 79–109.

El-Hakim, M., Bakalowicz, M., 2007. Significance and origin of very large regulating power of some karst aquifers in the Middle East. Implication on karst aquifer classification. J. Hydrol. 333, 329–339. http://dx.doi.org/10.1016/j.jhydrol.2006.09.003.

El Yaouti, F., El Mandour, A., Khattach, D., Kaufmann, O., 2008. Modelling groundwater flow and advective contaminant transport in the Bou-Areg unconfined aquifer (NE Morocco). J. Hydro-environ. Res. 1-18. http://dx.doi.org/10.1016/j.jher.2008.08.003.

Emblanch, C., Fidelibus, M.D., Futo, I., Hertelendi, E., Lambrakis, N., Vengosh, A., Zojer, H., Zuppi, G.M., 2005a. Environmental tracing methods. In Tulipano et al. (eds.), Groundwater management of coastal karstic aquifers. Luxemburg: COST Action 621, Final Report, EUR 21366, COST Office, 363.

Emblanch, C., Fidelibus, M.D., Hertelendi, E., Kogovsek, J., Zojer, H., 2005b. Environmental tracing for outlining fresh groundwater flow in a coastal karstic aquifer. In Tulipano et al. (eds.), Groundwater management of coastal karstic aquifers. Luxemburg: COST Action 621, Final Report, EUR 21366, COST Office, 363.

Ertas, T., Topal, T., 2008. Quality and durability assessments of the armourstones for two rubble mound breakwaters (Mersin, Turkey). Environ. Geol. 53, 1235–1247. http://dx.doi.org/10.1007/s00254-007-0712-z.

ESCWA 2009. ESCWA water development report 3: Role of Desalination in Addressing Water Scarcity. United Nations, New York: USA, 46p.

Essink, G., 2001. Improving fresh groundwater supply-problems and solutions. Ocean Coast. Manag. 44, 429–449. http://dx.doi.org/10.1016/S0964-5691(01)00057-6.

EU, 1998. Council directive 98/83/EC of 3 November 1998 on the quality of water intended for human consumption. Official Journal of the European Communities L 330/32.

Faimon, J., Ličbinska, M., Zajiček, P., Sracek, O., 2012. Partial pressures of CO_2 in epikarst zone deduced from hydrogeochemistry of permanent drips, the Moravian karst, Czech Republic, Acta Carsologica 41(1), 47-57.

FAO, 1973. Project de development hydro-agricole du sud du Liban: Thermometrie aeroportee par infra-rouge. Beirut, Lebanon.

FAO, 1997. Seawater intrusion in coastal aquifers: guidelines for study, monitoring and control. Water reports 11, Food and Agriculture Organization of the United Nations, Italy.

Fattahi, M.H., Talebbeydokhti, N., Shamsai, A., 2010. Application of Double Continuum Porosity Equivalent Method to Investigate the Karst Problem of Salman Farsi Dam in Iran. The National Conference on Water Crisis Management, Azad University, Iran.

Fernández-Torquemada, Y., Sánchez-Lizaso, J.L., González-Correa, J.M., 2005. Preliminary results of the monitoring of the brine discharge produced by the SWRO desalination plant of Alicante (SE Spain). Desalin. 182, 395–402. http://dx.doi.org/10.1016/j.desal.2005.03.023.

Fidelibus, M.D., 2003. Environmental tracing in coastal aquifers: old problems and new solutions. In Coastal Aquifers Intrusion Technology: Mediterranean Countries. Publ. IGME, Madrid, 9–111.

Fidelibus, M.D., Giménez, E., Morell, I., Tulipano, L., 1993. Salinization processes in the Castellon Plain aquifer (Spain). Study and modelling of saltwater intrusion into aquifers. 12th Saltwater Intrusion Meeting, CIMNE, Barcelona, 267–283.

Fiket Ž, Rožmarić M., Krmpotić M., Benedik L., 2015. Levels of major and trace elements, including rare earth elements, and ^{238}U in Croatian tap waters. Environ. Sci. Pollut. Res. 22, 6789–6799. http://dx.doi.org/10.1007/s11356-014-3869-5.

FilmTec's Technical Manual, 2014. FILMTEC™ Reverse Osmosis Membranes Technical Manual. Dow Water & Process Solutions, form No. 609-00071-1009, Midland, USA.

Fishbein, L., 1981. Sources, Transport and Alterations of Metal Compounds: An Overview. I. Arsenic, Beryllium, Cadmium, Chromium, and Nickel. Environ. Health Perspect. 40, 43-64.

Ford, D., Williams, P., 2007. Karst Hydrogeology and Geomorphology. John Wiley and Sons, England.

Fritzmann, C., Löwenberg, J., Wintgens, T., Melin, T., 2007. State-of-the-art of reverse osmosis desalination. Desalin. 216, 1–76. http://dx.doi.org/10.1016/j.desal.2006.12.009.

Frondini, F., Zucchini, A., Comodi, P., 2014. Water–rock interactions and trace elements distribution in dolomite aquifers: The Sassolungo and Sella systems (Northern Italy). Geochem. J. 48, 231-246. http://dx.doi.org/10.2343/geochemj.2.0301.

Fu, T., Chen, H., Wang, K., 2016. Structure and water storage capacity of a small karst aquifer based on stream discharge in southwest China. J. Hydrol. 534, 50–62. http://dx.doi.org/10.1016/j.jhydrol.2015.12.042.

Gat, J.R., Carmi, I., 1970. Evolution of the isotopic composition of atmospheric waters in the Mediterranean Sea area. J. Geophys. Res. 75, 3039–304.

Geofizika, 1965. Report on geophysical investigations in the southern coastal zone. Zagreb: Geofizika Enterprise for Applied Geophysics.

Ghasemizadeh, R., Hellweger, F., Butscher, C., Padilla, I., Vesper, D., Field, M., Alshawabkeh, A., 2012. Review: Groundwater flow and transport modeling of karst aquifers, with particular reference to the North Coast Limestone aquifer system of Puerto Rico. Hydrogeol. J. 20, 1441−1461. http://dx.doi.org/10.1007/s10040-012-0897-4.

Gillespie, M.R., Kemp, S.J., Vickers, B.P., Waters, C., Gowing, C.J., 2001. Cation-Exchange Capacity (CEC) of Selected Lithologies from England, Wales and Scotland. Environment Agency R&D Technical Report P2-222/TR, British Geological Survey, Keyworth, Nottingham.

Glynn, P.D., Reardon, E.J., 1990. Solid-solution aqueous-solution equilibria—Thermodynamic theory and representation. Am. J. Sci. 290, 164-201.

Goldberg, S., Forster, H.S., 1998. Factors affecting molybdenum adsorption by soils and minerals. Soil Sci. 163, 109–114.

Gonneea, M.E., Charette, M.A, Liu, Q., Herrera-Silveira, J.A., Morales-Ojeda, S.M., 2014. Trace element geochemistry of groundwater in a karst subterranean estuary (Yucatan Peninsula, Mexico). Geochimica et Cosmochimica Acta 132, 31–49. http://dx.doi.org/10.1016/j.gca.2014.01.037.

Gopinath, S., Srinivasamoorthy, K., Saravanan, K., Suma, C.S., Prakash, R., Senthilnathan, D., Chandrasekaran, N., Srinivas, Y., Sarma, V.S., 2016. Modeling saline water intrusion in Nagapattinam coastal aquifers, Tamilnadu, India. Model. Earth Syst. Environ. 2:2. http://dx.doi.org/10.1007/s40808-015-0058-6.

Grakist, G., Maas, K., Rosbergen, W., Kappelhof, J., 2002. Keeping our wells fresh. Proc. 17th Salt Water Intrusion Meeting, Delft, the Netherlands, 337–340.

Greenlee, L.F., Lawler, D.F., Freeman, B.D., Marrot, B., Moulin, P., 2009. Reverse osmosis desalination: water sources, technology, and today's challenges. Water Res. 43, 2317–2348. http://dx.doi.org/10.1016/j.watres.2009.03.010.

Guo, W., Langevin, C.D., 2002. User's guide to SEAWAT: a computer program for the simulation of three-dimensional variable-density ground-water flow. USGS Techniques of Water Resources Investigations Book 6, Chapter A7. Reston, Virginia, USGS.

Habtemichael, Y.T., Fuentes, H.R., 2016. Hydrogeochemical analysis of processes through modeling of seawater intrusion impacts in Biscayne aquifer water quality, USA. Aquat. Geochem. 1-13. http://dx.doi.org/10.1007/s10498-016-9287-1.

Hamada, G.M., Almajed, A.A., Okasha, T.M., Algathe, A.A., 2013. Uncertainty analysis of Archie's parameters determination techniques in carbonate reservoirs. J. Petrol. Explor. Prod. Technol. 3, 1–10. http://dx.doi.org/10.1007/s13202-012-0042-x.

Hasan, M., Rotich, N., John, M., Louhi-Kultanen, M., 2017. Salt recovery from wastewater by air-cooled eutectic freeze crystallization. Chem. Eng. J. 326, 192-200. http://dx.doi.org/10.1016/j.cej.2017.05.136.

Hassan, G., 2011. The national wind atlas of Lebanon. Beirut: UNDP-CEDRO project.

HDR, 2009. An analysis of the correlation between lead released from galvanized iron piping and the contents of lead in drinking water. HDR Engineering Inc., Washington.

Heathcote, J.A., 1985. Carbonate chemistry of recent chalk groundwater in a part of East-Anglia, UK. J. Hydrol. 78, 215–227.

Hem, J.D., 1992. Study and interpretation of the chemical characteristics of natural water. U.S. Geological Survey, Water Supply Paper 2254.

Hendizadeh, R., Kompanizare, M., Hashemi, M.R., Rakhshandehroo, G.R., 2016. Steady critical discharge rates from vertical and horizontal wells in fresh–saline aquifers with sharp interfaces. Hydrogeol. J. 24, 865–876. http://dx.doi.org/10.1007/s10040-015-1351-1.

Henthorne, L., Boysen, B., 2015. State-of-the-art of reverse osmosis desalination pretreatment. Desalin. 356, 129–139. http://dx.doi.org/10.1016/j.desal.2014.10.039.

Henry, H. R., 1959. Salt intrusion into fresh-water aquifers. J. Geophys. Res. 64(11), 1911–1919. http://dx.doi.org/10.1029/JZ064i011p01911.

Herman, J., Back, W., Pomar, L., 1985. Geochemistry of groundwater in the mixing zone along the east coast of Mallorca, Spain. Karst Water Resources, Proc. Ankara - Antalya Symposium. IAHS 161, 467-479.

Herzberg B., 1901. Die Wasserversorgung einiger Nordseebäder (The water supply of some North Sea resorts). Jour. Gasbeleuchtung Wasserversorg (Journal of gas lighting and water supply) 44, 815–844 (in German).

Himi, M., Tapias, J., Benabdelouahab, S., Salhi, A., Rivero, L., Elgettafi, M., El Mandour, A., Stitou, J., Casas, A., 2017. Geophysical characterization of saltwater intrusion in a

coastal aquifer: The case of Martil-Alila plain (North Morocco). J. Afr. Earth Sci. 126, 136-147. http://dx.doi.org/10.1016/j.jafrearsci.2016.11.011.

Hinkle, D.E., Wiersma, W., Jurs, S.G., 2003. Applied statistics for the behavior sciences. Houghton Mifflin Company, New York.

IPCC (Intergovernmental Panel on Climate Change), 2007. Contribution of Working Groups I, II and III to the fourth assessment report of the Intergovernmental Panel on Climate Change. Geneva: IPCC.

Jaber, I.S., Ahmed, M.R., 2004. Technical and economic evaluation of brackish groundwater desalination by reverse osmosis (RO) process. Desalination 165, 209–213. http://dx.doi.org/10.1016/j.desal.2004.06.051.

Jacob, C., 2007. Seawater desalination: boron removal by ion exchange technology. Desalination 205, 47–52. http://dx.doi.org/10.1016/j.desal.2006.06.007.

Janssen, R.P., Verweij, W., 2003. Geochemistry of some rare earth elements in groundwater, Vierlingsbeek, The Netherlands. Water Res. 37, 1320–1350. http://dx.doi.org/10.1016/S0043-1354(02)00492-X.

Javadi, A., Hussain, M., Sherif, M., Farmani, R., 2015.Multi-objective optimization of different management scenarios to control seawater intrusion in coastal aquifers. Water Resour. Manage. 29, 1843–1857. http://dx.doi.org/10.1007/s11269-015-0914-1.

Jemcov, I., Petric, M., 2009. Measured precipitation vs. effective infiltration and their influence on the assessment of karst systems based on results of the time series analysis. J. Hydrol. 379, 304–314. http://dx.doi.org/10.1016/j.jhydrol.2009.10.016.

Kacimov, A.R., Sherif, M.M., Perret, J.S., Al-Mushikhi, A., 2009. Control of sea-water intrusion by salt-water pumping: Coast of Oman. Hydrogeol. J. 17, 541–558. http://dx.doi.org/10.1007/s10040-008-0425-8.

Kafri, U., Arad, A., 1979. Current subsurface intrusion of Mediterranean seawater—a possible source of groundwater salinity in the Rift Valley system, Israel. J. Hydrol. 44, 267–287.

Karagiannis, I.C., Soldatos, P.G., 2008. Water desalination cost literature: review and assessment. Desalin. 223:448–456. http://dx.doi.org/10.1016/j.desal.2007.02.071.

Kavouri, K.P., Karatzas, G.P., Plagnes, V., 2017. A coupled groundwater-flow-modelling and vulnerability-mapping methodology for karstic terrain management. Hydrogeol. J. 25 (5), 1301-1317. http://dx.doi.org/10.1007/s10040-017-1548-6.

Kempe, S., Al-Malabeh, A., Al-Shreideh, A., Henschel, H., 2006. Al-Daher Cave (Bergish), Jordan, the first extensive Jordanian limestone cave: a convective Carlsbad-type cave? J. Cave Karst Stud. 68 (3), 107–114.

Kerrou, J., Renard, P., Cornaton, F., Perrochet, P., 2013. Stochastic forecasts of seawater intrusion towards sustainable groundwater management: application to the Korba aquifer (Tunisia). Hydrogeol. J. 21, 425–440. http://dx.doi.org/10.1007/s10040-012-0911-x.

Khadra, W.M., 2003. Hydrogeology of the Damour-Upper Sannine- Maameltain Aquifer. MS Thesis. American University of Beirut, Beirut, Lebanon.

Khadra, W.M., Stuyfzand, P.J., 2014. Separating baseline conditions from anthropogenic impacts: example of the Damour coastal aquifer (Lebanon). Hydrol. Sci. J. 59, 1872-1893. http://dx.doi.org/10.1080/02626667.2013.841912.

Khadra, W.M., Stuyfzand, P.J., 2016. Mass balancing to define major hydrogeochemical processes in salinizing dolomitic limestone aquifers: Example from Eastern Mediterranean (Lebanon). In Werner A.D. (ed.), Proc. 24th Salt Water Intrusion Meeting and the 4th Asia-Pacific Coastal Aquifer Management Meeting, Cairns, Australia, 110-116.

Khadra, W.M., Stuyfzand, P.J., Khadra, I.M., 2017a. Mitigation of saltwater intrusion by 'integrated fresh-keeper' wells combined with high recovery reverse osmosis. Sci. Total Environ. 574, 796–805. http://dx.doi.org/10.1016/j.scitotenv.2016.09.156.

Khadra, W.M., Stuyfzand, P.J., van Breukelen, B.M., 2017b. Hydrochemical effects of saltwater intrusion in a limestone and dolomitic limestone aquifer in Lebanon. Appl. Geochem. 79, 36-51. http://dx.doi.org/10.1016/j.apgeochem.2017.02.005.

Khayat, Z.A., 2001. Groundwater conditions in the Koura- Zgharta Miocene limestone aquifer. MS Thesis. American University of Beirut, Beirut, Lebanon.

Kihm, J.H., Kim, J.M., Song, S.H., Lee, G.S., 2007. Three-dimensional numerical simulation of fully coupled groundwater flow and land deformation due to groundwater pumping in an unsaturated fluvial aquifer. J. Hydrol. 335, 1-14. http://dx.doi.org/10.1016/j.jhydrol.2006.09.031.

Kim, K.-Y., Chon, C.-M., Park, K.-H., 2007. A simple method for locating the fresh water–salt water interface using pressure data. Groundwater 45(6), 723-728. http://dx.doi.org/10.1111/j.1745-6584.2007.00349.x.

Klein, W.A., Manda A.K., Griffin M.T., 2014. Refining management strategies for groundwater resources. Hydrogeol. J. 22, 1727–1730. http://dx.doi.org/10.1007/s10040-014-1177-2.

Koh, D.-C., Chae, G.-T., Ryu, J.-S., Lee, S.-G., Ko, K.-S., 2016. Occurrence and mobility of major and trace elements in groundwater from pristine volcanic aquifers in Jeju Island, Korea. Appl. Geochem. 65, 87-102. http://dx.doi.org/10.1016/j.apgeochem.2015.11.004.

Kooiman, J.W., Stuyfzand, P.J., Maas, C., Kappelhof, J.W., 2004. Pumping brackish groundwater to prepare drinking water and keep salinizing wells fresh: a feasibility study. Proc. 18th Salt Water Intrusion Meeting, Cartagena, Spain, 625–635.

Kopsiaftis, G., Mantoglou, A., Giannoulopoulos, P., 2009. Variable density coastal aquifer models with application to an aquifer on Thira Island. Desalination 237, 65-80. http://dx.doi.org/10.1016/j.desal.2007.12.023.

Korfali, S., Jurdi, M., 2007. Assessment of domestic water quality: case study, Beirut, Lebanon. Environ. Monit. Assess. 135, 241–251. http://dx.doi.org/10.1007/s10661-007-9646-x.

Korfali, S., Jurdi, M., 2009. Provision of safe domestic water for the promotion and protection of public health: a case study of the city of Beirut, Lebanon. Environ. Geochem. Health 31, 283–295. http://dx.doi.org/10.1007/s10653-008-9218-1.

Kourgialas, N.N., Dokou, Z., Karatzas, G.P., 2016. Saltwater intrusion in an irrigated agricultural area: combining density-dependent modeling and geophysical methods. Environ. Earth Sci. 75, 15. http://dx.doi.org/10.1007/s12665-015-4856-y.

Kovačič, G., 2010. Hydrogeological study of the Malenščica karst spring (SW Slovenia) by means of a time series analysis. Acta Carsologica 39(2), 201–215.

Kovács, A., 2003. Geometry and hydraulic parameters of karst aquifers: A hydrodynamic modeling approach. PhD Thesis, Université de Neuchâtel, Switzerland.

Kovács, A., Sauter, M., 2007. Modelling karst hydrodynamics. In: Goldscheider N, Drew D (eds.) Methods in karst hydrogeology. International Contribution to Hydrogeology, IAH, vol 26. Taylor and Francis/Balkema, London, 201–222.

Kresic, N., 2007. Hydrogeology and Groundwater Modeling, 2nd edition. CRC Press, New York.

Lababidi, H., Shatela, A., Acra, A., 1987. The progressive salination of ground water in Beirut, Lebanon. Int. J. Environ. Studies 30, 203–208.

Labregère, D., Delhomme, J. P., Priestley, A., 2006. Mitigating salt water advance using horizontal wells: risk based comparison of different approaches. Proc. 1st SWIM-SWICA Joint Saltwater Intrusion Conference, Cagliari-Chia Laguna, Italy, 273-280.

Lafare, A.E.A., Peach, D.W., Hughes, A.G., 2016. Use of seasonal trend decomposition to understand groundwater behaviour in the Permo-Triassic Sandstone aquifer, Eden Valley, UK. Hydrogeol. J. 24, 141–158. http://dx.doi.org/10.1007/s10040-015-1309-3.

Langevin, C.D., 2003. Simulation of submarine ground water discharge to a marine estuary: Biscayne Bay, Florida. Groundwater 41(6), 758–771. http://dx.doi.org/10.1111/j.1745-6584.2003.tb02417.x.

Langevin, C.D., 2008. Modeling axisymmetric flow and transport. Ground Water 46 (4), 579–590. http://dx.doi.org/10.1111/j.1745-6584.2008.00445.x.

Langevin, C.D., Guo, W., 2006. MODFLOW/MT3DMS–Based Simulation of Variable-Density Ground Water Flow and Transport. Groundwater 44(3), 339-351. http://dx.doi.org/10.1111/j.1745-6584.2005.00156.x.

Langevin, C.D., Shoemaker, W.B., Guo, W., 2003. MODFLOW-2000, the U.S. Geological Survey modular ground-water model—Documentation of the SEAWAT-2000 version with the variable-density flow process (VDF) and the integrated MT3DMS Transport Process (IMT): U.S. Geological Survey Open-File Report 03-426.

Langmuir, D., 1997. Aqueous Environmental Geochemistry. Prentice Hall, New Jersey.

Larocque, M., Mangin, A., Razack, M., Banton, O., 1998. Contribution of correlation and spectral analyses to the regional study of a large karst aquifer (Charente, France). J. Hydrol. 205, 217–231. https://doi.org/10.1016/S0022-1694(97)00155-8.

Lebanese Ministry of Environment, 2001. Lebanon State of the Environment Report. Beirut: ECODIT/LEDO.

Lee, J.Y., Song, S.H., 2007. Groundwater chemistry and ionic ratios in a western coastal aquifer of Buan, Korea: implication for seawater intrusion. Geosci. J. 11(3), 259–270. http://dx.doi.org/10.1007/BF02913939.

Lee, J.Y., Lee, K.K., 2000. Use of hydrologic time series data for identification of recharge mechanism in a fractured bedrock aquifer system. J. Hydrol. 229, 190–201. https://doi.org/10.1016/S0022-1694(00)00158-X.

Lin, C.Y., Musta, B., Abdullah, M.H., 2013. Geochemical processes, evidence and thermodynamic behavior of dissolved and precipitated carbonate minerals in a modern seawater/freshwater mixing zone of a small tropical island. Appl. Geochem. 29, 13–31. http://dx.doi.org/10.1016/j.apgeochem.2012.10.029.

Lipson, D.S., McCray, J.E., Thyne, G.D., 2007. Using PHREEQC to Simulate Solute Transport in Fractured Bedrock. Ground Water 45 (4), 468-472. http://dx.doi.org/10.1111/j.1745-6584.2007.00318.x.

Louwyck, A., Vandenbohede, A., Bakker, M., Lebbe, L., 2012. Simulation of axi-symmetric flow towards wells: a finite-difference approach. Comput. Geosci. 44, 136–145. http://dx.doi.org/10.1016/j.cageo.2011.09.004.

Luengo-Oroz, N., Bellomo, S., D'Allessandro, W., 2014. High vanadium concentrations in groundwater at El Hierro (Canary Islands, Spain). 10th International Hydrogeological Congress of Greece, Thessaloniki, 427-435.

Magaritz, M., Luzier, J.E., 1985. Water-rock interactions and seawater-freshwater mixing effects in the coastal dunes aquifer, Coos Bay, Oregon. Geochimica et Cosmochimica Acta 49, 2515-2525.

Maihemuti, B., Ghasemizadeh, R., Yu, X., Padilla, I., Alshawabkeh, A., 2015. Simulation of Regional Karst Aquifer System and Assessment of Groundwater Resources in Manatí-Vega Baja, Puerto Rico. J. Water Resour. Prot. 7, 909-922. http://dx.doi.org/10.4236/jwarp.2015.712075.

Maimone M., Harley B., Fitzgerald R., Moe H., Hossain R., Heywood B, 2004. Coastal Aquifer Planning Elements. In Cheng and Quazar (eds.) Coastal aquifer management: monitoring, modeling, and case studies. CRC Press LLC, USA.

Maliva, R.G., 2014. Economics of managed aquifer recharge. Water 6, 1257–1279. http://dx.doi.org/10.3390/w6051257.

Maloszewski, P., Zuber, A., 1985. On the theory of tracer experiments in fissured rocks with a porous matrix. J. Hydrol. 79, 333–358. http://dx.doi.org/10.1016/0022-1694(85)90064-2.

Maloszewski, P., Stichler, W., Zuber, A., 2004. Interpretation of environmental tracers in groundwater systems with stagnant water zones. Isotopes Environ. Health Stud. 40, 21–33. http://dx.doi.org/10.1080/10256010310001645717.

Mandel, S., Gilboa, Y., Mercado, A., 1972. Groundwater flow in calcareous aquifers in the vicinity of Barcelona, Spain. Bull. Int. Assoc. Hydrol. Sci. 17, 77–83.

Mangin, A., 1994. Karst hydrogeology. In: Groundwater Ecology, Gibert et al. (eds). Academic Press, San Diego, CA, p. 43–67.

Masciopinto, C., 2006. Simulation of coastal groundwater remediation: the case of Nardò fractured aquifer in Southern Italy. Environ. Model. Softw. 21, 85–97. http://dx.doi.org/10.1016/j.envsoft.2004.09.028.

Masciopinto, C., 2013. Management of aquifer recharge in Lebanon by removing seawater intrusion from coastal aquifers. J. Environ. Manag. 130, 306–312. http://dx.doi.org/10.1016/j.jenvman.2013.08.021.

Matthess, G. 1982. The properties of groundwater. John Wiley & Sons, New York.

Mayer, A., May, W., Lukkarila, C., Diehl, J., 2007. Estimation of fault-zone conductance by calibration of a regional groundwater flow model: Desert Hot Springs, California, Hydrogeol. J. 15, 1093. http://dx.doi.org/10.1007/s10040-007-0158-0.

McDonald, M.G., Harbaugh, A.W., 1988. A modular three-dimensional finite-difference ground-water flow model. U.S. Geological Survey Techniques of Water Resources Investigations, book 6, chap A1.

Medema, G.J., Stuyfzand, P.J., 2002. Removal of micro-organisms upon basin recharge, deep well injection and river bank filtration in the Netherlands. In Dillon (ed.), Management of aquifer recharge for sustainability, Proc. 4th Int. symp. on artificial recharge, Adelaide, Australia, Balkema, 125-131.

MED-EUWI, 2007. Mediterranean groundwater report: Technical report on groundwater management in the Mediterranean and the Water Framework Directive. Joint Mediterranean EUWI/WFD Process, EU. http://www.semide.net/initiatives/medeuwi/JP/GroundWater.

Mendizabal, I., Stuyfzand, P.J., 2009. Guidelines for interpreting hydrochemical patterns in data from public supply well fields and their value for natural background groundwater quality determination. J. Hydrol. 379, 151–163. http://dx.doi.org/10.1016/j.jhydrol.2009.10.001.

Mendizabal, I., Stuyfzand, P.J., Wiersma, A.P., 2010. Hydrochemical system analysis of public supply well fields, to reveal water-quality patterns and define groundwater bodies: The Netherlands. Hydrogeol. J. 19(1), 83-100. http://dx.doi.org/10.1007/s10040-010-0614-0.

Meteorological Service, 2010. Meteorological Data Archive, Lebanon Weather, 1985-2010. Unpublished weather reports from Beirut International Airport weather station. General Directorate of Civil Aviation, Beirut, Lebanon.

Missimer, T.M., Ghaffour, N., Dehwah, A.H.A., Rachman, R., Maliva, R.G., Amy, G., 2013. Subsurface intakes for seawater reverse osmosis facilities: Capacity limitation, water quality improvement, and economics. Desalin. 322, 37–51. http://dx.doi.org/10.1016/j.desal.2013.04.021.

MoEW, 2010. National water sector strategy. Ministry of Energy and Water, Beirut, Lebanon.

MoEW, UNDP, 2014. Assessment of groundwater resources of Lebanon. Ministry of Energy and Water (MoEW) and UNDP, Beirut, Lebanon.

MoE/UNDP/ECODIT, 2011. State and Trends of the Lebanese Environment. Ministry of Environment, Beirut, Lebanon.

MoE/UNDP/GEF, 2016. Lebanon's third national communication to the UNFCCC. Beirut, Lebanon.

Mohsen M.S., Al-Jayyousi O.R., 1999. Brackish water desalination: an alternative for water supply enhancement in Jordan. Desalin. 124, 163-174. http://dx.doi.org/10.1016/S0011-9164(99)00101-0.

Mondal, N.C., Singh, V.S., Puranik, S.C., Singh, V.P., 2010. Trace element concentration in groundwater of Pesarlanka Island, Krishna Delta, India. Environ. Monit. Assess. 163, 215–227. http://dx.doi.org/10.1007/s10661-009-0828-6.

Monti, J., Misut, P., Busciolano, R., 2009. Simulation of variable-density ground-water flow and saltwater intrusion beneath Manhasset Neck, Nassau County, New York, 1905-2005. U.S. Geological Scientific Investigations Report 2008-5166.

Mooi, E., Sarstedt, M., 2011. A concise guide to market research: The process, data, and methods using IBM SPSS Statistics. Springer-Verlag Berlin Heidelberg.

Morse, J.W., Mackenzie, F.T., 1990. Geochemistry of Sedimentary Carbonates, Elsevier Science, the Netherlands.

Moskalyk, R.R., Alfanti, A.M., 2003. Processing of vanadium: a review. Miner. Eng. 16, 793–805. http://dx.doi.org/10.1016/S0892-6875(03)00213-9.

Moudjeber, D.E., Mahmoudi, H., Djennad, M., Sioutopoulos, D.C., Mitrouli, S.T., Karabelas, A.J., 2014. Brackish water desalination in the Algerian Sahara—plant design considerations for optimal resource exploitation. Desalin. Water Treat. 1–13 http://dx.doi.org/10.1080/19443994.2013.875947.

Mulligan, A.E., Langevin, C., Post, V.E.A., 2011. Tidal boundary conditions in SEAWAT. Ground Water 49(6), 866-879. http://dx.doi.org/10.1111/j.1745-6584.2010.00788.x.

Nader, F.H., 2000. Petrographic and geochemical characterization of the Jurassic-Cretaceous carbonate sequence of the Nahr Ibrahim region, Lebanon. M.S. Thesis, American University of Beirut, Lebanon.

Nader, F.H., Abdel-Rahman, A.M., Haidar, A.T., 2006. Petrographic and chemical traits of Cenomanian platform carbonates (central Lebanon): implications for depositional environments. Cretaceous Res. 27, 689-706. http://dx.doi.org/10.1016/j.cretres.2006.03.009.

Nederlof, M.M., Hoogendoorn, J.H., 2005. Desalination of brackish groundwater: the concentrate dilemma. Desalin. 182, 441–447. http://dx.doi.org/10.1016/j.desal.2005.03.024.

Neukum, C., Song, J., Köhler, H.J., Hennings, S., Azzam, R., 2015. Groundwater flow modeling in a karst area, Blau Valley, Germany. In: Andreo et al (eds), Hydrogeological and environmental investigations in karst systems, Environ. Earth Sci. 1, Springer-Verlag Berlin Heidelberg, p. 323-329. http://dx.doi.org/10.1007/978-3-642-17435-3_36.

Ning, R.Y., Troyer, T.L., 2009. Tandem reverse osmosis process for zero-liquid discharge. Desalin. 237, 238–242. http://dx.doi.org/10.1016/j.desal.2007.11.060.

Nocchi, M., Salleolini, M., 2013. A 3D density-dependent model for assessment and optimization of water management policy in a coastal carbonate aquifer exploited for water supply and fish farming. J. Hydrol. 492, 200–218. http://dx.doi.org/10.1016/j.jhydrol.2013.03.048.

Obikoya, I.B., Bennell, J.D., 2012. Geophysical investigation of the fresh-saline water interface in the coastal Area of Abergwyngregyn. J. Environ. Prot. 3, 1039-1046. http://dx.doi.org/10.4236/jep.2012.39121.

O'Connor, A.E., Luek, J.L., McIntosh, H, Beck, A.J., 2015. Geochemistry of redox-sensitive trace elements in a shallow subterranean estuary. Marine Chem. 172, 70–81. http://dx.doi.org/10.1016/j.marchem.2015.03.001.

O´Leary, D.W., Friedman, J.D., Pohn, H.A., 1976. Linear, lineation, lineation: some proposed new standards for old terms. Bull. Geol. Soc. Am. 87, 1463-1469.

Ortuño, F., Molinero, J., Garrido, T., Custodio, E., 2012. Seawater injection barrier recharge with advanced reclaimed water at Llobregat delta aquifer (Spain).Water Sci. Technol. 66 (10), 2083–2089. http://dx.doi.org/10.2166/wst.2012.423.

Ouelhazi, H., Lachaal, F., Charef, A., Challouf, B., Chaieb, H., Horriche, F., 2014. Hydrogeological investigation of groundwater artificial recharge by treated wastewater in semi-arid regions: Korba aquifer (Cap-Bon Tunisia). Arab. J. Geosci. 7, 4407–4421. http://dx.doi.org/10.1007/s12517-013-1090-3.

Padilla, A., Pulido-Bosch, A., 1995. Study of hydrographs of karstic aquifers by means of correlation and cross-spectral analysis. J. Hydrol. 168, 73–89. https://doi.org/10.1016/0022-1694(94)02648-U.

Padilla, A., Pulido-Bosch, A., Mangin, A., 1994. Relative importance of baseflow and quickflow from hydrographs of karst spring. Groundwater 32(2), 267–277. http://dx.doi.org/10.1111/j.1745-6584.1994.tb00641.x.

Panagopoulos, G., 2012. Application of MODFLOW for simulating groundwater flow in the Trifilia karst aquifer, Greece. Environ. Earth Sci. 67, 1877–1. http://dx.doi.org/10.1007/s12665-012-1630-2.

Panagopoulos, G., Lambrakis, N., 2006. The contribution of time series analysis to the study of the hydrodynamic characteristics of the karst systems: Application on two typical karst aquifers of Greece (Trifilia, Almyros Crete). J. Hydrol. 329, 368– 376. http://dx.doi.org/10.1016/j.jhydrol.2006.02.023.

Papadopoulou, MP, Karatzas, GP, Koukadaki, MA, Trichakis, Y, 2005. Modeling the saltwater intrusion phenomenon in coastal aquifers - a case study in the industrial zone of Herakleio in Crete. Global NEST J 7(2), 197–203.

Papadopoulou, M.P., Varouchakis, E.A., Karatzas, G.P., 2010. Terrain discontinuity effects in the regional flow of a complex karstified aquifer. Environ. Modeling Assess. 15 (5), 319–328. http://dx.doi.org/10.1007/s10666-009-9207-5.

Pardo-Igúzquiza, E., Durán, J.J., Robledo-Ardilaet, P.A., 2015. A Three-Dimensional Karst Aquifer Model: The Sierra de Las Nieves Case (Málaga, Spain). In: Andreo et al. (eds.), Hydrogeological and Environmental Investigations in Karst Systems, Environ. Earth Sci. 1, Springer-Verlag Berlin Heidelberg, p. 271-276. http://dx.doi.org/10.1007/978-3-642-17435-3_30.

Parkhurst, D.L., Appelo, C.A.J., 1999. User's Guide to PHREEQC (Version 2), A Computer Program for Speciation, Batch-reaction, One-dimensional Transport, and Inverse Geochemical Calculations: U.S. Geological Survey Water-Resources Investigations Report 99-4259.

Parkhurst, D.L., Appelo, C.A.J., 2013. Description of input and examples for PHREEQC Version 3—a computer program for speciation, batch-reaction, one-dimensional transport, and inverse geochemical calculations. U.S. Geological Survey Techniques and methods, book 6, chap. A43. http://www.hydrochemistry.eu/ph3/manual3.pdf.

Payal, Z., 2014. Innovative method for saltwater intrusion control. Int. J. Eng. Sci. Res. Tech. 3 (2), 892–896.

Perelman, A.I., 1972. Geochemie epigenetischer prozesse (die hypergene Zone). Akademie Verlag, Berlin.

Pérez-González, A., Urtiaga, A.M., Ibáñez, R., Ortiz, I., 2012. State of the art and review on the treatment technologies of water reverse osmosis concentrates. Water Res. 46, 267–283. http://dx.doi.org/10.1016/j.watres.2011.10.046.

Petelet-Giraud, E., Négrel, P., Gourcy, L., Schmidt, C., Schirmer, M., 2007. Geochemical and isotopic constraints on groundwater-surface water interactions in a highly anthropized site. The Wolfen/Bitterfeld megasite (Mulde subcatchment, Germany). Environ. Pollut. 148, 707–717.

Pichler, T., Mozaffari, A., 2015. Occurrence, distribution and mobility of geogenic molybdenum and arsenic in a limestone aquifer matrix. Appl. Geochem. 63, 623-633, http://dx.doi.org/10.1016/j.apgeochem.2015.08.006.

Plummer, L.N., Back, W.W., 1980. The mass balance approach—Application to interpreting the chemical evolution of hydrologic systems. Am. J. Sci. 280, 130–142.

Plummer, L.N., Prestemon, E.C., Parkhurst, D.L., 1994. An interactive code (NETPATH) for modeling NET geochemical reactions along a flow PATH, Version 2.0: U.S. Geological Survey Water-Resources Investigations Report 94-4169.

Polemio, M., Romanazzi, A., 2014. Hydrogeological modeling for sustainable groundwater management under climate change effects for a karstic coastal aquifer (Southern Italy). Proc. 23rd Salt Water Intrusion Meeting, Husum, Germany.

Pool, M., Carrera, J., 2010. Dynamics of negative hydraulic barriers to prevent seawater intrusion. Hydrogeology Journal 18: 95–105.

Porter, D.E., Michener, W.K., Siewicki, T., Edwards, D., Corbett, C., 1996. Geographic Information Processing Assessment of the Impacts of Urbanization. In Vernberg et al. (eds.), Sustainable Development in the Southeastern Coastal Zone, Univ. South Carolina Press.

Post, V.E.A., 2002. 'Chemistry for modellers' aqueous geochemistry in coastal areas. Proc. 17th Salt Water Intrusion Meeting, Deflt, The Netherlands, 3-12.

Post, V.E.A., 2005. Fresh and saline groundwater interaction in coastal aquifers: is our technology ready for the problems ahead? Hydrogeol. J. 13, 120–123.

Price, R.M., Herman, J.S., 1991. Geochemical investigation of salt-water intrusion into a coastal carbonate aquifer: Mallorca, Spain. Geol. Soc. Am. Bull. 103, 1270-1279.

Prinos, S.T., Wacker, M.A., Cunningham, K.J., Fitterman, D.V., 2014. Origins and delineation of saltwater intrusion in the Biscayne aquifer and changes in the distribution of saltwater in Miami-Dade County, Florida. U.S. Geological Survey. Scientific Investigations Report 2014–5025.

Prinz, D., 2016. Managed Aquifer Recharge in the Hazmieh area to prevent seawater intrusion in Beirut – Lebanon. Deutsche Gesellschaft für Internationale Zusammenarbeit (GIZ) GmbH, Bonn, Germany.

Prommer, H., Barry, D.A., Zheng, C., 2003. MODFLOW/MT3DMS based reactive multi-component transport modelling. Ground Water 41(2), 247- 257.

Pulido-Leboeuf, P., 2004. Seawater intrusion and associated processes in a small coastal complex aquifer (Castell de Ferro, Spain). Appl. Geochem. 19, 1517-1527. http://dx.doi.org/10.1016/j.apgeochem.2004.02.004.

Quinn, J.J., Tomasko, D., Kuiper, J.A., 2006. Modeling complex flow in a karst aquifer. Sediment. Geol. 184 (3–4), 343–351. http://dx.doi.org/10.1016/j.sedgeo.2005.11.009.

Rahardianto, A., McCool, B.C., Cohen, Y., 2010. Accelerated desupersaturation of reverse osmosis concentrate by chemically-enhanced seeded precipitation. Desalin. 264 (3), 256–267. http://dx.doi.org/10.1016/j.desal.2010.06.018.

Rastogi, A, Choi, GW, Ukarande, SK, 2004. Diffused interface model to prevent ingress of seawater in multi-layer coastal aquifers. J. Special Hydrol. 4, 1–31.

Reichard, E.G., Johnson, T.A., 2005. Assessment of regional management strategies for controlling seawater intrusion. J. Water Resour. Plann. Manage. 131(4), 280-291.

Reimann, T., Giese, M., Geyer, T., Liedl, R., Maréchal, J-C., Shoemaker, W.B., 2014. Representation of water abstraction from a karst conduit with numerical discrete continuum models. Hydrol. Earth System Sci. 18, 227-241. http://dx.doi.org/10.5194/hess-18-227-2014.

Rezaei, M., Sanz, E., Raeisi, E., Ayora, C., Vázquez-Suñé, E., Carrera, J., 2005. Reactive transport modeling of calcite dissolution in the fresh-salt water mixing zone. J. Hydrol. 311, 282–298. http://dx.doi.org/10.1016/j.jhydrol.2004.12.017.

Romanazzi, A., Gentile, F., Polemio, M., 2015. Modelling and management of a Mediterranean karstic coastal aquifer under the effects of seawater intrusion and climate change. Environ. Earth Sci. 74, 115–128. http://dx.doi.org/10.1007/s12665-015-4423-6.

Ru Y, Jinno K, Hosokawa T, Nakagawa K, 2001. Study on effect of subsurface dam in coastal seawater intrusion. In 1st Int. conf. saltwater intrusion and coastal aquifers, monitoring, modelling, and management, Essaouira, Morocco.

Russo, S.L., Amanzio, G., Ghione, R., De Maio, M., 2015. Recession hydrographs and time series analysis of springs monitoring data: application on porous and shallow aquifers in mountain areas (Aosta Valley). Environ. Earth Sci. 73, 7415–7434. http://dx.doi.org/10.1007/s12665-014-3916-z.

Saad, Z., Kazpard, V., Geyh, M., Slim, K., 2004. Chemical and isotopic composition of water from springs and wells in the Damour River Basin and the Coastal Plain in Lebanon. J. Environ. Hydrol. 12, 1–13.

Saad, Z., Kazpard, V., El Samrani, A., Slim, K., 2005. Chemical and isotopic composition of rainwater in coastal and highland regions in Lebanon. J. Environ. Hydrol. 13, 1–11.

Saadeh, M., 2008. Influence of overexploitation and seawater intrusion on the quality of groundwater in Greater Beirut. PhD Thesis, Aachen University, Germany.

Sacks, L.A., Tihansky, A.B., 1996. Geochemical and Isotopic Composition of Ground Water, with Emphasis on Sources of Sulfate, in the Upper Floridan Aquifer and Intermediate Aquifer System in Southwest Florida. U.S. Geological Survey, Water-Resources Investigations Report 96-4146.

Saller, S.P., Ronayne, M.J., Long, A.J., 2013. Comparison of a karst groundwater model with and without discrete conduit flow. Hydrogeol. J. 21, 1555–1566. http://dx.doi.org/10.1007/s10040-013-1036-6.

Sana, A., Baawain, M., Al-Sabti, A., 2013. Feasibility Study of Using Treated Wastewater to Mitigate Seawater Intrusion along Northern Coast of Oman. Int. J. of Water Resour. Arid Environ. 2(2), 56-63.

Sanford, W.E., Konikow, L.F., 1989. Porosity development in coastal carbonate aquifers. Geol. 17, 249-252.

Sanford, W.E., Pope, J.P., 2010. Current challenges using models to forecast seawater intrusion: lessons from the Eastern Shore of Virginia, USA. Hydrogeol. J. 18, 73–93. http://dx.doi.org/10.1007/s10040-009-0513-4.

Scanlon, B.R., Mace, R.E., Barrett, M.E., Smith, B., 2003. Can we simulate regional groundwater flow in a karst aquifer using equivalent porous media models? Case study, Barton Springs Edwards aquifer, USA. J. Hydrol. 276, 137-158. https://doi.org/10.1016/S0022-1694(03)00064-7.

Schepper, G., 2010. Evaluation de la Faisabilite d'un Projet de Recharge Artificielle. MS Thesis. Centre d'Hydrogéologie, Université de Neuchâtel, Neuchâtel, Switzerland.

Scholze, O., Hillmer, G., Schneider, W., 2002. Protection of the groundwater resources of Metropolis CEBU (Philippines) in consideration of saltwater intrusion into the coastal aquifer. In: 17th Salt water intrusion meeting, Delft, the Netherlands.

Schulz, S., de Rooij, G. H., Michelsen, N., Rausch, R., Siebert, C., Schüth, C., Al-Saud, M., and Merz, R., 2016. Estimating groundwater recharge for an arid karst system using a combined approach of time-lapse camera monitoring and water balance modelling. Hydrol. Process. 30, 771-782. http://dx.doi.org/10.1002/hyp.10647.

Schulze-Makuch, D., 2005. Longitudinal Dispersivity Data and Implications for Scaling Behavior. Ground Water 43 (3), 443-456. http://dx.doi.org/10.1111/j.1745-6584.2005.0051.x.

Schwarz, G.E., 1978. Estimating the dimension of a model. Ann. Statist. 6 (2), 461-464.

Schwartz, F., Zhang, H., 2003. Fundamentals of Ground Water, John Wiley & Sons, USA.

Sebben, M.L., Werner, A.D., Graf, T., 2015. Seawater intrusion in fractured coastal aquifers: a preliminary numerical investigation using a fractured Henry problem. Adv. Water Resour. 85, 93-108. http://dx.doi.org/10.1016/j.advwatres.2015.09.013.

Shand, P, Edmunds, W.M., 2008. The baseline inorganic chemistry of European groundwaters, In Edmunds and Shand (eds.), Natural groundwater quality. Blackwell Publishing Ltd, 22–58.

Sherif, M., Hamza, K., 2001. Mitigation of seawater intrusion by pumping brackish water. J Trans. Porous Media 43, 29–44.

Sherif, M., Kacimov, A., 2008. Pumping of brackish and saline water in coastal aquifers: an effective tool for alleviation of seawater intrusion. Proc. 20th Salt Water Intrusion Meeting, Naples, Florida, USA.

Sherif, M., Kacimov, A., Javadi, A., Ebraheem, A., 2012. Modeling groundwater flow and seawater intrusion in the coastal aquifer of Wadi Ham, UAE. Water Resour. Manag. 26, 751–774. http://dx.doi.org/10.1007/s11269-011-9943-6.

Sherif, M., Almulla, M., Shetty, A., 2013. Seawater Intrusion Assessment and Mitigation in the Coastal Aquifer of Wadi Ham. In Wetzelhuetter (ed.), Groundwater in the Coastal Zones of Asia-Pacific, Coastal Research Library, 271-294.

Shi, J., Ma, R., Liu, J., Zhang, Y., 2013. Suitability assessment of deep groundwater for drinking, irrigation and industrial purposes in Jiaozuo City, Henan Province, north China. Chin. Sci. Bull. 58(25), 3098-3110. http://dx.doi.org/10.1007/s11434-013-5952-6.

Shoemaker, W.B., Edwards, K.M., 2003. Potential for Saltwater Intrusion into the Lower Tamiami Aquifer near Bonita Springs, Southwestern Florida. U.S. Geological Survey Water-Resources Investigations Report 03-4262.

Shoemaker, W.B., Kuniansky, E.L., Birk, S., Bauer, S., Swain, E.D., 2008. Documentation of a conduit flow process (CFP) for MODFLOW-2005. U.S. Geological Survey Techniques and Methods 6-A24.

Simmons, C.T., Bauer-Gottwein, P., Graf, T., Kinzelbach, W., Kooi, H., Li, L., 2010. Variable density groundwater flow: from modelling to applications. In Wheater et al. (eds.), Groundwater Modelling in Arid and Semi-Arid Areas, International Hydrology Series. London: Cambridge University Press.

Slama, F., 2010. Field Experimentation and Modelling of Salts Transfer in Korba Coastal Plain: Impact of Seawater Intrusion and Irrigation Practices. PhD Thesis. University of Neuchatel, Centre of Hydrogeology.

Smedley, P.L., Edmunds, W.M., 2002. Redox patterns and trace-element behavior in the East Midlands Triassic Sandstone Aquifer, UK. Ground Water 40, 44–58.

Smedley, P.L., Cooper, D.M., Ander, E.L., Milne, C.J., Lapworth, D.J., 2014. Occurrence of molybdenum in British surface water and groundwater: Distributions, controls and implications for water supply. Appl. Geochem. 40, 144–154. http://dx.doi.org/10.1016/j.apgeochem.2013.03.014.

Sola, F., Vallejos, A., Moreno, L., López, Geta, J.A., Pulido Bosch, A., 2013. Identification of hydrogeochemical process linked to marine intrusion induced by pumping of a semiconfined Mediterranean coastal aquifer. Int. J. Environ. Sci. Technol. 10, 63–76. http://dx.doi.org/10.1007/s13762-012-0087-x.

Sophiya, M.S., Syed, T.H., 2013. Assessment of vulnerability to seawater intrusion and potential remediation measures for coastal aquifers: a case study from eastern India. Environ. Earth Sci. 70, 1197–1209. http://dx.doi.org/10.1007/s12665-012-2206-x.

Soupios, P., Kourgialas, N., Dokou, Z., Karatzas, G., Panagopoulos, G., Vafidis, A., Manoutsoglou, E., 2015. Modeling saltwater intrusion at an agricultural coastal area using geophysical methods and the FEFLOW model. In: Lollino et al. (eds), Engineering Geology for Society and Territory – Volume 3, Springer International Publishing Switzerland, p. 249-252.

Spiessl, S.M., Prommer, H., Licha, T., Sauter, M., Zheng, C., 2007. A process-based reactive hybrid transport model for coupled discrete conduit–continuum systems. J. Hydrol. 347, 23-34. http://dx.doi.org/10.1016/j.jhydrol.2007.08.026.

Sprenger, C., Hartog, N., Hernández, M., Vilanova, E., Grützmacher, G., Scheibler, F., Hannappel, S., 2017. Inventory of managed aquifer recharge sites in Europe: historical development, current situation and perspectives. Hydrogeol J (In press). http://dx.doi.org/10.1007/s10040-017-1554-8.

Steiakakis, E., Vavadakis, D., Kritsotakis, M., Voudouris, K., Anagnostopoulou, C., 2016. Drought impacts on the fresh water potential of a karst aquifer in Crete, Greece. Environ. Earth Sci. 75, 507. http://dx.doi.org/10.1007/s12665-016-5509-5.

Stein, S., Russak, A., Sivan, O., Yechieli, Y., Rahav, E., Oren, Y., Kasher, R., 2016. Saline groundwater from coastal aquifers as a source for desalination. Environ. Sci. Technol. 50 (4), 1955–1963. http://dx.doi.org/10.1021/acs.est.5b03634.

Stewart M.T., 1999. Geophysical investigations. In Bear et al. (eds.) Seawater intrusion in coastal aquifers: concepts, methods and practices. Kluwer Academic Publishers, the Netherlands.

Stigter, T.Y., van Ooijen, S.P., Post, V.E., Appelo, C.A., Carvalho Dill, A.M., 1998. A hydrogeological and hydrochemical explanation of the groundwater composition under irrigated land in a Mediterranean environment, Algarve, Portugal. Journal of Hydrology, 208, 262–279. http://dx.doi.org/10.1016/S0022-1694(98)00168-1.

Stuyfzand, P.J., 1986. A new hydrochemical classification of water types: principles and application to the coastal dunes aquifers system of the Netherlands. Proc. 9th Salt Water Intrusion Meeting. Delft: Delft University of Technology, 641–655.

Stuyfzand, P.J., 1987. Influences of filtration and storage of groundwater samples on sample composition. Trends Anal. Chem. (TrAC) 6, 50–54.

Stuyfzand P.J, 1989a. Hydrology and water quality aspects of Rhine bank groundwater in the Netherlands. J. Hydrol. 106, 341-363.

Stuyfzand P.J, 1989b. Quality changes of river Rhine and Meuse water upon basin recharge in the Netherlands' coastal dunes: 30 years of experience. In Johnson and Finlayson (eds.), Artificial recharge of Groundwater. Proc. Int. Symp. Anaheim USA, Am. Soc. Civil Eng., New York, 233-245.

Stuyfzand, P.J., 1989c. A new hydrochemical classification of water types. In Ragone (ed.), Regional characterization of water quality, Proceedings of Baltimore Symposium. Wallingford: International Association of Hydrological Sciences: IAHS Publ. 182, 89–98.

Stuyfzand, P.J. 1993a. Hydrochemistry and hydrology of the coastal dune area of the Western Netherlands. Ph.D Thesis Vrije Univ. Amsterdam, published by KIWA, The Netherlands.

Stuyfzand, P.J. 1993b. Behaviour of major and trace constituents in fresh and salt intrusion waters, in the Western Netherlands. In Custodio and Galofré (eds.), Study and modelling of saltwater intrusion into aquifers. Proc. 12th Salt Water Intrusion Meeting, Barcelona, Spain, 143-160.

Stuyfzand, P.J., 1998. Simple models for reactive transport of pollutants and main constituents during artificial recharge and bank filtration. In Peters et al. (eds.), Artificial recharge of groundwater, Proc. 3rd Int. symp. on artificial recharge, Amsterdam, the Netherlands, Balkema, 427-434.

Stuyfzand, P.J., 1999. Patterns in groundwater chemistry resulting from groundwater flow. Hydrogeol. J. 7, 15–27. http://dx.doi.org/10.1007/s100400050177.

Stuyfzand P.J., 2002. Quantifying the environmental impact and sustainability of artificial recharge systems. In Dillon (ed.), Management of aquifer recharge for sustainability, Proc. 4th Int. symp. on artificial recharge, Adelaide, Australia, Balkema, 77-82.

Stuyfzand, P.J., 2005. Mapping groundwater bodies with artificial or induced recharge, by determination of their origin and chemical facies. Proc. 5th Int. symp. on management of aquifer recharge. Berlin, 839–850.

Stuyfzand, P.J., 2008. Base exchange indices as indicators of salinization or freshening of (Coastal). Proc. 20th Salt Water Intrusion Meeting, Naples, Florida, USA, 262–265.

Stuyfzand, P.J, 2011. Hydrogeochemical processes during riverbank filtration and artificial recharge of polluted surface waters: Zonation, identification, and quantification. In Chittaranjan and Shamrukh (eds.), Riverbank Filtration for Water Security in Desert Countries. Series: NATO Science for Peace and Security Series C: Environmental Security. 1st Edition, Springer, 97-128.

Stuyfzand, P.J., 2012. Hydrogeochemcal (HGC 2.1), for storage, management, control, correction and interpretation of water quality data in Excel® spread sheet. Nieuwegein: KWR report BTO 2012. 244(s).

Stuyfzand, P.J, 2015a. Trace element patterns in Dutch coastal dunes after 50 years of artificial recharge with Rhine River water. Environ. Earth Sci. 73, 7833–7849. http://dx.doi.org/10.1007/s12665-014-3770-z.

Stuyfzand, P.J, 2015b. Hydrogeochemcal (HGC 2.2), for storage, management, control, correction and interpretation of water quality data in Excel® spread sheet. Nieuwegein: KWR report BTO 2012. 244(s).

Stuyfzand, P.J., Timmer, H., 1999. Deep well injection at the Langerak and Nieuwegein sites in the Netherlands: chemical reactions and their modeling. Kiwa-report SWE 99.006, 44p.

Stuyfzand P.J, Kappelhof, J., 2005. Floating, high-capacity desalting islands on renewable multi-energy supply. Desalin. 77: 259-266.

Stuyfzand, P.J., Stuurman, R.J., 2006. Origin, distribution and chemical mass balances of non-anthropogenic, brackish and (hyper)saline groundwaters in the Netherlands. Proc. 1st SWIM-SWICA joint saltwater intrusion conference. Cagliari, Italy, 151–164.

Stuyfzand, PJ, Mendizabal, I., 2010. Trace element concentrations of groundwater from public supply well fields, and their relation with marine sedimentary environments of the aquifer and postdepositional salinity changes. Proc. 21st Salt Water Intrusion Meeting, Azores, Portugal.

Stuyfzand, P.J., Raat, K.J., 2010. Benefits and hurdles of using brackish groundwater as a drinking water source in the Netherlands. Hydrogeol. J. 18, 117–130. http://dx.doi.org/10.1007/s10040-009-0527-y.

Stuyfzand P.J, Maas K., Kappelhof J., Kooiman J., 2004. Pumping brackish groundwater to prepare drinking water and keep salinized wells fresh. 18th Salt Water Intrusion Meeting, Cartagena, Spain.

Stuyfzand, P.J., Juhàsz-Holterman, M.H.A., de Lange W.J., 2006. Riverbank filtration in the Netherlands: well fields, clogging and geochemical reactions. In Stephen A. Hubbs (ed.), Riverbank Filtration Hydrology, Proc. NATO Advanced Research Workshop on Riverbank Filtration Hydrology, Bratislava, Springer NATO Science Series IV, Earth and Envir Sciences 60, 119-153.

Stuyfzand, P.J., Smidt, E., Zuurbier, K.G., Hartog, N., Dawoud, M.A., 2017. Observations and Prediction of Recovered Quality of Desalinated Seawater in the Strategic ASR Project in Liwa, Abu Dhabi. Water 9, 177. http://dx.doi.org/10.3390/w9030177.

Sugio, S., Nakada, K., Urish, D., 1987. Subsurface seawater intrusion barrier analysis. J. Hydraul. Eng. 113 (6), 767–779.

Sun, D., Semprich, S., 2013. Using Compressed Air Injection to Control Seawater Intrusion in a Confined Coastal Aquifer. Transp Porous Med 100:259–278.

Sun, H., Alexander, J., Gove, B., Koch, 2015. Mobilization of arsenic, lead, and mercury under conditions of sea water intrusion and road deicing salt application. J. Contam. Hydrol. 180, 12-24. http://dx.doi.org/10.1016/j.jconhyd.2015.07.002.

Teutsch, G., 1993. An extended double-porosity concept as a practical modeling approach for a karstified terrain. Hydrogeological Processes in Karst Terranes (Proceedings of the Antalya Symposium and Field Seminar, October 1990), IAHS, Wallingford, UK, p. 281–292.

Therrien, R., McLaren, R.G., Sudicky, E.A., Panday, S.M., 2010. HydroGeoSphere A three-dimensional numerical model describing fully integrated subsurface and surface flow and solute transport. Groundwater Simulations Group, Univ. of Waterloo, Waterloo, Canada.

Todd, D. K., 1953. Sea-water intrusion in coastal aquifers. Eos Trans. 34(5), 749–754. http://dx.doi.org/10.1029/TR034i005p00749.

Topal, T., Kaya, Y., 2016. Assessment of deterioration and collapse mechanisms of dolomitic limestone at Hasankeyf Antique City before and after reservoir impounding (Turkey). Environ. Earth Sci. 75:131. http://dx.doi.org/10.1007/s12665-015-5062-7.

Tribovillard, N., A. Riboulleau, T. Lyons, Baudin, F., 2004. Enhanced trapping of molybdenum by sulfurized marine organic matter of marine origin in Mesozoic limestones and shales, Chem. Geol. 213(4), 385-401.

Triki, Z., Bouaziz, M.N., Boumaza, M., 2014. Techno-economic feasibility of wind-powered reverse osmosis brackish water desalination systems in southern Algeria. Desalination and Water Treatment 52: 1745–1760.

Troeger, U., 2010. Managing the Thermal Aquifer System of Caldas Novas – Brazil. Proc. 7th Int. symp. on management of aquifer recharge. Abu Dhabi, 591–596.

Tulipano, L., Cotecchia, V., Fidelibus, M.D., 1990. An example of multitracing approach in the studies of karstic and coastal aquifers. In Gunay et al. (eds.), Hydrogeological processes in Karst Terranes. Antalya symposium 1990. Wallingford: International Association of Hydrological Sciences, IAHS Publ. 207, 381–389.

Tulipano, L., Fidelibus M.D., Panagopoulos A., 2005. Groundwater management of coastal karstic aquifers. Luxemburg: COST Action 621, Final Report, EUR 21366, COST Office, 363.

Turek, M., Was, J., Dydo, P., 2009. Brackish water desalination in RO–single pass EDR system. Desalin. Water Treat. 7, 263-266. http://dx.doi.org/10.5004/dwt.2009.710.

US EPA, 2008. EPA's Report on the Environment (ROE). U.S. Environmental Protection Agency, Washington, D.C., EPA/600/R-07/045F. Available online at http://www.epa.gov/roe.

Vandenbohede, A., Wallis, I., Van Houtte, E., Van Ranst, E., 2013. Hydrogeochemical transport modeling of the infiltration of tertiary treated wastewater in a dune area, Belgium. Hydrogeol. J. 21, 1307–1321.

Vanderzalm, J., Page, D., Dillon P., Lawson, J., Grey, N., Sexton, D. and Williamson, D. 2014. A risk-based management plan for Mount Gambier stormwater recharge system: stormwater recharge to the Gambier Limestone aquifer. Goyder Institute for Water Research Technical Report 14/7, Adelaide, South Australia.

Van Genuchten, M.T., 1985. A general approach for modeling solute transport in structured soils. Memoirs Int. Ass. Hydrogeol. 17(2), 513-526.

Volker, R.E., Rushton, K.R., 1982. An assessment of the importance of some parameters for seawater intrusion in aquifers and a comparison of dispersive and sharp-interface modelling approaches. J. Hydrol. 56(3-4), 239-250. http://dx.doi.org//10.1016/0022-1694(82)90015-4.

Wallis, I., Prommer, H., Post, V., Vandenbohede, A., Simmons, C.T., 2013. Simulating MODFLOW-based reactive transport under radially symmetric flow conditions. Groundwater 51 (3), 398–413. http://dx.doi.org/10.1111/j.1745-6584.2012.00978.x.

Walsh, V., Price, R., 2010. Determination of vertical and horizontal pathways of injected fresh wastewater into a deep saline aquifer (Florida, USA) using natural chemical tracers. Hydrogeol. J. 18, 1027-1042.

Wang, X., Jardani, A., Jourde, H., Lonergan, L., Cosgrove, J., Gosselin, O., Massonnat, G., 2016. Characterisation of the transmissivity field of a fractured and karstic aquifer, Southern France. Adv. Water Resour. 87, 106-121. http://dx.doi.org/10.1016/j.advwatres.2015.10.014.

Weinstein, Y., Less, G., Kafri, U., Herut, B., 2007. Submarine groundwater discharge in the southeastern Mediterranean (Israel). Radioact. Environ. 8, 360–372. http://dx.doi.org/10.1016/S1569-4860(05)08029-0.

Whitaker, F.F., Smart, P.L., 1993. Dolomitization by saline ground waters within the north-western great Bahama Bank: an overview. Proc. 6th symposium on the geology of the Bahamas, 165-179.

WHO, 2001. Beryllium and beryllium compounds. Concise International Chemical Assessment Document 32. WHO, Geneva.

WHO, 2008. Guidelines for drinking-water quality: incorporating 1st and 2nd addenda, Vol.1, Recommendations, 3rd edition. WHO, Geneva.

Wicks, C., Herman, J, 1995. The Effect of Zones of High Porosity and Permeability on the Configuration of the Saline-Freshwater Mixing Zone. Ground Water 33(5), 733-740. http://dx.doi.org/10.1111/j.1745-6584.1995.tb00019.x.

Wolthek, N., Raat, K., de Ruijter, J.A., Kemperman, A., Oosterhof, A., 2013. Desalination of brackish groundwater and concentrate disposal by deep well injection. Desalin. Water Treat. 51, 1131–1136. http://dx.doi.org/10.1080/19443994.2012.694205.

World Bank, 2011. Adaptation to a Changing Climate in the Arab Countries. MNA Flagship Report, Report N° 64635, Washington, DC.

Wright, M.T., Belitz, K., 2010. Factors controlling the regional distribution of vanadium in groundwater. Ground Water 48 (4), 515–525. http://dx.doi.org/10.1111/j.1745-6584.2009.00666.x.

Xanke, J., Goeppert, N., Sawarieh, A., Liesch, T., Kinger, J., Ali, W., Hötzl, H., Hadidi, K., Goldscheider, N., 2015. Impact of managed aquifer recharge on the chemical and isotopic composition of a karst aquifer, Wala reservoir, Jordan. Hydrogeol. J. 23: 1027–1040. http://dx.doi.org/10.1007/s10040-015-1233-6.

Xanke, J., Jourde, H., Liesch, T., Goldscheider, N., 2016. Numerical long-term assessment of managed aquifer recharge from a reservoir into a karst aquifer in Jordan. J. Hydrol. 540: 603–614. http://dx.doi.org/10.1016/j.jhydrol.2016.06.058.

Xu, Z., 2016. Data analysis and numerical modeling of seawater intrusion through conduit network in a coastal karst aquifer. PhD Thesis, Florida State University, USA.

Yan, Z., Chen, C., Fan, P., Wang, M., Fang, X., 2015. Pore structure characterization of ten typical rocks in China. Electron. J. Geotech. Eng. 20, 479-494.

Yassine Hajj Chehadeh, A.H.M., 2015. Tectonic evolution and seismic hazard analysis of the Damour-Beit Ed Dine Fault System. MSc Thesis, American University of Beirut, Lebanon.

Yuce, G., 2007. A Geochemical study of the groundwater in the Misli basin and environmental implications. Environ. Geol. 51, 857–868. http://dx.doi.org/10.1007/s00254-006-0460-5.

Zghibi, A., Merzougui, A., Zouhri, L., Tarhouni, J., 2014. Understanding groundwater chemistry using multivariate statistics techniques to the study of contamination in the Korba unconfined aquifer system of Cap-Bon (North-east of Tunisia). J. Afr. Earth Sci. 89, 1-15. http://dx.doi.org/10.1016/j.jafrearsci.2013.09.004.

Zhao, J., Lin, J., Wu, J., Yang, Y., Wu, J., 2016. Numerical modeling of seawater intrusion in Zhoushuizi district of Dalian City in northern China. Environ. Earth Sci. 75, 805. http://dx.doi.org/10.1007/s12665-016-5606-5.

Zheng, C., Wang, P., 1999. MT3Dms−A modular three-dimensional multispecies transport model for simulation of advection, dispersion and chemical reactions of contaminants in ground-water systems. University of Alabama, Tuscaloosa.

Zheng, C., Bennett, G.D., 2002. Applied contaminant transport modeling, 2nd edition, Wiley-Interscience, New York.

Curriculum Vitae

Wisam M. Khadra was born in 1978 in Saida, Lebanon. He finished his Lebanese Baccalaureate II - Mathematics in 1995 at the National Evangelical Institute for Girls and Boys, then entered the American University of Beirut (AUB) to study natural sciences at the Department of Geology. He obtained a B.Sc. in Geology in 1998 and a M.Sc. in Geology (subspecialty in Hydrogeology) in 2003. In October 2003, he was hired as an instructor of Geology at AUB where he has taught undergraduate geology courses to more than 2,600 students. His areas of teaching cover: environmental physical geography, natural disasters, structural geology, physical geology and hydrogeology. In 2011, he started his Ph.D. program at VU University Amsterdam (the Netherlands), but transferred in October 2015 to Delft University of Technology (Technische Universiteit Delft; TU Delft) to complete his work and obtain a Ph.D. at the Faculty of Civil Engineering and Geosciences (section of Geo-environmental Engineering at the Department of Geoscience and Engineering,). During the last years, he had several contributions to hydrological theory and methodology, and served as a reviewer for different international journals. Besides his academic involvement, W. Khadra works as a private consultant in hydrogeology for the Lebanese private and public sectors.

List of Publications

I. Peer Reviewed papers

- Khadra, W.M., Stuyfzand, P.J. Simulation of saltwater intrusion in a poorly karstified coastal aquifer in Lebanon (Eastern Mediterranean). *Hydrogeology Journal* (Under review).
- Khadra, W.M., Stuyfzand, P.J., van Breukelen, B.M., 2017. Hydrochemical effects of saltwater intrusion in a limestone and dolomitic limestone aquifer in Lebanon. *Applied Geochemistry* 79, 36-51.
- Khadra, W.M., Stuyfzand, P.J., Khadra, I.M., 2017. Mitigation of saltwater intrusion by 'integrated fresh-keeper' wells combined with high recovery reverse osmosis. *Science of the Total Environment* 574, 796-805.
- Khadra, W.M., Stuyfzand, P.J., 2014. Separating baseline conditions from anthropogenic Impacts: example of the Damour coastal aquifer (Lebanon). *Hydrological Sciences Journal* 59, 1872-1893.

II. Lightly Reviewed papers

- Khadra, W.M., Stuyfzand, P.J., 2016. Mass balancing to define major hydrogeochemical processes in salinizing dolomitic limestone aquifers: Example from Eastern Mediterranean (Lebanon). In Werner A.D. (ed.), *Proceedings of the 24th Salt Water Intrusion Meeting and the 4th Asia-Pacific Coastal Aquifer Management Meeting*, 4-8 July, 2016, Cairns, Australia, pp. 110-116.

- Amin, I.E., Khadra, W.M., 2003. Seawater Intrusion in Central Lebanon: A Case Study of the Damour Aquifer. In J.A. López-Geta et al. (eds.), Coastal Aquifers Intrusion Technology: Mediterranean Countries, Volume II. Instituto Geológico Minero Y Minero de España (IGME), Madrid, Spain, pp. 289 – 294.

III. Abstracts in International Conferences

- Korfali, S.I, Al-Hakawati, N., Khadra, W.M., 2014. Evaluation of metals and their potential hazard in the Awali River surface sediments. *30th SEGH (Society of Environmental Geochemistry and Health) International Conference*, 30June-4July, Newcastle, UK.

- Amin, I.E., Khayat, Z.A., Khadra, W.M., Hamzeh, M.M., 2008. Major problems affecting the principal aquifers in Lebanon. Annual Meeting and Exposition of the Geological Society of America, Soil Science Society of America, American Society of Agronomy, Crop Science Society of America, Gulf Coast Association of Geological Societies with the Gulf Coast Section of SEPM, 5-9 October, Houston, Texas, USA.

Coastal aquifer management has recently emerged as a main scope in groundwater hydrology, especially in arid and semi-arid zones. About two thirds of the human population are currently gathered close to shorelines relying on coastal groundwater resources. Worldwide, these systems are subject to quality deterioration due to a multitude of anthropogenic impacts and subsequent saltwater intrusion (SWI).

Many hydrological and hydrochemical features of SWI have been disclosed during the past century through numerous case studies, column studies, scale models, flow and reactive transport modeling. Yet, many scientific and engineering challenges remain, some of which need to be addressed for a better prospecting of future coastal freshwater reserves. The scope of this work is to contribute to the analysis and remediation of SWI by studying the following aspects: (1) response of carbonate aquifers with varying Ca/Mg content to SWI, (2) behavior of trace elements (TEs) where fresh and intruded seawater mix, (3) derivation of groundwater baseline levels in polluted settings, notably salinized aquifers, (4) identification and quantification of major hydrogeochemical processes stimulated by SWI, (5) reliability of complex models (especially in karst) with variable-density and solute transport formulations, and (6) feasibility of SWI mitigation strategies.

In order to reach the scope, some existing tools have been adapted and new tools developed to analyze and mitigate SWI. All together, they offer an interesting toolbox for investigating SWI anywhere. They were successfully applied to a stressed dolomitic limestone aquifer system in Lebanon (Eastern Mediterranean).